

Properties of the Volume Operator in Loop Quantum Gravity II: Detailed Presentation

Johannes Brunnemann^{1*}, David Rideout^{2†}

¹Department of Mathematics, University of Hamburg, 20146 Hamburg, Germany

²Perimeter Institute for Theoretical Physics, Waterloo, Ontario N2L 2Y5, Canada

October 24, 2018

Abstract

The properties of the Volume operator in Loop Quantum Gravity, as constructed by Ashtekar and Lewandowski, are analyzed for the first time at generic vertices of valence greater than four. We find that the occurrence of a smallest non-zero eigenvalue is dependent upon the geometry of the underlying graph, and is not a property of the Volume operator itself. The present analysis benefits from the general simplified formula for matrix elements of the Volume operator derived in [24], making it feasible to implement it on a computer as a matrix which is then diagonalized numerically. The resulting eigenvalues serve as a database to investigate the spectral properties of the volume operator. Analytical results on the spectrum at 4-valent vertices are included. This is a companion paper to [25], providing details of the analysis presented there.

Contents

1	Introduction	2
2	Definition and Derivation of the Volume Operator	3
2.1	Classical Starting Point	3
2.2	Regularization Scheme	4
2.3	Right Invariant Vector Fields as Angular Momentum Operators	7
2.4	Matrix Elements in Terms of $3nj$ -Symbols	8
2.5	Removal of the Arbitrariness of the Edge Labeling	9
3	Explicit Matrix Elements of the Volume Operator	9
3.1	Starting Point for Matrix Element Implementation	9
3.2	Explicit Matrix Element Expressions	12
3.3	The Arguments: Special $6j$ -Symbols	16
4	Mathematical Preparations for Implementation on a Computer	17
4.1	Recoupling Scheme Basis	17
4.2	Sign Factor Combinatorics	19
5	Computational Details	29
5.1	Recoupling Scheme Implementation	29
5.2	Realizable Sign Factors via Poisson Sprinkling Process	30
5.3	Eigenvalue Computation and Numerical Errors	30
5.4	The Cactus Framework	30
6	Numerical Results on Volume Spectrum	31
6.1	General Remarks	31
6.2	Gauge Invariant 4-Vertex	33
6.3	Gauge Invariant 5-Vertex	34
6.4	Gauge Invariant 6-Vertex	45
6.5	Gauge Invariant 7-Vertex	53
6.6	Numerical Errors	54
6.7	Histograms of Entire Data Set	60

*brunnemann@math.uni-hamburg.de

†drideout@perimeterinstitute.ca

7 Analytical Results at the Gauge Invariant 4-Vertex	60
7.1 Setup: Explicit Expression for the Volume Operator as D -dimensional Matrix \widehat{Q}_D	60
7.2 Simplicity of the Spectrum of the Matrix \widehat{Q}_D	61
7.3 Eigenvectors of the Matrix \widehat{Q}_D	62
7.4 Upper and Lower Bounds on the Eigenvalues of \widehat{Q}_D	63
8 Summary	71
9 Acknowledgments	71
A Representations of $SU(2)$	72
A.1 General Conventions — Defining Representation $j = \frac{1}{2}$	72
A.2 General Conventions for $(2j + 1)$ -dimensional $SU(2)$ -Representation Matrices	73
B Angular Momentum Theory	73
B.1 Basic Definitions	73
B.2 Fundamental Recoupling	74
B.3 Recoupling of n Angular Momenta — $3nj$ -Symbols	74
B.4 Properties of Recoupling Schemes	76
C Properties of the $6j$-Symbols	77
C.1 Definition	77
C.2 Explicit Evaluation of the $6j$ -Symbols	77
C.3 Symmetry Properties	78
C.4 Orthogonality and Sum Rules	78
D Spin Networks and Representation Theory	78
D.1 Spin Network Functions	79
D.2 Right Invariant Vector Fields	79
D.3 Correspondence to Angular Momentum Theory	80
D.4 Historical Remark	81
References	83

1 Introduction

During the last 15 years major achievements have been obtained towards constructing a quantum theory of gravity in a background independent way. Within the framework of Loop Quantum Gravity (LQG) [1, 2, 3] it has been possible to reformulate General Relativity as a constrained¹ gauge field theory which is then quantized using a refined version² of canonical quantization which is based on [5]. In order to complete this program several conceptual and technical problems have to be solved. One major task is to understand and evaluate the action of the operators in the quantum theory which correspond to the classical constraints. Following the program of Refined Algebraic Quantization these operators have to be imposed on the up to now kinematical theory. A key ingredient [7, 8] for this is the understanding of the quantum operator corresponding to the classical volume of a region in three dimensional Riemannian space.

Note that there are different versions of this operator due to Ashtekar and Lewandowski [16] and due to Rovelli and Smolin [13] resulting from two different regularization schemes. We will focus here on the first version which considers diffeomorphism invariant properties of the graphs, namely the relative orientation of the graph edges underlying the kinematical basis states encoded in sign factors, whereas the latter is insensitive to this information. Moreover the latter regularization [13] seems to lead to difficulties when one attempts to reconstruct the action of the electric flux operators from the volume operator [22, 23]. In what follows we will always imply the operator due to Ashtekar and Lewandowski when using the phrase ‘volume operator’. This paper contains the details on the results presented in the companion paper [25], on the properties of the volume operator in Loop Quantum Gravity. We recommend the reader to have a look at [25] first in order to get an overview before getting into the details. Note that the basic notation which is used throughout this paper is introduced in [25]. Also an introduction to details of Loop Quantum Gravity essential for our analysis is provided in [25] and will not be reproduced here.

This paper is organized as follows. In section 2 we recall the construction (regularization scheme) of the volume operator from the classical volume expression of a spatial region in order to clarify the origin of the combinatorial

¹ Upon rewriting General Relativity in Hamilton’s formalism, the background independence of the underlying theory is manifested in the occurrence of constraints which must be fulfilled by physical configurations in the thus constructed model. By ‘background independence’ we refer to independence from a choice of fixed background geometry.

²This quantization program is referred to as Refined Algebraic Quantization (RAQ), see [1] for a pedagogical introduction.

sign factor and the recoupling in the resulting operator expression. Here we closely follow [15]. Starting from [24] we then present in section 3 a more elaborate discussion of the computation of the matrix elements of the volume operator, in particular all cases of special arguments of the general matrix element formula obtained in [24] are worked out in detail. Subsequently in section 4 we show how considerations of gauge invariance impose conditions on the combinatorial sign factors, which reveals a kind of ‘self-regulating’ property of this operator with respect to high valent vertices, providing a suppression of the volume contribution of certain high valent vertices. Next we present a detailed analysis on the set of diffeomorphism inequivalent embeddings which exist for the edges of an N -valent vertex into a spatial three dimensional Riemannian manifold. This analysis is accompanied by a numerical Monte Carlo sprinkling computation. Section 5 then describes the technical details of the computational implementation. In the following section 6 the results of the detailed numerical analysis of the volume spectrum is presented. The eigenvalues are computed via singular value decomposition, utilizing the LAPACK library [35]. The numerical work employs the Cactus computational framework [36], which provides automatic parallelism, facilitates use of the LAPACK library (including managing inter-language procedure calls), and places the code in a modular context from which it can easily be used by others for future investigations. Finally in section 7 we present new analytic results on properties of the volume operator at four-valent gauge invariant vertices. We show that its spectrum is simple and give an expression of the volume eigenstates in terms of its matrix elements and its eigenvalues. Moreover we show how one can (under mild assumptions on the four spins at the vertex) obtain an analytic lower bound of the smallest non-zero eigenvalue, solving an outstanding problem of [24]. Our results are then briefly summarized in section 8; for a detailed summary we refer the reader to the companion paper [25]. An appendix contains background material regarding spin networks and angular momentum theory, in order to make the present series of papers self contained and accessible to non-specialists.

2 Definition and Derivation of the Volume Operator

Let us briefly introduce our notation first. Note that a basic introduction to LQG is given in the companion paper [25] and will not be reproduced here. For more details the reader is referred to [1, 2, 3].

As General Relativity is treated in Hamiltonian formalism as an $SU(2)$ -gauge field theory, four dimensional space time is foliated into three dimensional spatial slices Σ with induced metric $q_{ab}(x)$ and orthogonal foliation direction parametrized by a real foliation parameter. The canonical variables are then densitized triads $E_i^a(x)$ and a connection $A_b^j(y)$, at $x, y \in \Sigma$. Usually $i, j = 1, 2, 3$ are $su(2)$ -directions, and $a, b = 1, 2, 3$ are spatial tensor indices. The set of classical (smooth, continuous) connection configurations is denoted by \mathcal{A} , the set of distributional connections is called $\overline{\mathcal{A}}$. The Poisson brackets of the $E_i^a(x)$ and the connection $A_b^j(y)$ are then given by

$$\{E_i^a(x), A_b^j(y)\} = \kappa \delta_b^a \delta_i^j \delta(x, y) \quad (2.1)$$

Here $\kappa = 8\pi G_N$, G_N being Newton’s constant. Electric fluxes $E_i(S)$ are constructed by integration of the dual electric field over two dimensional orientable surfaces $S \subset \Sigma$ and the integral of the connection along one dimensional oriented piecewise analytic edges $e \subset \Sigma$ giving the holonomy $h_e(A)$ for each $A \in \mathcal{A}$. In this way (2.1) is regularized. A collection of edges is called a graph γ . Its set of edges is called $E(\gamma)$. It is constructed such that two edges mutually intersect at most in their beginning/end point, called a vertex v in the vertex set $V(\gamma)$. Continuous maps $f = f_\gamma \circ p_\gamma$ are called cylindrical functions, the set of cylindrical functions is denoted by CYL. Here $p_\gamma : \mathcal{A} \rightarrow \{h_e(A)\}_{e \in E(\gamma)} \in SU(2)^{|E(\gamma)|}$ and $f_\gamma : \{h_e(A)\}_{e \in E(\gamma)} \in SU(2)^{|E(\gamma)|} \rightarrow \mathbb{C}$. Sometimes we will also refer to f_γ as cylindrical functions. Moreover one finds that spin network functions (SNF) $T_{\gamma \vec{j} \vec{m} \vec{n}}(A) = \prod_{e \in E(\gamma)} \sqrt{2j_e + 1} [\pi_{j_e}(h_e(A))]_{m_e n_e}$ serve as a basis for CYL. Here $[\pi_{j_e}(h_e(A))]_{m_e n_e}$ is a representation matrix element function of an irreducible $SU(2)$ representation of weight j_e which is associated to every $e \in E(\gamma)$, and $m_e, n_e = -j_e, \dots, j_e$ denote the matrix element.

2.1 Classical Starting Point

In this section we will closely follow the construction presented in [15].

Let us review the most important steps in order to write down a well defined operator \hat{V} acting on the kinematical Hilbert space of LQG. The classical expression for the volume of an open, connected three dimensional spatial region R given by:

$$\begin{aligned} V(R) &= \int_R d^3x \sqrt{\det q(x)} \\ &= \int_R d^3x \sqrt{\left| \frac{1}{3!} \epsilon^{ijk} \epsilon_{abc} E_i^a(x) E_j^b(x) E_k^c(x) \right|} \end{aligned} \quad (2.2)$$

where we choose the Riemannian signature $\det(q) > 0 \forall x$ and have used the fact that the square root of the determinant of the spatial metric $q_{ab}(x)$ can be re-expressed in terms of the densitized triads $E_i^a(x)$, as introduced in [25].

2.2 Regularization Scheme

The regularization procedure displayed here will be similar to the regularization of (2.1) by smearing the dual of electric fields $E_i^a(x)$ over two dimensional surfaces S and the connection $A_b^j(y)$ along one dimensional edges e in order to obtain its holonomy $h_e(A)$, however the idea is here to define the smearing surfaces somewhat intrinsically, adapted to a graph γ being the support for a cylindrical function f_γ .

Let us introduce the characteristic function $\chi_\Delta(p, x)$ of a cube in a coordinate frame x centered at a point p and spanned by the three vectors $\vec{\Delta}_\rho = \Delta_\rho \vec{n}_\rho$, the \vec{n}_ρ being normal vectors in the frame x . The cube Δ has coordinate volume $\text{vol}(\Delta) = 2^3 \Delta_1 \Delta_2 \Delta_3 \det(\vec{n}_1, \vec{n}_2, \vec{n}_3)$. Then $\chi_\Delta(p, x)$ can be defined as

$$\chi_\Delta(p, x) = \prod_{\rho=1}^3 \Theta\left(\Delta_\rho - |\langle \vec{n}_\rho, (x-p) \rangle|\right) \quad (2.3)$$

and $\langle \cdot | \cdot \rangle$ is the Euclidean inner product, $\Theta(z)$ is the usual unit step function with $\Theta(z) = 0$ if $z < 0$, $\Theta(z) = \frac{1}{2}$ if $z = 0$ and $\Theta(z) = 1$ if $z > 0$.

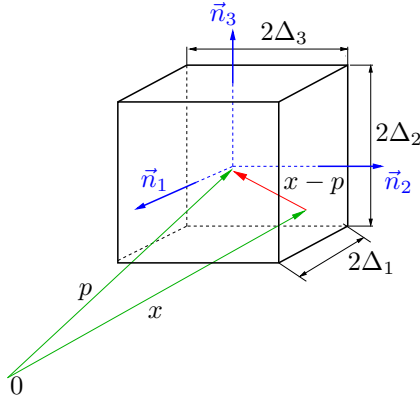


Figure 1: The regulator $\chi_\Delta(p, x)$

If we take the limit $\Delta \rightarrow 0$ (by decreasing $\Delta_\rho \rightarrow 0$ for $\rho = 1, 2, 3$) we realize that

$$\lim_{\Delta \rightarrow 0} \frac{1}{\text{vol}(\Delta)} \chi_\Delta(p, x) = \delta^{(3)}(p, x) \quad (2.4)$$

where $\delta^{(3)}$ indicates the delta distribution in three dimensions. Now upon introducing the smeared quantity

$$E(p, \Delta, \Delta', \Delta'') := \frac{1}{\text{vol}(\Delta) \text{vol}(\Delta') \text{vol}(\Delta'')} \int_R d^3x \int_R d^3y \int_R d^3z \chi_\Delta(p, x) \chi_{\Delta'}(p, \frac{x+y}{2}) \chi_{\Delta''}(p, \frac{x+y+z}{3}) \times \frac{1}{3!} \epsilon^{ijk} \epsilon_{abc} E_i^a(x) E_j^b(y) E_k^c(z) \quad (2.5)$$

one notices that

- (i) Taking the limits $\Delta_\rho, \Delta'_{\rho'}, \Delta''_{\rho''} \rightarrow 0$ in any combination and at any rate with respect to each other we come back to $\frac{1}{3!} \epsilon^{ijk} \epsilon_{abc} E_i^a(p) E_j^b(p) E_k^c(p)$ due to (2.4).
- (ii) (i) holds for any choice of linearly independent normal vectors $\vec{n}_\rho, \vec{n}_{\rho'}, \vec{n}_{\rho''}$.
- (iii)

$$V(R) = \lim_{\Delta \rightarrow 0} \lim_{\Delta' \rightarrow 0} \lim_{\Delta'' \rightarrow 0} \int_R d^3p \sqrt{|E(p, \Delta, \Delta', \Delta'')|} \quad (2.6)$$

The classical Poisson bracket (2.1) contains functional derivatives with respect to the electric field $E_i^a(x)$ and the connection $A_b^j(y)$. Upon quantization the electric field $E_i^a(x)$ acts as a functional derivative

$$E_i^a(x) \longrightarrow \hat{E}_i^a(x) := -i\hbar\kappa \frac{\delta}{\delta A_a^i(x)} \quad (2.7)$$

and we have (symbolically), for the action of this functional derivative on a holonomy $h_e(A)$ of an edge e with $x = e(t_x)$ being a point of e , (here $\tau_i = -i\sigma_i$ denotes a basis for the Lie algebra $su(2)$, σ_i are the Pauli matrices) :

$$\begin{aligned} \frac{\delta h_e(A)}{\delta A_a^i(x)} &= \frac{1}{2} \left[\lim_{\tilde{t} \downarrow t_x} + \lim_{\tilde{t} \uparrow t_x} \right] \int_0^1 dt \left[\delta^3(e(\tilde{t}), x) \dot{e}^a(t) h_{e[0,t]} \frac{\tau_i}{2} h_{e[t,1]} \right] \\ &= \begin{cases} \frac{1}{2} \dot{e}^a(t_x) \frac{\tau_i}{2} h_{e[0,1]} & x = e(t)|_{t=0} \\ \dot{e}^a(t_x) h_{e[0,t]} \frac{\tau_i}{2} h_{e[t,1]} & x = e(t)|_{0 < t < 1} \\ \frac{1}{2} \dot{e}^a(t_x) h_{e[0,1]} \frac{\tau_i}{2} & x = e(t)|_{t=1} \end{cases} \end{aligned} \quad (2.8)$$

Then we can formulate the action of a smeared version of (2.7) contained in the regulated expression (2.5)

$$\hat{E}_i^a(p, \Delta) := \frac{1}{\text{vol}(\Delta)} \int_{\sigma} d^3x \chi_{\Delta}(x) \hat{E}_i^a(x) \quad (2.9)$$

on a function $f_{\gamma}(h_{e_1}, \dots, h_{e_N})$ cylindrical with respect to the graph γ , e.g. for $x = e(t)|_{0 < t < 1}$ as

$$\hat{E}_i^a(p, \Delta) f_{\gamma} = -\frac{i\ell_P^2}{\text{vol}(\Delta)} \sum_{e \in E(\gamma)} \int_0^1 dt \chi_{\Delta}(p, e(t)) \dot{e}^a(t) \text{tr} \left[h_{e[0,t]} \frac{\tau_i}{2} h_{e[t,1]} \frac{\partial}{\partial h_{e[0,1]}} \right] f_{\gamma}(h_{e_1}, \dots, h_{e_N}) \quad (2.10)$$

where the trace is taken with respect to the defining representation of $SU(2)$ and we have used the chain rule and Leibnitz rule in order to evaluate the functional derivative on f_{γ} .

Now obviously the regulated expression (2.5) contains three expressions of the form (2.10), which have to be applied successively if one wants to evaluate the action of (2.5) on a cylindrical function. This involves a careful analysis of the action (2.8) of the individual functional derivatives, in particular if they act on one edge simultaneously, which results in expressions where different τ -matrices have to be inserted into the holonomy at different values of the curve parameter t .

The action of $E(p, \Delta, \Delta', \Delta'')$ on a cylindrical function then schematically reads

$$\begin{aligned} E(p, \Delta, \Delta', \Delta'') f_{\gamma} &= \left[\sum_{e' e''} M \cdot \epsilon_{abc} \times \right. \\ &\times \left. \int_0^1 dt \int_0^1 dt' \int_0^1 dt'' \chi_{\Delta}(p, e(t)) \chi_{\Delta'}(p, \frac{e(t)+e'(t')}{2}) \chi_{\Delta''}(p, \frac{e(t)+e'(t')+e''(t'')}{3}) \dot{e}(t)^a \dot{e}'(t')^b \dot{e}''(t'')^c \hat{O}_{e' e''}(t, t', t'') \right] f_{\gamma} \end{aligned} \quad (2.11)$$

Here $M = \frac{i\ell_P^6}{3! \text{vol}(\Delta) \text{vol}(\Delta') \text{vol}(\Delta'')}$ and the sum has to be extended to all triples of (not necessarily distinct) edges $(e' e'')$. By successive application of the three functional derivatives and Leibnitz rule, one obtains expressions $\hat{O}_{e' e''}(t, t', t'')$ which are combinations of traces of holonomies containing inserted τ matrices and partial derivatives with respect to holonomies of the appropriate edges.

In order to evaluate the characteristic functions $\chi_{\Delta}(p, x)$, $\chi_{\Delta'}(p, \frac{x+y}{2})$, $\chi_{\Delta''}(p, \frac{x+y+z}{3})$ contained in expression (2.5) one considers a coordinate transformation in the integrals: for a given triple (e, e', e'') of (not necessarily) distinct edges contained in the edge set $E(\gamma)$, the vector valued function

$$x_{ee'e''}(t, t', t'') := \frac{e(t) + e'(t') + e''(t'')}{3} \quad (2.12)$$

whose Jacobian is given by

$$\det \left(\frac{\partial x_{ee'e''}^a}{\partial(t, t', t'')} \right) = \det \begin{pmatrix} \frac{\partial x^1}{\partial t} & \frac{\partial x^2}{\partial t} & \frac{\partial x^3}{\partial t} \\ \frac{\partial x^1}{\partial t'} & \frac{\partial x^2}{\partial t'} & \frac{\partial x^3}{\partial t'} \\ \frac{\partial x^1}{\partial t''} & \frac{\partial x^2}{\partial t''} & \frac{\partial x^3}{\partial t''} \end{pmatrix} = \frac{1}{3^3} \epsilon_{abc} \dot{e}(t)^a \dot{e}'(t')^b \dot{e}''(t'')^c \quad (2.13)$$

equals, up to a numerical prefactor, the tangent vectors³ contracted with the totally antisymmetric ϵ_{abc} in (2.5), which is the reason for the choice of arguments in the characteristic function $\chi_{\Delta''}$.

³As implied by inserting (2.7), (2.8) into the classical expression (2.5).

The observation is now that taking the limit $\Delta''_{p''} \rightarrow 0$, and simultaneously demanding that $\chi_{\Delta'}(p, \frac{e(t)+e'(t')+e''(t'')}{3}) \stackrel{!}{=} 1$, implies that $e(t_{int}) \stackrel{!}{=} e'(t'_{int}) \stackrel{!}{=} e''(t''_{int}) \stackrel{!}{=} p$, that is the edges e, e', e'' have to intersect at p at the according curve parameters $t_{int}, t'_{int}, t''_{int}$.⁴ Therefore the point p is a vertex v in the vertex set $V(\gamma)$ of the graph γ . Moreover due to the convention that edges can at most intersect at their beginning and endpoints,⁵ we can without loss of generality assume that (e, e', e'') are outgoing from $p = v$, which consequently serves as their beginning point and hence $t_{int} = t'_{int} = t''_{int} = 0$.

We can thus pull the remaining characteristic functions $\chi_{\Delta}(p, e(t)) = \chi_{\Delta'}(p, \frac{e(t)+e'(t')}{2}) = 1$ out of the integral. The remaining part of the integral then is schematically given as

$$\begin{aligned} \lim_{\Delta'' \rightarrow 0} E(p, \Delta, \Delta', \Delta'') f_{\gamma} &= \\ &= \left[\sum_{e, e', e''} \frac{i \ell_p^6 3^3 \chi_{\Delta}(p, v) \chi_{\Delta'}(p, v)}{3! \text{vol}(\Delta) \text{vol}(\Delta')} \hat{O}_{e, e', e''}(0, 0, 0) \int_0^1 dt \int_0^1 dt' \int_0^1 dt'' \delta^{(3)}(p, x_{e, e', e''}) \det \left(\frac{\partial x_{e, e', e''}^a}{\partial(t, t', t'')} \right) \right] f_{\gamma} \end{aligned} \quad (2.14)$$

In order to get a non vanishing expression from (2.14) the triple (e, e', e'') must consist of three distinct edges with linearly independent tangents in $p = v$.

Now perform a change of variables

$$\begin{aligned} d^3 t \left| \det \left(\frac{\partial x_{e, e', e''}^a}{\partial(t, t', t'')} \right) \right| &= d^3 t \underbrace{\text{sgn} \left[\det \left(\frac{\partial x_{e, e', e''}^a}{\partial(t, t', t'')} \right) \right]}_{\epsilon(e, e', e'')} \cdot \det \left(\frac{\partial x_{e, e', e''}^a}{\partial(t, t', t'')} \right) \\ &=: d^3 t \epsilon(e, e', e'') \cdot \det \left(\frac{\partial x_{e, e', e''}^a}{\partial(t, t', t'')} \right) \\ &= d^3 x_{e, e', e''} \end{aligned} \quad (2.15)$$

in order to evaluate the $\delta^{(3)}$ -distribution in (2.14). Note that *it is here where the sign factor $\epsilon(e, e', e'')$ enters*. For this purpose we have to insert a $1 = [\epsilon(e, e', e'')]^2$ and, observing that integrating the $\delta^{(3)}(p, x_{e, e', e''})$ over the positive octant only gives an additional prefactor of $\frac{1}{8}$, we arrive at

$$\lim_{\Delta'' \rightarrow 0} E(p, \Delta, \Delta', \Delta'') f_{\gamma} = \left[\sum_{e, e', e'' \in E(\gamma)} \frac{i \ell_p^6 3^3 \chi_{\Delta}(p, v) \chi_{\Delta'}(p, v)}{3! 8 \cdot 8 \text{vol}(\Delta) \text{vol}(\Delta')} \epsilon(e, e', e'') \hat{O}_{e, e', e''}(0, 0, 0) \right] f_{\gamma} \quad (2.16)$$

where

$$\hat{O}_{e, e', e''}(0, 0, 0) = \frac{1}{8} \epsilon_{ijk} X_e^i X_{e'}^j X_{e''}^k \quad (2.17)$$

and $X_e^i := \text{tr} \left(\tau_i h_{e[0,1]} \frac{\partial}{\partial h_{e[0,1]}} \right)$ denotes the right invariant vector fields of $\text{SU}(2)$ resulting from the action of the functional derivatives (2.8). Note that we can choose the order of the right invariant vector fields arbitrarily in (2.17), because they commute if they act on distinct edges, that is distinct copies of $\text{SU}(2)$.

The second prefactor $\frac{1}{8}$ in (2.16) stems from the fact that we only evaluate one sided functional derivatives according to (2.8): For a vertex v in the vertex set $V(\gamma)$ of the graph γ , the point p is the beginning point of the outgoing edges e, e', e'' , that is $p = e(t)|_{t=0} = e'(t')|_{t'=0} = e''(t'')|_{t''=0}$.

Inserting (2.16) back into (2.6) we may synchronize the remaining limits $\Delta, \Delta' \rightarrow 0$ by choosing $\Delta = \Delta'$ and take $\chi_{\Delta}(p, v) = [\chi_{\Delta}(p, v)]^2$ out of the square root. Taking the limit $\Delta \rightarrow 0$ then results in the operator describing the volume of a spatial region R , namely the volume operator $\hat{V}(R)_{\gamma}$ acting on the cylindrical function f_{γ} over a graph γ as:

$$\hat{V}(R)_{\gamma} f_{\gamma} = \int_R d^3 p \sqrt{\widehat{\det(q)}(p)_{\gamma}} f_{\gamma} = \int_R d^3 p \hat{V}(p)_{\gamma} f_{\gamma} \quad (2.18)$$

where

$$\hat{V}(p)_{\gamma} = \ell_p^3 \sum_{v \in V(\gamma)} \delta^{(3)}(p, v) \hat{V}_{v, \gamma} \quad (2.19)$$

$$\hat{V}_{v, \gamma} = \sqrt{\left| i \cdot \tilde{Z} \sum_{\substack{e_I, e_J, e_K \in E(\gamma) \\ e_I \cap e_J \cap e_K = v}} \epsilon(e_I, e_J, e_K) \epsilon_{ijk} X_I^i X_J^j X_K^k \right|} \quad (2.20)$$

⁴ The decoration '!' in ' $\stackrel{!}{=}$ ' simply indicates that the equality is required to hold.

⁵This can always be achieved by subdividing and redirecting the edges of a graph γ , see [25].

Here \tilde{Z} is a constant depending on the regularization procedure. Its numerical value according to [15] and above is found to be $\tilde{Z} = \frac{\beta^3}{3! \cdot 8} \cdot \left(\frac{3}{4}\right)^3$, however we will keep it unspecified in our calculations, since the Immirzi parameter β can be freely chosen. It only contributes an overall constant scaling to the spectrum of the volume operator. Mostly we will set $Z = 1$ below and reinsert it when necessary.

The sum has to be taken over all vertices $v \in V(\gamma)$ of the graph γ and at each vertex v over all possible triples (e_I, e_J, e_K) of outgoing edges⁶ of the graph γ . Here $\epsilon(e_I, e_J, e_K)$ is the sign of the cross product of the three tangent vectors of the edges (e_I, e_J, e_K) at the vertex v .

Again the X_I^i are the right invariant vector fields on $SU(2)$ fulfilling the commutator relation

$$[X_I^i, X_J^j] = -2 \delta_{IJ} \epsilon^{ijk} X_I^k \quad (2.21)$$

2.3 Right Invariant Vector Fields as Angular Momentum Operators

One can introduce the self-adjoint right invariant vector fields $Y_J^j := -\frac{i}{2} X_J^j$ fulfilling the usual angular momentum commutation relations $[Y_I^i, Y_J^j] = i \delta_{IJ} \epsilon^{ijk} Y_I^k$.

Their action on cylindrical functions f_γ and hence spin network functions $T_{\gamma \vec{j} \vec{m} \vec{n}}(A)$ can be associated to the action of ordinary angular momentum operators J_I^i acting on a (recoupled) abstract spin system $|\vec{a} J M ; n\rangle$ as analyzed in [22, 23]. This correspondence is summarized in the companion paper [25] and recalled in more detail in section D.3 in the appendix of this paper. We can therefore equivalently replace:

$$\epsilon_{ijk} X_I^i X_J^j X_K^k f_\gamma \leftrightarrow \left(-\frac{2}{i}\right)^3 \epsilon_{ijk} J_I^i J_J^j J_K^k |\vec{a} J M ; n\rangle \quad (2.22)$$

Using furthermore the antisymmetry of ϵ_{ijk} and the fact that $[J_I^i, J_J^j] = 0$ whenever $I \neq J$ we can restrict the summation in (2.20) to $I < J < K$ if we simultaneously write a factor $3!$ in front of the sum. The result is:

$$\hat{V}_{v,\gamma} = \sqrt{\left| \tilde{Z} \cdot 3! \cdot 2^3 \sum_{I < J < K} \epsilon(e_I, e_J, e_K) \epsilon_{ijk} J_I^i J_J^j J_K^k \right|} \quad (2.23)$$

We then make use of the identity

$$\epsilon_{ijk} J_I^i J_J^j J_K^k = \frac{i}{4} [(J_{IJ})^2, (J_{JK})^2] \quad (2.24)$$

where $(J_{IJ})^2 = \sum_{k=1}^3 (J_I^k + J_J^k)^2$. This relation can be derived by writing down every commutator as $[(J_{IJ})^2, (J_{JK})^2] = \sum_{i,j=1}^3 [(J_I^i + J_J^i)^2, (J_J^j + J_K^j)^2]$, using the identity $[a, bc] = [a, b]c + b[a, c]$ for the commutator, the angular momentum commutation relations ($[J^i, J^j] = i\epsilon^{ijk} J^k$) and the fact that $[J_I^i, J_J^j] = 0$ whenever $I \neq J$.

We may then summarize:

$$\hat{V}_{v,\gamma} = \sqrt{\left| Z \cdot \sum_{I < J < K} \epsilon(e_I, e_J, e_K) \hat{q}_{IJK} \right|} = \left| |Z| \cdot Q \right|^{\frac{1}{2}} = \left| |Z|^2 \cdot Q^\dagger Q \right|^{\frac{1}{4}} \quad (2.25)$$

where $\hat{q}_{IJK} := [(J_{IJ})^2, (J_{JK})^2]$ and $Z = \tilde{Z} \cdot \frac{i}{4} \cdot 3! \cdot 2^3 = i \cdot \beta^3 \cdot \frac{27}{256}$, β again denotes the Immirzi parameter. Note that the actual numerical value of Z varies in different regularizations [16, 15]⁷. However [22] shows how it can be fixed to $Z = \beta^3 \cdot \frac{3!i}{4} \cdot C_{reg}$, with $C_{reg} = \frac{1}{3!8}$, by demanding consistency of the volume quantization to the usual quantization of the electric fluxes. We will set $Z = 1$ in our subsequent analysis, as it only gives an overall numerical scaling of the volume spectrum.

Here we have introduced the shorthand $Q^\dagger Q$. Q is by definition a sum of antisymmetric matrices and hence antisymmetric itself. Multiplying it by its transposed conjugate Q^\dagger , one obtains a totally symmetric real matrix. Its eigenvalues $\lambda_{Q^\dagger Q} \geq 0$ are real and come in pairs $\lambda_{Q^\dagger Q} = |\lambda_Q|^2$. Equation (2.25) can be understood as follows: The Volume operator \hat{V} has the same eigenstates as Q or $Q^\dagger Q$, but its eigenvalues are defined as $\lambda_{\hat{V}} := |\lambda_Q|^{\frac{1}{2}} = |\lambda_{Q^\dagger Q}|^{\frac{1}{4}}$.

Our task is then to calculate the spectra of totally antisymmetric real matrices of the form:

$$Q := \sum_{I < J < K \leq N} \epsilon(IJK) \hat{q}_{IJK} \quad (2.26)$$

where $\epsilon(IJK) = \text{sgn}(\det(\dot{e}_I(v), \dot{e}_J(v), \dot{e}_K(v)))$ denotes the sign of the determinant of the tangents of the three edges e_I, e_J, e_K intersecting at the vertex v , and N is the valence of v .

⁶As mentioned before, one can without loss of generality always redirect edges such that there are only outgoing edges at each vertex.

⁷The latter regularization [15], which we have presented here, differs by a numerical factor of $\frac{27}{8}$ from the former [16]. The former exactly reproduces the value of C_{reg} obtained in [22].

2.4 Matrix Elements in Terms of $3nj$ -Symbols

Now we can apply the recoupling theory of n angular momenta as introduced in the companion paper [25]. Further details are provided in appendix section B. The aim is to represent \hat{q}_{IJK} in a recoupling scheme basis. We will do this with respect to the standard basis⁸ $|\vec{a}(12)\rangle$, where we can now easily restrict our calculations to gauge invariant spin network states by demanding the total angular momentum J and the total magnetic quantum number M to vanish, i.e. we will take into account only recoupling schemes which couple the outgoing spins at the vertex v to resulting angular momentum 0. In terms of the recoupling schemes these states are given by:

$$|\vec{g}(IJ) \vec{j} J = 0 M = 0\rangle := |\vec{g}(IJ)\rangle \quad (2.27)$$

where we have introduced an abbreviation, since the quantum numbers \vec{j} , $J = 0$, $M = 0$ are the same for every gauge invariant spin network state with respect to a fixed N -valent vertex v with edge spins $\vec{j} := (j_1, \dots, j_N)$.

We will now represent $\hat{q}_{IJK} := [(J_{IJ})^2, (J_{JK})^2]$ in the standard recoupling scheme basis where $|\vec{a}\rangle := |\vec{a}(12)\rangle$, $|\vec{a}'\rangle := |\vec{a}'(12)\rangle$. The point is that by construction a recoupling scheme basis $|\vec{g}(IJ)\rangle$ diagonalizes the operator $(G_2)^2 = (J_{IJ})^2 = (J_I + J_J)^2$:

$$(G_2)^2 |\vec{g}(IJ)\rangle = g_2(IJ)(g_2(IJ) + 1) |\vec{g}(IJ)\rangle \quad (2.28)$$

Furthermore every recoupling scheme $|\vec{g}(IJ)\rangle$ can be expanded in terms of the standard basis via its expansion coefficients, the $3nj$ -symbols. So it is possible to express [15]

$$\begin{aligned} \langle \vec{a}(12) | \hat{q}_{IJK} | \vec{a}'(12) \rangle &= \\ &= \langle \vec{a}(12) | [(J_{IJ})^2, (J_{JK})^2] | \vec{a}'(12) \rangle \\ &= \langle \vec{a}(12) | (J_{IJ})^2 (J_{JK})^2 | \vec{a}'(12) \rangle - \langle \vec{a}(12) | (J_{JK})^2 (J_{IJ})^2 | \vec{a}'(12) \rangle \\ &= \sum_{\vec{g}(IJ)} g_2(IJ)(g_2(IJ) + 1) [\langle \vec{a}(12) | \vec{g}(IJ) \rangle \langle \vec{g}(IJ) | (J_{JK})^2 | \vec{a}'(12) \rangle - \langle \vec{a}(12) | (J_{JK})^2 | \vec{g}(IJ) \rangle \langle \vec{g}(IJ) | \vec{a}'(12) \rangle] \\ &= \sum_{\vec{g}(IJ), \vec{g}(JK), \vec{g}''(12)} g_2(IJ)(g_2(IJ) + 1) g_2(JK)(g_2(JK) + 1) \langle \vec{g}(IJ) | \vec{g}''(12) \rangle \langle \vec{g}(JK) | \vec{g}''(12) \rangle \times \\ &\quad \times [\langle \vec{g}(IJ) | \vec{a}(12) \rangle \langle \vec{g}(JK) | \vec{a}'(12) \rangle - \langle \vec{a}(12) | \vec{g}(JK) \rangle \langle \vec{g}(IJ) | \vec{a}'(12) \rangle] \\ &= \sum_{\vec{g}''(12)} \left[\sum_{\vec{g}(IJ)} g_2(IJ)(g_2(IJ) + 1) \langle \vec{g}(IJ) | \vec{g}''(12) \rangle \langle \vec{g}(IJ) | \vec{a}(12) \rangle \times \right. \\ &\quad \left. \times \sum_{\vec{g}(JK)} g_2(JK)(g_2(JK) + 1) \langle \vec{g}(JK) | \vec{g}''(12) \rangle \langle \vec{g}(JK) | \vec{a}'(12) \rangle \right] \\ &\quad - \left[\vec{a}(12) = \vec{a}'(12) \right] \end{aligned} \quad (2.29)$$

$$= \sum_{\vec{g}''(12)} \left[F^{IJ}(\vec{a}(12), \vec{g}''(12)) \times F^{JK}(\vec{a}'(12), \vec{g}''(12)) \right] - \left[\vec{a}(12) = \vec{a}'(12) \right] \quad (2.30)$$

where we have introduced the shorthand

$$F^{IJ}(\vec{a}(12), \vec{g}''(12)) := \sum_{\vec{g}(IJ)} g_2(IJ)(g_2(IJ) + 1) \langle \vec{g}(IJ) | \vec{g}''(12) \rangle \langle \vec{g}(IJ) | \vec{a}(12) \rangle \quad (2.31)$$

We can nicely see from (2.29) that we obtain a real antisymmetric matrix possessing purely imaginary eigenvalues (we could alternatively consider the purely complex version by multiplying all matrix elements by the imaginary unit i). We have inserted the suitable recoupling schemes $|\vec{g}(IJ)\rangle$, $|\vec{g}(JK)\rangle$ diagonalizing $(J_{IJ})^2$ and $(J_{JK})^2$ and their expansion in terms of the standard basis $|\vec{g}(12)\rangle$ by using the completeness of the recoupling schemes $|\vec{g}(IJ)\rangle$ for arbitrary $I \neq J$ ⁹

$$\mathbb{1} = \sum_{\vec{g}(IJ)} |\vec{g}(IJ)\rangle \langle \vec{g}(IJ)| \quad (2.32)$$

So we have as a first step expressed the matrix elements of \hat{q}_{IJK} in terms of $3nj$ -symbols.

⁸See appendix section B.4 for the definition.

⁹The summation has to be extended over all possible intermediate recoupling steps g_2, \dots, g_{n-1} , that is $|j_r - j_q| \leq g_k(j_q, j_r) \leq j_q + j_r$, allowed by the Clebsch-Gordan Theorem.

2.5 Removal of the Arbitrariness of the Edge Labeling

We have described how one can represent the volume operator as a matrix acting on a linear vector space whose basis states are labelled by the multilabel \vec{a} of the standard recoupling schemes. As can be seen from definition B.3 in the appendix there exists a unitary basis transformation between any two different orders of recoupling, e.g. $\vec{g}(IJ), \vec{a}(12)$:

$$|\vec{g}(IJ) J M ; \vec{n}\rangle = \sum_{\vec{a}(12)} \langle \vec{a}(12) J M ; \vec{n} | \vec{g}(IJ) J M ; \vec{n} \rangle \cdot |\vec{a}(12) J M ; \vec{n}\rangle \quad (2.33)$$

where the matrix elements $\langle \vec{a}(12) J M ; \vec{n} | \vec{g}(IJ) J M ; \vec{n} \rangle =: U_{\vec{a}\vec{g}}$ of this basis transformation are the so called $3nj$ -symbols. Now this basis transformation is unitary as can easily be seen because the recoupling schemes are orthonormal

$$\langle \vec{a}(12) J M ; \vec{n} | \vec{a}'(12) J' M' ; \vec{n}' \rangle = U_{\vec{a}\vec{a}'} = \delta_{\vec{a}\vec{a}'} \delta_{JJ'} \delta_{MM'} \delta_{\vec{n}\vec{n}'} \quad (2.34)$$

and provide a complete orthonormal basis

$$\begin{aligned} \langle \vec{a}(12) J M ; \vec{n} | \vec{a}'(12) J M ; \vec{n} \rangle &= \\ &= \delta_{\vec{a}'\vec{a}(12)} \\ &= \sum_{\vec{g}(IJ)} \langle \vec{a}(12) J M ; \vec{n} | \vec{g}(IJ) J M ; \vec{n} \rangle \langle \vec{g}(IJ) J M ; \vec{n} | \vec{a}'(12) J M ; \vec{n} \rangle \\ &= \sum_{\vec{g}(IJ)} U_{\vec{a}\vec{g}} U_{\vec{g}\vec{a}'} \end{aligned} \quad (2.35)$$

Moreover the $3nj$ -symbols are real (the overline denotes complex conjugation) and symmetric

$$\begin{aligned} \overline{\langle \vec{a}(12) J M ; \vec{n} | \vec{g}(IJ) J M ; \vec{n} \rangle} &= \overline{U_{\vec{a}\vec{g}}} = U_{\vec{a}\vec{g}} = \langle \vec{a}(12) J M ; \vec{n} | \vec{g}(IJ) J M ; \vec{n} \rangle \\ &= U_{\vec{g}\vec{a}} = \langle \vec{g}(IJ) J M ; \vec{n} | \vec{a}(12) J M ; \vec{n} \rangle \end{aligned} \quad (2.36)$$

Thus we have

$$UU^\dagger = UU^T = U^2 = \mathbb{1} \quad (2.37)$$

Because the change of the recoupling order can be implemented as a unitary transformation, we have for the matrix representation Q of the volume operator of (2.26), after a transformation from the standard basis $\vec{a}(12)$ to a new basis $\vec{g}(IJ)$:

$$Q_{\vec{g}'\vec{g}} := \langle \vec{g}' | Q | \vec{g} \rangle = \langle \sum_{\vec{a}'} U_{\vec{g}'\vec{a}'} \vec{a}' | Q | \sum_{\vec{a}} U_{\vec{g}\vec{a}} \vec{a} \rangle = \sum_{\vec{a}'\vec{a}} U_{\vec{g}'\vec{a}'}^\dagger U_{\vec{g}\vec{a}} \langle \vec{a}' | Q | \vec{a} \rangle = \sum_{\vec{a}'\vec{a}} U_{\vec{g}'\vec{a}'}^\dagger U_{\vec{g}\vec{a}} Q_{\vec{a}'\vec{a}} \quad (2.38)$$

The matrix Q is being transformed as $Q \mapsto U^{-1}QU$ because $U^\dagger = U^{-1}$. Such a unitary transformation does not change the spectrum of Q , hence *the spectrum of the volume operator is independent of the chosen order of recoupling*.

We use this property to drastically decrease the number of assignments of spins to edges we must use in the numerical analysis, because we can always choose a particular edge labelling e_1, \dots, e_N in which the spins are sorted

$$j_1 \leq j_2 \leq \dots \leq j_N = j_{max} \quad (2.39)$$

Such a labeling then corresponds to

$$D(\vec{j}) = \frac{N}{N_1! \cdot N_2! \cdot \dots \cdot N_p!} \quad (2.40)$$

arbitrarily labeled spin assignments, where N_i is number of elements in one of p sets of mutually identical spins, $\sum_{i=1}^p N_i = N$. Throughout the remainder of the paper we refer to such a sorted assignment of spins to vertex edges as a *spin configuration* (or \vec{j} -configuration).

3 Explicit Matrix Elements of the Volume Operator

3.1 Starting Point for Matrix Element Implementation

The simplified closed expression for (2.29), which has been derived in [24], serves as a starting point for our computations. Its derivation will not be reproduced here. However, in order to make it implementable on the computer, we will recall the crucial intermediate results of [24] and give the detailed outcome of the main formula for the matrix elements for all combinations of its arguments.

Let us first state the complete results on $F^{IJ}(\vec{a}(12), \vec{g}''(12))$ as contained in (2.29). We find:

$$\begin{aligned}
& \boxed{I = 1 \quad J = 2} \quad a_2(a_2 + 1) \prod_{n=2}^N \delta_{g''_n a_n} \\
& \boxed{I = 1 \quad J = 3} \quad \left[\frac{1}{2}(-1)^{-j_1-j_2}(-1)^{j_3+1} X(j_1 \ j_3)^{\frac{1}{2}} A(g''_2 \ a_2) \begin{Bmatrix} j_2 & j_1 & g''_2 \\ 1 & a_2 & j_1 \end{Bmatrix} (-1)^{a_3} \begin{Bmatrix} a_3 & j_3 & g''_2 \\ 1 & a_2 & j_3 \end{Bmatrix} \right. \\
& \quad \left. + C(j_1 \ j_3) \delta_{g''_2 a_2} \right] \prod_{k=3}^N \delta_{g''_k a_k} \\
& \boxed{I = 1 \quad J > 3} \quad \left[\frac{1}{2}(-1)^{-j_1-j_2}(-1)^{j_J+1} X(j_1 \ j_J)^{\frac{1}{2}} A(g''_2 \ a_2) \begin{Bmatrix} j_2 & j_1 & g''_2 \\ 1 & a_2 & j_1 \end{Bmatrix} \times \right. \\
& \quad \times \prod_{n=3}^{J-1} A(g''_n a_n) (-1)^{-j_n+g''_{n-1}+a_{n-1}+1} \begin{Bmatrix} j_n & g''_{n-1} & g''_n \\ 1 & a_n & a_{n-1} \end{Bmatrix} \times (-1)^{a_J} \begin{Bmatrix} a_J & j_J & g''_{J-1} \\ 1 & a_{J-1} & j_J \end{Bmatrix} \\
& \quad \left. + C(j_1 \ j_J) \prod_{k=2}^{J-1} \delta_{g''_k a_k} \right] \prod_{k=J}^N \delta_{g''_k a_k} \\
& \boxed{I = 2 \quad J = 3} \quad \left[\frac{1}{2}(-1)^{-j_1-j_2}(-1)^{j_3+1} (-1)^{a_2-g''_2} X(j_2 \ j_3)^{\frac{1}{2}} A(g''_2 \ a_2) \begin{Bmatrix} j_1 & j_2 & g''_2 \\ 1 & a_2 & j_2 \end{Bmatrix} (-1)^{a_3} \begin{Bmatrix} a_3 & j_3 & g''_2 \\ 1 & a_2 & j_3 \end{Bmatrix} \right. \\
& \quad \left. + C(j_2 \ j_3) \delta_{g''_2 a_2} \right] \prod_{k=3}^N \delta_{g''_k a_k} \\
& \boxed{I = 2 \quad J > 3} \quad \left[\frac{1}{2}(-1)^{-j_1-j_2}(-1)^{j_J+1} (-1)^{a_2-g''_2} X(j_2 \ j_J)^{\frac{1}{2}} A(g''_2 \ a_2) \begin{Bmatrix} j_1 & j_2 & g''_2 \\ 1 & a_2 & j_2 \end{Bmatrix} \times \right. \\
& \quad \times \prod_{n=3}^{J-1} A(g''_n a_n) (-1)^{-j_n+g''_{n-1}+a_{n-1}+1} \begin{Bmatrix} j_n & g''_{n-1} & g''_n \\ 1 & a_n & a_{n-1} \end{Bmatrix} \times (-1)^{a_J} \begin{Bmatrix} a_J & j_J & g''_{J-1} \\ 1 & a_{J-1} & j_J \end{Bmatrix} \\
& \quad \left. + C(j_2 \ j_J) \prod_{k=2}^{J-1} \delta_{g''_k a_k} \right] \prod_{k=J}^N \delta_{g''_k a_k} \tag{3.1} \\
& \boxed{I > 2 \quad J = I + 1} \quad \left[\frac{1}{2}(-1)^{-2 \sum_{n=1}^{I-1} j_n} (-1)^{j_{I+1}-j_I} (-1)^{a_{I-1}+1} (-1)^{a_I-g''_I} X(j_I \ j_{I+1})^{\frac{1}{2}} A(g''_I \ a_I) \times \right. \\
& \quad \times \begin{Bmatrix} a_{I-1} & j_I & g''_I \\ 1 & a_I & j_I \end{Bmatrix} \times (-1)^{a_{I+1}} \begin{Bmatrix} a_{I+1} & j_{I+1} & g''_I \\ 1 & a_I & j_{I+1} \end{Bmatrix} \\
& \quad \left. + C(j_I \ j_{I+1}) \prod_{k=2}^I \delta_{g''_k a_k} \right] \prod_{l=2}^{I-1} \delta_{g''_l a_l} \prod_{k=I+1}^N \delta_{g''_k a_k} \\
& \boxed{I > 2 \quad J > I + 1} \quad \left[\frac{1}{2}(-1)^{-2 \sum_{n=1}^{I-1} j_n} (-1)^{-\sum_{n=I+1}^{J-1} j_n} (-1)^{j_J-j_I} (-1)^{a_{I-1}+1} (-1)^{a_I-g''_I} X(j_I \ j_J)^{\frac{1}{2}} A(g''_I \ a_I) \begin{Bmatrix} a_{I-1} & j_I & g''_I \\ 1 & a_I & j_I \end{Bmatrix} \times \right. \\
& \quad \times \prod_{n=I+1}^{J-1} A(g''_n a_n) (-1)^{g''_{n-1}+a_{n-1}+1} \begin{Bmatrix} j_n & g''_{n-1} & g''_n \\ 1 & a_n & a_{n-1} \end{Bmatrix} \times (-1)^{a_J} \begin{Bmatrix} a_J & j_J & g''_{J-1} \\ 1 & a_{J-1} & j_J \end{Bmatrix} \\
& \quad \left. + C(j_I \ j_J) \prod_{k=2}^{J-1} \delta_{g''_k a_k} \right] \prod_{l=2}^{I-1} \delta_{g''_l a_l} \prod_{k=J}^N \delta_{g''_k a_k}
\end{aligned}$$

Where we have used the shorthands

$$\begin{aligned}
C(a, b) &= a(a+1) + b(b+1) & X(a, b) &= 2a(2a+1)(2a+2)2b(2b+1)(2b+2) \\
A(a, b) &= \sqrt{(2a+1)(2b+1)}
\end{aligned} \tag{3.2}$$

The explicit expressions $F^{IJ}(\vec{a}(12), \vec{g}''(12))$ of (3.1) serve as the building blocks in order to calculate the matrix elements $\langle \vec{a}(12) \mid \hat{q}_{IJK} \mid \vec{a}'(12) \rangle$ given in (2.30). One can evaluate (2.30) as written down above by using the appropriate expressions from (3.1).

However there is still some simplification possible [24]. When looking at (3.1), obviously each expression comes as a sum of two terms. So multiplying two expressions $F^{IJ}(\cdot) \times F^{JK}(\cdot)$ as in the first term on the right hand side of (2.30) would result in four terms. We will now show that by symmetry all product terms containing a symmetric $C(\cdot)$ factor vanish, as we antisymmetrize with respect to the interchange $[\vec{a}(12) \rightleftharpoons \vec{a}'(12)]$. For every term containing $C(\cdot)$ we effectively get a prefactor of $\prod_{k=2}^N \delta_{g_k'' a_k}$ or $\prod_{k=2}^N \delta_{g_k'' a_k'}$ if we appropriately concatenate the products of δ -factors in (3.1). Therefore the product terms $C(j_I, j_J) \times C(j_J, j_K)$ are obviously symmetric under $[\vec{a}(12) \rightleftharpoons \vec{a}'(12)]$ and vanish under antisymmetrization.

Let us discuss the δ -factors in (3.1) in order to exclude mixed terms containing one $C(\cdot)$. We will present here only the discussion for products containing $C(j_J, j_K)$ in $F^{JK}(\vec{a}'(12), \vec{g}''(12))$. The discussion of $C(j_I, j_J)$ in $F^{IJ}(\vec{a}(12), \vec{g}''(12))$ is completely analogous.

For every term containing $C(j_J, j_K)$ we effectively get a prefactor of $\prod_{k=2}^N \delta_{g_k'' a_k'}$ if we concatenate the products of δ -factors. Therefore when considering a product of the form (2.30), with a non- $C(j_I, j_J)$ -term contributed by $F^{IJ}(\cdot)$ and a $C(j_J, j_K)$ -term coming from $F^{JK}(\cdot)$, every g_k'' in the $F^{IJ}(\cdot)$ -term can be replaced by a_k' . That is $\boxed{\vec{g}''(12) = \vec{a}'(12)}$. But then the mixed terms containing one $C(j_J, j_K)$ become symmetric wrt. $[\vec{a}(12) \rightleftharpoons \vec{a}'(12)]$ for the following reasons:

- $(-1)^{a_2 - a_2'} = (-1)^{a_2' - a_2}$ because $(a_2' - a_2) \in \mathbb{Z}$
- $A(a_k', a_k)$ is symmetric by construction
- all (but 2) $6j$ -symbols occurring in definition (3.1) for $F^{IJ}(\cdot)$ are of the form

$$\left\{ \begin{matrix} j_I & g_{n-1}'' & g_n'' \\ 1 & a_n & a_{n-1} \end{matrix} \right\} = \left\{ \begin{matrix} j_I & a_n & a_{n-1} \\ 1 & g_{n-1}'' & g_n'' \end{matrix} \right\}$$

by the symmetry properties¹⁰ of the $6j$ -symbols. But $\vec{g}''(12) = \vec{a}'(12)$.

- due to the $\prod_{k=2}^{I-1} \delta_{g_k'' a_k}$ $\prod_{n=J}^N \delta_{g_n'' a_n}$ in the non- $C(j_I, j_J)$ terms of $F^{IJ}(\cdot)$:

$$\text{the remaining } 6j\text{-symbols } \left\{ \begin{matrix} a_{I-1} & a_I & j_I \\ 1 & j_I & g_I'' \end{matrix} \right\} \text{ and } (-1)^{a_J} \left\{ \begin{matrix} a_J & j_J & g_{J-1}'' \\ 1 & a_{J-1} & j_J \end{matrix} \right\} \text{ are then symmetric}$$

wrt. $\vec{a}(12) \rightleftharpoons \vec{a}'(12)$, because $\vec{g}''(12) = \vec{a}'(12)$
and hence, $g_{J-1}'' = a_{J-1}'$, $a_{I-1} = g_{I-1}'' = a_{I-1}'$, $g_I'' = a_I'$, $a_J = g_J'' = a_J'$.

Thus when calculating (2.30) using (3.1) we are always left with the single product not containing a symmetric $C(j_I, j_J)$ or $C(j_J, j_K)$ -part. Note, however, that for cases containing $\boxed{I=1 \ J=2}$ in (3.1) we get a contribution.

Let us finally take a closer look at the δ -products in the remaining non-symmetric product terms of (2.30). In these products we have for $I < J < K$:

$$\left[\prod_{k=2}^{I-1} \delta_{g_k'' a_k} \prod_{l=J}^N \delta_{g_l'' a_l} \right] \left[\prod_{m=2}^{J-1} \delta_{g_m'' a_m'} \prod_{n=K}^N \delta_{g_n'' a_n'} \right] = \prod_{k=2}^{I-1} \delta_{a_k a_k'} \prod_{m=I}^{J-1} \delta_{g_m'' a_m'} \prod_{l=J}^{K-1} \delta_{g_l'' a_l} \prod_{n=K}^N \delta_{a_n a_n'} \quad (3.3)$$

We have thus to look at the symmetries between $I \dots K-1$ only. Here we find:

$$\begin{aligned} \text{For the first term in (2.30)} \quad & \vec{a}(12) \quad \vec{a}'(12) \quad \prod_{m=I}^{J-1} \delta_{g_m'' a_m'} \prod_{l=J}^{K-1} \delta_{g_l'' a_l} \\ \text{and the second term in (2.30)} \quad & \vec{a}'(12) \quad \vec{a}(12) \quad \prod_{m=I}^{J-1} \delta_{g_m'' a_m} \prod_{l=J}^{K-1} \delta_{g_l'' a_l'} \\ & (\vec{a}(12) \rightarrow \vec{a}'(12), \quad \vec{a}'(12) \rightarrow \vec{a}(12)) \end{aligned} \quad (3.4)$$

Using again symmetry properties of the $6j$ -symbols, and integer-arguments for the (-1) -exponents, together with (3.4), we can show, as in the case of symmetric terms, that almost all terms are symmetric with respect to the interchange $\vec{a}(12) \rightleftharpoons \vec{a}'(12)$.

So we are left with the discussion of the following terms: One easily sees that for a product $F^{IJ}(\cdot) \times F^{JK}(\cdot)$ (of two terms from (3.1) using the according arguments given in (2.30)) one has:

$$(-1)^{a_{I-1}} (-1)^{a_I - a_I'} (-1)^{a_J} \left\{ \begin{matrix} a_J & j_J & a_{J-1}' \\ 1 & a_{J-1} & j_J \end{matrix} \right\} \times (-1)^{a_{J-1}'} (-1)^{a_J' - a_J} \left\{ \begin{matrix} a_{J-1}' & a_J & j_J \\ 1 & j_J & a_J' \end{matrix} \right\} \quad (3.5)$$

¹⁰ $6j$ -symbols are invariant under the interchange of 2 columns and the simultaneous flip of two columns, see appendix C.3.

Here $a_{I-1} = a'_{I-1}$ by (3.4), $(a_I - a'_I) \in \mathbb{Z}$, and the a_J exponents cancel. Thus the remaining part of the product terms in (2.30) not symmetric wrt. the interchange $\vec{a}(12) \rightarrow \vec{a}'(12)$, $\vec{a}'(12) \rightarrow \vec{a}(12)$ is given by

$$(-1)^{a'_J} (-1)^{a'_{J-1}} \begin{Bmatrix} a_J & j_J & a'_{J-1} \\ 1 & a_{J-1} & j_J \end{Bmatrix} \begin{Bmatrix} a'_{J-1} & a_J & j_J \\ 1 & j_J & a'_J \end{Bmatrix} \quad (3.6)$$

We will give the explicit matrix element expressions (2.30) in the following section.

3.2 Explicit Matrix Element Expressions

The discussion above leads us to consider the following 14 special cases for the matrix element $\langle \vec{a}(12) | \hat{q}_{IJK} | \vec{a}'(12) \rangle$:

$$\begin{aligned} I = 1 \quad J = 2 \quad K = 3 \\ K > 3 \\ I = 1 \quad J = 3 \quad K = J + 1 \\ K > J + 1 \\ I = 1 \quad J > 3 \quad K = J + 1 \\ K > J + 1 \\ I = 2 \quad J = 3 \quad K = 4 \\ K > 4 \\ I = 2 \quad J > 3 \quad K = J + 1 \\ K > J + 1 \\ I > 2 \quad J = I + 1 \quad K = J + 1 \\ K > J + 1 \\ I > 2 \quad J > I + 1 \quad K = J + 1 \\ K > J + 1 \end{aligned} \quad (3.7)$$

Using combinations of the according cases (3.1) as written down in (2.30) one obtains,¹¹ using the shorthand $\mathbb{q}_{IJK} := \langle \vec{a}(12) | \hat{q}_{IJK} | \vec{a}'(12) \rangle$:

3.2.1 $I = 1 \quad J = 2 \quad K = 3$

$$\begin{aligned} \mathbb{q}_{123} = & \left[a_2(a_2 + 1) - a'_2(a'_2 + 1) \right] \frac{1}{2} (-1)^{-j_1 - j_2} (-1)^{j_3 + 1} (-1)^{a'_2 - a_2} (-1)^{a'_3} X(j_2 \ j_3)^{\frac{1}{2}} A(a'_2 \ a_2) \times \\ & \times \begin{Bmatrix} j_1 & j_2 & a_2 \\ 1 & a'_2 & j_2 \end{Bmatrix} \begin{Bmatrix} a'_3 & j_3 & a_2 \\ 1 & a'_2 & j_3 \end{Bmatrix} \times \prod_{n=3}^N \delta_{a'_n \ a_n} \end{aligned} \quad (3.8)$$

3.2.2 $I = 1 \quad J = 2 \quad K > 3$

$$\begin{aligned} \mathbb{q}_{12K} = & \left[a_2(a_2 + 1) - a'_2(a'_2 + 1) \right] \frac{1}{2} (-1)^{-j_1 - j_2} (-1)^{j_K + 1} (-1)^{a'_2 - a_2} X(j_2 \ j_K)^{\frac{1}{2}} A(a_2 \ a'_2) \times \begin{Bmatrix} j_1 & j_2 & a_2 \\ 1 & a'_2 & j_2 \end{Bmatrix} \\ & \times \prod_{n=3}^{K-1} A(a_n \ a'_n) (-1)^{-j_n + a_{n-1} + a'_{n-1} + 1} \begin{Bmatrix} j_n & a_{n-1} & a_n \\ 1 & a'_n & a'_{n-1} \end{Bmatrix} \times (-1)^{a'_K} \begin{Bmatrix} a'_K & j_K & a_{K-1} \\ 1 & a'_{K-1} & j_K \end{Bmatrix} \\ & \times \prod_{n=K}^N \delta_{a'_n \ a_n} \end{aligned} \quad (3.9)$$

¹¹For completeness all Kronecker- δ 's at the end of the following equations range from $K \dots N$, however if we consider gauge invariant states, besides $a'_N = a_N = J \stackrel{!}{=} 0$, we automatically have $a'_{N-1} = a_{N-1} \stackrel{!}{=} j_N$ in every case.

3.2.3 $I = 1 \quad J = 3 \quad K = J + 1$

$$\begin{aligned} \mathbb{Q}_{134} = & \left[\frac{1}{4} (-1)^{j_1+j_2} (-1)^{j_4} (-1)^{a'_4} X(j_1 \ j_3)^{\frac{1}{2}} X(j_3 \ j_4)^{\frac{1}{2}} A(a'_2 \ a_2) A(a'_3 \ a_3) \times \begin{Bmatrix} j_2 & j_1 & a'_2 \\ 1 & a_2 & j_1 \end{Bmatrix} \begin{Bmatrix} a'_4 & j_4 & a'_3 \\ 1 & a_3 & j_4 \end{Bmatrix} \right] \\ & \times \left[(-1)^{a'_2} (-1)^{a'_3} \begin{Bmatrix} a_3 & j_3 & a'_2 \\ 1 & a_2 & j_3 \end{Bmatrix} \begin{Bmatrix} a'_2 & j_3 & a_3 \\ 1 & a'_3 & j_3 \end{Bmatrix} - (-1)^{a_2} (-1)^{a_3} \begin{Bmatrix} a'_3 & j_3 & a_2 \\ 1 & a'_2 & j_3 \end{Bmatrix} \begin{Bmatrix} a_2 & j_3 & a'_3 \\ 1 & a_3 & j_3 \end{Bmatrix} \right] \\ & \times \prod_{n=4}^N \delta_{a'_n \ a_n} \end{aligned} \quad (3.10)$$

3.2.4 $I = 1 \quad J = 3 \quad K > J + 1$

$$\begin{aligned} \mathbb{Q}_{13K} = & \left[\frac{1}{4} (-1)^{j_1+j_2} (-1)^{-\sum_{n=4}^{K-1} j_n} (-1)^{j_K} (-1)^{a'_K} X(j_1 \ j_3)^{\frac{1}{2}} X(j_3 \ j_K)^{\frac{1}{2}} A(a'_2 \ a_2) A(a'_3 \ a_3) \right] \\ & \times \begin{Bmatrix} j_2 & j_1 & a'_2 \\ 1 & a_2 & j_1 \end{Bmatrix} \times \prod_{n=4}^{K-1} A(a_n \ a'_n) (-1)^{a_{n-1}+a'_{n-1}+1} \begin{Bmatrix} j_n & a_{n-1} & a_n \\ 1 & a'_n & a'_{n-1} \end{Bmatrix} \times \begin{Bmatrix} a'_K & j_K & a_{K-1} \\ 1 & a'_{K-1} & j_K \end{Bmatrix} \\ & \times \left[(-1)^{a'_2} (-1)^{a'_3} \begin{Bmatrix} a_3 & j_3 & a'_2 \\ 1 & a_2 & j_3 \end{Bmatrix} \begin{Bmatrix} a'_2 & j_3 & a_3 \\ 1 & a'_3 & j_3 \end{Bmatrix} - (-1)^{a_2} (-1)^{a_3} \begin{Bmatrix} a'_3 & j_3 & a_2 \\ 1 & a'_2 & j_3 \end{Bmatrix} \begin{Bmatrix} a_2 & j_3 & a'_3 \\ 1 & a_3 & j_3 \end{Bmatrix} \right] \\ & \times \prod_{n=K}^N \delta_{a'_n \ a_n} \end{aligned} \quad (3.11)$$

3.2.5 $I = 1 \quad J > 3 \quad K = J + 1$

$$\begin{aligned} \mathbb{Q}_{1JJ+1} = & \left[\frac{1}{4} (-1)^{\sum_{n=1}^{J-1} j_n} (-1)^{j_{J+1}} (-1)^{a'_{J+1}} X(j_1 \ j_J)^{\frac{1}{2}} X(j_J \ j_{J+1})^{\frac{1}{2}} A(a'_2 \ a_2) A(a_J \ a'_J) \right. \\ & \times \begin{Bmatrix} j_2 & j_1 & a'_2 \\ 1 & a_2 & j_1 \end{Bmatrix} \times \prod_{n=3}^{J-1} A(a'_n \ a_n) (-1)^{a'_{n-1}+a_{n-1}+1} \begin{Bmatrix} j_n & a'_{n-1} & a'_n \\ 1 & a_n & a_{n-1} \end{Bmatrix} \times \begin{Bmatrix} a'_{J+1} & j_{J+1} & a_J \\ 1 & a'_J & j_{J+1} \end{Bmatrix} \left. \right] \\ & \times \left[(-1)^{a'_{J-1}} (-1)^{a'_J} \begin{Bmatrix} a_J & j_J & a'_{J-1} \\ 1 & a_{J-1} & j_J \end{Bmatrix} \begin{Bmatrix} a'_{J-1} & j_J & a_J \\ 1 & a'_J & j_J \end{Bmatrix} - (-1)^{a_{J-1}} (-1)^{a_J} \begin{Bmatrix} a'_J & j_J & a_{J-1} \\ 1 & a'_{J-1} & j_J \end{Bmatrix} \begin{Bmatrix} a_{J-1} & j_J & a'_J \\ 1 & a_J & j_J \end{Bmatrix} \right] \\ & \times \prod_{n=J+1}^N \delta_{a'_n \ a_n} \end{aligned} \quad (3.12)$$

3.2.6 $I = 1 \quad J > 3 \quad K > J + 1$

$$\begin{aligned} \mathbb{Q}_{1JK} = & \left[\frac{1}{4} (-1)^{\sum_{n=1}^{J-1} j_n} (-1)^{-\sum_{n=J+1}^{K-1} j_n} (-1)^{j_K} (-1)^{a'_K} X(j_1 \ j_J)^{\frac{1}{2}} X(j_J \ j_K)^{\frac{1}{2}} A(a'_2 \ a_2) A(a_J \ a'_J) \right. \\ & \times \begin{Bmatrix} j_2 & j_1 & a'_2 \\ 1 & a_2 & j_1 \end{Bmatrix} \times \prod_{n=3}^{J-1} A(a'_n \ a_n) (-1)^{a'_{n-1}+a_{n-1}+1} \begin{Bmatrix} j_n & a'_{n-1} & a'_n \\ 1 & a_n & a_{n-1} \end{Bmatrix} \\ & \times \prod_{n=J+1}^{K-1} A(a'_n \ a_n) (-1)^{a'_{n-1}+a_{n-1}+1} \begin{Bmatrix} j_n & a'_{n-1} & a'_n \\ 1 & a_n & a_{n-1} \end{Bmatrix} \times \begin{Bmatrix} a'_K & j_K & a_{K-1} \\ 1 & a'_{K-1} & j_K \end{Bmatrix} \left. \right] \\ & \times \left[(-1)^{a'_{J-1}} (-1)^{a'_J} \begin{Bmatrix} a_J & j_J & a'_{J-1} \\ 1 & a_{J-1} & j_J \end{Bmatrix} \begin{Bmatrix} a'_{J-1} & j_J & a_J \\ 1 & a'_J & j_J \end{Bmatrix} - (-1)^{a_{J-1}} (-1)^{a_J} \begin{Bmatrix} a'_J & j_J & a_{J-1} \\ 1 & a'_{J-1} & j_J \end{Bmatrix} \begin{Bmatrix} a_{J-1} & j_J & a'_J \\ 1 & a_J & j_J \end{Bmatrix} \right] \\ & \times \prod_{n=K}^N \delta_{a'_n \ a_n} \end{aligned} \quad (3.13)$$

3.2.7 $I = 2 \quad J = 3 \quad K = 4$

$$\begin{aligned} \mathbb{Q}_{234} &= \left[\frac{1}{4} (-1)^{j_1+j_2+j_4} (-1)^{a'_4} X(j_2 \ j_3)^{\frac{1}{2}} X(j_3 \ j_4)^{\frac{1}{2}} A(a'_2 \ a_2) A(a_3 \ a'_3) \begin{Bmatrix} j_1 & j_2 & a'_2 \\ 1 & a_2 & j_2 \end{Bmatrix} \begin{Bmatrix} a'_4 & j_4 & a_3 \\ 1 & a'_3 & j_4 \end{Bmatrix} \right] \\ &\times \left[(-1)^{a_2} (-1)^{a'_3} \begin{Bmatrix} a_3 & j_3 & a'_2 \\ 1 & a_2 & j_3 \end{Bmatrix} \begin{Bmatrix} a'_2 & j_3 & a_3 \\ 1 & a'_3 & j_3 \end{Bmatrix} - (-1)^{a'_2} (-1)^{a_3} \begin{Bmatrix} a'_3 & j_3 & a'_2 \\ 1 & a_2 & j_3 \end{Bmatrix} \begin{Bmatrix} a_2 & j_3 & a_3 \\ 1 & a'_3 & j_3 \end{Bmatrix} \right] \\ &\times \prod_{n=4}^N \delta_{a'_n \ a_n} \end{aligned} \quad (3.14)$$

3.2.8 $I = 2 \quad J = 3 \quad K > 4$

$$\begin{aligned} \mathbb{Q}_{23K} &= \left[\frac{1}{4} (-1)^{j_1+j_2} (-1)^{-\sum_{n=4}^{K-1} j_n} (-1)^{j_K} (-1)^{a'_K} X(j_2 \ j_3)^{\frac{1}{2}} X(j_3 \ j_K)^{\frac{1}{2}} A(a'_2 \ a_2) A(a_3 \ a'_3) \right. \\ &\times \left. \begin{Bmatrix} j_1 & j_2 & a'_2 \\ 1 & a_2 & j_2 \end{Bmatrix} \times \prod_{n=4}^{K-1} A(a_n \ a'_n) (-1)^{a_{n-1}+a'_{n-1}+1} \begin{Bmatrix} j_n & a_{n-1} & a_n \\ 1 & a'_n & a'_{n-1} \end{Bmatrix} \times \begin{Bmatrix} a'_K & j_K & a_{K-1} \\ 1 & a'_{K-1} & j_K \end{Bmatrix} \right] \\ &\times \left[(-1)^{a_2} (-1)^{a'_3} \begin{Bmatrix} a_3 & j_3 & a'_2 \\ 1 & a_2 & j_3 \end{Bmatrix} \begin{Bmatrix} a'_2 & j_3 & a_3 \\ 1 & a'_3 & j_3 \end{Bmatrix} - (-1)^{a'_2} (-1)^{a_3} \begin{Bmatrix} a'_3 & j_3 & a'_2 \\ 1 & a_2 & j_3 \end{Bmatrix} \begin{Bmatrix} a_2 & j_3 & a_3 \\ 1 & a'_3 & j_3 \end{Bmatrix} \right] \\ &\times \prod_{n=K}^N \delta_{a'_n \ a_n} \end{aligned} \quad (3.15)$$

3.2.9 $I = 2 \quad J > 3 \quad K = J + 1$

$$\begin{aligned} \mathbb{Q}_{2JJ+1} &= \left[\frac{1}{4} (-1)^{\sum_{n=1}^{J-1} j_n} (-1)^{a_2-a'_2} (-1)^{j_{J+1}} (-1)^{a'_{J+1}} X(j_2 \ j_J)^{\frac{1}{2}} X(j_J \ j_{J+1})^{\frac{1}{2}} A(a'_2 \ a_2) A(a_J \ a'_J) \right. \\ &\times \left. \begin{Bmatrix} j_1 & j_2 & a'_2 \\ 1 & a_2 & j_2 \end{Bmatrix} \times \prod_{n=3}^{J-1} A(a_n \ a'_n) (-1)^{a_{n-1}+a'_{n-1}+1} \begin{Bmatrix} j_n & a_{n-1} & a_n \\ 1 & a'_n & a'_{n-1} \end{Bmatrix} \times \begin{Bmatrix} a'_{J+1} & j_{J+1} & a_J \\ 1 & a'_J & j_{J+1} \end{Bmatrix} \right] \\ &\times \left[(-1)^{a'_J} (-1)^{a'_{J-1}} \begin{Bmatrix} a_J & j_J & a'_{J-1} \\ 1 & a_{J-1} & j_J \end{Bmatrix} \begin{Bmatrix} a'_{J-1} & j_J & a_J \\ 1 & a'_J & j_J \end{Bmatrix} - (-1)^{a_J} (-1)^{a_{J-1}} \begin{Bmatrix} a'_J & j_J & a_{J-1} \\ 1 & a'_{J-1} & j_J \end{Bmatrix} \begin{Bmatrix} a_{J-1} & j_J & a'_J \\ 1 & a_J & j_J \end{Bmatrix} \right] \\ &\times \prod_{n=J+1}^N \delta_{a'_n \ a_n} \end{aligned} \quad (3.16)$$

3.2.10 $I = 2 \quad J > 3 \quad K > J + 1$

$$\begin{aligned} \mathbb{Q}_{2JK} &= \left[\frac{1}{4} (-1)^{\sum_{n=1}^{J-1} j_n} (-1)^{-\sum_{n=J+1}^{K-1} j_n} (-1)^{a_2-a'_2} (-1)^{j_K} (-1)^{a'_K} X(j_2 \ j_J)^{\frac{1}{2}} X(j_J \ j_K)^{\frac{1}{2}} A(a'_2 \ a_2) A(a_J \ a'_J) \right. \\ &\times \left. \begin{Bmatrix} j_1 & j_2 & a'_2 \\ 1 & a_2 & j_2 \end{Bmatrix} \times \prod_{n=3}^{J-1} A(a_n \ a'_n) (-1)^{a_{n-1}+a'_{n-1}+1} \begin{Bmatrix} j_n & a_{n-1} & a_n \\ 1 & a'_n & a'_{n-1} \end{Bmatrix} \right. \\ &\quad \times \left. \prod_{n=J+1}^{K-1} A(a_n \ a'_n) (-1)^{a_{n-1}+a'_{n-1}+1} \begin{Bmatrix} j_n & a_{n-1} & a_n \\ 1 & a'_n & a'_{n-1} \end{Bmatrix} \times \begin{Bmatrix} a'_K & j_K & a_{K-1} \\ 1 & a'_{K-1} & j_K \end{Bmatrix} \right] \\ &\times \left[(-1)^{a'_J} (-1)^{a'_{J-1}} \begin{Bmatrix} a_J & j_J & a'_{J-1} \\ 1 & a_{J-1} & j_J \end{Bmatrix} \begin{Bmatrix} a'_{J-1} & j_J & a_J \\ 1 & a'_J & j_J \end{Bmatrix} - (-1)^{a_J} (-1)^{a_{J-1}} \begin{Bmatrix} a'_J & j_J & a_{J-1} \\ 1 & a'_{J-1} & j_J \end{Bmatrix} \begin{Bmatrix} a_{J-1} & j_J & a'_J \\ 1 & a_J & j_J \end{Bmatrix} \right] \\ &\times \prod_{n=K}^N \delta_{a'_n \ a_n} \end{aligned} \quad (3.17)$$

3.2.11 $I > 2 \quad J = I + 1 \quad K = J + 1$

$$\begin{aligned}
\mathfrak{Q}_{II+1I+2} &= \left[\frac{1}{4} (-1)^{j_I+j_{I+2}} (-1)^{a_{I-1}} (-1)^{a'_{I+2}} X(j_I \ j_{I+1})^{\frac{1}{2}} X(j_{I+1} \ j_{I+2})^{\frac{1}{2}} A(a'_I \ a_I) A(a_{I+1} \ a'_{I+1}) \right. \\
&\times \left. \left\{ \begin{matrix} a_{I-1} & j_I & a'_I \\ 1 & a_I & j_I \end{matrix} \right\} \times \left\{ \begin{matrix} a'_{I+2} & j_{I+2} & a_{I+1} \\ 1 & a'_{I+1} & j_{I+2} \end{matrix} \right\} \right] \\
&\times \left[(-1)^{a_I} (-1)^{a'_{I+1}} \left\{ \begin{matrix} a_{I+1} & j_{I+1} & a'_I \\ 1 & a_I & j_{I+1} \end{matrix} \right\} \left\{ \begin{matrix} a'_I & j_{I+1} & a_{I+1} \\ 1 & a'_{I+1} & j_{I+1} \end{matrix} \right\} - (-1)^{a'_I} (-1)^{a_{I+1}} \left\{ \begin{matrix} a'_{I+1} & j_{I+1} & a_I \\ 1 & a'_I & j_{I+1} \end{matrix} \right\} \left\{ \begin{matrix} a_I & j_{I+1} & a_{I+1} \\ 1 & a'_{I+1} & j_{I+1} \end{matrix} \right\} \right] \\
&\times \prod_{n=2}^{I-1} \delta_{a'_n \ a_n} \prod_{n=I+2}^N \delta_{a'_n \ a_n}
\end{aligned} \tag{3.18}$$

3.2.12 $I > 2 \quad J = I + 1 \quad K > J + 1$

$$\begin{aligned}
\mathfrak{Q}_{II+1K} &= \left[\frac{1}{4} (-1)^{j_I} (-1)^{-\sum_{n=I+2}^{K-1} j_n} (-1)^{a_{I-1}} (-1)^{j_K} (-1)^{a'_K} X(j_I \ j_{I+1})^{\frac{1}{2}} X(j_{I+1} \ j_K)^{\frac{1}{2}} A(a'_I \ a_I) A(a_{I+1} \ a'_{I+1}) \right. \\
&\times \left. \left\{ \begin{matrix} a_{I-1} & j_I & a'_I \\ 1 & a_I & j_I \end{matrix} \right\} \times \prod_{n=I+2}^{K-1} A(a'_n \ a_n) (-1)^{a_{n-1}+a'_{n-1}+1} \left\{ \begin{matrix} j_n & a_{n-1} & a_n \\ 1 & a'_n & a'_{n-1} \end{matrix} \right\} \times \left\{ \begin{matrix} a'_K & j_K & a_{K-1} \\ 1 & a'_{K-1} & j_K \end{matrix} \right\} \right] \\
&\times \left[(-1)^{a_I} (-1)^{a'_{I+1}} \left\{ \begin{matrix} a_{I+1} & j_{I+1} & a'_I \\ 1 & a_I & j_{I+1} \end{matrix} \right\} \left\{ \begin{matrix} a'_I & j_{I+1} & a_{I+1} \\ 1 & a'_{I+1} & j_{I+1} \end{matrix} \right\} - (-1)^{a'_I} (-1)^{a_{I+1}} \left\{ \begin{matrix} a'_{I+1} & j_{I+1} & a_I \\ 1 & a'_I & j_{I+1} \end{matrix} \right\} \left\{ \begin{matrix} a_I & j_{I+1} & a_{I+1} \\ 1 & a'_{I+1} & j_{I+1} \end{matrix} \right\} \right] \\
&\times \prod_{n=2}^{I-1} \delta_{a'_n \ a_n} \prod_{n=K}^N \delta_{a'_n \ a_n}
\end{aligned} \tag{3.19}$$

3.2.13 $I > 2 \quad J > I + 1 \quad K = J + 1$

$$\begin{aligned}
\mathfrak{Q}_{IJJ+1} &= \left[\frac{1}{4} (-1)^{\sum_{n=I}^{J-1} j_n} (-1)^{a_{I-1}} (-1)^{a_I-a'_I} (-1)^{j_{J+1}} (-1)^{a'_{J+1}} X(j_I \ j_J)^{\frac{1}{2}} X(j_J \ j_{J+1})^{\frac{1}{2}} A(a'_I \ a_I) A(a_J \ a'_J) \right. \\
&\times \left. \left\{ \begin{matrix} a_{I-1} & j_I & a'_I \\ 1 & a_I & j_I \end{matrix} \right\} \times \prod_{n=I+1}^{J-1} A(a'_n \ a_n) (-1)^{a_{n-1}+a'_{n-1}+1} \left\{ \begin{matrix} j_n & a_{n-1} & a_n \\ 1 & a'_n & a'_{n-1} \end{matrix} \right\} \times \left\{ \begin{matrix} a'_{J+1} & j_{J+1} & a_J \\ 1 & a'_J & j_{J+1} \end{matrix} \right\} \right] \\
&\times \left[(-1)^{a'_{J-1}} (-1)^{a'_J} \left\{ \begin{matrix} a_J & j_J & a'_{J-1} \\ 1 & a_{J-1} & j_J \end{matrix} \right\} \left\{ \begin{matrix} a'_{J-1} & j_J & a_J \\ 1 & a'_J & j_J \end{matrix} \right\} - (-1)^{a_{J-1}} (-1)^{a_J} \left\{ \begin{matrix} a'_J & j_J & a_{J-1} \\ 1 & a'_{J-1} & j_J \end{matrix} \right\} \left\{ \begin{matrix} a_{J-1} & j_J & a'_J \\ 1 & a_J & j_J \end{matrix} \right\} \right] \\
&\times \prod_{n=2}^{I-1} \delta_{a'_n \ a_n} \prod_{n=J+1}^N \delta_{a'_n \ a_n}
\end{aligned} \tag{3.20}$$

3.2.14 $I > 2 \quad J > I + 1 \quad K > J + 1$

$$\begin{aligned}
\mathfrak{Q}_{IJK} &= \left[\frac{1}{4} (-1)^{\sum_{n=I}^{J-1} j_n} (-1)^{-\sum_{n=J+1}^{K-1} j_n} (-1)^{a_{I-1}} (-1)^{a_I-a'_I} (-1)^{j_K} (-1)^{a'_K} X(j_I \ j_J)^{\frac{1}{2}} X(j_J \ j_K)^{\frac{1}{2}} A(a'_I \ a_I) A(a_J \ a'_J) \right. \\
&\times \left. \left\{ \begin{matrix} a_{I-1} & j_I & a'_I \\ 1 & a_I & j_I \end{matrix} \right\} \times \prod_{n=I+1}^{J-1} A(a'_n \ a_n) (-1)^{a_{n-1}+a'_{n-1}+1} \left\{ \begin{matrix} j_n & a_{n-1} & a_n \\ 1 & a'_n & a'_{n-1} \end{matrix} \right\} \right. \\
&\quad \times \left. \prod_{n=J+1}^{K-1} A(a'_n \ a_n) (-1)^{a_{n-1}+a'_{n-1}+1} \left\{ \begin{matrix} j_n & a_{n-1} & a_n \\ 1 & a'_n & a'_{n-1} \end{matrix} \right\} \times \left\{ \begin{matrix} a'_K & j_K & a_{K-1} \\ 1 & a'_{K-1} & j_K \end{matrix} \right\} \right] \\
&\times \left[(-1)^{a'_{J-1}} (-1)^{a'_J} \left\{ \begin{matrix} a_J & j_J & a'_{J-1} \\ 1 & a_{J-1} & j_J \end{matrix} \right\} \left\{ \begin{matrix} a'_{J-1} & j_J & a_J \\ 1 & a'_J & j_J \end{matrix} \right\} - (-1)^{a_{J-1}} (-1)^{a_J} \left\{ \begin{matrix} a'_J & j_J & a_{J-1} \\ 1 & a'_{J-1} & j_J \end{matrix} \right\} \left\{ \begin{matrix} a_{J-1} & j_J & a'_J \\ 1 & a_J & j_J \end{matrix} \right\} \right] \\
&\times \prod_{n=2}^{I-1} \delta_{a'_n \ a_n} \prod_{n=K}^N \delta_{a'_n \ a_n}
\end{aligned} \tag{3.21}$$

3.3 The Arguments: Special $6j$ -Symbols

In all cases discussed, very special $6j$ -symbols occur: All of them contain a 1 as an argument. $6j$ -symbols of this kind possess short closed expressions and they restrict the arguments allowed (see [29]).

3.3.1 Different Cases and their Classification

The following four types of $6j$ -symbols occur in (3.8), ..., (3.21):

$$\begin{aligned}
I[b, c] &:= \left\{ \begin{array}{ccc} a & b & c \\ 1 & c-1 & b-1 \end{array} \right\} = (-1)^{a+b+c} \left[\frac{(a+b+c)(a+b+c+1)(-a+b+c-1)(-a+b+c)}{(2b-1)2b(2b+1)(2c-1)2c(2c+1)} \right]^{\frac{1}{2}} \\
II[b, c] &:= \left\{ \begin{array}{ccc} a & b & c \\ 1 & c-1 & b \end{array} \right\} = (-1)^{a+b+c} \left[\frac{2(a+b+c+1)(-a+b+c)(a-b+c)(a+b-c+1)}{2b(2b+1)(2b+2)(2c-1)2c(2c+1)} \right]^{\frac{1}{2}} \\
III[b, c] &:= \left\{ \begin{array}{ccc} a & b & c \\ 1 & c-1 & b+1 \end{array} \right\} = (-1)^{a+b+c} \left[\frac{(a-b+c-1)(a-b+c)(a+b-c+1)(a+b-c+2)}{(2b+1)(2b+2)(2b+3)(2c-1)2c(2c+1)} \right]^{\frac{1}{2}} \\
IV[b, c] &:= \left\{ \begin{array}{ccc} a & b & c \\ 1 & c & b \end{array} \right\} = (-1)^{a+b+c+1} \frac{2[b(b+1)+c(c+1)-a(a+1)]}{[2b(2b+1)(2b+2)2c(2c+1)(2c+2)]^{\frac{1}{2}}}
\end{aligned} \tag{3.22}$$

So we always have $6j$ -symbols of the general form

$$\left\{ \begin{array}{ccc} a & p & q \\ 1 & r & s \end{array} \right\} \tag{3.23}$$

This leads us to consider nine possible cases of argument combinations:

$\frac{p-s}{+1}$	$\frac{p=s+1}{p=s+1}$	$q=r+1$ (1)	$q=r$ (2)	$q=r-1$ (3)
0	$\frac{p=s}{p=s}$	(4)	(5)	(6)
-1	$\frac{p=s-1}{p=s-1}$	(7)	(8)	(9)

(3.24)

Using the symmetry properties (C.5), (C.6) of the $6j$ -symbols, these 9 combinations are covered by the 4 types of $6j$ -symbols contained in (3.22)(with the appropriate arguments in brackets):

$$\begin{aligned}
(1) \quad & \left\{ \begin{array}{ccc} a & p & q \\ 1 & q-1 & p-1 \end{array} \right\} & \longrightarrow I[b=p, c=q] \\
(2) \quad & \left\{ \begin{array}{ccc} a & p & q \\ 1 & q & p-1 \end{array} \right\} = \left\{ \begin{array}{ccc} a & q & p \\ 1 & p-1 & q \end{array} \right\} & \longrightarrow II[b=q, c=p] \\
(3) \quad & \left\{ \begin{array}{ccc} a & p & q \\ 1 & q+1 & p-1 \end{array} \right\} = \left\{ \begin{array}{ccc} a & q & p \\ 1 & p-1 & q+1 \end{array} \right\} & \longrightarrow III[b=q, c=p] \\
(4) \quad & \left\{ \begin{array}{ccc} a & p & q \\ 1 & q-1 & p \end{array} \right\} & \longrightarrow II[b=p, c=q] \\
(5) \quad & \left\{ \begin{array}{ccc} a & p & q \\ 1 & q & p \end{array} \right\} & \longrightarrow IV[b=p, c=q] \\
(6) \quad & \left\{ \begin{array}{ccc} a & p & q \\ 1 & q+1 & p \end{array} \right\} = \left\{ \begin{array}{ccc} a & q+1 & p \\ 1 & p & q \end{array} \right\} = \left\{ \begin{array}{ccc} a & p & q+1 \\ 1 & q & p \end{array} \right\} & \longrightarrow II[b=p, c=q+1] \\
(7) \quad & \left\{ \begin{array}{ccc} a & p & q \\ 1 & q-1 & p+1 \end{array} \right\} & \longrightarrow III[b=p, c=q] \\
(8) \quad & \left\{ \begin{array}{ccc} a & p & q \\ 1 & q & p+1 \end{array} \right\} = \left\{ \begin{array}{ccc} a & q & p+1 \\ 1 & p & q \end{array} \right\} & \longrightarrow II[b=q, c=p+1] \\
(9) \quad & \left\{ \begin{array}{ccc} a & p & q \\ 1 & q+1 & p+1 \end{array} \right\} = \left\{ \begin{array}{ccc} a & q+1 & p+1 \\ 1 & p & q \end{array} \right\} & \longrightarrow I[b=q+1, c=p+1]
\end{aligned} \tag{3.25}$$

3.3.2 Inequalities to be Fulfilled for the Arguments of I, II, III, IV

Following the general definition (C.1) of the $6j$ -symbols certain inequalities for their arguments must hold. Due to the special form of the arguments these 12 inequalities reduce to a set of 5 inequalities for each case:

$$\begin{aligned}
I[b, c] &= \left\{ \begin{array}{ccc} a & b & c \\ 1 & c-1 & b-1 \end{array} \right\} & \Delta(a, b, c) : & \begin{array}{l} a+b-c \geq 0 \\ a-b+c \geq 0 \end{array} \\
& & \Delta(a, c-1, b-1) : & -a+c+b \geq 2 \\
& & \Delta(1, b, b-1) : & b \geq 1 \\
& & \Delta(1, c-1, c) : & c \geq 1 \\
\\
II[b, c] &= \left\{ \begin{array}{ccc} a & b & c \\ 1 & c-1 & b \end{array} \right\} & \Delta(a, b, c) : & a+b-c \geq 0 \\
& & \Delta(a, c-1, b) : & \begin{array}{l} a-b+c \geq 1 \\ -a+b+c \geq 1 \end{array} \\
& & \Delta(1, b, b) : & b \geq \frac{1}{2} \\
& & \Delta(1, c-1, c) : & c \geq 1 \\
\\
III[b, c] &= \left\{ \begin{array}{ccc} a & b & c \\ 1 & c-1 & b+1 \end{array} \right\} & \Delta(a, b, c) : & \begin{array}{l} a+b-c \geq 0 \\ -a+b+c \geq 0 \end{array} \\
& & \Delta(a, c-1, b+1) : & a-b+c \geq 2 \\
& & \Delta(1, b, b+1) : & b \geq 0 \\
& & \Delta(1, c-1, c) : & c \geq 1 \\
\\
IV[b, c] &= \left\{ \begin{array}{ccc} a & b & c \\ 1 & c & b \end{array} \right\} & \Delta(a, b, c) : & \begin{array}{l} a+b-c \geq 0 \\ a-b+c \geq 0 \\ -a+b+c \geq 0 \end{array} \\
& & \Delta(a, c, b) : & -- \\
& & \Delta(1, b, b) : & b \geq \frac{1}{4} \\
& & \Delta(1, c, c) : & c \geq \frac{1}{2}
\end{aligned}$$

Moreover we have an integer condition, namely in each case $\boxed{a+b+c \in \mathbb{N}}$ must be fulfilled. All other $6j$ -symbols containing a 1 but different argument ranges as given above or not fulfilling the integer condition vanish identically.

4 Mathematical Preparations for Implementation on a Computer

Here we address the remaining mathematical issues necessary for numerical computation of the volume spectrum. Recall from (2.25) that we have to calculate the spectra of totally antisymmetric real matrices of the form:

$$Q := \sum_{I < J < K \leq N} \epsilon(IJK) \hat{q}_{IJK} \quad (4.1)$$

where again $\epsilon(IJK) = \text{sgn}(\det(\dot{e}_I(v), \dot{e}_J(v), \dot{e}_K(v)))$ denotes the sign of the determinant of the tangents of the three edges e_I, e_J, e_K intersecting at the vertex v . The actual computation is twofold: firstly we have to compute the recoupling scheme basis in order to apply the matrix element expressions of section 3.2 for the computation of the constituent matrices \hat{q}_{IJK} . Secondly the possible sign factors $\epsilon(IJK)$ have to be computed.

4.1 Recoupling Scheme Basis

Let us first describe the computation of the recoupling basis. As it turns out, the number of gauge invariant recoupling schemes contained in all possible recouplings of a set of spins can be surprisingly small. To our knowledge an exact result for this number is known only for the special case where all spins equal $j = \frac{1}{2}$ [21].

By definition B.2 in the appendix a standard recoupling scheme is the successive recoupling of all N angular momenta j_1, \dots, j_N at the vertex v : Fix a labelling of the edges. Then recouple j_1, j_2 to a resulting angular momentum $a_2(j_1 j_2)$. We have due to the Clebsch-Gordan-Theorem $|j_1 - j_2| \leq a_2(j_1 j_2) \leq j_1 + j_2$. Now couple a_2, j_3 to a resulting angular momentum $a_3(a_2 j_3)$ where again $|a_2 - j_3| \leq a_3(a_2 j_3) \leq a_2 + j_3$. This continues until we arrive at the last recoupling step where $J \stackrel{!}{=} a_N(a_{N-1} j_N)$ and thus $|a_{N-1} - j_N| \leq J \leq a_{N-1} + j_N$. If we work with gauge invariant recoupling schemes we have $J = 0$ and therefore must have $j_N \stackrel{!}{=} a_{N-1}$.

The challenge is now to find, for a given spin configuration j_1, \dots, j_N , all possible gauge invariant states, that is all recoupling sequences as illustrated below for which

$$a_k^{(min)} := |a_{k-1} - j_k| \leq a_k(a_{k-1} j_k) \leq (a_{k-1} + j_k) =: a_k^{(max)} \quad (2 \leq k \leq N-1) \quad (4.2)$$

(with $a_1 = j_1$) and additionally $a_{N-1} \stackrel{!}{=} j_N$. Let us moreover define the dimension for each intermediate recoupling step as

$$\dim(a_k) := a_k^{(max)} - a_k^{(min)} + 1 \quad (4.3)$$

This expression has to be understood iteratively, since for the k^{th} recoupling step the $(k-1)^{\text{th}}$ step provides one initial spin as illustrated in figure 2.

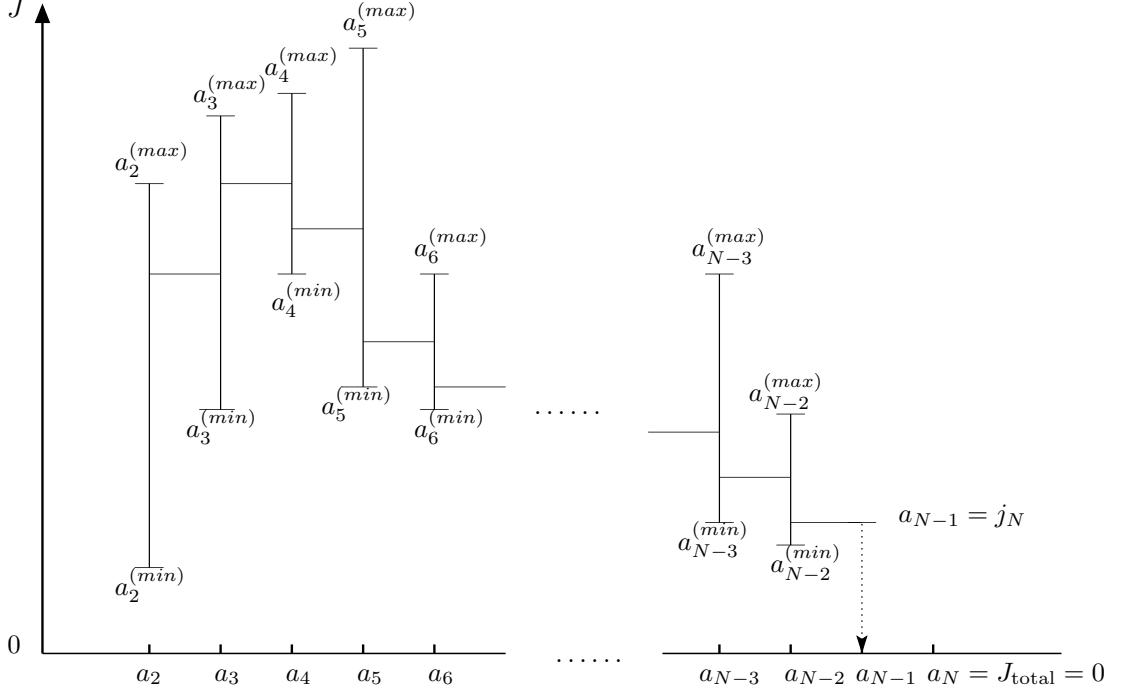


Figure 2: Schematic depiction of the recoupling computation described in section 4.1. The figure is meant to be read from left to right. Each vertical line represents the range of possible values for the recoupled angular momentum a_i . The horizontal lines show a particular choice for each recoupling, which subsequently affects the range of possible values for the next recoupling a_{i+1} . At the rightmost edge of the diagram we see that, to enforce gauge invariance, we restrict $a_N \stackrel{!}{=} J = 0$. This in turn requires that $a_{N-1} \stackrel{!}{=} j_N$.

4.1.1 Estimate for the Number of Eigenvalues

Throughout our analysis, when referring to numbers of eigenvalues, we of course take into account their degeneracies. Thus counting eigenvalues is equivalent to adding the numbers of recoupling states for each of the vertex states.

As described in the previous section the construction of a recoupling state $|a_2(j_1 j_2) \dots a_{N-1}(a_{N-2} j_{N-1}) J(a_{N-1} j_N) M \rangle$ is a successive process in which the possibilities at the k^{th} step are given by the inequality (4.2). Moreover due to (2.39) in section 2.5 we may assume $j_1 \leq j_2 \leq \dots \leq j_N \leq j_{max}$. We can iteratively estimate $\dim(a_k)$ as

$$\dim(a_2) \leq 2j_N + 1 \quad \rightsquigarrow \quad \dim(a_3) \leq 3j_N + 1 \quad \rightsquigarrow \quad \dots \quad \rightsquigarrow \quad \dim(a_{N-2}) \leq (N-2)j_N + 1 \quad (4.4)$$

Note that due to gauge invariance $\dim(a_{N-1}) = \dim(a_N = J) = 1$. So the dimension of the gauge invariant subspace contained in the $[\prod_{k=1}^N (2j_k + 1)]$ -dimensional tensor space is bounded from above by

$$\dim \left(|a_2(j_1 j_2) \dots J(a_{N-1} j_N) = 0 M \rangle \right) \leq \prod_{l=2}^{N-2} [l \cdot j_N + 1] \leq \prod_{l=2}^{N-2} [l \cdot j_N + l] = [j_N + 1]^{N-3} \cdot (N-2)! \quad (4.5)$$

which is at the same time a bound for the maximum number of eigenvalues contributed by a fixed spin configuration. The number of spin configurations $j_1 \leq j_2 \leq \dots \leq j_N$ can be calculated as follows: Assume an N -dimensional orthonormal lattice with cubes of edge length 1 as elementary cells. Choose a lattice origin, and associate each j_k

($k = 1 \dots N$) with a direction of the cube at the origin. If we exclude $j_k = 0$ then we can get the number of spin configurations $N_{j\text{-configs}}$ for a particular j_N by counting the number of lattice points as:

$$N_{j\text{-configs}} = \sum_{b_{N-1}=1}^{b_N} \sum_{b_{N-2}=1}^{b_{N-1}} \dots \sum_{b_2=1}^{b_3} b_2 = \frac{1}{(N-1)!} b_N (b_N + 1) \cdot \dots \cdot (b_N + N - 2) = \binom{b_N + N - 2}{N - 1} \quad (4.6)$$

where we have defined $b_k := 2j_k$ and used that $\sum_{k=1}^L k = \frac{1}{2}L(L+1)$. Thus we can estimate the number $N_{\text{evals}}|_{j_N}$ of eigenvalues contributed by spin configurations $j_1 \leq j_2 \leq \dots \leq j_N$ with fixed j_N :

$$\begin{aligned} N_{\text{evals}}|_{j_N} &\leq [j_N + 1]^{N-3} \cdot (N-2)! \cdot \binom{b_N + N - 2}{N - 1} = \\ &= \frac{1}{N-1} \left\{ [2j_N]^{N-1} + [2j_N]^{N-2} (1 + \dots + N-2) + \mathcal{O} \left[[j_N]^{N-3} \right] \right\} \left\{ [j_N]^{N-3} + (N-3)[j_N]^{N-4} + \mathcal{O} \left[[j_N]^{N-5} \right] \right\} \\ &= \frac{1}{N-1} \left\{ 2^{N-1} [j_N]^{2N-4} + \left(2^{N-1} (N-3) + 2^{N-3} (N-1)(N-2) \right) [j_N]^{2N-5} + \mathcal{O} \left[[j_N]^{2N-6} \right] \right\} \end{aligned} \quad (4.7)$$

Here we have computed the coefficients of the two highest orders in j_N . We thus expect that the number of eigenvalues resulting from spin configurations $j_1 \leq j_2 \leq \dots \leq j_N$, j_N fixed may be given by a polynomial in j_N of degree $2N - 4$. This result will be used in order to give a polynomial fit to the number of eigenvalues obtained in the eigenvalue computations of section 6.

4.2 Sign Factor Combinatorics

Beside the recoupling part in the definition (2.25), the sign factors $\epsilon(IJK)$ provide sensitivity of the volume operator to the diffeomorphism invariant structure of the edge embeddings at a particular vertex. The following discussion summarizes this up to now not fully understood problem and sketches the starting point for a detailed analysis. We find that there is a fascinating interplay between gauge invariance and the spatial embedding of a given graph, showing a possible link between edge spins and the (spatial) diffeomorphism invariant information encoded in the edge structure of a graph.

4.2.1 Gauge Invariance at the Operator Level

At the operator level gauge invariance

$$(J_{(tot)})^2 := \sum_{k=1}^3 \left(\sum_{K=1}^N J_K^k \right)^2 = 0 \quad (4.8)$$

implies that

$$J_N^k \stackrel{!}{=} - \sum_{L=1}^{N-1} J_L^k \quad \forall k = 1, 2, 3 \quad (4.9)$$

This can be used in (2.25) in order to eliminate all \hat{q}_{IJN} containing N as an edge labels as follows: Because $\hat{q}_{IJK} = \text{const} \cdot \epsilon_{ijk} J_I^i J_J^j J_K^k$ we have

$$\begin{aligned} Q &= \text{const} \cdot \sum_{I < J < K \leq N} \epsilon(IJK) \epsilon_{ijk} J_I^i J_J^j J_K^k \\ &= \text{const} \cdot \left[\sum_{I < J < K < N} \epsilon(IJK) \epsilon_{ijk} J_I^i J_J^j J_K^k + \sum_{I < J < (K=N)} \epsilon(IJN) \epsilon_{ijk} J_I^i J_J^j J_N^k \right] \end{aligned} \quad (4.10)$$

Using (4.9) we can rewrite the second sum term on the right hand side of (4.10) as

$$\begin{aligned}
& \sum_{I < J < (K=N)} \epsilon(IJN) \epsilon_{ijk} J_I^i J_J^j J_N^k = - \sum_{I < J < N} \sum_{L=1}^{N-1} \epsilon(IJN) \epsilon_{ijk} J_I^i J_J^j J_L^k = \\
& = - \sum_{I < J < N} \left[\sum_{L=1}^I \epsilon(IJN) \epsilon_{ijk} J_I^i J_J^j J_L^k + \sum_{L=I+1}^J \epsilon(IJN) \epsilon_{ijk} J_I^i J_J^j J_L^k + \sum_{L=J+1}^{N-1} \epsilon(IJN) \epsilon_{ijk} J_I^i J_J^j J_L^k \right] \\
& \quad \boxed{\text{Configurations with 2 identical edge labels } L = I \text{ or } L = J \text{ will not contribute} \\
& \quad \text{to the sum due to the antisymmetry of } \epsilon_{ijk}} \\
& = - \left[\sum_{L < I < J < N} \epsilon(IJN) \epsilon_{ijk} J_I^i J_J^j J_L^k + \sum_{I < L < J < N} \epsilon(IJN) \epsilon_{ijk} J_I^i J_J^j J_L^k + \sum_{I < J < L < N} \epsilon(IJN) \epsilon_{ijk} J_I^i J_J^j J_L^k \right] \\
& \quad \boxed{[J_I^i, J_L^k] = 0 \text{ for } I \neq L.} \\
& = - \left[\sum_{L < I < J < N} \epsilon(IJN) \epsilon_{ijk} J_L^k J_I^i J_J^j + \sum_{I < L < J < N} \epsilon(IJN) \epsilon_{ijk} J_I^i J_L^k J_J^j + \sum_{I < J < L < N} \epsilon(IJN) \epsilon_{ijk} J_I^i J_J^j J_L^k \right] \\
& = - \left[\sum_{L < I < J < N} \epsilon(IJN) \epsilon_{kij} J_L^k J_I^i J_J^j - \sum_{I < L < J < N} \epsilon(IJN) \epsilon_{ikj} J_I^i J_L^k J_J^j + \sum_{I < J < L < N} \epsilon(IJN) \epsilon_{ijk} J_I^i J_J^j J_L^k \right] \quad (4.11)
\end{aligned}$$

Upon introducing a suitable relabelling of the sum variables in (4.11), taking each sum term into the form of the first line in (4.10), we conclude that the volume operator, if acting on a gauge invariant spin network function, can be rewritten as

$$\begin{aligned}
\hat{V} & := \sqrt{\left| Z \cdot \sum_{I < J < K < N} [\epsilon(IJK) - \epsilon(JKN) + \epsilon(IKN) - \epsilon(IJN)] \hat{q}_{IJK} \right|} \\
\hat{V} & := \sqrt{\left| Z \cdot \sum_{I < J < K < N} \sigma(IJK) \hat{q}_{IJK} \right|} \quad \text{with } \sigma(IJK) := \epsilon(IJK) - \epsilon(IJN) + \epsilon(IKN) - \epsilon(JKN) \quad (4.12)
\end{aligned}$$

which is the final expression for the volume operator acting on gauge invariant recoupling states. We would like to mention here that (4.12) can be interpreted as a kind of ‘self-regulating’ property of the volume operator when applied to certain ‘pathological’ edge configurations, as illustrated in the following paragraphs.

Consider the following explicit construction of a configuration of N edges outgoing from a vertex v , where each ordered edge triple e_I, e_J, e_K , $I < J < K$ contributes with a negative sign factor $\epsilon(I, J, K)$. Since we are only interested in the sign factor we can make simplifying assumptions, in particular we may arbitrarily choose certain numerical values. Consider the vertex v as the origin of a 3 dimensional coordinate system with axes x, y, z . Now consider a circle with radius $r = 1$ centered at $y = 1$, parallel to the x - z plane. Let every edge tangent vector \dot{e}_K end at a point on the circle with coordinates $(\cos \phi_K, 1, \sin \phi_K)$ and $\phi_K = 2\pi \frac{K}{N}$. Now one may check that for each ordered triple e_I, e_J, e_K with $I < J < K \leq N$ we have:

$$\det(\dot{e}_I, \dot{e}_J, \dot{e}_K) = -4 \cdot \sin \left[\pi \frac{K-I}{N} \right] \sin \left[\pi \frac{K-J}{N} \right] \sin \left[\pi \frac{J-I}{N} \right] \quad (4.13)$$

Since for all arguments x of the sine functions we have $0 < x \leq \pi$, all of these functions are ≥ 0 and therefore we get $\epsilon(I, J, K) = \text{sgn}(\det(\dot{e}_I, \dot{e}_J, \dot{e}_K)) = -1$ for all ordered edge triples e_I, e_J, e_K , $I < J < K$ at v .

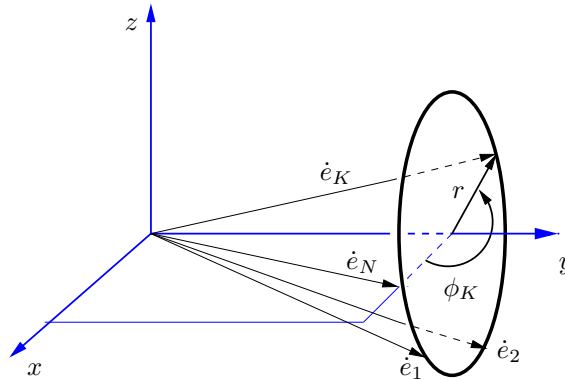


Figure 3: ‘Pathological’ edge configuration

As one can see, this edge configuration is quite special — it is as if all edges lie in one octant only (if we rotate the coordinate system) or on one 2 dimensional surface as the hull of a cone. Such an edge configuration would appear 1

or 2, rather than 3 dimensional. However, upon imposing gauge invariance, we conclude from (4.12) that such an edge configuration would effectively contribute zero volume, *coming from only the orientation of the edges and independent of the spin configuration*¹².

In [11],[12] an upper bound for the coherent state expectation value of the operator corresponding to the inverse scale factor in a Friedmann-Robertson-Walker universe was derived. This upper bound provided boundedness of the expectation value, independently of whether the coherent states are peaked on classically singular data. However, the authors were unable to exclude the growing of the expectation value as the valence of the vertex on which it is evaluated is increased. They supposed this to be an effect of a too rough estimate, assuming all $\epsilon(IJK)$ factors to be identical 1 or -1. However by the explicit construction of the edge configuration shown in figure 3, one can see that there indeed exist graphs leading to an unbounded coherent state expectation value of the inverse scale factor operator. This problem is now cured upon imposing gauge invariance via (4.12), which is why we refer to this issue as a ‘self-regulating’ property of the volume operator.

A similar problem arises with respect to a state as presented in figure 3: in principle we can produce volume eigenvalues which increase with the number of edge triples at a vertex. See the discussion in section 6 of [25].

4.2.2 Numerical Computation of Sign-Factor Configurations $\vec{\epsilon}$ Using a Monte Carlo Process

Consider an N -valent vertex v . For each of the $\binom{N}{3}$ triples of edges $1 \leq I < J < K \leq N$ we have a sign factor $\epsilon(IJK)$. Hereafter we refer to an assignment of the $\binom{N}{3}$ such sign factors at a vertex as a *sign configuration* $\vec{\epsilon} := \{\epsilon(IJK)\}_{I < J < K \leq N} = (\epsilon(123), \epsilon(124), \dots, \epsilon(12N), \epsilon(134), \dots, \epsilon(13N), \dots, \epsilon(N-2, N-1, N))$. The remaining question in the definition (2.25) is what sign configurations can be realized in the tangent space at the N -vertex¹³ $v \in \Sigma$ at all. This turns out to be a highly nontrivial problem.

Our first attempt to solve this problem is via a Monte Carlo simulation. We note that the set of directions of tangent vectors to the embedded edges at a vertex is equivalent to the set of points of a unit 2-sphere. Thus the embedding of an N -valent vertex is equivalent to an N -tuple of points on the sphere. We can explore the collection of such realizable embeddings by randomly selecting sets of N points on the sphere, via a Poisson process (by which we mean simply that the points are ‘sprinkled’ at unit density with respect to the area element on the sphere). For each such ‘sprinkling’ of the N points, we can compute the sign factors $\epsilon(IJK)$, for each of the $\binom{N}{3}$ triples $1 \leq I < J < K \leq N$. The particular algorithm we employ is to sprinkle N points, compute the resulting sign configuration, and then store in a database (hash table) the number of times $n_{\vec{\epsilon}}$ this sign configuration has arisen so far. We continue this process until the smallest such $n_{\vec{\epsilon}}$ exceeds a fixed threshold. (In practice this threshold can be set at 1, because the number of sign configurations is enormous.)

One should note that the numbers $n_{\vec{\epsilon}}$ computed by the above algorithm have no intrinsic meaning in and of themselves, since we might do a coordinate transformation on the unit sphere, which changes the probability measure used during the sprinkling process. Moreover this method is unable to give sign configurations $\vec{\epsilon}$ containing coplanar triples (IJK) with $\epsilon(IJK) = 0$, because they form a set of measure zero with respect to area on the 2-sphere. This is the technical reason why the present work will not consider these coplanar sign configurations, and is restricted to $\epsilon(IJK) = \pm 1$.

Nevertheless, using this method we can compute all the sign configurations $\vec{\epsilon}$ containing only linearly independent triples, as demonstrated in section 4.2.3 below. Using (4.12) it is then straightforward to compute the effective signs $\sigma(IJK) = 0, \pm 2, \pm 4$ resulting from gauge invariance and the restriction $\epsilon(IJK) = \pm 1$:

The following table details our results:

valence N of v	number of triples: $\binom{N}{3}$	maximal number of theoretically possible $\vec{\epsilon}$ -sign configs $T_{max} = 2^{\binom{N}{3}}$	number of re- alized $\vec{\epsilon}$ -sign configs T_R	fraction $\frac{T_R}{T_{max}}$	total number of realized $\vec{\sigma}$ -configs	multiplicity $\chi_{\vec{\sigma}=\vec{0}}$ of $\vec{\sigma} = \vec{0}$ -config
4	4	16	16	1	5	6
5	10	1024	384	0.375	171	24
6	20	2^{20}	23,808	0.023	16,413	120
7	35	2^{35}	3,486,720	$1.015 \cdot 10^{-5}$	3,079,875	720

Table 1: Possible sign factor combinations a vertices of valence 4-7.

In the next to last column we have listed the number of realizable $\vec{\sigma}$ -configurations, which is the number of assignments of $\sigma(IJK) = \pm 4, \pm 2$, or 0 to edge triples e_I, e_J, e_K with edge labels $1 \leq I < J < K \leq N$ according

¹²The spin configuration must allow for gauge invariance at v of course.

¹³Recall that Σ denotes the 3-dimensional spatial foliation hypersurfaces used in the (3+1)-formulation of General Relativity; see the companion paper [25] for details.

to (4.12). They are defined as $\vec{\sigma} := \{\sigma(IJK)\}_{I < J < K < N} = (\sigma(123), \sigma(124), \dots, \sigma(12N-1), \sigma(134), \dots, \sigma(13N-1), \dots, \sigma(N-3, N-2, N-1))$.

Note that there is a unique map $\mathcal{S} : \vec{\epsilon} \mapsto \vec{\sigma}$ where $\vec{\sigma} := \{\sigma(IJK)\}_{\substack{e_I, e_J, e_K \in E(v) \\ I < J < K}}$. However \mathcal{S} is not invertible, in particular it will happen that for different $\vec{\epsilon}, \vec{\epsilon}'$ -configurations we have $\mathcal{S}(\vec{\epsilon}) = \mathcal{S}(\vec{\epsilon}') = \vec{\sigma}$. We denote the number of $\vec{\epsilon}$ -configurations giving the same $\vec{\sigma}$ -configuration by $\chi_{\vec{\sigma}}$ and call $\chi_{\vec{\sigma}}$ the redundancy of $\vec{\sigma}$.

In the last column we have written down the number $\chi_{\vec{\sigma}=\vec{0}}$ of distinct sign configurations $\vec{\epsilon}$ which lead to a $\vec{\sigma}$ -configuration for which $\sigma(IJK) = 0 \quad \forall I < J < K < N$. Note that this number seems to be given by $(N-1)!$.

4.2.3 Analytical Computation of the Sign Configurations $\vec{\epsilon}$

The results from the previous section are somewhat unsatisfactory, in that one may be concerned that the Monte Carlo process does not reveal every realizable sign configuration. For example how do we know that we do not terminate the sprinklings too early? Additionally, the Monte Carlo technique will never find linearly dependent triples of tangent vectors. Therefore it is highly desirable to have an analytic proposal at hand in order to compute the number of sign configurations directly, without using Monte Carlo methods. Here we present such a proposal, which will be worked out in more detail in a forthcoming paper [26].

In what follows we are going to derive a set of inequalities that must be fulfilled by a sign configuration in order for it to correspond to a realizable configuration of tangent vectors, meaning it must be embeddable in 3-dimensional Riemannian space. By its definition we have $\epsilon[IJK] = \text{sgn}(\det(\dot{e}_I(v), \dot{e}_J(v), \dot{e}_K(v)))$ and for the tangent vectors $\dot{e}_I(v)$

we introduce the shorthands $\dot{e}_I(v) =: \vec{v}_I = \begin{pmatrix} v_I^1 \\ v_I^2 \\ v_I^3 \end{pmatrix}$, which are vectors in the tangent space to v . Then the determinants $\det(\dot{e}_I(v), \dot{e}_J(v), \dot{e}_K(v))$ can be expressed as

$$\det(\dot{e}_I(v), \dot{e}_J(v), \dot{e}_K(v)) =: \epsilon[IJK] \cdot Q[IJK] = \sum_{i \ j \ k} \epsilon_{ijk} v_I^i v_J^j v_K^k \quad (4.14)$$

where $Q[IJK] := |\det(\dot{e}_I(v), \dot{e}_J(v), \dot{e}_K(v))| \geq 0$ by construction. For an N -valent vertex v we have $\binom{N}{3} = \frac{1}{6}N(N-1)(N-2)$ ordered triples with according sign factors.

Let us for simplicity assume linear independence of all tangent vectors at the vertex v , that is $Q[IJK] \neq 0 \quad \forall I < J < K \leq N$ in what follows, which implies that $\epsilon[IJK] \neq 0$ and $\epsilon[IJK] = \pm 1$ for all ordered triples IJK . This ignores of course a certain class of configurations, however the calculation presented here can be extended to the linearly dependent case in an obvious way, c.f. section 4.2.5.

Without loss of generality we may then introduce a basis in the tangent space of v given by the first three tangent vectors $\vec{v}_1, \vec{v}_2, \vec{v}_3$ as

$$\vec{v}_1 = \begin{pmatrix} 1 \\ 0 \\ 0 \end{pmatrix} \quad \vec{v}_2 = \begin{pmatrix} 0 \\ 1 \\ 0 \end{pmatrix} \quad \vec{v}_3 = \begin{pmatrix} 0 \\ 0 \\ 1 \end{pmatrix} \quad (4.15)$$

Note that (4.15) implies that $\epsilon[123] = 1$. This is a restriction since it fixes a positive orientation of this triple. However we will express all the other vectors with respect to that choice. Configurations in which $\vec{v}_1, \vec{v}_2, \vec{v}_3$ have negative orientation $\epsilon[123] = -1$ will give a global minus sign to all $\epsilon[IJK]$. We will work with the choice $\epsilon[123] = 1$ in what follows but we keep in mind that for every sign configuration we are going to discuss with respect to $\epsilon[123] = 1$, there exists a corresponding second one with inverted signs and $\epsilon[123] = -1$. It will be sufficient to discuss only the $\epsilon[123] = 1$ case, apply the found selection rules for realizable sign configurations, and multiply the obtained number of realizable configurations by 2. The second restriction $Q[123] = 1$ implied by the choice (4.15) is just the normalization of the coordinate volume to 1. This only gives a positive global numerical factor which does not affect the signs $\epsilon[IJK]$.

Employing all these conventions we can cast (4.14) in the following form:

$$\begin{aligned}
& \epsilon[123] Q[123] = 1 \quad \rightsquigarrow \text{global factor 2} \\
(I) \quad & \epsilon[12I] Q[12I] = v_I^3 \quad \boxed{3 < I \leq N} \\
(II) \quad & \epsilon[13I] Q[13I] = -v_I^2 \quad \boxed{3 < I \leq N} \\
(III) \quad & \epsilon[23I] Q[23I] = v_I^1 \quad \boxed{3 < I \leq N} \\
(1) \quad & \epsilon[1IJ] Q[1IJ] = -v_I^3 v_J^2 + v_I^2 v_J^3 \quad \boxed{3 < I < J \leq N} \\
(2) \quad & \epsilon[2IJ] Q[2IJ] = v_I^3 v_J^1 - v_I^1 v_J^3 \quad \boxed{3 < I < J \leq N} \\
(3) \quad & \epsilon[3IJ] Q[3IJ] = -v_I^2 v_J^1 + v_I^1 v_J^2 \quad \boxed{3 < I < J \leq N} \\
(4) \quad & \epsilon[IJK] Q[IJK] = -v_I^3 v_J^2 v_K^1 + v_I^3 v_J^1 v_K^2 - v_I^2 v_J^1 v_K^3 + v_I^2 v_J^3 v_K^1 - v_I^1 v_J^3 v_K^2 + v_I^1 v_J^2 v_K^3 \quad \boxed{3 < I < J < K \leq N}
\end{aligned} \tag{4.16}$$

The relations (4.16) may be rewritten by eliminating the vector components v_K^k in (1)...(4) by plugging into (I), (II), (III). Then

$$\begin{aligned}
(1) \quad & \epsilon[1IJ] Q[1IJ] = \epsilon[12I] \epsilon[13J] Q[12I] Q[13J] - \epsilon[13I] \epsilon[12J] Q[13I] Q[12J] \\
(2) \quad & \epsilon[2IJ] Q[2IJ] = \epsilon[12I] \epsilon[23J] Q[12I] Q[23J] - \epsilon[23I] \epsilon[12J] Q[23I] Q[12J] \\
(3) \quad & \epsilon[3IJ] Q[3IJ] = \epsilon[13I] \epsilon[23J] Q[13I] Q[23J] - \epsilon[23I] \epsilon[13J] Q[23I] Q[13J] \\
(4) \quad & \epsilon[IJK] Q[IJK] = \epsilon[12I] \epsilon[13J] \epsilon[23K] Q[12I] Q[13J] Q[23K] - \epsilon[12I] \epsilon[23J] \epsilon[13K] Q[12I] Q[23J] Q[13K] \\
& \quad + \epsilon[13I] \epsilon[23J] \epsilon[12K] Q[13I] Q[23J] Q[12K] - \epsilon[13I] \epsilon[12J] \epsilon[23K] Q[13I] Q[12J] Q[23K] \\
& \quad + \epsilon[23I] \epsilon[12J] \epsilon[13K] Q[23I] Q[12J] Q[13K] - \epsilon[23I] \epsilon[13J] \epsilon[12K] Q[23I] Q[13J] Q[12K]
\end{aligned} \tag{4.17}$$

A further simplification can be brought to (4.17) if we realize that our assumption $\epsilon[IJK] \neq 0 \quad \forall I < J < K \leq N$ implies that $v_K^k \neq 0 \quad \forall K = 4 \dots N, k = 1, 2, 3$ due to equations (I), (II), (III) in (4.16). We are therefore free to set $|v_I^3| = Q[12I] \stackrel{!}{=} 1$ which only scales the individual vector¹⁴ \vec{v}_I and thus the moduli $Q[IJK]$ but does not change the direction \vec{v}_I points to. That is setting $|v_I^3| = 1$ does not affect the signs $\epsilon[IJK]$. Additionally we define the manifestly positive quantities $x_I := |v_I^1| = Q[23I]$ and $y_I := |v_I^2| = Q[13I]$.

Using the fact that $(\epsilon[IJK])^2 = 1$ we can bring all sign factors to the right hand side of (4.17). Now since by construction $Q[IJK]$ is a manifestly positive quantity we can express (4.17) as a system of inequalities:

$$\begin{aligned}
(1) \quad & 0 < \epsilon[1IJ] \left[\epsilon[12I] \epsilon[13J] y_J - \epsilon[13I] \epsilon[12J] y_I \right] \\
(2) \quad & 0 < \epsilon[2IJ] \left[\epsilon[12I] \epsilon[23J] x_J - \epsilon[23I] \epsilon[12J] x_I \right] \\
(3) \quad & 0 < \epsilon[3IJ] \left[\epsilon[13I] \epsilon[23J] y_I x_J - \epsilon[23I] \epsilon[13J] x_I y_J \right] \\
(4) \quad & 0 < \epsilon[IJK] \left[\epsilon[12I] \epsilon[13J] \epsilon[23K] y_J x_K - \epsilon[12I] \epsilon[23J] \epsilon[13K] x_J y_K \right. \\
& \quad + \epsilon[13I] \epsilon[23J] \epsilon[12K] y_I x_J - \epsilon[13I] \epsilon[12J] \epsilon[23K] y_I x_K \\
& \quad \left. + \epsilon[23I] \epsilon[12J] \epsilon[13K] x_I y_K - \epsilon[23I] \epsilon[13J] \epsilon[12K] x_I y_J \right]
\end{aligned} \tag{4.18}$$

Now we divide¹⁵ (1) by $y_J > 0$, (2) by $x_J > 0$, (3) by $(x_J \cdot y_J) > 0$, (4) by $(x_K \cdot y_K) > 0$ and introduce the quotients

$$Y_J^I := \frac{y_I}{y_J} = (Y_I^J)^{-1} \quad X_J^I := \frac{x_I}{x_J} = (X_I^J)^{-1} \tag{4.19}$$

with the obvious property that for $\boxed{I < J < K}$ we have transitivity, that is

$$Y_K^I = Y_J^I \cdot Y_K^J \quad \text{and} \quad X_K^I = X_J^I \cdot X_K^J \tag{4.20}$$

¹⁴This can be equivalently thought of as scaling the vector \vec{v}_I by dividing all its components v_I^k by $|v_I^3|$, giving a new vector \vec{v}_I' pointing in the same direction as \vec{v}_I but with components $v_I'^k = \frac{v_I^k}{|v_I^3|}$.

¹⁵Note again that due to our conventions $y_K > 0$ and $x_K > 0 \quad \forall K = 4 \dots N$.

We can then bring (4.18) into its final form

$$\begin{aligned}
(1) \quad & 0 < \epsilon[1IJ] \left[\epsilon[12I] \epsilon[13J] - \epsilon[13I] \epsilon[12J] Y_J^I \right] \\
(2) \quad & 0 < \epsilon[2IJ] \left[\epsilon[12I] \epsilon[23J] - \epsilon[23I] \epsilon[12J] X_J^I \right] \\
(3) \quad & 0 < \epsilon[3IJ] \left[\epsilon[13I] \epsilon[23J] Y_J^I - \epsilon[23I] \epsilon[13J] X_J^I \right] \\
(4) \quad & 0 < \epsilon[IJK] \left[\epsilon[12I] \epsilon[13J] \epsilon[23K] Y_K^J - \epsilon[12I] \epsilon[23J] \epsilon[13K] X_K^J \right. \\
& + \epsilon[13I] \epsilon[23J] \epsilon[12K] Y_J^I Y_K^J X_K^J - \epsilon[13I] \epsilon[12J] \epsilon[23K] Y_J^I Y_K^J \\
& \left. + \epsilon[23I] \epsilon[12J] \epsilon[13K] X_J^I X_K^J - \epsilon[23I] \epsilon[13J] \epsilon[12K] X_J^I X_K^J Y_K^J \right]
\end{aligned} \tag{4.21}$$

We will subsequently discuss the properties of first the set (1), (2), (3) and secondly (4) as contained in (4.21) in two separate subsections.

The system (1), (2), (3)

If we introduce the short hand signs

$$\begin{aligned}
\rho_1^{[IJ]} &= \epsilon[1IJ] \epsilon[12I] \epsilon[13J] & \rho_3^{[IJ]} &= \epsilon[2IJ] \epsilon[12I] \epsilon[23J] & \rho_5^{[IJ]} &= \epsilon[3IJ] \epsilon[13I] \epsilon[23J] \\
\rho_2^{[IJ]} &= -\epsilon[1IJ] \epsilon[13I] \epsilon[12J] & \rho_4^{[IJ]} &= -\epsilon[2IJ] \epsilon[23I] \epsilon[12J] & \rho_6^{[IJ]} &= -\epsilon[3IJ] \epsilon[23I] \epsilon[13J]
\end{aligned} \tag{4.22}$$

we can rewrite the equations (1), (2), (3) of (4.21) as the simple system

$$\begin{aligned}
(1) \quad & 0 < \rho_1^{[IJ]} + \rho_2^{[IJ]} Y_J^I \\
(2) \quad & 0 < \rho_3^{[IJ]} + \rho_4^{[IJ]} X_J^I \\
(3) \quad & 0 < \rho_5^{[IJ]} Y_J^I + \rho_6^{[IJ]} X_J^I
\end{aligned} \tag{4.23}$$

Each of the 3 inequalities in (4.23) has 4 different sign-combinations:

Solutions to inequality (1)

case	$\rho_1^{(IJ)}$	$\rho_2^{(IJ)}$	condition
1.1	+	+	$0 < Y_J^I$
1.2	+	-	$0 < Y_J^I < 1$
1.3	-	+	$1 < Y_J^I$
1.4	-	-	no solution

Solutions to inequality (2)

case	$\rho_3^{(IJ)}$	$\rho_4^{(IJ)}$	condition
2.1	+	+	$0 < X_J^I$
2.2	+	-	$0 < X_J^I < 1$
2.3	-	+	$1 < X_J^I$
2.4	-	-	no solution

Solutions to inequality (3)

case	$\rho_5^{(IJ)}$	$\rho_6^{(IJ)}$	condition
3.1	+	+	$0 < X_J^I \quad 0 < Y_J^I$
3.2	+	-	$X_J^I < Y_J^I$
3.3	-	+	$Y_J^I < X_J^I$
3.4	-	-	no solution

(4.24)

It remains to discuss the complete set of solutions¹⁶ for the coupled inequality system (1), (2), (3) in (4.23), where we will exclude those sign configurations which contain the cases 1.4 or 2.4 or 3.4 of (4.24) since they do not contribute a solution. One finds the following table of solutions. It has to be read as follows: Each row gives a combination of 3 solutions contained in (4.24) (for example the first row indicates a combination of solution 1.1 for inequality (1), 2.1 for inequality (2), 3.1 for inequality (3) as given in (4.24)). Then the resulting sign combinations are written as '+ ' \equiv 1 and '- ' \equiv -1. Finally the conditions implied by the given set of solutions are written down.

¹⁶That is, consistent combinations of the signs.

(1)	(2)	(3)	$\rho_1^{[I,J]}$	$\rho_2^{[I,J]}$	$\rho_3^{[I,J]}$	$\rho_4^{[I,J]}$	$\rho_5^{[I,J]}$	$\rho_6^{[I,J]}$	conditions given by (1),(2),(3)	final condition
1	1	1	+	+	+	+	+	+	$0 < Y_J^I 0 < X_J^I$	$0 < Y_J^I 0 < X_J^I$
1	1	2	+	+	+	+	+	-	$0 < Y_J^I 0 < X_J^I X_J^I < Y_J^I$	$0 < X_J^I < Y_J^I$
1	1	3	+	+	+	+	-	+	$0 < Y_J^I 0 < X_J^I Y_J^I < X_J^I$	$0 < Y_J^I < X_J^I$
1	2	1	+	+	+	-	+	+	$0 < Y_J^I 0 < X_J^I < 1$	$0 < Y_J^I 0 < X_J^I < 1$
1	2	2	+	+	+	-	+	-	$0 < Y_J^I 0 < X_J^I < 1 X_J^I < Y_J^I$	$0 < X_J^I < 1 X_J^I < Y_J^I$
1	2	3	+	+	+	-	-	+	$0 < Y_J^I 0 < X_J^I < 1 Y_J^I < X_J^I$	$0 < Y_J^I < X_J^I < 1$
1	3	1	+	+	-	+	+	+	$0 < Y_J^I 1 < X_J^I$	$0 < Y_J^I 1 < X_J^I$
1	3	2	+	+	-	+	+	-	$0 < Y_J^I 1 < X_J^I X_J^I < Y_J^I$	$1 < X_J^I < Y_J^I$
1	3	3	+	+	-	+	-	+	$0 < Y_J^I 1 < X_J^I Y_J^I < X_J^I$	$0 < Y_J^I < X_J^I 1 < X_J^I$
2	1	1	+	-	+	+	+	+	$0 < Y_J^I < 1 0 < X_J^I$	$0 < Y_J^I < 1 0 < X_J^I$
2	1	2	+	-	+	+	+	-	$0 < Y_J^I < 1 0 < X_J^I X_J^I < Y_J^I$	$0 < X_J^I < Y_J^I < 1$
2	1	3	+	-	+	+	-	+	$0 < Y_J^I < 1 0 < X_J^I Y_J^I < X_J^I$	$0 < Y_J^I < 1 Y_J^I < X_J^I$
2	2	1	+	-	+	-	+	+	$0 < Y_J^I < 1 0 < X_J^I < 1$	$0 < Y_J^I < 1 0 < X_J^I < 1$
2	2	2	+	-	+	-	+	-	$0 < Y_J^I < 1 0 < X_J^I < 1 X_J^I < Y_J^I$	$0 < X_J^I < Y_J^I < 1$
2	2	3	+	-	+	-	-	+	$0 < Y_J^I < 1 0 < X_J^I < 1 Y_J^I < X_J^I$	$0 < Y_J^I < X_J^I < 1$
2	3	1	+	-	-	+	+	+	$0 < Y_J^I < 1 1 < X_J^I$	$0 < Y_J^I < 1 < X_J^I$
2	3	2	+	-	-	+	+	-	$0 < Y_J^I < 1 1 < X_J^I X_J^I < Y_J^I$	no solution
2	3	3	+	-	-	+	-	+	$0 < Y_J^I < 1 1 < X_J^I Y_J^I < X_J^I$	$0 < Y_J^I < 1 < X_J^I$
3	1	1	-	+	+	+	+	+	$1 < Y_J^I 0 < X_J^I$	$1 < Y_J^I 0 < X_J^I$
3	1	2	-	+	+	+	+	-	$1 < Y_J^I 0 < X_J^I X_J^I < Y_J^I$	$1 < Y_J^I 0 < X_J^I < Y_J^I$
3	1	3	-	+	+	+	-	+	$1 < Y_J^I 0 < X_J^I Y_J^I < X_J^I$	$1 < Y_J^I < X_J^I$
3	2	1	-	+	+	-	+	+	$1 < Y_J^I 0 < X_J^I < 1$	$0 < X_J^I < 1 < Y_J^I$
3	2	2	-	+	+	-	+	-	$1 < Y_J^I 0 < X_J^I < 1 X_J^I < Y_J^I$	$0 < X_J^I < 1 < Y_J^I$
3	2	3	-	+	+	-	-	+	$1 < Y_J^I 0 < X_J^I < 1 Y_J^I < X_J^I$	no solution
3	3	1	-	+	-	+	+	+	$1 < Y_J^I 1 < X_J^I$	$1 < Y_J^I 1 < X_J^I$
3	3	2	-	+	-	+	+	-	$1 < Y_J^I 1 < X_J^I X_J^I < Y_J^I$	$1 < X_J^I < Y_J^I$
3	3	3	-	+	-	+	-	+	$1 < Y_J^I 1 < X_J^I Y_J^I < X_J^I$	$1 < Y_J^I < X_J^I$

(4.25)

By inspection of the definition of the ρ -signs in (4.22), due to the arguments of sign factors we notice that

$$\rho_1^{[I,J]} \cdot \rho_2^{[I,J]} \cdot \dots \cdot \rho_6^{[I,J]} = -1 \quad (4.26)$$

and (ignoring the cases 2 – 3 – 2 and 3 – 2 – 3 which give no solution) we will only have 12 cases contained in (4.25) with an odd number of minus signs among the ρ 's. The remaining solutions are given in the following table:

case	(1)	(2)	(3)	$\rho_1^{[IJ]}$	$\rho_2^{[IJ]}$	$\rho_3^{[IJ]}$	$\rho_4^{[IJ]}$	$\rho_5^{[IJ]}$	$\rho_6^{[IJ]}$	final condition
1	1	1	2	+	+	+	+	+	-	$0 < X_J^I < Y_J^I$
2	1	1	3	+	+	+	+	-	+	$0 < Y_J^I < X_J^I$
3	1	2	1	+	+	+	-	+	+	$0 < Y_J^I 0 < X_J^I < 1$
4	1	3	1	+	+	-	+	+	+	$0 < Y_J^I 1 < X_J^I$
5	2	1	1	+	-	+	+	+	+	$0 < Y_J^I < 1 0 < X_J^I$
6	2	2	2	+	-	+	-	+	-	$0 < X_J^I < Y_J^I < 1$
7	2	2	3	+	-	+	-	-	+	$0 < Y_J^I < X_J^I < 1$
8	2	3	3	+	-	-	+	-	+	$0 < Y_J^I < 1 < X_J^I$
9	3	1	1	-	+	+	+	+	+	$1 < Y_J^I 0 < X_J^I$
10	3	2	2	-	+	+	-	+	-	$0 < X_J^I < 1 < Y_J^I$
11	3	3	2	-	+	-	+	+	-	$1 < X_J^I < Y_J^I$
12	3	3	3	-	+	-	+	-	+	$1 < Y_J^I < X_J^I$

(4.27)

Note that for a 5-valent vertex ($N = 5$) we only need to consider the solutions 1 – 12 as provided by (4.27) for the pair $(I, J) = (4, 5)$, however for $N > 5$ we have for every triple $I < J < K < N$ three relevant copies of the system (4.23) which read as

$$\begin{aligned}
(1)^{[IJ]} \quad 0 < \rho_1^{[IJ]} &+ \rho_2^{[IJ]} Y_J^I & (1)^{[JK]} \quad 0 < \rho_1^{[JK]} &+ \rho_2^{[JK]} Y_K^J \\
(2)^{[IJ]} \quad 0 < \rho_3^{[IJ]} &+ \rho_4^{[IJ]} X_J^I & (2)^{[JK]} \quad 0 < \rho_3^{[JK]} &+ \rho_4^{[JK]} X_K^J \\
(3)^{[IJ]} \quad 0 < \rho_5^{[IJ]} Y_J^I &+ \rho_6^{[IJ]} X_J^I & (3)^{[JK]} \quad 0 < \rho_5^{[JK]} Y_K^J &+ \rho_6^{[JK]} X_K^J \\
(1)^{[IK]} \quad 0 < \rho_1^{[IK]} &+ \rho_2^{[IK]} Y_J^I Y_K^J & & \\
(2)^{[IK]} \quad 0 < \rho_3^{[IK]} &+ \rho_4^{[IK]} X_J^I X_K^J & & \\
(3)^{[IK]} \quad 0 < \rho_5^{[IK]} Y_J^I Y_K^J &+ \rho_6^{[IK]} X_J^I X_K^J & &
\end{aligned} \tag{4.28}$$

wherein for the pair (IK) we have again used that $Y_K^I = Y_J^I Y_K^J$ and $X_K^I = X_J^I X_K^J$ by definition. Moreover we have used definition (4.22) in order to introduce the ρ -signs which can be seen as a coordinate transformation from the sign factors $\epsilon[JKI]$ to the ρ 's. However, the definitions of the ρ -signs are redundant as the following three identities are obvious:

$$\begin{aligned}
\rho_1^{[IJ]} \rho_2^{[IJ]} \rho_1^{[JK]} \rho_2^{[JK]} &= \epsilon[12I] \epsilon[13I] \epsilon[13K] \epsilon[12K] = -\rho_1^{[IK]} \rho_2^{[IK]} \\
\rho_3^{[IJ]} \rho_4^{[IJ]} \rho_3^{[JK]} \rho_4^{[JK]} &= \epsilon[12I] \epsilon[23I] \epsilon[23K] \epsilon[12K] = -\rho_3^{[IK]} \rho_4^{[IK]} \\
\rho_5^{[IJ]} \rho_6^{[IJ]} \rho_5^{[JK]} \rho_6^{[JK]} &= \epsilon[13I] \epsilon[23I] \epsilon[23K] \epsilon[13K] = -\rho_5^{[IK]} \rho_6^{[IK]}
\end{aligned} \tag{4.29}$$

A short MATHEMATICA calculation reveals that the coupled inequality system (4.28) has 312 solutions if we impose the restrictions (4.29). Each is given by a consistent combination of solutions for each of the three subsystems $[IJ], [JK], [IK]$: Each such solution of the subsystems can be labelled according to the cases of the first column in (4.27).

The inequality (4)

Let us now additionally consider inequality number (4) contained in (4.21). This can be rewritten, upon using the obvious identities induced by (4.22) and collecting terms with equal prefactors as follows:

$$\begin{aligned}
0 < \epsilon[JKI] &\left[\epsilon[12I] \epsilon[3JK] (\rho_5^{[JK]} Y_K^J + \rho_6^{[JK]} X_K^J) \right. \\
&- \epsilon[13I] \epsilon[2JK] Y_J^I Y_K^J (\rho_4^{[JK]} X_K^J + \rho_3^{[JK]}) \\
&\left. + \epsilon[23I] \epsilon[1JK] X_J^I X_K^J (\rho_2^{[JK]} Y_K^J + \rho_1^{[JK]}) \right]
\end{aligned} \tag{4.30}$$

Here we notice that the terms in the round brackets precisely resemble the terms on the right hand side of the inequalities $(1)^{[JK]}, (2)^{[JK]}, (3)^{[JK]}$ contained in the inequality system (4.28), and are thus positive by construction if

we want to obtain a solution. Let us abbreviate the sign-prefactors in (4.30) by

$$\begin{aligned}
\kappa_3^{[IJK]} &:= \epsilon[12I] \epsilon[3JK] = \epsilon[12I] \epsilon[13J] \epsilon[23K] \rho_5^{[JK]} \\
\kappa_2^{[IJK]} &:= -\epsilon[13I] \epsilon[2JK] = -\epsilon[13I] \epsilon[12J] \epsilon[23K] \rho_3^{[JK]} \\
\kappa_1^{[IJK]} &:= \epsilon[23I] \epsilon[1JK] = \epsilon[23I] \epsilon[12J] \epsilon[13K] \rho_1^{[JK]}
\end{aligned} \tag{4.31}$$

where we have again used (4.22) on the right hand side. Let us take a closer look at products of sign factors on the right hand sides of (4.31). According to (4.22) the following identities hold:

$$\begin{aligned}
\rho_5^{[IK]} \rho_6^{[IK]} &= -\epsilon[13I] \epsilon[23K] \epsilon[23I] \epsilon[13K] \rightsquigarrow \epsilon[23I] \epsilon[13K] = -\epsilon[13I] \epsilon[23K] \rho_5^{[IK]} \rho_6^{[IK]} \\
\rho_1^{[IJ]} \rho_2^{[IJ]} &= -\epsilon[12I] \epsilon[13J] \epsilon[13I] \epsilon[12J] \rightsquigarrow \epsilon[13I] \epsilon[12J] = -\epsilon[12I] \epsilon[13J] \rho_1^{[IJ]} \rho_2^{[IJ]}
\end{aligned} \tag{4.32}$$

Let us define the new sign-factor

$$\begin{aligned}
\lambda^{[IJK]} &:= \epsilon[23I] \epsilon[12J] \epsilon[13K] = \epsilon[12J] \epsilon[23I] \epsilon[13K] \\
&= -\epsilon[13I] \epsilon[12J] \epsilon[23K] \rho_5^{[IK]} \rho_6^{[IK]} \\
&= -\epsilon[23K] \rho_5^{[IK]} \rho_6^{[IK]} \epsilon[13I] \epsilon[12J] \\
&= \epsilon[12I] \epsilon[13J] \epsilon[23K] \rho_1^{[IJ]} \rho_2^{[IJ]} \rho_5^{[IK]} \rho_6^{[IK]}
\end{aligned} \tag{4.33}$$

Using (4.33) we can now express the κ 's of (4.31) completely in terms of ρ -signfactors and the overall sign $\lambda^{[IJK]}$:

$$\begin{aligned}
\kappa_1^{[IJK]} &= \lambda^{[IJK]} \rho_1^{[JK]} \\
\kappa_2^{[IJK]} &= \lambda^{[IJK]} \rho_5^{[IK]} \rho_6^{[IK]} \rho_3^{[JK]} \\
\kappa_3^{[IJK]} &= \lambda^{[IJK]} \rho_1^{[IJ]} \rho_2^{[IJ]} \rho_5^{[IK]} \rho_6^{[IK]} \rho_5^{[JK]}
\end{aligned} \tag{4.34}$$

In the last step we use (4.31), (4.34) to finally express (4.30) in terms of ρ -signfactors and the overall sign $\lambda^{[IJK]}$:

$$\begin{aligned}
0 < \epsilon[IJK] \lambda^{[IJK]} \left[\rho_1^{[IJ]} \rho_2^{[IJ]} \rho_5^{[IK]} \rho_6^{[IK]} \rho_5^{[JK]} \left(\rho_5^{[JK]} Y_K^J + \rho_6^{[JK]} X_K^J \right) \right. \\
\left. + \rho_5^{[IK]} \rho_6^{[IK]} \rho_3^{[JK]} Y_J^I Y_K^J \left(\rho_4^{[JK]} X_K^J + \rho_3^{[JK]} \right) + \rho_1^{[JK]} X_J^I X_K^J \left(\rho_2^{[JK]} Y_K^J + \rho_1^{[JK]} \right) \right]
\end{aligned} \tag{4.35}$$

The advantage of reformulating (4.30) as (4.35) is that we can give now a general tree of solutions to the total system (4.21) for an arbitrary edge triple $I < J < K \leq N$: Using the ρ -signs we can label each such solution again by a solution to the coupled triple inequality system (4.28) and additionally by an *overall* sign $S := \epsilon[LJK] \lambda^{[IJK]}$. For every solution of the triple system (4.28) we seek compatible signs $S := \epsilon[IJK] \lambda^{[IJK]} = \pm 1$. If a solution exists the sign $S := \epsilon[IJK] \lambda^{[IJK]}$ is written down in the subsequent table in the fourth column. We find that the total inequality system (4.21) obeys 372 solutions given in the table below.

IJ	JK	IK	S	IJ	JK	IK	S	IJ	JK	IK	S	IJ	JK	IK	S	IJ	JK	IK	S	IJ	JK	IK	S
1	1	6	-1	3	1	5	1	5	1	3	-1	7	1	1	1	9	1	3	1	11	1	1	-1
1	1	10	-1	3	1	9	1	5	1	3	1	7	1	2	1	9	1	4	1	11	2	1	-1
1	1	11	-1	3	2	5	-1	5	1	4	1	7	2	2	-1	9	2	3	1	11	2	2	-1
1	2	6	-1	3	2	5	1	5	2	3	1	7	2	2	1	9	2	4	1	11	2	2	1
1	2	6	1	3	2	9	1	5	2	4	1	7	3	3	-1	9	3	1	-1	11	3	3	1
1	2	7	1	3	3	6	-1	5	3	1	1	7	4	3	-1	9	3	1	1	11	3	4	1
1	2	8	1	3	3	7	-1	5	3	2	1	7	4	4	-1	9	3	2	1	11	4	4	-1
1	2	10	-1	3	3	10	-1	5	4	1	1	7	4	4	1	9	4	1	1	11	4	4	1
1	2	11	-1	3	4	6	-1	5	4	2	1	7	5	5	-1	9	4	2	1	11	5	5	1
1	2	12	-1	3	4	7	-1	5	5	6	1	7	6	6	1	9	5	6	-1	11	5	9	1
1	2	12	1	3	4	8	-1	5	5	7	1	7	6	7	1	9	5	6	1	11	6	6	-1
1	3	5	1	3	4	8	1	5	5	8	1	7	7	7	-1	9	5	7	1	11	6	10	-1
1	3	9	1	3	4	10	-1	5	6	5	-1	7	7	7	1	9	5	8	1	11	6	11	-1
1	4	5	1	3	4	10	1	5	6	5	1	7	8	7	-1	9	5	10	-1	11	7	6	-1
1	4	9	-1	3	4	11	1	5	7	5	1	7	8	8	-1	9	5	11	-1	11	7	7	-1
1	4	9	1	3	4	12	1	5	8	5	1	7	9	5	-1	9	5	12	-1	11	7	7	1
1	5	3	1	3	5	1	-1	5	9	6	1	7	9	9	-1	9	5	12	1	11	7	8	1
1	5	4	1	3	5	2	-1	5	9	7	1	7	10	6	1	9	6	5	1	11	7	10	-1
1	6	1	-1	3	6	3	1	5	9	8	-1	7	10	7	1	9	6	9	1	11	7	11	-1
1	7	1	-1	3	7	3	-1	5	9	8	1	7	10	10	1	9	7	5	1	11	7	11	1
1	7	1	1	3	7	3	1	5	9	10	-1	7	11	6	1	9	7	9	1	11	7	12	1
1	7	2	1	3	8	3	-1	5	9	10	1	7	11	7	-1	9	8	5	1	11	8	8	1
1	8	1	1	3	8	4	-1	5	9	11	-1	7	11	7	1	9	8	9	-1	11	8	11	1
1	8	2	1	3	9	1	-1	5	9	12	-1	7	11	8	-1	9	8	9	1	11	8	12	1
1	9	3	1	3	9	2	-1	5	10	5	-1	7	11	10	1	9	9	10	-1	11	9	9	1
1	9	4	1	3	10	3	1	5	10	9	-1	7	11	11	-1	9	9	11	-1	11	10	10	-1
1	10	1	-1	3	11	3	-1	5	11	5	-1	7	11	11	1	9	9	12	-1	11	10	11	-1
1	11	1	-1	3	11	3	1	5	11	9	-1	7	11	12	-1	9	10	9	-1	11	11	11	-1
1	11	1	1	3	11	4	-1	5	12	5	-1	7	12	7	-1	9	10	9	1	11	11	11	1
1	12	1	1	3	12	3	-1	5	12	5	1	7	12	8	-1	9	11	9	-1	11	12	11	1
1	12	2	1	3	12	4	-1	5	12	9	-1	7	12	12	-1	9	12	9	-1	11	12	12	1
2	1	6	-1	4	1	5	1	6	1	1	-1	8	1	1	1	10	1	1	-1	12	1	1	-1
2	1	7	-1	4	1	9	1	6	1	1	1	8	1	2	1	10	2	1	-1	12	1	1	1
2	1	7	1	4	2	5	1	6	2	1	-1	8	2	2	1	10	2	2	-1	12	1	2	1
2	1	8	1	4	2	9	1	6	2	2	-1	8	3	3	-1	10	3	3	-1	12	2	2	1
2	1	10	-1	4	3	6	-1	6	3	3	-1	8	3	3	1	10	3	3	1	12	3	3	1
2	1	11	-1	4	3	7	-1	6	4	3	-1	8	3	4	1	10	4	3	-1	12	3	4	1
2	1	11	1	4	3	7	1	6	4	4	-1	8	4	4	1	10	4	4	-1	12	4	4	1
2	1	12	1	4	3	8	1	6	5	5	-1	8	5	5	-1	10	5	5	-1	12	5	5	1
2	2	7	1	4	3	10	-1	6	6	6	-1	8	5	5	1	10	5	5	1	12	5	9	1
2	2	8	1	4	3	11	-1	6	6	6	1	8	6	6	1	10	5	9	1	12	6	6	-1
2	2	12	1	4	3	11	1	6	7	6	-1	8	6	7	1	10	6	6	-1	12	6	6	1
2	3	5	1	4	3	12	1	6	7	7	-1	8	6	8	1	10	6	10	-1	12	6	7	1
2	3	9	1	4	4	8	1	6	8	6	-1	8	7	7	1	10	7	6	-1	12	6	8	1
2	4	5	1	4	4	11	1	6	8	7	-1	8	7	8	1	10	7	7	-1	12	6	10	-1
2	4	9	1	4	4	12	1	6	8	8	-1	8	8	8	-1	10	7	10	-1	12	6	11	-1
2	5	3	1	4	5	1	-1	6	9	5	-1	8	8	8	1	10	8	6	-1	12	6	12	-1
2	5	4	1	4	5	2	-1	6	9	9	-1	8	9	5	-1	10	8	7	-1	12	6	12	1
2	6	1	-1	4	5	2	1	6	9	9	1	8	9	9	-1	10	8	8	-1	12	7	7	1
2	6	2	-1	4	6	3	1	6	10	6	1	8	10	6	1	10	8	8	1	12	7	8	1
2	6	2	1	4	6	4	1	6	10	10	1	8	10	7	1	10	8	10	-1	12	7	12	1
2	7	2	1	4	7	3	1	6	11	6	1	8	10	8	-1	10	8	10	1	12	8	8	1
2	8	2	1	4	7	4	1	6	11	10	1	8	10	8	1	10	8	11	1	12	8	12	1
2	9	3	1	4	8	4	-1	6	11	11	1	8	10	10	-1	10	8	12	1	12	9	9	-1
2	9	4	-1	4	8	4	1	6	12	6	-1	8	10	10	1	10	9	9	1	12	9	9	1
2	9	4	1	4	9	1	-1	6	12	6	1	8	10	11	-1	10	10	10	-1	12	10	10	-1
2	10	1	-1	4	9	2	-1	6	12	7	-1	8	10	12	-1	10	10	10	1	12	10	11	-1
2	10	2	-1	4	10	3	1	6	12	8	-1	8	11	8	-1	10	11	10	1	12	10	12	-1
2	11	1	-1	4	10	4	-1	6	12	10	1	8	11	11	-1	10	11	11	1	12	11	11	-1
2	11	2	-1	4	10	4	1	6	12	11	1	8	11	12	-1	10	12	10	1	12	11	12	-1
2	12	2	-1	4	11	4	-1	6	12	12	-1	8	12	8	-1	10	12	11	1	12	12	12	-1
2	12	2	1	4	12	4	-1	6	12	12	1	8	12	12	-1	10	12	12	1	12	12	12	1

(4.36)

4.2.4 Results

Table (4.36) can be taken as a starting point to compute all possible sign configurations $\vec{\epsilon}$ for a given N -valent vertex v . Here it will be of particular interest whether one can get conclusions for high valent vertices from the consistency of all the triple solutions, such that as more and more ϵ signs must be equal most of the $\sigma[IJK]$ prefactors must vanish. We expect that it will be possible to develop an effective algorithm starting from (4.36) [26]. A preliminary MATHEMATICA calculation reveals, for the numbers of linearly independent triples at valences $N = 4, 5, 6$, the results shown in table 2.

Comparing this table with the results of the Monte Carlo sprinkling process reveals that, in the case of 4, 5, and

n	Number of triples $\binom{N}{3}$	Number of potential sign configurations $T_{\max} = 2^{\binom{N}{3}}$	Number of realizable sign configurations T_R	$\frac{T_R}{T_{\max}}$
4	4	16	16	1
5	10	1024	384	0.375
6	20	2^{20}	23,808	0.023

Table 2: Analytic check of the sprinkling results of table 1 using the inequality system method of this section.

6-valent vertices, we have found all possible (non-coplanar) sign configurations from the sprinkling.

4.2.5 Remark on Linearly Dependent Tangents

In this section we sketch how edges having tangents which are linearly dependent can be treated. Given the set of tangent vectors of the edges at a vertex v , consider first only the maximal set of edges having linearly independent tangents using the procedure described above¹⁷. Calculate the possible sign configurations for this set of edges. Then consider the remaining edges having linearly dependent tangents for each of the obtained sign configurations as follows:

For three linearly dependent tangent vectors $\vec{v}_K, \vec{v}_L, \vec{v}_M$ we find constants $\alpha_{MK}, \alpha_{ML} \in \mathbb{R}$ such that $\vec{v}_M = \alpha_{MK} \cdot \vec{v}_K + \alpha_{ML} \cdot \vec{v}_L$. In particular we have for the components $v_M^i, i = 1, 2, 3$

$$\begin{aligned}
 v_M^i &= \alpha_{MK} \cdot v_K^i + \alpha_{ML} \cdot v_L^i \\
 &\downarrow \\
 \text{sgn}[v_M^i] \cdot |v_M^i| &= \text{sgn}[\alpha_{MK}] \text{sgn}[v_K^i] \cdot |\alpha_{MK} v_K^i| + \text{sgn}[\alpha_{ML}] \text{sgn}[v_L^i] \cdot |\alpha_{ML} v_L^i|
 \end{aligned} \tag{4.37}$$

These conditions then have to be imposed in the procedure above, giving further restrictions to possible sign configurations in (4.36) on the complete set of triples. A detailed numerical computation based on the analysis presented here will be given in [26].

5 Computational Details

In this section we discuss the details of our implementation of the numerical computation of the volume spectrum.

Our code takes the valence N of a vertex and the maximum spin j_{\max} as input parameters. It computes eigenvalues for the N -vertex for all spin configurations $j_1 \leq j_2 \leq \dots \leq j_N \leq j_{\max}$, subject to the constraint that $\sum_{i=1}^N j_i$ is an integer, since otherwise there is no gauge invariant recoupling scheme. Since the edge spins take on a countable set of values, we store doubled spins as (1 byte) integers on the computer.

5.1 Recoupling Scheme Implementation

As discussed in section 4.1, we must compute the set of all possible recouplings of the edge spins to total angular momentum $J = 0$. We do this with a recursive procedure, as follows. Each basis vector \vec{a} begins with j_1 as its first component. The second component a_2 can potentially take any value $|j_1 - j_2| \leq a_2 \leq j_1 + j_2$ which differs from those bounds by an integer. For each of these potential values, the third component a_3 can take any value $|a_2 - j_3| \leq a_3 \leq a_2 + j_3$ (which also differs by an integer from the bounds), and so on. Thus the recursive procedure adds a value for the next component of a potential basis vector \vec{a} . When it reaches a_{N-2} it considers only values for which it is possible to arrive at $a_{N-1} = j_N$, which is required to get $a_N = J = 0$. Any instances of the recursion for which this is not possible are abandoned at this stage.

The particular algorithm employed stores each of the components of \vec{a} obtained so far for each instance of the recursion. Since the majority of these instances will be abandoned at ‘stage a_{N-2} ’, this is somewhat inefficient, and can cause problems when dealing with high valences (or particularly large spins). A more efficient use of memory would be to employ some tree-like algorithm which only stores, for each instance of the recursion, the potential values of the ‘newest’ component of \vec{a} .

Another issue with this algorithm is that it traverses every potential sequence of values for the spin recouplings, and only very close to the end does it abandon sequences which cannot possibly recouple to total angular momentum zero. It may be more efficient to make this determination as soon as possible, so the computer does not waste cycles traversing ‘not possibly gauge invariant’ recoupling schemes.

It turns out that in practice neither of these issues make any difference, because the computable values of valence and spin are much more tightly bounded by consideration of the vast number of sign configurations \vec{c} . The CPU time required to compute eigenvalues, and disk space required to store them, vastly outweigh any concerns about the efficiency of the recoupling algorithm.

¹⁷Such a set will always exist, since in order to have non-vanishing volume we must always have at least one linearly independent triple.

5.2 Realizable Sign Factors via Poisson Sprinkling Process

The Monte Carlo computation of the set of realizable sign configurations is described in section 4.2.2. Here we comment on the Poisson sprinkling into S^2 .

We describe points on S^2 via the usual (θ, ϕ) coordinates, and wish to select N points at random such that, for any region of the sphere of area A , the number of points sprinkled into that region is Poisson distributed with mean $\frac{NA}{4\pi}$. Given random variables x, y which are uniformly distributed in the unit interval, we select N points from

$$\begin{aligned}\theta &= \arccos(2x - 1) \\ \phi &= 2\pi y\end{aligned}\tag{5.1}$$

This gives $\theta \in [0, \pi]$ and $\phi \in [0, 2\pi]$. If we form an area element by taking the product of their differentials, we get $(-)\sin\theta d\theta d\phi = 4\pi dx dy$, indicating that this gives the correct area element on the sphere. (The sign clearly has no significance).¹⁸

5.3 Eigenvalue Computation and Numerical Errors

As explained in section 2.3, we have a real antisymmetric matrix Q , or a real symmetric matrix $Q^\dagger Q$, whose eigenvalues we wish to compute. LAPACK [35] is an extensive, efficient linear algebra library written in Fortran 77, available from Netlib [37]. One of the computations it performs is a singular value decomposition of a real matrix A into USV^T , where U and V are orthogonal, and S is diagonal. The diagonal elements of S are the *singular values*. The singular decomposition of Q is

$$Q = USV^T\tag{5.3}$$

Multiplying on the right with Q^T gives

$$QQ^T = USV^T V S^T U^T = USS^T U^T = US^2 U^{-1}$$

which is the diagonalization of $QQ^T = QQ^\dagger$. Thus the eigenvalues of QQ^\dagger are simply the square of the singular values of Q . As discussed in section 2.3, these eigenvalues are simply the square of those of Q (which are pure imaginary and come in complex conjugate pairs). Thus the singular values of Q are non-positive real numbers and come in pairs, and their modulus is the square of that of the eigenvalues of \hat{V} . (Note that due to the definition of \hat{V} we are only concerned with the modulus of its eigenvalues.)

LAPACK employs an efficient recursive algorithm to compute the singular values, which it returns with fixed relative accuracy. (e.g. as compared to the ‘symmetric eigenvalue problem’ (c.f. section 6.6.5), for which the errors scale with the 1-norm of the input matrix.) The absolute error of the singular values is bounded by

$$\delta s_i \leq c\epsilon s_{\max}\tag{5.4}$$

where ϵ is machine epsilon (around 10^{-16}), s_{\max} is the largest singular value for that matrix, and c is a constant which governs the convergence criterion of the algorithm. For our calculations $c \approx 90$.

The effect of these numerical errors on our dataset is extremely small, and is described in detail in section 6.6.

5.4 The Cactus Framework

The Cactus framework [36] is a modular, open source, problem solving environment for high performance computing. It was originally developed to deal with the complex and computationally intensive problem of numerical relativity, where one seeks to extract the detailed form of gravitational waves which are emitted from astrophysical events such as binary star or black hole coalescence. The extensive needs of that computational task have led to what is now a very generic and extensible framework, which enables a wide class of applications to be easily placed on supercomputers. For this reason it seemed a natural framework to use for the development of code to explore Loop Quantum Gravity, and in particular to perform this volume spectrum computation.

The name ‘Cactus’ is meant to describe the framework metaphorically as a collection of modules, called ‘thorns’, which are bound together by the ‘flesh’. The thorns declare their characteristics, e.g. public variables called ‘grid functions’, to the flesh, which then generates code to allow the thorns to communicate and interoperate cleanly. To maintain portability Cactus defines its own datatypes, so it can guarantee their size and presence on all architectures it supports.

Perhaps the greatest benefit which Cactus affords is automatic parallelization. Cactus contains a software layer called a *driver*, which hides the details of implementing parallel code from the application programmer. For our

¹⁸ To say this another way, we can regard (5.1) as a coordinate transformation on the 2-sphere. The area element in the (θ, ϕ) coordinates is related to that in the Cartesian coordinates by

$$\tilde{d}x \wedge \tilde{d}y = J \tilde{d}\theta \wedge \tilde{d}\phi\tag{5.2}$$

where J is the Jacobian of the coordinate transformation. Inverting (5.1) and expanding leads to the same equality as above.

computation it allowed us to easily run on a distributed memory supercomputer, without much more difficulty than that required to develop the code to run on a single processor.

The volume spectrum computation described above is composed of three stages. First, given a spin configuration, one must compute the recoupling basis, as described in sections 4.1 and 5.1. Next, with the recoupling basis in hand, one computes the $\binom{N-1}{3}$ sub-matrices \hat{q}_{IJK} of Q for each triple $1 \leq I < J < K < N$, shown in (2.26). These submatrices are shown in full detail in equations (3.8) through (3.21). The final task is to combine the resulting submatrices, according to (2.26), for each $\vec{\sigma}$ -configuration (c.f. section 4.2.2). This last task is easily parallelized, by splitting the set of $\vec{\sigma}$ -configurations among the processors. This is implemented within Cactus by storing a $\vec{\sigma}$ -configuration within the 64 bit integer type ‘CCTK_INT8’¹⁹. The thorn which implements the volume computation then declares a one dimensional CCTK_INT8 grid function, which is automatically distributed among the processors by the standard Cactus driver PUGH.

A second benefit of using Cactus is that it provides a degree of language independence. The LAPACK library is written in Fortran 77, a language which is now quite old and inconvenient to work with. With Cactus one can write thorn code in C, C++, or any variant of Fortran, and Cactus takes care of all issues regarding inter-language communication. All of the code developed for this Volume computation is written in C, save one routine in Fortran 90 which performs all the calls to the LAPACK library.

Additionally Cactus is ‘familiar with’ external packages such as LAPACK and BLAS (upon which LAPACK depends). It provides thorns which automatically detect and link to these libraries, which makes it extremely easy to port the code to a new machine.

Last, but not least, is the modularity and extensibility of Cactus. The underlying philosophy behind its design is to facilitate code sharing and building a ‘community code base’ upon which all workers in a field can draw. A user is not required to release his or her thorns, of course, but the modularity of the thorn-flesh design makes it easy to incorporate code developed by others in one’s own code, so that one can build on the developments of others rather than each user having to start from scratch. We intend to release the code which generated the results of this paper.²⁰ It is hoped that this software will be a first step in constructing a community code base for performing high performance computations within Loop Quantum Gravity.

6 Numerical Results on Volume Spectrum

We will now show the results of our computations. It is in general remarkable that the $\vec{\sigma}$ -configuration will determine the shape of the spectrum as well as the behavior of the smallest non-zero eigenvalues (in particular the presence of a volume gap), and the largest eigenvalues as we increase the maximum spin j_{max} .

6.1 General Remarks

Let us begin by briefly reviewing the particular computation we have performed. Recall that given a graph γ we have a set of edges $E(\gamma)$ and a set of vertices $V(\gamma)$. Each edge $e \in E(\gamma)$ carries a representation of $SU(2)$ with weight j_e , that is we have a set $\vec{j} := \{j_e\}_{e \in E(\gamma)}$ of spins. In the gauge invariant setup we furthermore have at every vertex $v \in V(\gamma)$ an intertwiner I_v projecting on to one trivial representation contained in the reduction of the tensor product of the $SU(2)$ -representations carried by the edges outgoing²¹ from v . Thus we have a set $\vec{I} := \{I_v\}_{v \in V(\gamma)}$. We denote the set of N edges outgoing from v by $E(v)$, and the set of spins incident at the vertex v by $\vec{j}_v := \{j_I\}_{I \in E(v)}$. By definition (2.25), (2.26), the action of the volume operator \hat{V} can be separated to the single vertices $v \in V(\gamma)$. We can thus restrict our analysis to \hat{V} acting on a single but arbitrary vertex v , since we can determine the action of \hat{V} on arbitrary graphs from that.

\hat{V} is sensitive to the sign factors $\epsilon(IJK) := \text{sgn}[\det(\dot{e}_I, \dot{e}_J, \dot{e}_K)]$ which are the sign of the determinant of the tangents $\dot{e}_I, \dot{e}_J, \dot{e}_K$ of each ordered triple (e_I, e_J, e_K) , ($I < J < K$) of edges outgoing from v . A particular sign configuration $\vec{\epsilon} := \{\epsilon(IJK)\}_{\substack{e_I, e_J, e_K \in E(v) \\ I < J < K}}$ is fixed by the chosen graph γ (as a representative of its orbit under the diffeomorphism group). Note again that, upon imposing gauge invariance due to (4.12), there is a unique map $\mathcal{S} : \vec{\epsilon} \mapsto \vec{\sigma}$ where $\vec{\sigma} := \{\sigma(IJK)\}_{\substack{e_I, e_J, e_K \in E(v) \\ I < J < K}}$. Note that \mathcal{S} is not invertible, in particular it will happen that for different $\vec{\epsilon}, \vec{\epsilon}'$ -configurations we have $\mathcal{S}(\vec{\epsilon}) = \mathcal{S}(\vec{\epsilon}') = \vec{\sigma}$. Let us denote the number of $\vec{\epsilon}$ -configurations giving the same $\vec{\sigma}$ -configuration by $\chi_{\vec{\sigma}}$. We call $\chi_{\vec{\sigma}}$ the redundancy of $\vec{\sigma}$. In the end we will compute the volume spectrum for diffeomorphism equivalence classes of vertex embeddings, each of which has a corresponding sign configuration $\vec{\epsilon}$. Since only the $\vec{\sigma}$ -configurations enter into the eigenvalue computation, we must simply keep in mind that each $\vec{\sigma}$ -configuration comes with degeneracy $\chi_{\vec{\sigma}}$.

Given a fixed N -valent vertex v with fixed spin configuration $\vec{j}_v = \{j_1 \leq j_2 \leq \dots \leq j_N\}$ and fixed sigma configuration $\vec{\sigma}$, we compute the resulting matrix Q given in (2.26). As mentioned earlier we will employ Planck

¹⁹It turns out 64 bits is enough to store the $\vec{\sigma}$ -configuration for a 7-vertex, but not for an 8-vertex. The code could easily be generalized to handle higher valences.

²⁰Instructions for downloading the code will appear shortly.

²¹Recall that we can always redirect edges such that at every $v \in V(\gamma)$ with valence greater or equal 3 we only have outgoing edges.

units, with ℓ_P^3 , and the Z appearing in (2.25) (which is a function of the Immirzi parameter β and the regularization procedure), set to 1. We then compute the eigenvalues λ_Q . The square root of the modulus of the λ_Q gives the eigenvalues of $\lambda_{\hat{V}}$ of \hat{V} . Note that the eigenvalues $\lambda_{\hat{V}} = \sqrt{|\pm \lambda_Q|}$ come in pairs or are identical to 0. We store one number from each of the eigenvalues pairs, along with the corresponding spin and sigma configurations, in binary data files.²²

Ideally we would like to compute the full spectrum of the volume operator. Since its action on spin networks can be reduced to that on a single vertex, we consider only the latter. While in principle one must compute the eigenvalues above for all valences N and spin configurations \vec{j} , it will be necessary, due to finite computational resources, to introduce a cutoff j_{max} on the maximum allowed spin in the spin configurations, and restrict ourselves to valences $N \leq 7$. We thus compute, for each valence $N \leq 7$, for every spin configuration $\vec{j}_v = \{j_1 \leq j_2 \leq \dots \leq j_N\}$, for every sigma configuration $\vec{\sigma}$ described in section 4.2, the set of eigenvalues λ_Q of the resulting matrix Q as given in (2.26). From that one arrives at the set of individual eigenvalues $\lambda_{\hat{V}}$ for \hat{V} . Each eigenvalue thus obtained is regarded as coming with a redundancy of $D(\vec{j}) \cdot \chi_{\vec{\sigma}}$. The first factor arises from the degeneracy of the spin configuration (2.40) as described in section 2.5, and the second from the degeneracy of the sigma configuration mentioned above.

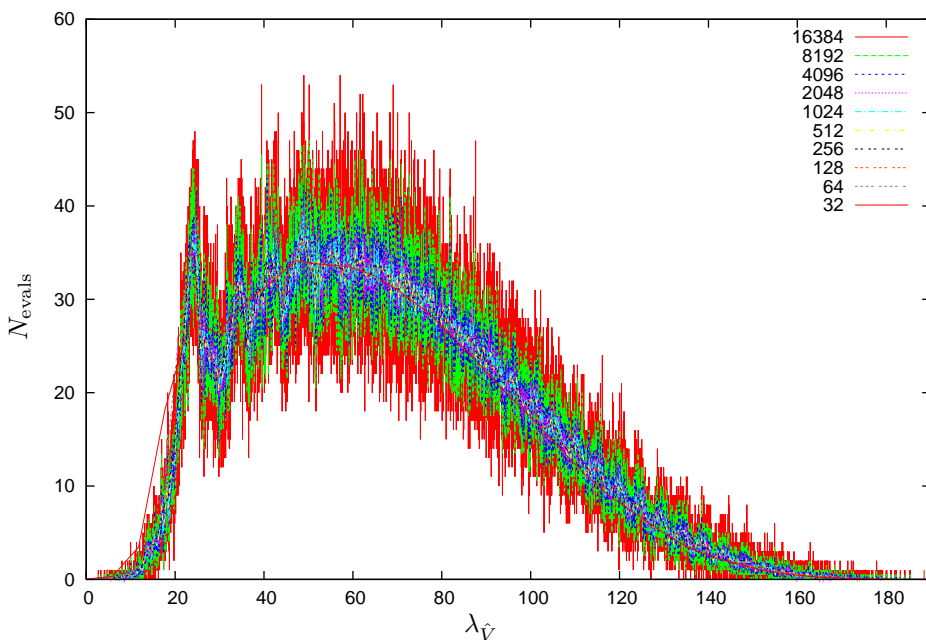


Figure 4: Illustration of effect of bin width on histograms.

In the following we display the collection of eigenvalues we have computed in a number of graphs. Most of these take the form of histograms: the real line between 0 and the maximum occurring eigenvalue $\lambda_{\hat{V}}^{(max)}$ is divided into N_{bins} equal width bins. The number of eigenvalues falling into each bin, taking into account the degeneracies mentioned above, is plotted. We ignore zero eigenvalues in all histograms. (In general there are *many* more zero eigenvalues than the number of eigenvalues in any histogram bin that we display.) We have attempted to choose the number of bins for the histograms such that we capture as much fine structure of this ‘spectral density function’ as possible, without using a too fine bin width such that the histogram appears ‘noisy’. Figure 4 illustrates the effect of bin width on the histogram. The histogram is like those described in section 6.3.2, showing the density of eigenvalues for a 5-vertex with $\vec{\sigma}$ -configuration = (0 -2 -4 -4) and all spins up to $j_{max} = \frac{23}{2}$. We see that decreasing the number of bins reduces the apparent noise in the curve. For a very small number of bins some fine detail of the density curve is washed out. Here, when increasing the bin width by a factor of 2, we also multiply the number of eigenvalues in that bin by $\frac{1}{2}$, so that the curves line up with the same vertical scale. Throughout the rest of the paper, whenever two histograms of varying bin width appear in the same plot, we employ this same normalization technique, so that the histograms can be displayed with the same vertical scale.

Additionally we will present various fits, which measure characteristic parameters of the eigenvalue set we have computed. For the number of eigenvalues as a function of j_{max} we employ a polynomial fit according to the estimate in section 4.1.1. Unless otherwise stated we have used for all other fits linear regression for logarithmic (in case of exponential dependencies) or double logarithmic (in case of possible polynomial dependencies) plots. This results from the fact that there is currently no applicable analytic model for the spectrum at hand, which could give us at least the functional dependencies of different characteristic spectral parameters. Therefore the fits we present here have to be

²²These are stored in a native binary format. The results described in this paper come from 188GB of data.

seen rather as a suggestion to a possible behavior than as a proof. Also the error ranges we give should be considered within this context.

6.2 Gauge Invariant 4-Vertex

The 4-vertex has been studied extensively in [24]. New analytic results concerning the degeneracy of the spectrum and on the smallest non-zero eigenvalue are presented in section 7. Here we present only a histogram of the eigenvalues in figure 5, for completeness, as well as a fit of the total number of eigenvalues.

Note that the 4-vertex has five realizable $\vec{\sigma}$ -configurations, with $\sigma(123)$ able to take any of its possible values -4, -2, 0, 2, or 4. The sign has no effect, so the only role of the $\vec{\sigma}$ -configuration, in this case, is to scale the overall spectrum by 0, 2, or 4. For consistency with the higher valences we include all eigenvalues contributed from these five $\vec{\sigma}$ -configurations in our analysis, whereas in [24] only the bare matrix \hat{q}_{123} was analyzed. Our numerical analysis extends the criterion for the smallest non-zero eigenvalue $\lambda_{\hat{V}}^{(\min)}$ given in [24] to a higher maximum spin of $j_{\max} = \frac{126}{2} = 63$. This sequence is contributed by spin configurations $j_1 = j_2 = \frac{1}{2}$ and $j_3 = j_4 = j_{\max}$. As shown in [24] these configurations give rise to an eigenvalue sequence $\lambda_{\hat{V}}^{(\min)}(j_{\max}) \propto \sqrt{2\sqrt{j_{\max}(j_{\max} + 1)}}$. This eigenvalue sequence as well as its spin configuration are in good agreement to the analytic lower bound (7.56) for the eigenvalues²³ λ_Q , as $\lambda_Q \geq j_{\max}$.

6.2.1 Histograms

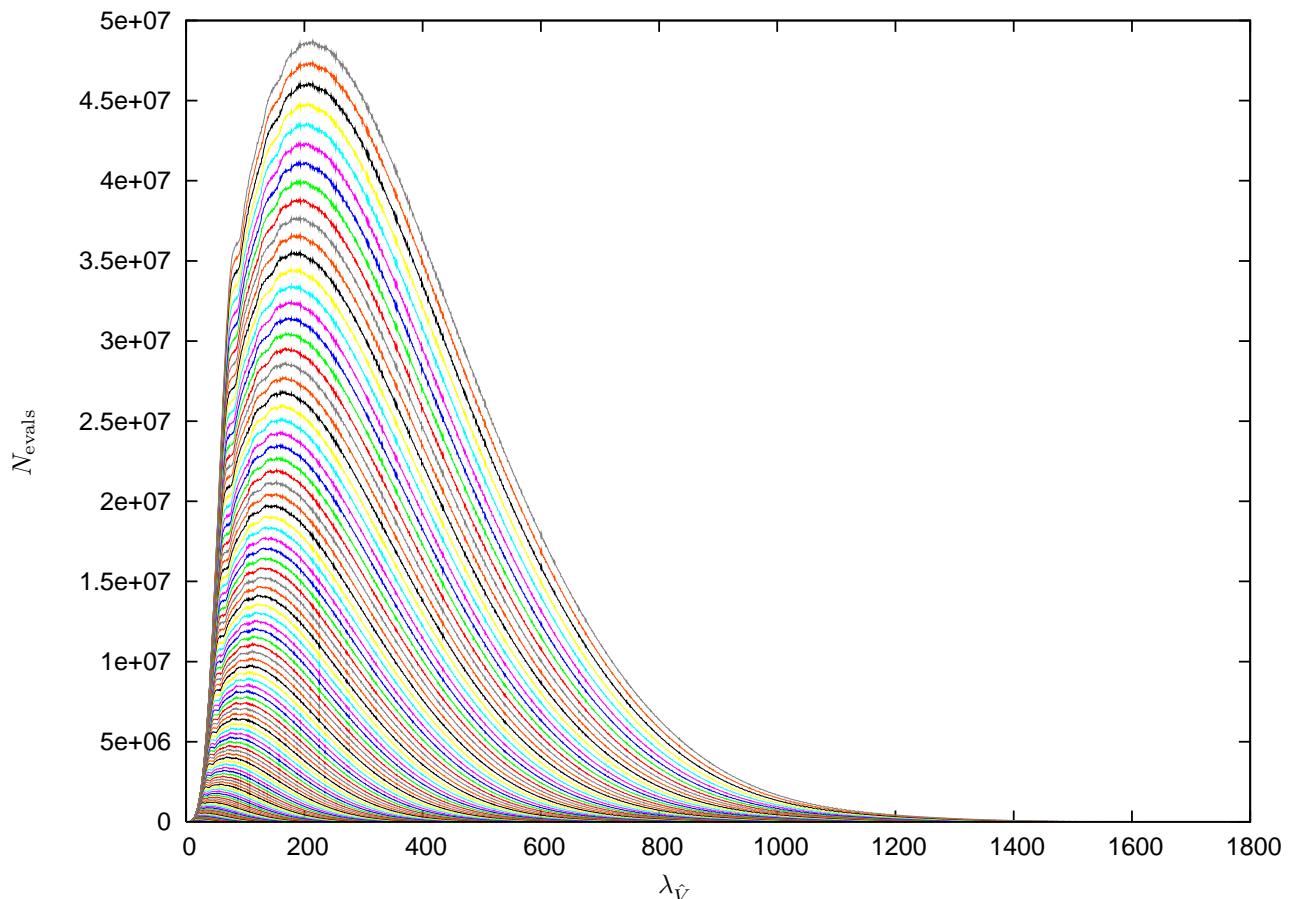


Figure 5: Overall 2048 bin histograms at the gauge invariant 4-vertex up to $j_{\max} = \frac{126}{2}$. There are 44,893,393,776 eigenvalues in all, of which 17,364,833,136 are zero.

Our results for the 4-vertex are depicted in figure 5, which was generated with $N_{\text{bins}} = 2048$. Each line represents the histogram of the eigenvalues for all $\vec{\sigma}$ -configurations and all values of edge spins up to a maximum spin j_{\max} (and all five $\vec{\sigma}$ -configurations). Thus the histogram for a given j_{\max} includes all eigenvalues which were used to generate the histogram for $j_{\max} - \frac{1}{2}$. We will refer to this diagram as an ‘overall’ histogram, for the given valence. Here the topmost line (gray) is the histogram for $j_{\max} = \frac{126}{2}$, the red line beneath it is the histogram for $j_{\max} = \frac{125}{2}$, and so forth. There are 17,364,833,136 zero eigenvalues not included in the histogram.

²³Recall that $\lambda_{\hat{V}} = \sqrt{|\pm \lambda_Q|}$.

6.2.2 Number of Eigenvalues

As a consistency check with the results in [24], we present, according to section 4.1.1, the total number number of eigenvalues (including zero eigenvalues) for all vertex configurations $j_1 \leq j_2 \leq j_3 \leq j_4 = j_{\max}$. Fitting to a polynomial of degree four in j_{\max} we obtain

$$N_{\text{evals}}^{(fit)}(j_{\max}) = \sum_{k=0}^4 r_k \cdot (j_{\max})^k \quad (6.1)$$

with coefficients (and their 95% confidence interval)

$$\begin{pmatrix} r_0 = 54.4937 & \pm 5.66522 \\ r_1 = -117.403 & \pm 1.22582 \\ r_2 = -10.6641 & \pm 0.07806 \\ r_3 = 213.333 & \pm 0.00184 \\ r_4 = 106.667 & \pm 0.000014 \end{pmatrix}$$

For this fit the quantity $\chi^2 := \sum_{j_{\max}=\frac{1}{2}}^{\frac{126}{2}} (N_{\text{evals}}(j_{\max}) - N_{\text{evals}}^{(fit)}(j_{\max}))^2$ takes the numerical value $\chi^2 = 4533.14$ for the set of 126 data points.

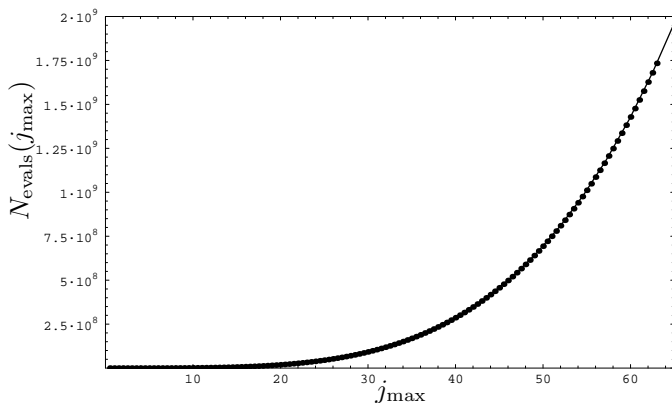


Figure 6: Number of eigenvalues at the 4-vertex. The solid line is a fit to a fourth order polynomial as given in the text.

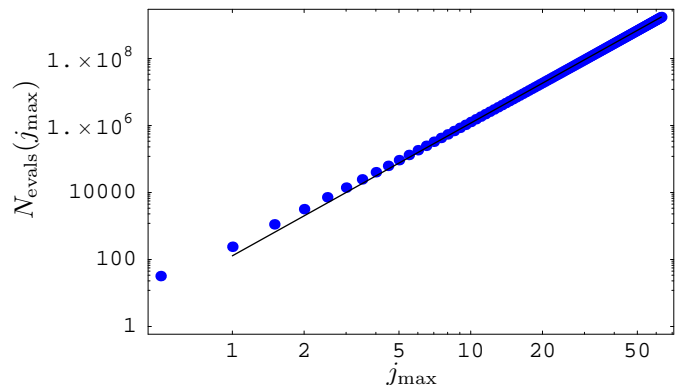


Figure 7: Number of eigenvalues at the 4-vertex in a double logarithmic plot using a two-parameter model. Again the computed data is represented by dots, the fit is a solid line.

As the number of eigenvalues is governed by the construction rules for the recoupling scheme basis, one can also give a model having a minimal number of parameters in order to get the behavior of N_{evals} in the leading order in j_{\max} as $N_{\text{evals}}^{(fit)}(j_{\max}) = r \cdot (j_{\max})^s$. In this case we obtain (using the non linear fit routine of Mathematica) $r = 128.981 \pm 0.428$ and $s = 3.96158 \pm 0.00082$, $\chi^2 = 1.18 \cdot 10^{13}$ which approximates the data quite well.

Note that in [24] the cumulative number of eigenvalues was analyzed, that is all eigenvalues, including zero eigenvalues, contributed from spin configurations $0 \leq j_1 \leq j_2 \leq j_3 \leq j_4 \leq j_{\max}$. In the present paper we have excluded all spin configurations with $0 = j_1$, because setting the spin of an edge to 0 corresponds to deleting that edge from the graph it belongs to. Moreover the present analysis considers the redundancy of the $\sigma_{123} = 0(6), \pm 2(4), \pm 4(1)$ prefactor: In brackets we have given the number $\chi_{\vec{\sigma}}$ of $\vec{\epsilon} = (\epsilon(123), \epsilon(124), \epsilon(134), \epsilon(234))$ configurations of linearly independent edge tangents which give rise to the according σ_{123} prefactor. As the sum over all $\chi_{\vec{\sigma}}$ is 16, we include this additional factor in our number of eigenvalue counting, as opposed to [24] which does not consider this factor. By taking into account this difference we exactly reproduce equation (95) in [24].

6.3 Gauge Invariant 5-Vertex

6.3.1 Histograms

According to section 4.2.2 we have 171 $\vec{\sigma}$ -configurations. Due to the modulus taken in the definition (4.12), configurations which differ by an overall sign can be identified. Therefore (excluding the $\sigma(IJK) = 0 \quad \forall I < J < K$ configuration) we are effectively left with 85 nontrivial $\vec{\sigma}$ -configurations. (There is clearly a symmetry in the $\vec{\sigma}$ -configurations whereby if one $\vec{\sigma}$ -configuration is realizable then its pair with all opposite signs is also realizable.)

We present here the histograms for the 5-vertex, for each maximum spin $j_{\max} \leq \frac{44}{2}$. These include all 85 $\vec{\sigma}$ -configurations. It turns out that, as opposed to the gauge invariant 4-vertex, the smallest eigenvalue does not always increase with j_{\max} . Rather this property is dictated by the particular $\vec{\sigma}$ -configuration, as can be seen in the discussion of the smallest eigenvalues below. Here this manifests itself in the growth of spectral density with j_{\max} at zero, as can

been seen in figure 9. Figure 10 demonstrates that, upon dividing the number of eigenvalues N_{evals} in each histogram bin by the total number of eigenvalues $N_{\text{evals}}(j_{\text{max}})$ (as given in section 6.3.5), one finds that this growth of the spectral density becomes more distinct at larger j_{max} .

Note that this cannot be traced back to numerical errors (see section 6.6 for a detailed discussion), but is a property of the volume operator itself: Eigenvalues are accumulated close to zero, resulting in a non-vanishing and in the limit $j_{\text{max}} \rightarrow \infty$ possibly infinite spectral density there. As we go from $\lambda_{\hat{V}} = 0$ to larger $\lambda_{\hat{V}}$ the eigenvalue density approaches a minimum and then goes over into a rising edge. This edge then finally decays into a long tail of the eigenvalue distribution, which can be traced back to the finite cutoff in j_{max} .

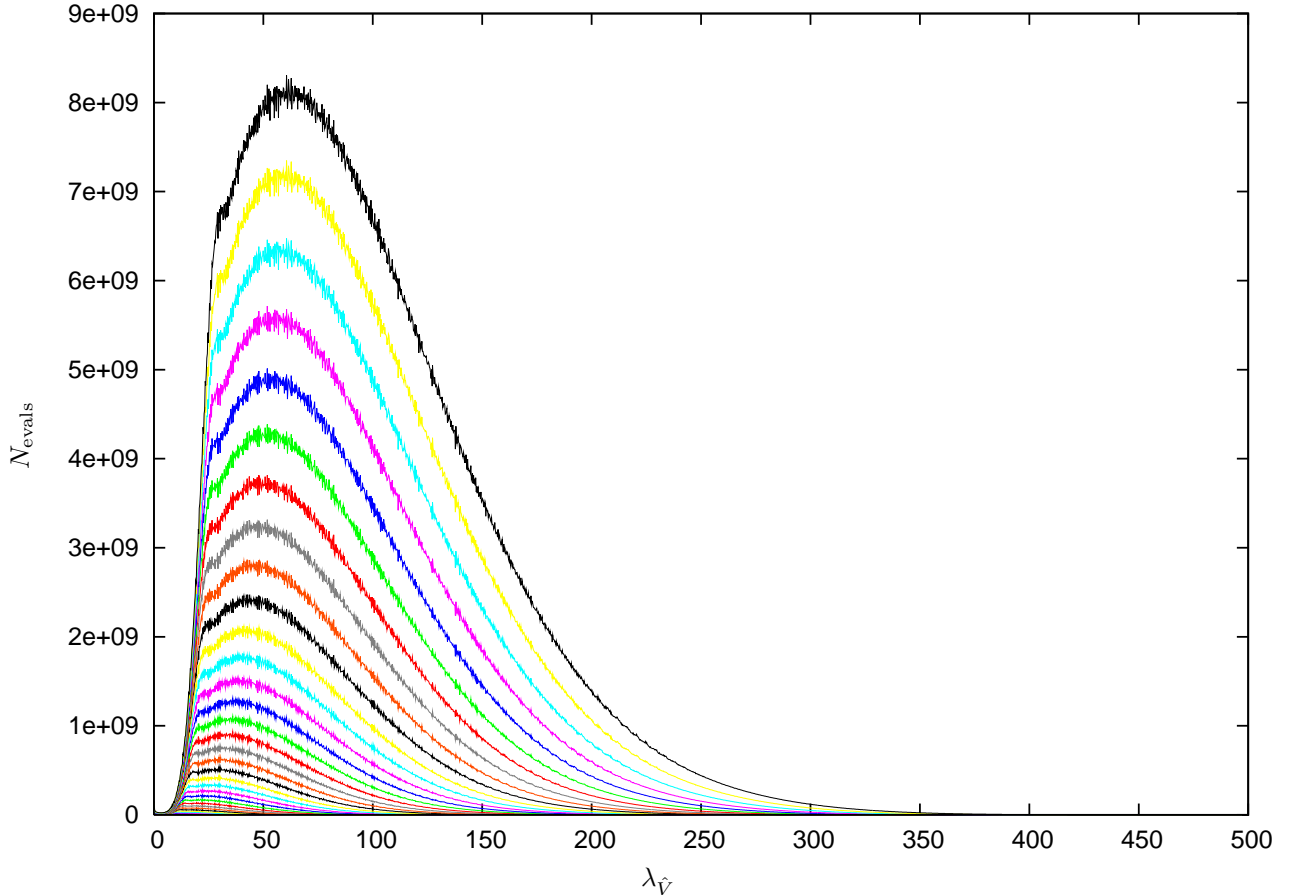


Figure 8: Overall 2048 bin histograms at the gauge invariant 5-vertex up to $j_{\text{max}} = \frac{44}{2}$. There are 4,680,292,624,128 eigenvalues in all, of which 450,641,502,288 are regarded as zero.

Figure 11 portrays 16 histograms, one for each value of $j_{\text{max}} = \frac{29}{2}, \dots, \frac{44}{2}$. Here each bin occupation number N_{bin} is divided by the maximum bin occupation number $N_{\text{bin}}^{\text{max}}(j_{\text{max}})$ of eigenvalues for that j_{max} , and in addition each eigenvalue is divided by the maximum eigenvalue at that j_{max} , $\lambda_{\hat{V}}^{\text{max}}(j_{\text{max}})$. Thus each of the histograms is normalized, such that we may see if they possess a universal shape which is independent of j_{max} . Here one can see that the 16 normalized histograms each have a quite similar shape.

6.3.2 Effect of Different $\vec{\sigma}$ -configurations

To give a feel for the effect of the $\vec{\sigma}$ -configuration, we show in figure 12 a sampling of histograms as in figure 8, but for various fixed $\vec{\sigma}$ -configurations. The first three $\vec{\sigma}$ -configurations shown (which have at least one $\sigma = \pm 4$) give a smallest non-zero eigenvalue which decreases with j_{max} (c.f. section 6.3.4). The next two $\vec{\sigma}$ -configurations give a smallest non-zero eigenvalue which increases with j_{max} . The last histogram is for the $\vec{\sigma}$ -configuration which gives a constant smallest non-zero eigenvalue. Some details regarding these histograms are given in table 3. The $\chi_{\vec{\sigma}}$ is defined in section 6.1. N_{zeros} is the total number of zero eigenvalues which occur for each $\vec{\sigma}$ -configuration. The last three histograms look sharper with fewer bins because there are more $\vec{\epsilon}$ -configurations corresponding to these $\vec{\sigma}$ -configurations, which causes more jitter in the spectrum.

Note how the $\vec{\sigma}$ -configuration affects many aspects of the spectrum, including the accumulation at zero, a dip in the spectral density at small eigenvalues around 10, the presence of a secondary peak at 30 or so, the presence of jagged edges for larger eigenvalues, and the magnitude of the largest eigenvalues which arise.

In figure 13 we show the histograms for each $\vec{\sigma}$ -configuration, without imposing any constraints on j_{max} (save that it is $\leq \frac{44}{2}$). Here we have also ignored the $\vec{\sigma}$ -configuration redundancy ($\chi_{\vec{\sigma}}$ of section 6.1), and weighted each

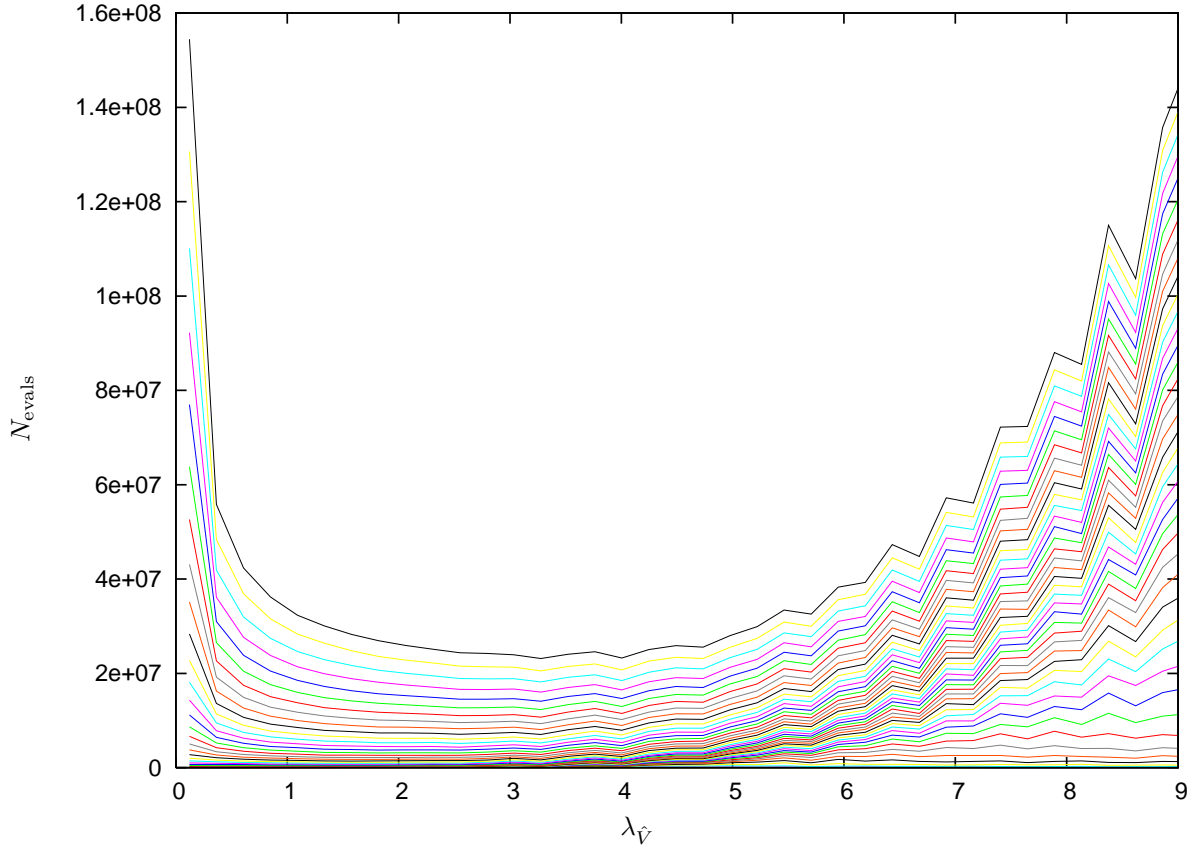


Figure 9: Zoom of eigenvalues close to 0 at the gauge invariant 5-vertex up to $j_{max} = \frac{44}{2}$.

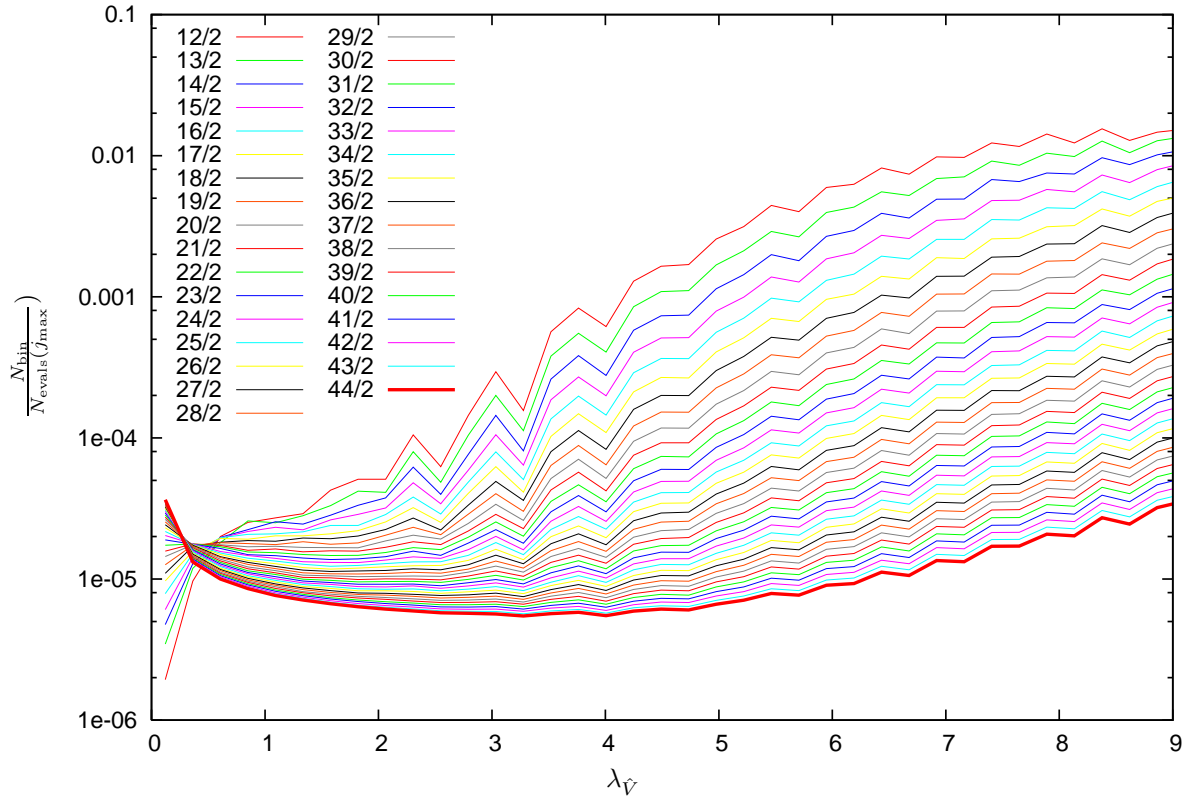


Figure 10: Zoom of log-plot of eigenvalues close to 0 at the gauge invariant 5-vertex up to $j_{max} = \frac{44}{2}$. We display the normalized histogram here: The number of eigenvalues per bin N_{bin} is divided by the total number of eigenvalues $N_{evals}(j_{max})$ (as given in section 6.3.5), such that the sum of all histogram bin occupation numbers gives 1. For larger j_{max} we clearly see a drastically increasing eigenvalue density close to zero.

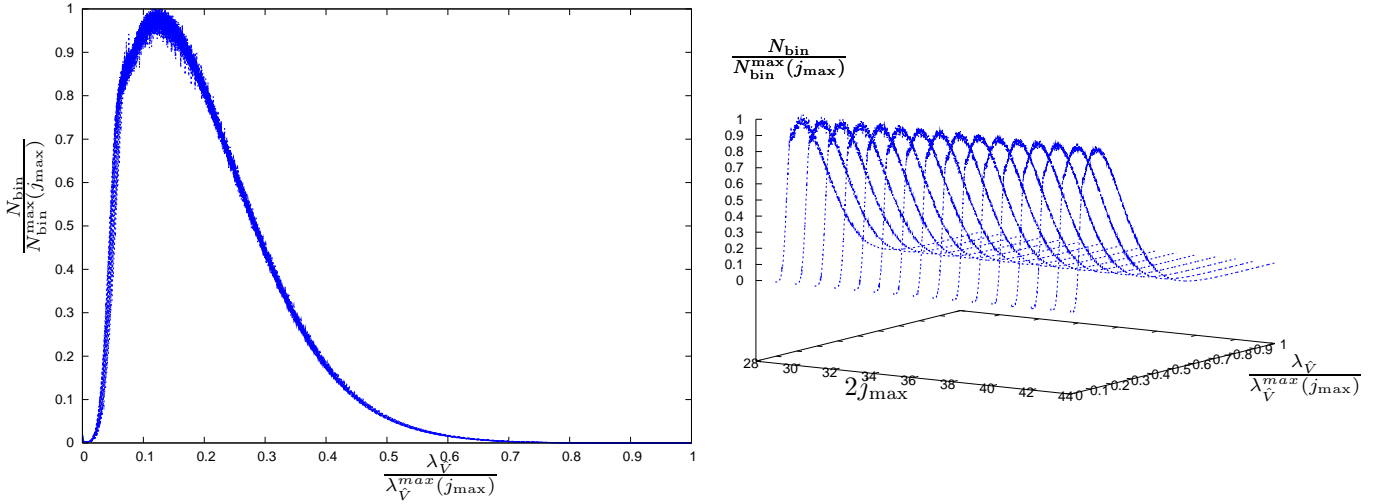
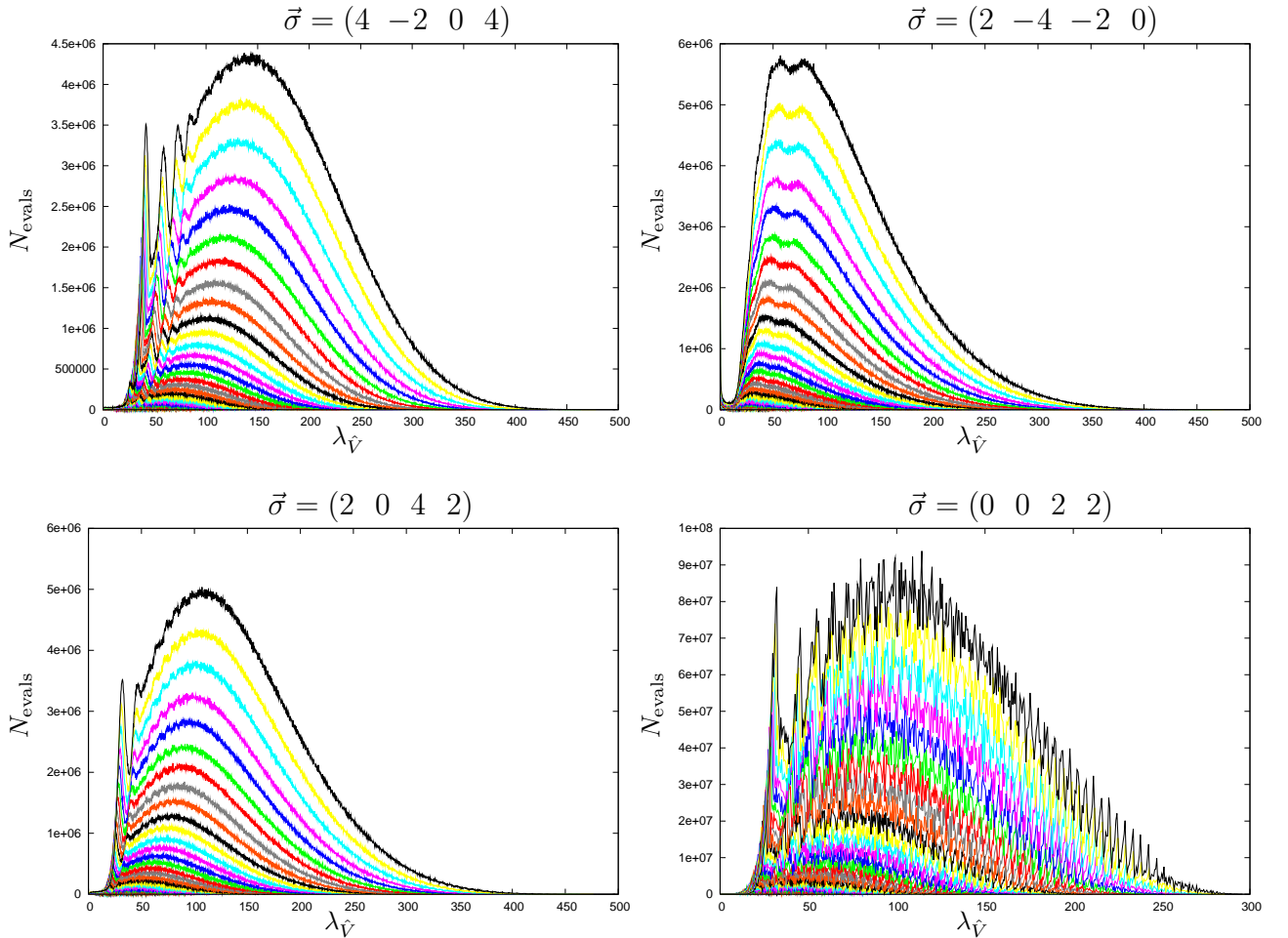


Figure 11: Normalized fixed- j_{\max} histograms for the 5-vertex for $j_{\max} = \frac{29}{2}, \dots, \frac{44}{2}$ (right figure). All histograms superposed are shown in the left figure.

$\vec{\sigma}$ -configuration	$\chi_{\vec{\sigma}}$	N_{zeros}	N_{bins}	behavior
4 -2 0 4	2	2,631,232,052	2048	decreasing $\lambda_{\hat{V}}^{(\min)}$
2 -4 -2 0	2	1,155,745,232	2048	decreasing $\lambda_{\hat{V}}^{(\min)}$
2 0 4 2	2	540,623,092	2048	decreasing $\lambda_{\hat{V}}^{(\min)}$
0 0 2 2	12	4,298,843,832	512	increasing $\lambda_{\hat{V}}^{(\min)}$
0 0 2 0	12	7,439,949,072	512	increasing $\lambda_{\hat{V}}^{(\min)}$
2 0 0 0	12	9,473,449,392	512	constant $\lambda_{\hat{V}}^{(\min)}$

Table 3: Details of some fixed $\vec{\sigma}$ -configuration histograms for the 5-vertex.



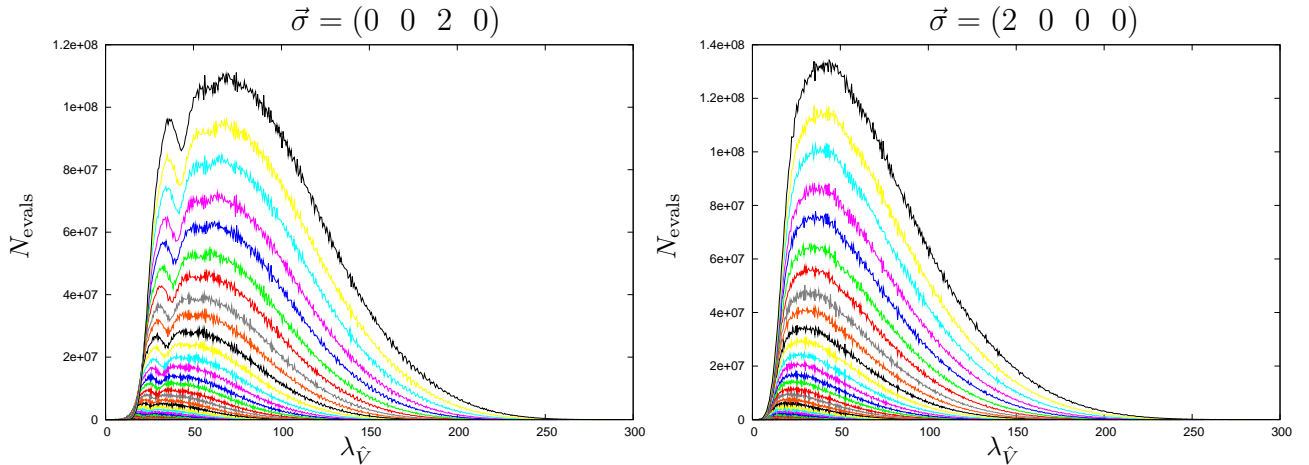


Figure 12: Histograms for individual $\vec{\sigma}$ -configurations of the 5-vertex.

individual $\vec{\sigma}$ -configuration equally. Each histogram has 2048 bins, save those of the $\vec{\sigma}$ -configurations corresponding to the $\vec{\sigma}$ -indices 30, 32–34, 36, and 40 from table 4 of section 6.3.4, which have only 512. These later ten histograms have their N_{evals} divided by 4, so they appear on the same scale as the other 75 histograms of figure 13. This ‘coarse graining’ improves the clarity of the figure, which is otherwise obscured by the rapidly fluctuating N_{evals} for these ten histograms.

6.3.3 Fitting of Histograms

The overall histogram for the 5-vertex, shown in figure 8, seems to possess an exponentially rising edge for eigenvalues around $\lambda_{\hat{\psi}} = 10$ to 30 or so. Note that as we consider larger and larger j_{max} , this edge does not change much as compared to the increase in the remainder of the histogram, save being extended to larger eigenvalues. Thus this exponentially rising edge may be a feature of the spectrum in the limit of $j_{\text{max}} \rightarrow \infty$. Figure 14 shows an exponential fit to this rising edge. The range of data points to fit, as well as the form of the fitting function, are chosen arbitrarily, as there is no directly applicable analytic model for the eigenvalue distribution available at the moment (though in [18] an expression for the 4-vertex was derived, see comments in [25]). Thus we would like to emphasize that the errors given for fits in the spectrum throughout this paper, although meaningful within the chosen set of data points, have to be taken in the context of the choice of fitting model and data point set we have made by hand. Our point here is to demonstrate that the spectrum in principle allows for an exponentially increasing number of eigenvalues. The fit gives the logarithm of the number of eigenvalues $N_{\text{evals}}(\lambda_{\hat{\psi}})$ as a function of the eigenvalue $\lambda_{\hat{\psi}}$ by:

$$\ln[N_{\text{evals}}(\lambda_{\hat{\psi}})]^{(fit)} = (14.87 \pm 0.20) + (0.43 \pm 0.02)\lambda_{\hat{\psi}} \quad \longrightarrow \quad N_{\text{evals}}^{(fit)}(\lambda_{\hat{\psi}}) \sim 2.87 \cdot 10^6 \cdot e^{0.43 \lambda_{\hat{\psi}}} \quad (6.2)$$

The quantity $\chi^2 := \sum_{k=1}^{20} (N_{\text{evals}}^{(fit)}(\lambda_{\hat{\psi}}^{(k)}) - N_{\text{evals}}^{(k)}(\lambda_{\hat{\psi}})) ^2$ has the numerical value $\chi^2 = 1.06 \cdot 10^{15}$ on the chosen set of 20 data points.

6.3.4 Extremal Eigenvalues

We have seen in section 6.3.2 that the $\vec{\sigma}$ -configuration has a considerable effect on the shape of the distribution of eigenvalues. Here we examine the largest and smallest eigenvalues which arise in the spectrum, as a function of j_{max} and $\vec{\sigma}$ -configuration. Figures 15 and 16 show the minimum and maximum non-zero eigenvalues of the spectrum, for a given $\vec{\sigma}$ -configuration and j_{max} .

As it turns out from the numerical analysis many of the $\vec{\sigma}$ -configurations give identical minimum eigenvalues $\lambda_{\hat{\psi}}^{(\text{min})}$ for each value of j_{max} , and we have separated them into equivalence classes, such that any two $\vec{\sigma}$ -configurations which have the same $\lambda_{\hat{\psi}}^{(\text{min})}(j_{\text{max}})$ will lie in the same equivalence class. The decision whether two $\vec{\sigma}$ -configurations belong to the same equivalence class is made as follows: Along with the smallest eigenvalue data we have recorded the numerical error bound of each eigenvalue according to section 5.3. We take the maximum numerical error which occurs among all the computed smallest eigenvalues as a threshold and look at the absolute differences in an elementwise subtraction of two eigenvalue lists. If the maximum numerical value of all the differences does not exceed the threshold then we consider the two $\vec{\sigma}$ -configurations as elements of the same equivalence class. These equivalence classes, which are detailed in tables 4 and 6, are used in the figures 15 and 16.

By inspection of figure 15, one can clearly see that some $\vec{\sigma}$ -configurations give rise to a minimum eigenvalue $\lambda_{\hat{\psi}}^{(\text{min})}$ which decreases with j_{max} , some give rise to a $\lambda_{\hat{\psi}}^{(\text{min})}$ which increases with j_{max} , and there is one in the middle for which $\lambda_{\hat{\psi}}^{(\text{min})}$ does not vary with j_{max} . These three behaviors of the minimum eigenvalues serve to classify the $\vec{\sigma}$ -configurations into three groups. In the following table we count the number of $\vec{\sigma}$ -configurations in each of these groups, and also

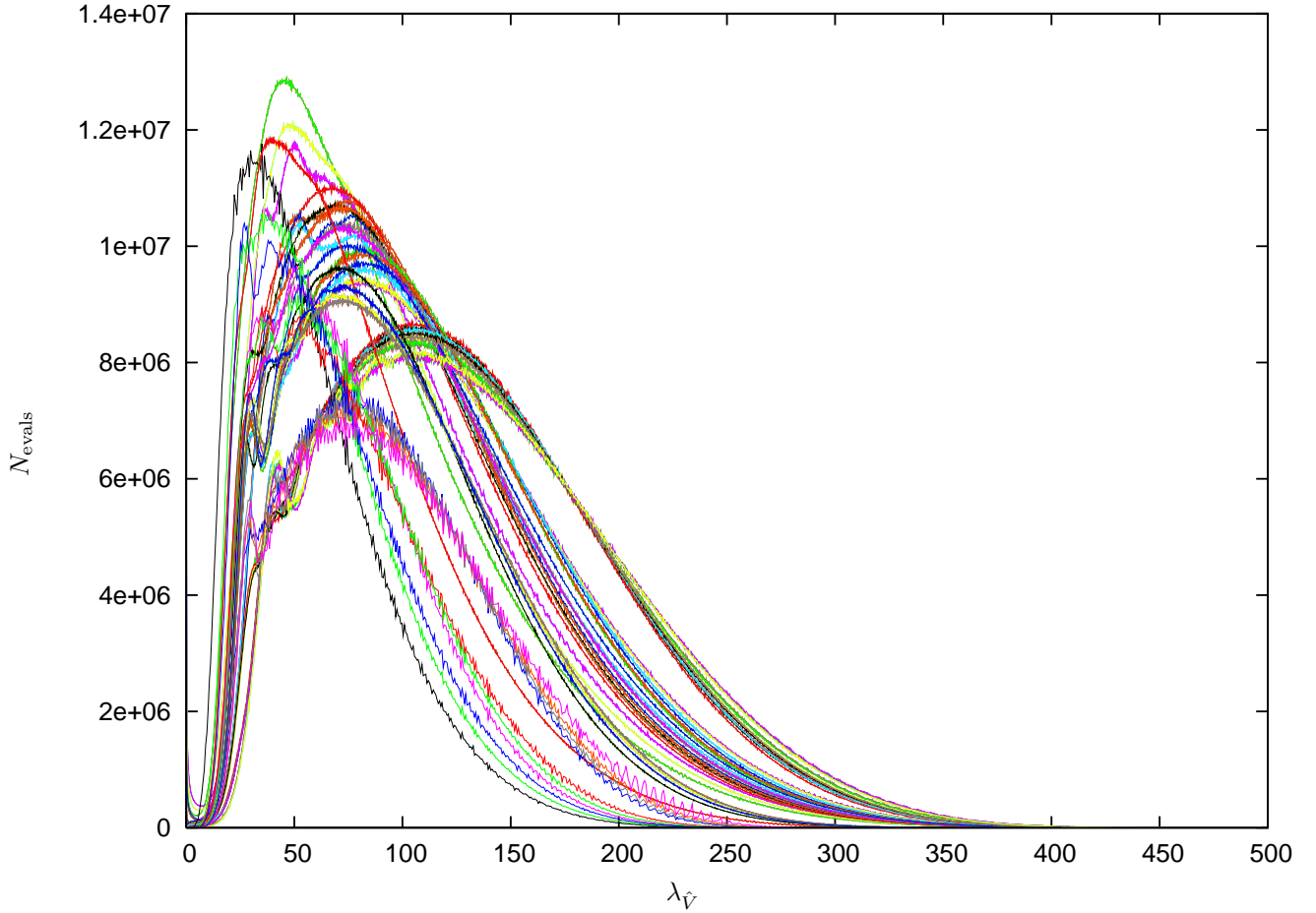


Figure 13: Histogram for each of the eighty-five $\vec{\sigma}$ -configurations of the 5-vertex.

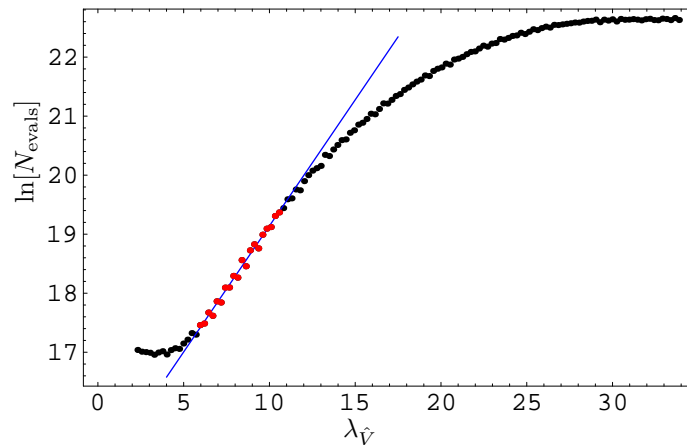


Figure 14: Logarithmic plot of the fit to the rising edge of the spectral density for the gauge invariant 5-vertex. The points shown in red were used in the fitting process, the blue solid line is the fitted function.

the number of inequivalent sequences $\lambda_{\vec{V}}^{(\min)}(j_{\max})$ which arise from the $\vec{\sigma}$ -configurations in each group. (We will often refer to ordered sequences of eigenvalues, such as $\lambda_{\vec{V}}^{(\min)}(j_{\max})$, $\lambda_{\vec{V}}^{(\max)}(j_{\max})$, as $j_{\max} \rightarrow \infty$, as *eigenvalue sequences*.) We find:²⁴

²⁴ Note that the list of equivalence classes given in tables 4 and 6 may be regarded as preliminary, because the eigenvalue sequences $\lambda_{\vec{V}}^{(\min)}(j_{\max})$ for two different $\vec{\sigma}$ -configurations may match only up to some finite j_{\max} . As observed already in [24], the structure of the volume spectrum becomes richer as we increase the cutoff j_{\max} , in particular new eigenvalue sequences may show up. Thus the number of equivalence classes could in principle increase at yet larger j_{\max} .

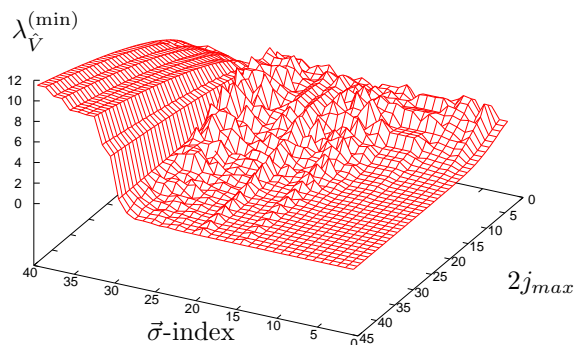


Figure 15: Smallest non-zero eigenvalues at the gauge invariant 5-vertex up to $j_{max} = \frac{44}{2}$. The $\vec{\sigma}$ -index is defined in table 4.

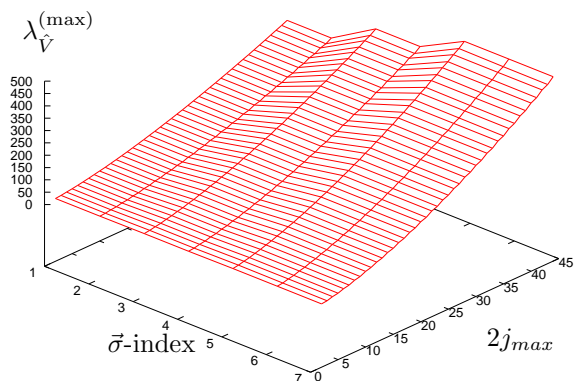


Figure 16: Largest Eigenvalues at the gauge invariant 5-vertex up to $j_{max} = \frac{44}{2}$. The $\vec{\sigma}$ -index is defined in table 6.

increasing σ -conf.	equiv. classes	10
	total	24
decreasing σ -conf.	equiv. classes	29
	total	60
constant σ -conf.	equiv. classes	1
	total	1

The analysis of the data for the smallest non-zero eigenvalues reveals that increasing smallest eigenvalues are contributed from $\vec{\sigma}$ -configurations containing only $(0, \pm 2)$ but not ± 4 , whereas decreasing eigenvalues are contributed by $\vec{\sigma}$ -configurations containing $(0, \pm 2, \pm 4)$. Table 4 lists the equivalence classes of $\vec{\sigma}$ -configurations showing a particular behavior for $\lambda_V^{(\min)}(j_{max})$ in detail. Recall the definition $\vec{\sigma} := \{\sigma(123), \sigma(124), \sigma(134), \sigma(234)\}$ where the arguments of $\sigma(IJK)$ are the edge labels for the particular edge triple (e_I, e_J, e_K) . We have assigned an index ‘ $\vec{\sigma}$ -index’ to every equivalence class of $\vec{\sigma}$ -configurations which relates it to the according curve in figure 15.

The fact that there is a $\vec{\sigma}$ -configuration giving constant smallest eigenvalues, independent of the value of j_{max} , seems to be puzzling, however this can be easily understood when we realize that this is the configuration $\vec{\sigma} := \{\sigma(123), \sigma(124), \sigma(134), \sigma(234)\} = \{2, 0, 0, 0\}$, as follows. If we look at equation (3.8), which gives the matrix elements for q_{123} , then the corresponding matrix only depends on the spins j_1, j_2, j_3 and the intermediate recoupling a_2 and a_3 . So it is effectively the matrix of the gauge invariant 4-vertex. Now even if j_5 becomes large, there still exist spin configurations with a large j_4 . Recall that the intermediate recouplings in a recoupling scheme at the gauge invariant 5-vertex are defined as: $a_2(j_1 j_2), a_3(a_2 j_3), a_4(a_3 j_4) \stackrel{!}{=} j_5$ where one has to apply the rules for the recoupling according to section 4.1. Now the smallest absolute numerical value for eigenvalues of the gauge invariant 4-vertex was found in [24] to be given by a configuration with $j_1 \sim j_2 \sim 1$ and $j_3 \sim a_3 = j_4 \sim j_{max}$.²⁵ But now we have this case embedded in a 5-vertex. This means that if j_3 is tiny then a_3 can be tiny as well (since $j_1 \leq j_2 \leq j_3 \leq j_4 \leq j_5$) whereas it might still happen that $j_3 + j_4 \sim j_5$. This case can occur for every $j_5 = j_{max}$, since we can still freely choose j_4, j_5 (because we consider all j_1, \dots, j_4 -combinations up to j_5). So we always get the same value. In the case of the 5-vertex, since the number of spins is odd, there is a sort of ‘struggling’ going on in the spin configuration which gives rise to the smallest eigenvalues, due to the condition that the sum of the 5 spins must be an integer (because otherwise we cannot recouple them to resulting zero spin). Thus different spin combinations can contribute the smallest eigenvalue: At the gauge invariant 4-vertex we saw that the smallest eigenvalue is contributed by spin configurations $j_1 = j_2 = \frac{1}{2}$ and $j_3 = j_4 = j_{max}$. Now assume a similar statement is true for the gauge invariant 5-vertex, for example²⁶ something like $j_1 = j_2 = \frac{1}{2}$ and $j_3 = j_4 = j_5 = j_{max}$. Then it is easy to see that while in case of the 4-vertex it does not matter if j_{max} is integer or half integer, this does matter at the 5-vertex. The combination here can only be realized if j_{max} is integer, otherwise there is no recoupling to resulting spin 0 possible. Thus for j_{max} half integer, a different spin combination will contribute the smallest non-zero eigenvalues. This is nicely demonstrated by the oscillating curves in figure 19.

Overall smallest eigenvalues As can be seen from the analysis of the data, the overall smallest non-zero eigenvalue, for each value of j_{max} , is always contributed by $\vec{\sigma} := \{\sigma(123), \sigma(124), \sigma(134), \sigma(234)\} = \{4, 2, 2, 0\} \equiv \{4, -2, -2, 0\} =: \vec{\sigma}_{min}$. It is contributed by the spin configurations listed in table 5 (here $j_5 = j_{max}$).

²⁵This result is proved below in section 7.4.2.

²⁶This is just a fictive example to illustrate our point.

$\vec{\sigma}$ -index	Decreasing $\vec{\sigma}$ -config.	$\vec{\sigma}$ -index	Decreasing $\vec{\sigma}$ -config.	$\vec{\sigma}$ -index	Constant $\vec{\sigma}$ -config.	$\vec{\sigma}$ -index	Increasing $\vec{\sigma}$ -config.
1	4 2 2 0 4 -2 -2 0	15	4 -2 -4 2 4 2 -4 -2	30	2 0 0 0	31	2 2 -2 0 2 2 2 0 2 -2 -2 0
2	4 4 2 0 4 4 -2 0 2 -4 -2 0 2 4 -2 0	16	2 0 -2 4 2 0 -2 -4	32	0 2 0 0	33	0 0 0 2
3	2 2 4 0 2 2 -4 0	17	4 4 0 -2 4 4 0 2	34	0 0 2 0	35	2 -2 0 2 2 2 0 -2 2 2 0 2
4	4 -2 0 2 4 2 0 -2	18	2 0 -4 2 2 0 4 2	36	0 2 0 -2 2 0 0 2 0 2 2 0 2 0 -2 0 2 2 0 0	37	0 2 2 -2 0 2 -2 -2 0 2 2 2
5	4 2 -4 0 4 -2 -4 0	19	0 4 2 2 0 4 -2 -2	38	2 -2 -2 2 2 2 2 2 2 2 -2 -2	39	2 0 -2 2 2 0 -2 -2 2 0 2 2
6	2 4 4 0 2 -4 -4 0	20	4 -2 -2 4 4 2 2 4	40	0 0 2 2		
7	4 0 2 2 4 0 -2 -2	21	0 2 4 -2 0 2 -4 -2				
8	2 -4 -2 4 2 4 -2 -4	22	0 2 2 -4 0 2 2 4				
9	0 4 -2 -4 0 4 2 -4	23	4 4 -2 -2 4 4 2 2				
10	2 -4 -4 2 2 4 4 2	24	4 -2 0 4 4 2 0 4				
11	0 4 4 -2 0 4 4 2	25	4 0 -2 4 4 0 2 4				
12	2 -4 0 2 2 4 0 2	26	2 4 0 -4 2 -4 0 4				
13	2 2 0 4 2 2 0 -4	27	0 2 -4 -4 0 2 4 4				
14	4 0 -4 -2 4 0 -4 2	28	2 2 4 4 2 2 -4 -4				
		29	2 0 -4 -4 2 0 4 4				

Table 4: Equivalence classes of $\vec{\sigma}$ -configurations with regard to $\lambda_{\vec{V}}^{(\min)}(j_{\max})$. The $\vec{\sigma}$ -configurations are grouped in accordance with the behavior of the smallest eigenvalues.

These minimum eigenvalues are plotted in figure 17, with the eigenvalue axis in log scale. Note that the eigenvalues become comparable to the numerical noise at around $j_{\max} = \frac{35}{2}$. This can also be seen in the breaking of the spin-pattern in table 5 for $j_5 = j_{\max} > \frac{35}{2}$. By inspection of figure 17 one can extract information on the behavior of $\lambda_{\vec{V}}^{(\min)}$ depending on j_{\max} . A linear fit for a chosen set of data (see caption of figure 18) reveals that $\lambda_{\vec{V}}^{(\min),(fit)}(2 \cdot j_{\max}) \approx e^{(3.395 \pm 0.073)} e^{-(0.394 \pm 0.003)2 \cdot j_{\max}}$. We find that $\chi^2 := \sum_{k=1}^{11} (\lambda_{\vec{V}}^{(\min),(fit)}(j_{\max}^{(k)}) - \lambda_{\vec{V}}^{(\min)}(j_{\max}^{(k)}))^2 = 7.7 \cdot 10^{-10}$ for the chosen set of 11 data points.

In order to show the generic behavior of the smallest eigenvalue sequences we have included figure 19. Note that the eigenvalue sequences are not always clearly separated from each other numerically, even when the eigenvalues are large compared to the numerical errors. They are also not always monotonically decreasing. This can be traced back to the following two reasons: Firstly certain eigenvalue subsequences show up only above a certain value of j_{\max} , therefore we can expect a ‘change of the smallest eigenvalue sequence’ as j_{\max} increases. Secondly, gauge invariance demands the sum of the five spins be an integer. Hence the spin configuration which gives rise to the matrix contributing the smallest eigenvalue can be forced to change, depending on the parity of j_{\max} : we may ‘jump’ between different eigenvalue sequences which contribute the smallest eigenvalue. These effects give rise to a sort of ‘oscillating’ curve, whose enveloping curve nevertheless still decreases. As the numerical noise is approached at $j_{\max} > \frac{35}{2}$ a clean distinction between the smallest two eigenvalue sequences is lost. Comparison with the numerical errors shown in figure 17, and figure 46, indicates that this is caused by numerical noise.

Overall largest eigenvalues In the same way as for the minimum eigenvalues, we place the $\vec{\sigma}$ -configurations into equivalence classes according to the maximum eigenvalue sequence $\lambda_{\vec{V}}^{(\max)}(j_{\max})$. In this case there are only seven equivalence classes, out of the 85 $\vec{\sigma}$ -configurations. They are listed in table 6. The $\vec{\sigma}$ -indices listed there are used to plot the maximum eigenvalue sequences $\lambda_{\vec{V}}^{(\max)}(j_{\max})$ in figure 16.

The overall largest eigenvalue sequence is contributed by those $\vec{\sigma}$ -configurations which are contained in the equivalence class of $\vec{\sigma}$ -index 7. These maximum eigenvalues are plotted in figure 20, with the eigenvalue axis in log scale. It is interesting to note that the $\vec{\sigma}$ -configuration which gives rise to the smallest eigenvalues, $\vec{\sigma} = \{4, 2, 2, 0\} \equiv \{4, -2, -2, 0\}$, also lies in the equivalence class of $\vec{\sigma}$ -configurations which gives rise to the largest eigenvalues. Figure 21 shows a fit to $\lambda_{\vec{V}}^{(\max)}$ as $\lambda_{\vec{V}}^{(\max),(fit)}(2 \cdot j_{\max}) = e^{0.067 \pm 0.043} \cdot (2 \cdot j_{\max})^{1.484 \pm 0.013}$, with $\chi^2 := \sum_{k=1}^{29} (\lambda_{\vec{V}}^{(\max),(fit)}(j_{\max}^{(k)}) - \lambda_{\vec{V}}^{(\max)}(j_{\max}^{(k)}))^2 = 57.3$ for the chosen set of 29 data points.

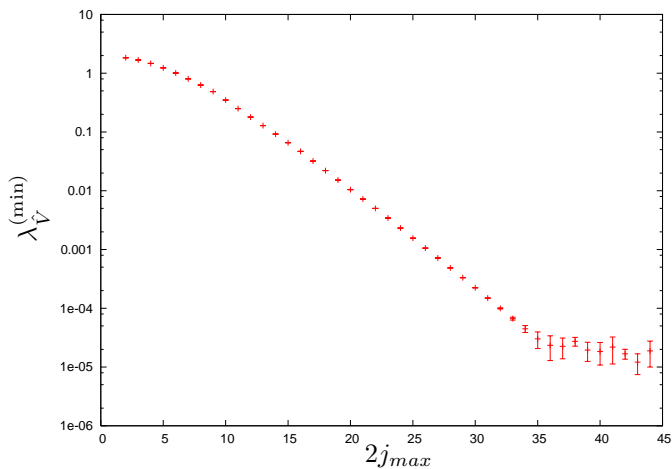


Figure 17: Smallest eigenvalue sequence at the gauge invariant 5-vertex, contributed by $\vec{\sigma}_{min} := \{\sigma(123), \sigma(124), \sigma(134), \sigma(234)\} = \{4, 2, 2, 0\}$. This is $\vec{\sigma}$ -index number 1 in figure 15.

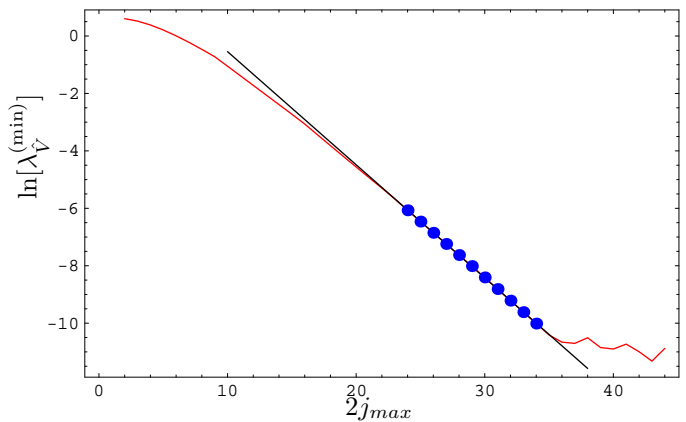


Figure 18: Fit of the logarithm $\ln[\lambda_{\hat{V}}^{(min)}]$ of the smallest eigenvalue sequence of figure 17. We have used $\lambda_{\hat{V}}^{(min)}(j_{max})$ for $j_{max} = \frac{24}{2}, \dots, \frac{34}{2}$ for the fitting (blue dots). The red line indicates the eigenvalue sequence of $\vec{\sigma}_{min}$, the black line the fit function.

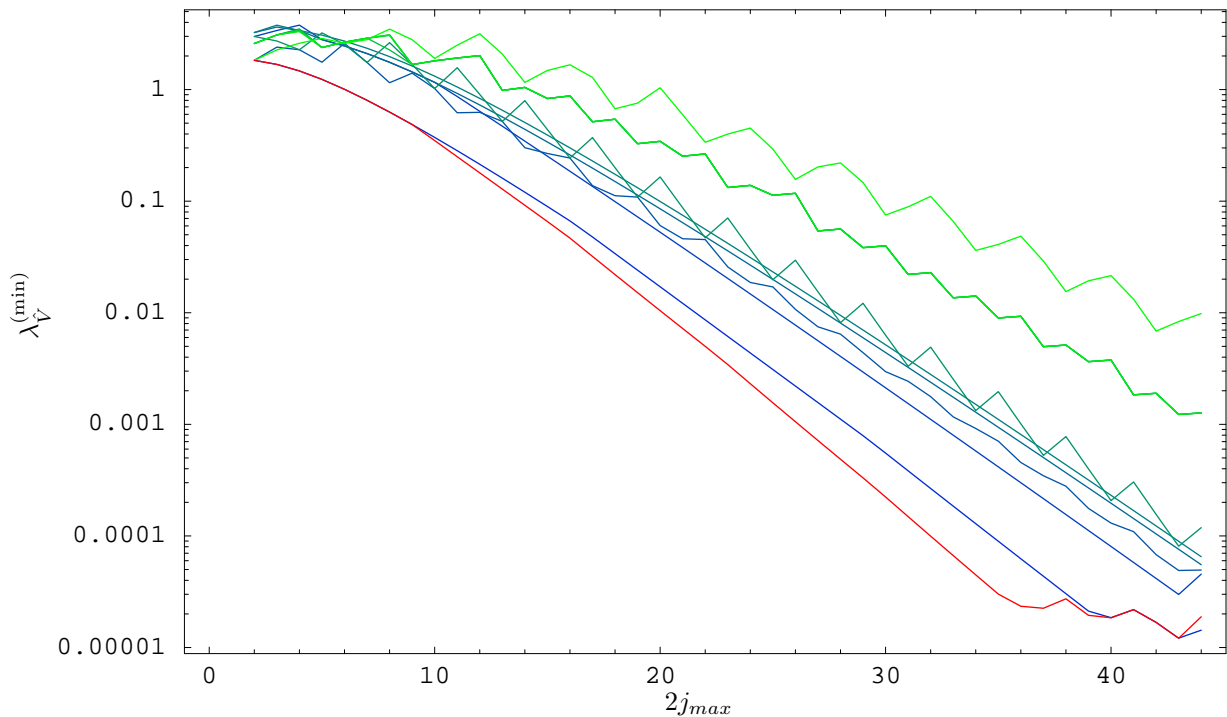


Figure 19: The twelve smallest eigenvalue sequences at the gauge invariant 5-vertex. The red line indicates $\vec{\sigma}_{min}$.

$2 \cdot j_1$	$2 \cdot j_2$	$2 \cdot j_3$	$2 \cdot j_4$	$2 \cdot j_5$
1	1	2	2	2
1	2	3	3	3
1	3	4	4	4
1	4	5	5	5
1	5	6	6	6
1	6	7	7	7
1	7	8	8	8
1	8	9	9	9
3	8	9	10	10
3	9	10	11	11
3	10	11	12	12
3	11	12	13	13
3	12	13	14	14
3	13	14	15	15
5	13	14	16	16
5	14	15	17	17
5	15	16	18	18
5	16	17	19	19
5	17	18	20	20
5	18	19	21	21
5	19	20	22	22
7	19	20	23	23
7	20	21	24	24
7	21	22	25	25
7	22	23	26	26
7	23	24	27	27
7	24	25	28	28
7	25	26	29	29
9	25	26	30	30
9	26	27	31	31
9	27	28	32	32
9	28	29	33	33
9	29	30	34	34
9	30	31	35	35
7	32	33	36	36
5	34	35	37	37
3	36	37	38	38
3	37	38	39	39
3	37	40	40	40
5	37	38	41	41
1	41	42	42	42
1	42	43	43	43
3	40	43	44	44

Table 5: The spin configurations contributing the smallest eigenvalues for $\vec{\sigma}_{min}$.

6.3.5 Number of Eigenvalues

According to (4.7) the number of eigenvalues $N_{\text{evals}}(j_{\text{max}})$ for configurations with $j_1 \leq j_2 \leq j_3 \leq j_4 \leq j_5 = j_{\text{max}}$ will be given by a polynomial of the order of $[j_{\text{max}}]^{2N-4} \equiv [j_{\text{max}}]^6$:

$$N_{\text{evals}}^{(fit)}(j_{\text{max}}) = \sum_{k=0}^6 r_k \cdot (j_{\text{max}})^k \quad (6.3)$$

with coefficients (and their 95% confidence interval)

$$\begin{pmatrix} r_0 = 106.59 & \pm 22515.70 \\ r_1 = 1523.19 & \pm 26095.85 \\ r_2 = -164.42 & \pm 9685.98 \\ r_3 = -8467.44 & \pm 1581.95 \\ r_4 = 9014.52 & \pm 126.55 \\ r_5 = 15678.82 & \pm 4.86 \\ r_6 = 5226.69 & \pm 0.07 \end{pmatrix}$$

For this fit the quantity $\chi^2 := \sum_{j_{\text{max}}=\frac{1}{2}}^{\frac{44}{2}} (N_{\text{evals}}(j_{\text{max}}) - N_{\text{evals}}^{(fit)}(j_{\text{max}}))^2$ takes the numerical value $\chi^2 = 2.26 \cdot 10^9$ for the set of 44 data points.

As in the case for the 4-vertex, one can also try a non linear two parameter fit $N_{\text{evals}}^{(fit)}(j_{\text{max}}) = r \cdot (j_{\text{max}})^s$, in order to measure the behavior of N_{evals} in the leading order in j_{max} . In this case we obtain $r = 9296.6 \pm 96.02$ and $s = 5.85582 \pm 0.00341$, $\chi^2 := \sum_{j_{\text{max}}=\frac{1}{2}}^{\frac{44}{2}} (N_{\text{evals}}(j_{\text{max}}) - N_{\text{evals}}^{(fit)}(j_{\text{max}}))^2 = 1.34 \cdot 10^{18}$ for the set of 44 data points (see figure 23).

$\vec{\sigma}$ - index	$\vec{\sigma}$ -config.	$\vec{\sigma}$ - index	$\vec{\sigma}$ -config.	$\vec{\sigma}$ - index	$\vec{\sigma}$ -config.	$\vec{\sigma}$ - index	$\vec{\sigma}$ -config.
1	0 0 2 2	5	2 2 4 4	6	2 -4 -4 2	7	2 4 4 0
	0 2 0 -2		2 2 -4 -4		2 4 4 2		2 -4 -4 0
	2 0 0 2		0 2 -4 -4		0 4 4 -2		4 2 -4 0
	0 0 0 2		0 2 4 4		0 4 4 2		4 -2 -4 0
2	0 2 2 0		2 0 -4 -4		4 -2 -4 2		2 2 4 0
	2 0 -2 0		2 0 4 4		4 2 -4 -2		2 2 -4 0
	0 0 2 0		2 -4 -2 4		4 0 -4 -2		4 4 2 0
	2 2 0 0		2 4 -2 -4		4 0 -4 2		4 4 -2 0
	0 2 0 0		0 4 -2 -4		0 2 4 -2		2 -4 -2 0
	2 0 0 0		0 4 2 -4		0 2 -4 -2		2 4 -2 0
3	2 -2 -2 2		4 -2 -2 4		4 4 -2 -2		4 2 2 0
	2 2 2 2		4 2 2 4		4 4 2 2		4 -2 -2 0
	2 2 -2 -2		2 4 0 -4		2 0 -4 2		
	0 2 2 -2		2 -4 0 4		2 0 4 2		
	0 2 -2 -2		4 0 -2 4		0 4 2 2		
	0 2 2 2		4 0 2 4		0 4 -2 -2		
	2 0 -2 2	0 2 2 -4	4 4 0 -2				
	2 0 -2 -2	0 2 2 4	4 4 0 2				
	2 0 2 2	4 -2 0 4	4 0 2 2				
	2 -2 0 2	4 2 0 4	4 0 -2 -2				
	2 2 0 -2	2 0 -2 4	2 -4 0 2				
	2 2 0 2	2 0 -2 -4	2 4 0 2				
	4	2 2 -2 0	2 2 0 4	4 -2 0 2			
		2 2 2 0	2 2 0 -4	4 2 0 -2			
2 -2 -2 0							

Table 6: Equivalence classes of $\vec{\sigma}$ -configurations with regard to $\lambda_{\vec{V}}^{(\max)}(j_{\max})$.

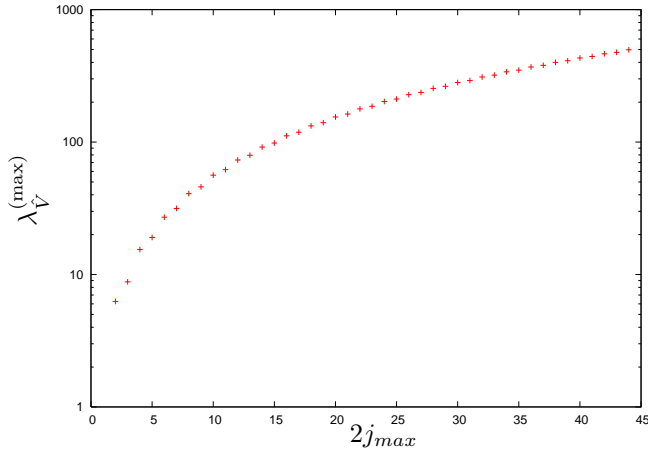


Figure 20: Largest eigenvalue sequence at the gauge invariant 5 vertex contributed by $\vec{\sigma}_{\min} := \{\sigma(123), \sigma(124), \sigma(134), \sigma(234)\}$ contained in the equivalence class with index number 7 in figure 16.

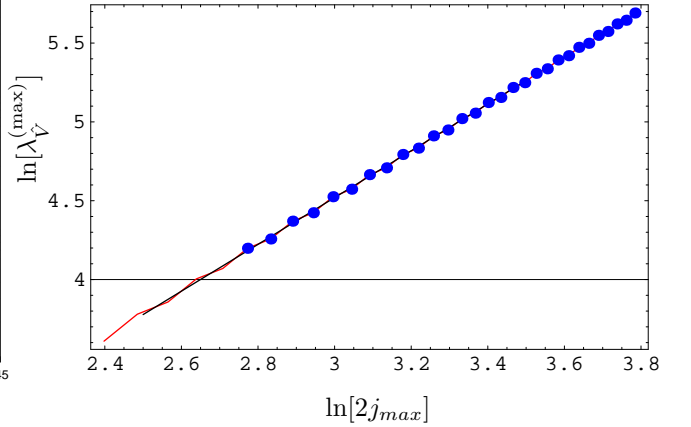


Figure 21: Fit of the logarithm $\ln[\lambda_{\vec{V}}^{(\max)}]$ of the largest eigenvalue sequence of figure 20 versus $\ln[2j_{\max}]$. We have used $\lambda_{\vec{V}}^{(\max)}(j_{\max})$ for $j_{\max} = \frac{16}{2}, \dots, \frac{44}{2}$ for the fitting (blue dots). The red line indicates the eigenvalue sequence, the black line the fit function given in the text.

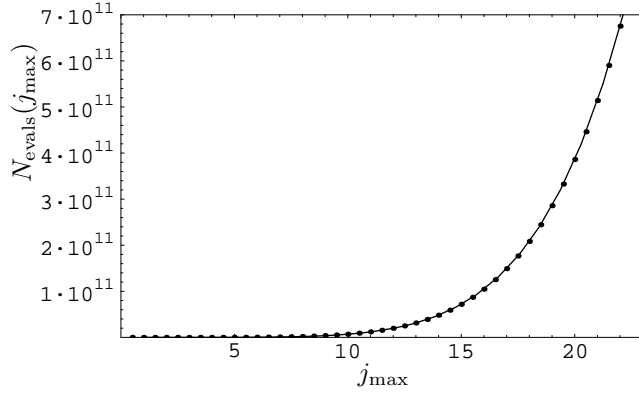


Figure 22: Number of eigenvalues (dots) at the 5-vertex, fitted by a sixth order polynomial (solid curve).

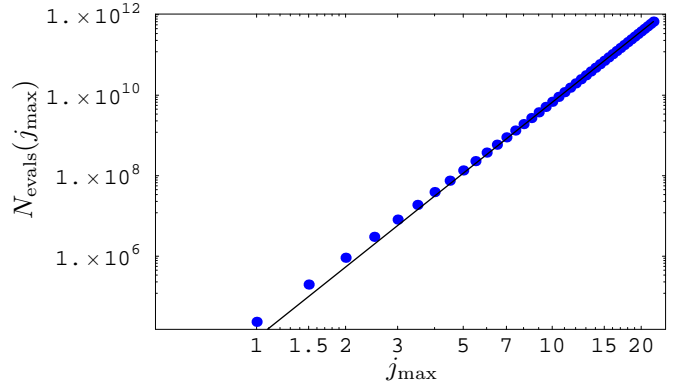


Figure 23: Number of eigenvalues at the 5-vertex in a double logarithmic plot for the two parameter minimum model.

6.4 Gauge Invariant 6-Vertex

There are 16413 $\vec{\sigma}$ -configurations for the 6-vertex, according to section 4.2.2. As mentioned in section 6.3.4, configurations which differ by an overall sign can be identified. Therefore (excluding $\sigma(IJK) = 0 \ \forall I < J < K$) we are left with 8206 non-trivial $\vec{\sigma}$ -configurations.

6.4.1 Histograms

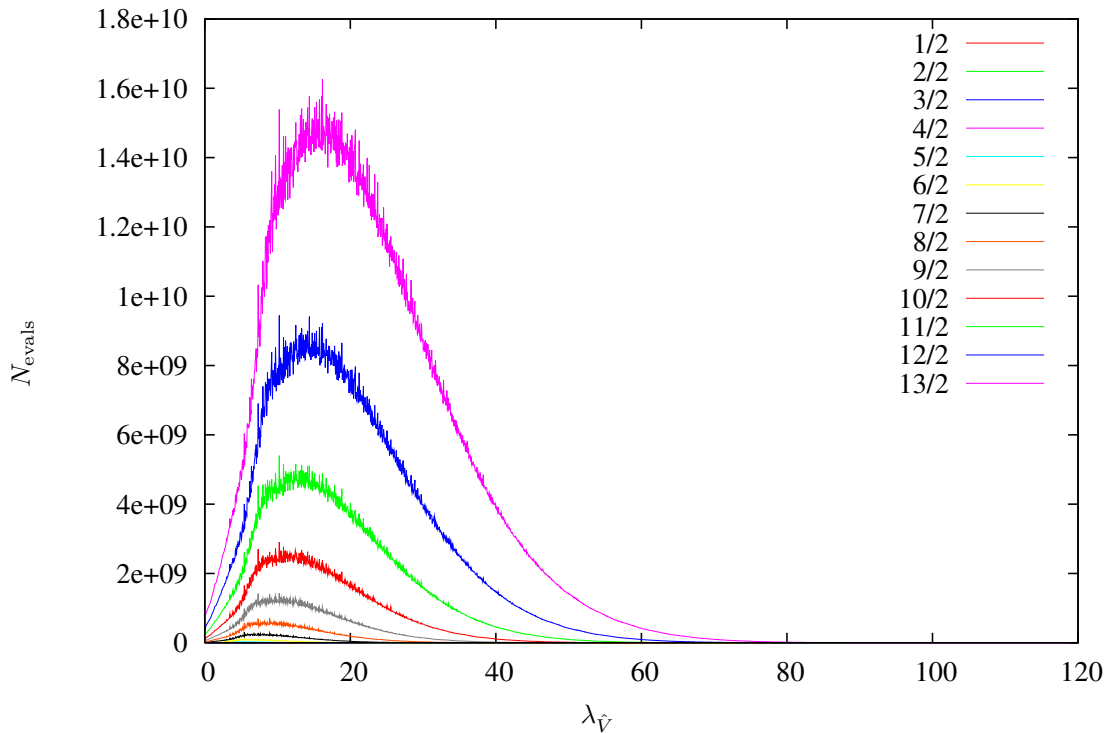


Figure 24: Overall histograms at the gauge invariant 6-vertex up to $j_{max} = \frac{13}{2}$. There are 7,349,844,794,112 eigenvalues in all, of which 212,946,944,688 are zero. $N_{bins} = 2048$.

As one can see in figure 24, the overall histograms for the gauge invariant 6-vertex show a similar behavior as those of the 4- and 5-vertex. However, there is no ‘lip’ in the spectral density close to zero visible (and quadrupling the number of bins does not alter this). Nevertheless the number of eigenvalues near zero increases with j_{max} and, as can be seen from section 6.4.3 below, the behavior of the smallest eigenvalue of a particular vertex configuration depends on its $\vec{\sigma}$ -configuration. Thus it seems that upon taking all eigenvalues from all $\vec{\sigma}$ -configurations the eigenvalues at the 6-valent vertex are rather equally spaced from 0 on, whereas the spectrum of the 5-vertex has an accumulation point

at 0. Nevertheless there are also single $\vec{\sigma}$ -configurations which show a lip in their spectral density, as demonstrated in figure 27.

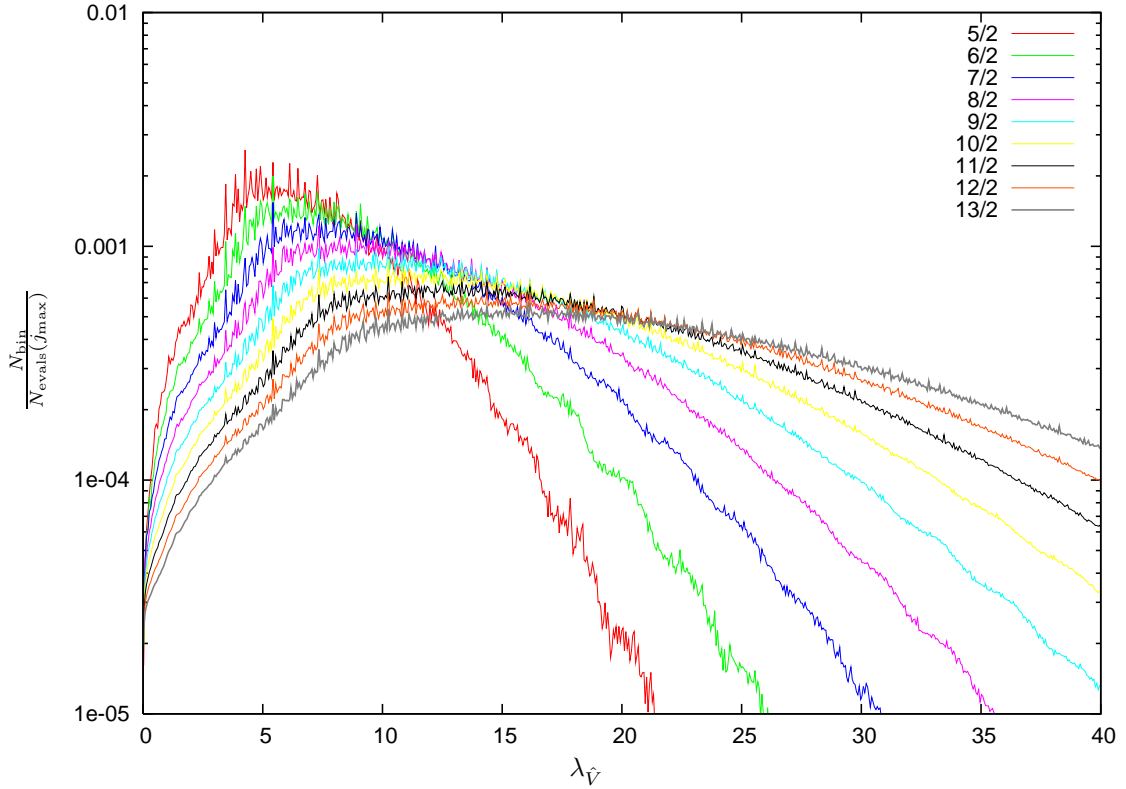


Figure 25: Normalized overall histogram for the 6-vertex. The vertical axis is in logscale. The histograms for the smallest four values of j_{\max} have been removed to give a clearer picture of the behavior at larger j_{\max} . $N_{\text{bins}} = 2048$.

In figure 25 we show the normalized overall histogram for the 6-vertex, analogous to figure 10 of section 6.3.1, in which each bin occupation number N_{bin} has been divided by the total number of eigenvalues $N_{\text{evals}}(j_{\max})$ at that j_{\max} . There we see that, as opposed to the situation with the 5-vertex, the normalized spectral density does decrease close to zero.

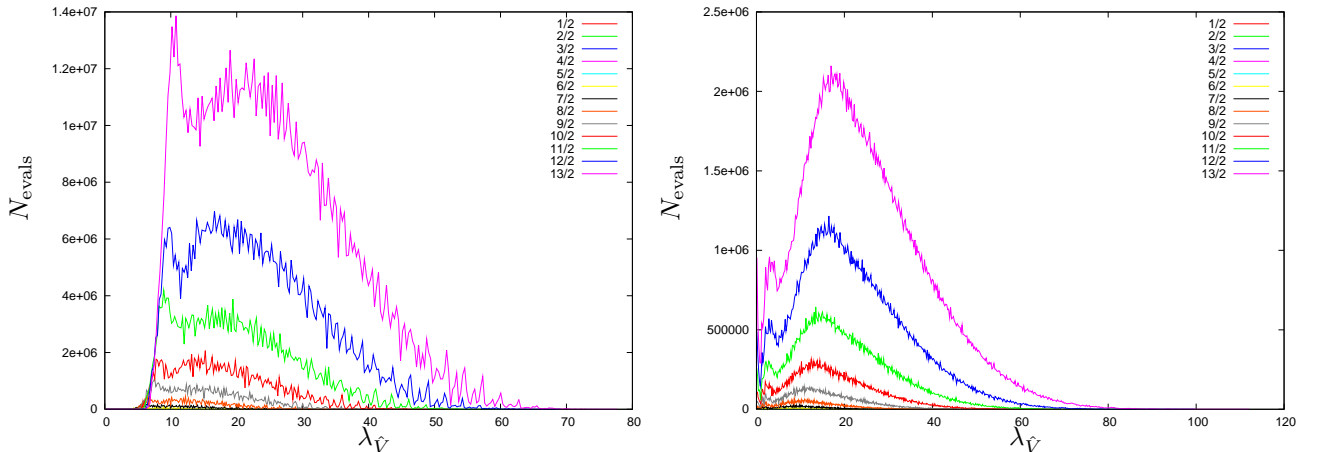


Figure 26: Two sample histograms for fixed $\vec{\sigma}$ -configuration. On the left $\vec{\sigma} = (0, 0, 0, 2, 2, 2, 2, 2, 2, 2)$ and on the right $\vec{\sigma} = (2, -4, -4, 0, 0, 0, 4, 2, 2, 0)$.

Figure 26 shows two histograms for fixed $\vec{\sigma}$ -configuration $\vec{\sigma} = (\sigma(123), \sigma(124), \sigma(125), \sigma(134), \sigma(135), \sigma(145), \sigma(234), \sigma(235), \sigma(245), \sigma(345))$. The $\vec{\sigma}$ -configuration on the left yields a minimum eigenvalue which increases with j_{\max} , while the $\vec{\sigma}$ -configuration on the right yields a decreasing minimum eigenvalue. Some details regarding these histograms are listed in table 7. Figure 27 shows the portion of the histograms on the right side of figure 26 for $\lambda_{\hat{V}} \leq 10$. There we see the lip quite clearly, which indicates that it is the ‘averaging’ over all $\vec{\sigma}$ -configurations which causes the lip to be flattened out in figure 24.

$\vec{\sigma}$ -configuration									$\chi_{\vec{\sigma}}$	N_{zeros}	N_{bins}	behavior
0	0	0	2	2	2	2	2	2	8	169,083,736	256	increasing $\lambda_{\hat{V}}^{(\min)}$
2	-4	-4	0	0	0	4	2	2	2	2,998,262	512	decreasing $\lambda_{\hat{V}}^{(\min)}$

Table 7: Details of two fixed $\vec{\sigma}$ -configuration histograms for the 6-vertex.

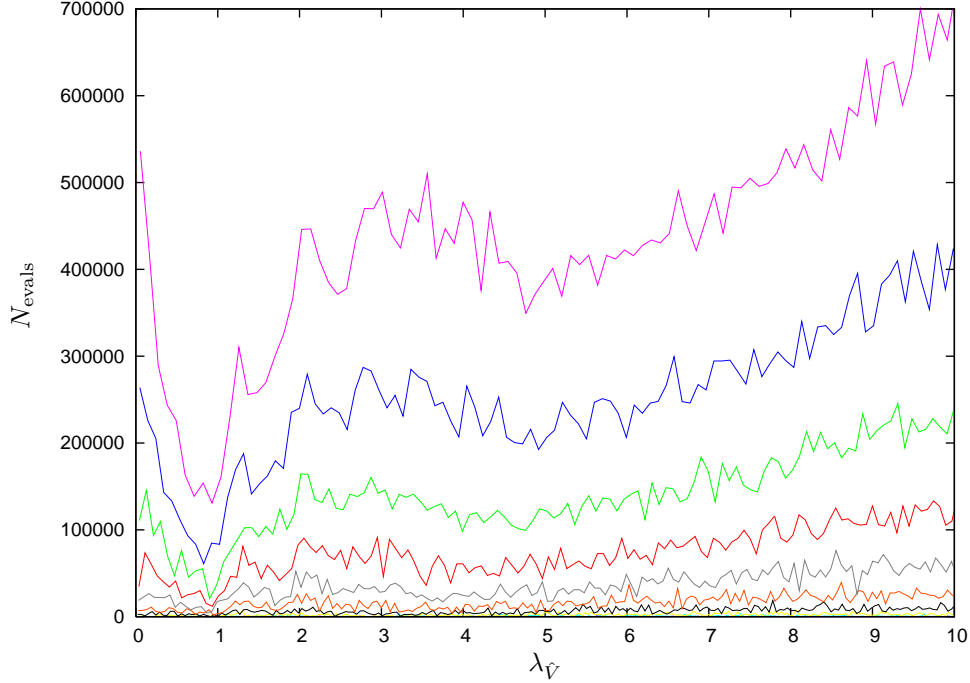


Figure 27: Zoom of the lip of the decreasing $\lambda_{\hat{V}}^{(\min)}$ histogram of figure 26. Here we use $N_{\text{bins}} = 1024$ to show more detail.

6.4.2 Fitting of Histograms

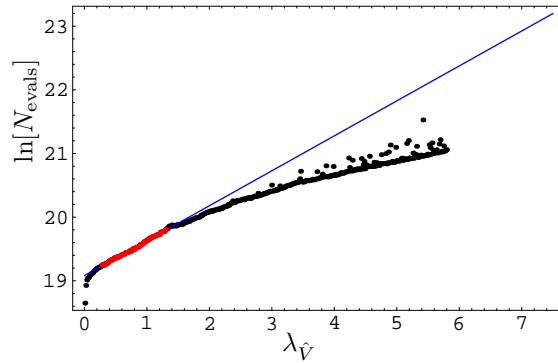


Figure 28: Logarithmic plot of the fit to the rising edge at the gauge invariant 6-vertex. The points that were used in the fitting process are indicated in red, the fitted function is the solid blue line.

As in section 6.3.3, figure 24 seems to possess a spectral density which rises exponentially with j_{max} . A fit to this rising edge is shown in figure 28, in which the logarithm of the number N_{evals} of eigenvalues as a function of the eigenvalue $\lambda_{\hat{V}}$ is given by:

$$\ln[N_{\text{evals}}(\lambda_{\hat{V}})]^{(fit)} = (19.081 \pm 0.007) + (0.549 \pm 0.008)\lambda_{\hat{V}} \quad \longrightarrow \quad N_{\text{evals}}^{(fit)}(\lambda_{\hat{V}}) \sim 0.19 \cdot 10^9 \cdot e^{0.55 \lambda_{\hat{V}}} \quad (6.4)$$

The quantity $\chi^2 := \sum_{k=1}^{71} (N_{\text{evals}}^{(fit)}(\lambda_{\hat{V}}^{(k)}) - N_{\text{evals}}^{(k)}(\lambda_{\hat{V}})) ^2$ has the numerical value $\chi^2 = 7.257 \cdot 10^{14}$ on the chosen set of 71 data points.

		$\lambda_{\hat{V}}^{(\min)}$	$\lambda_{\hat{V}}^{(\max)}$
increasing σ -conf.	equiv. classes	58	30
	total	323	8206
decreasing σ -conf.	equiv. classes	3645	-
	total	7856	-
constant σ -conf.	equiv. classes	5	-
	total	27	-

Table 8: Numbers of equivalence classes of $\vec{\sigma}$ -configurations for increasing and decreasing minimum eigenvalue, and maximum eigenvalue, for the 6-vertex. The information whether a configuration is increasing, decreasing or constant is obtained by comparing the (minimum) eigenvalue for $j_{\max} = 2$ with that from $j_{\max} = \frac{13}{2}$.

6.4.3 Extremal Eigenvalues

Table 8 shows the number of equivalence classes of $\vec{\sigma}$ -configurations for both the decreasing and increasing minimum eigenvalues, as in section 6.3.4.

Smallest Eigenvalue

Figure 29 shows how the smallest eigenvalue varies with j_{\max} for a sample of 21 $\vec{\sigma}$ -configurations. As is the case for the 5-vertex, some $\vec{\sigma}$ -configurations lead to rising minimum eigenvalues, and some to falling. Figure 30 shows the same for a collection of $\vec{\sigma}$ -configurations which only yield a decreasing minimum eigenvalues.

As it turns out, it is not possible to identify a genuine smallest eigenvalue sequence for the 6-vertex, at least not in the computed spin parameter range. This is due to the fact that the different eigenvalue sequences intersect each other and can hardly be separated. Figure 31 illustrates this property. Nevertheless we can define a smallest eigenvalue sequence by taking into account the ordering of the smallest eigenvalue sequences at a fixed j_{\max} . The chosen sequence is displayed as red curve in figure 31, it is obtained by comparing all eigenvalue sequences at $j_{\max} = \frac{13}{2}$. It is contributed by the spin configurations shown in table 9 (here $j_6 = j_{\max}$).

$2 \cdot j_1$	$2 \cdot j_2$	$2 \cdot j_3$	$2 \cdot j_4$	$2 \cdot j_5$	$2 \cdot j_6$
1	1	1	1	1	1
1	1	1	1	1	2
2	2	3	3	3	3
1	1	3	3	4	4
1	1	3	3	5	5
1	1	5	5	6	6
1	2	2	3	7	7
1	1	7	7	8	8
1	1	7	7	9	9
1	1	9	9	10	10
1	1	9	9	11	11
1	1	11	11	12	12
1	1	11	11	13	13

Table 9: The spin configurations contributing the smallest eigenvalues for $\vec{\sigma}_{\min} = (2, 0, 0, 0, 0, 0, 0, 0, -2, 0), (2, 0, 0, 0, 0, 0, 0, 0, 2, 0)$.

We can then (as in case if the 5-vertex) apply a fitting of $\ln[\lambda_{\hat{V}}^{(\min)}]$ versus $2j_{\max}$. A linear fit for a chosen set of data (see caption of figure 32) reveals that $\lambda_{\hat{V}}^{(\min)}(j_{\max}) = e^{(3.723 \pm 1.119)} e^{-(1.215 \pm 0.130)2 \cdot j_{\max}}$. Here $\chi^2 := \sum_{k=1}^{11} (\lambda_{\hat{V}}^{(\min), (fit)}(j_{\max}^{(k)}) - \lambda_{\hat{V}}^{(\min)}(j_{\max}^{(k)}))^2 = 0.32$ for the chosen set of 11 spin configurations.

Largest Eigenvalue

In figure 33 we show the maximum eigenvalues for the 30 equivalence classes (according to the maximum eigenvalues) of $\vec{\sigma}$ -configurations.

Figure 34 displays a fit to the largest of the maximum eigenvalue sequences. The fitting function is $\lambda_{\hat{V}}^{(\max)}(j_{\max}) = e^{0.270 \pm 0.026} \cdot (2 \cdot j_{\max})^{1.4108 \pm 0.012}$. Moreover $\chi^2 := \sum_{k=1}^{10} (\lambda_{\hat{V}}^{(\max), (fit)}(j_{\max}^{(k)}) - \lambda_{\hat{V}}^{(\max)}(j_{\max}^{(k)}))^2 = 0.23$ for the chosen set of 10 values of j_{\max} .

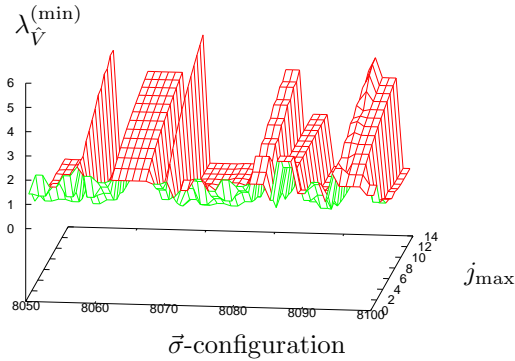


Figure 29: Minimum eigenvalue vs. j_{\max} for an arbitrary sampling of 21 $\vec{\sigma}$ -configurations. (In all plots for the 6-vertex, the integers labeling the $\vec{\sigma}$ -configurations have no intrinsic meaning.)

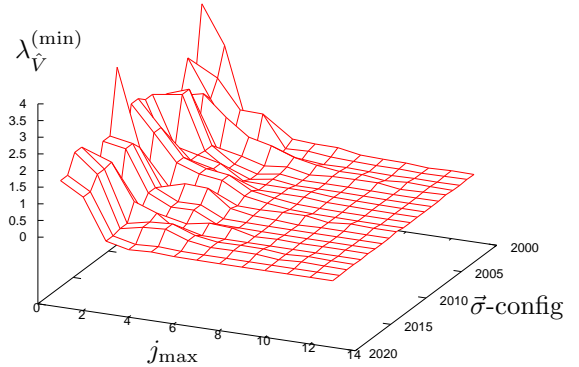


Figure 30: Minimum eigenvalue vs. j_{\max} for a sampling of 21 $\vec{\sigma}$ -configurations for which all $\lambda_V^{(\min)}$ decrease with j_{\max} .

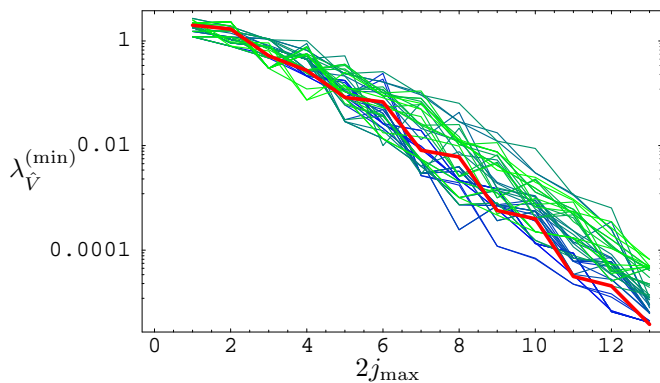


Figure 31: The 50 smallest eigenvalue sequences (sorted with respect to the smallest eigenvalue at $j_{\max} = \frac{13}{2}$) at the gauge invariant 6-vertex. The red line indicates the smallest eigenvalues from $\vec{\sigma}_{\min}$ in this ordering.

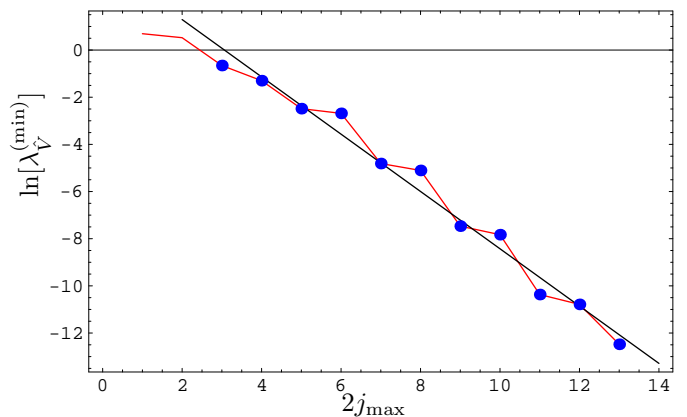


Figure 32: A curve for for the smallest eigenvalue sequence of the 6-vertex, which occurs for $\vec{\sigma}_{\min} = (2, 0, 0, 0, 0, 0, 0, -2, 0), (2, 0, 0, 0, 0, 0, 0, 0, 2, 0)$. We have used $\lambda_V^{(\min)}(j_{\max})$ for $j_{\max} = \frac{3}{2}, \dots, \frac{13}{2}$ for the fitting (blue dots). The red line indicates the eigenvalue sequence of $\vec{\sigma}_{\min}$, the black line the fit function. The error bars for these data points appear in figure 51.

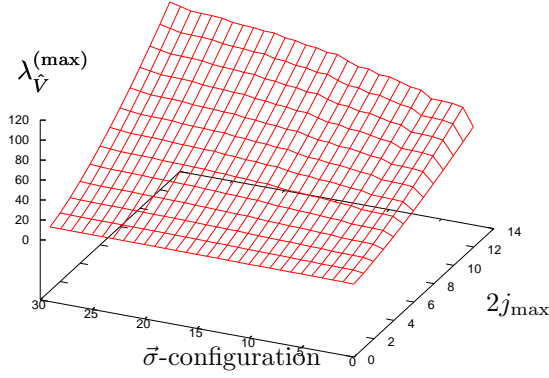


Figure 33: Maximum eigenvalue vs. j_{\max} for the 30 $\vec{\sigma}$ -configuration equivalence classes at the 6-vertex.

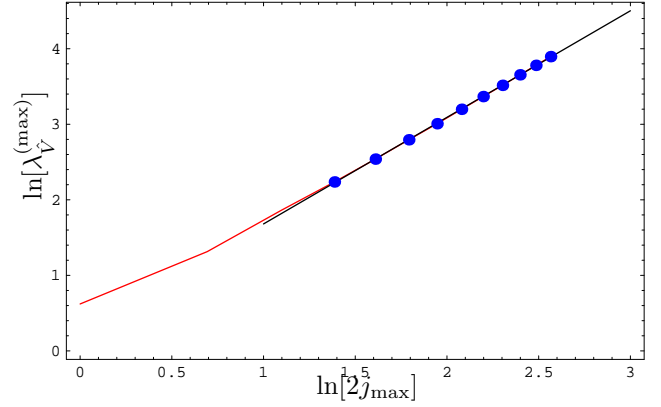


Figure 34: Fit of the logarithm $\ln[\lambda_{\vec{V}}^{(\max)}]$ of the largest eigenvalue sequence of figure 33 ($\vec{\sigma}$ -configuration index 30) versus $\ln[2j_{\max}]$. We have used $\lambda_{\vec{V}}^{(\max)}(j_{\max})$ for $j_{\max} = \frac{4}{2}, \dots, \frac{13}{2}$ for the fitting (blue dots). The red line indicates the eigenvalue sequence, the black line the fit function given in the text.

6.4.4 Number of Eigenvalues

According to (4.7) the number of eigenvalues $N_{\text{evals}}(j_{\max})$ for configurations with $j_1 \leq j_2 \leq j_3 \leq j_4 \leq j_5 \leq j_6 = j_{\max}$ will be given by a polynomial of the order of $[j_{\max}]^{2N-4} \equiv [j_{\max}]^8$:

$$N_{\text{evals}}^{(fit)}(j_{\max}) = \sum_{k=0}^8 r_k \cdot (j_{\max})^k \quad (6.5)$$

with coefficients (and their 95% confidence interval)

$$\begin{pmatrix} r_0 = 5.39 \cdot 10^6 \pm 2.20 \cdot 10^7 \\ r_1 = -2.42 \cdot 10^7 \pm 9.63 \cdot 10^7 \\ r_2 = 4.05 \cdot 10^7 \pm 1.56 \cdot 10^8 \\ r_3 = -3.38 \cdot 10^7 \pm 1.28 \cdot 10^8 \\ r_4 = 1.55 \cdot 10^7 \pm 5.89 \cdot 10^7 \\ r_5 = -4.74 \cdot 10^6 \pm 1.60 \cdot 10^7 \\ r_6 = 3.78 \cdot 10^6 \pm 2.55 \cdot 10^6 \\ r_7 = 2.50 \cdot 10^6 \pm 0.22 \cdot 10^6 \\ r_8 = 644618.00 \pm 7799.21 \end{pmatrix}$$

For this fit the quantity $\chi^2 := \sum_{j_{\max}=\frac{1}{2}}^{\frac{44}{2}} (N_{\text{evals}}(j_{\max}) - N_{\text{evals}}^{(fit)}(j_{\max}))^2$ takes the numerical value $\chi^2 = 3.64 \cdot 10^{11}$.

As in the case for the 4 and 5-vertex, one can also do a non linear fit to a minimal model $N_{\text{evals}}^{(fit)}(j_{\max}) = r \cdot (j_{\max})^s$, in order to get the behavior of N_{evals} in the leading order in j_{\max} . In this case we obtain $r = 2.94389 \cdot 10^6 \pm 85970$ and $s = 7.47748 \pm 0.01586$, $\chi^2 := \sum_{j_{\max}=\frac{1}{2}}^{\frac{44}{2}} (N_{\text{evals}}(j_{\max}) - N_{\text{evals}}^{(fit)}(j_{\max}))^2 = 3.49 \cdot 10^{19}$ for the set of 13 data points (see figure 36).

6.4.5 Cubic 6-Vertex

Here we include results for a 6-vertex which has linearly dependent edge tangent vectors. The cubic 6-vertex arises due to its convenient topology and geometry, and is frequently used in order to construct arbitrarily large periodic graphs with definite vertex structure. It is used in particular when working with coherent states, as in [9], as well in the recently initiated program [10]. As it turns out cubic 6-vertex configurations provide a volume gap: the smallest non-zero eigenvalue grows with the maximum spin.

Histogram

The cumulative histogram in figure 38 nicely illustrates two main parts of the spectrum: a rising edge for small $\lambda_{\vec{V}} \sim 10$, which at larger $\lambda_{\vec{V}}$ is dominated by the cutoff imposed by finite j_{\max} .

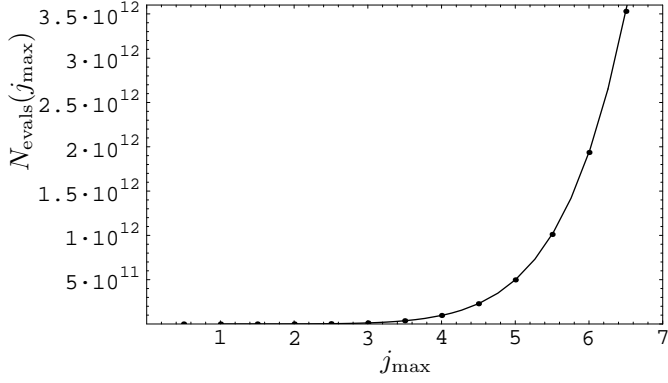


Figure 35: Number of eigenvalues at the 6-vertex fitted by a polynomial of degree eight (solid line).

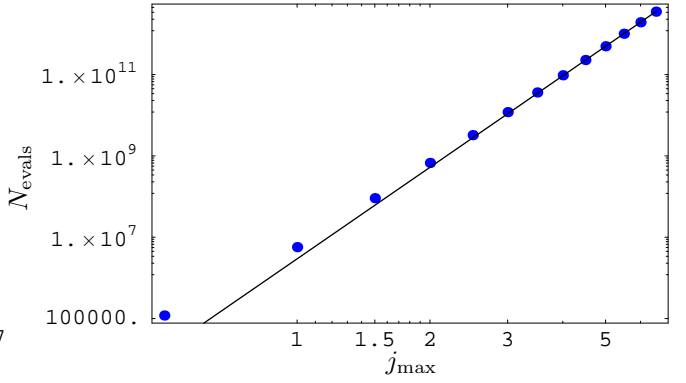


Figure 36: Log-log plot of the number of eigenvalues at the 6-vertex. The solid line shows a two parameter fit to the data.

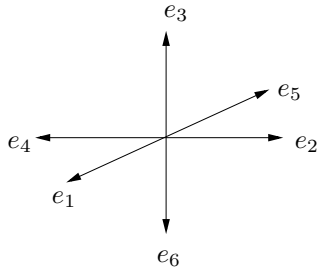


Figure 37: Cubic 6-vertex: setup and sign configuration.

$$\begin{aligned}
 \epsilon(123) &= 1 \\
 \epsilon(124) &= 0 & \epsilon(134) &= 1 \\
 \epsilon(125) &= 0 & \epsilon(135) &= 0 & \epsilon(145) &= 0 \\
 \epsilon(126) &= -1 & \epsilon(136) &= 0 & \epsilon(146) &= 1 & \epsilon(156) &= 0 \\
 \\
 \epsilon(234) &= 0 \\
 \epsilon(235) &= -1 & \epsilon(245) &= 0 \\
 \epsilon(236) &= 0 & \epsilon(246) &= 0 & \epsilon(256) &= -1 \\
 \\
 \sigma(123) &= 2 & \epsilon(345) &= -1 \\
 \sigma(124) &= 2 & \epsilon(346) &= 0 & \epsilon(356) &= 0 \\
 \sigma(125) &= 2 & & & \epsilon(456) &= 1 \\
 \\
 \sigma(134) &= 2 & \sigma(234) &= 0 \\
 \sigma(135) &= 0 & \sigma(235) &= -2 \\
 \\
 \sigma(145) &= -2 & \sigma(245) &= -2 & \sigma(345) &= -2
 \end{aligned}$$

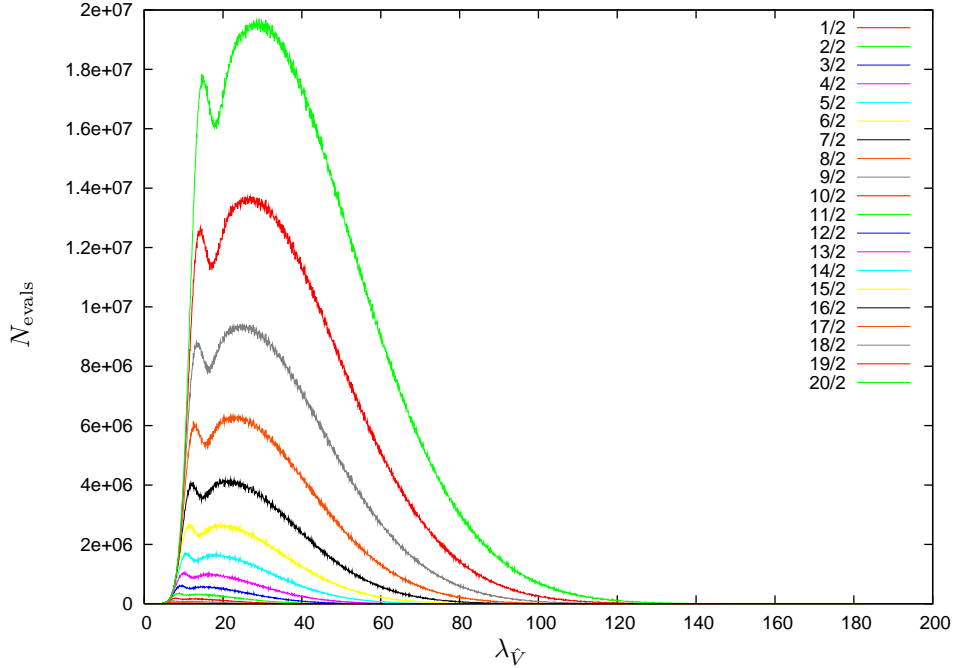


Figure 38: Overall histograms at the gauge invariant cubic 6-vertex up to $j_{max} = \frac{20}{2}$. There are 11,121,868,100 eigenvalues in all, of which 535,933,540 are zero. $N_{bins} = 2048$.

Extremal Eigenvalues

As one can see from the plot in figure 39, the cubic gauge invariant 6-vertex belongs to the class of $\vec{\sigma}$ -configurations having an increasing smallest non-zero eigenvalue $\lambda_V^{(min)}$ as the maximal spin j_{max} is increased. The oscillatory behavior

of the smallest non-zero eigenvalue can be traced back to different spin configurations which contribute the smallest eigenvalue for fixed $j_6 = j_{\max}$. We find (except for $j_1 = j_2 = j_3 = j_4 = j_5 = j_6 = j_{\max} = \frac{1}{2}$):

	j_1	j_2	j_3	j_4	j_5	j_6
j_{\max} half integer	$j_{\max} - 1$	$j_{\max} - \frac{1}{2}$	$j_{\max} - \frac{1}{2}$	$j_{\max} - \frac{1}{2}$	$j_{\max} - \frac{1}{2}$	j_{\max}
j_{\max} integer	$j_{\max} - \frac{1}{2}$	$j_{\max} - \frac{1}{2}$	$j_{\max} - \frac{1}{2}$	$j_{\max} - \frac{1}{2}$	j_{\max}	j_{\max}

This nicely illustrates the effect of gauge invariance, namely that the sum of all spins must be an integer in order to have the chance to recouple them to resulting 0 angular momentum.

The plot for the largest eigenvalues is given in figure 40.

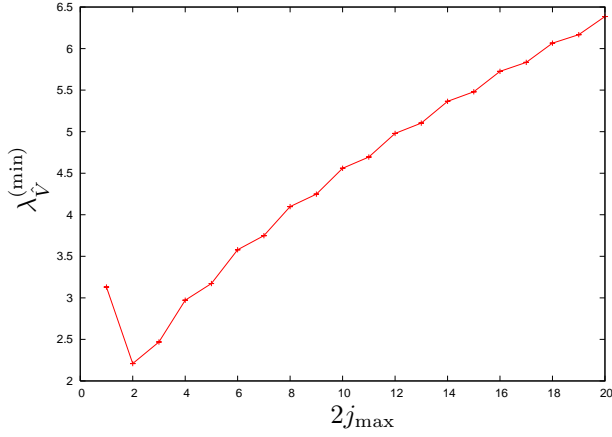


Figure 39: Smallest eigenvalues at the gauge invariant cubic 6-vertex up to $j_{\max} = \frac{20}{2}$.

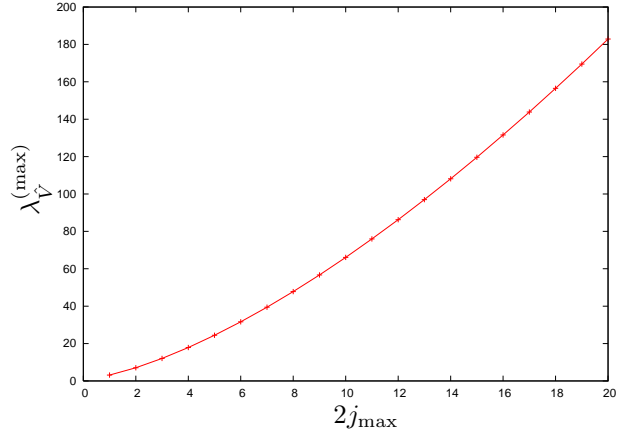


Figure 40: Largest eigenvalues at the gauge invariant cubic 6-vertex up to $j_{\max} = \frac{20}{2}$.

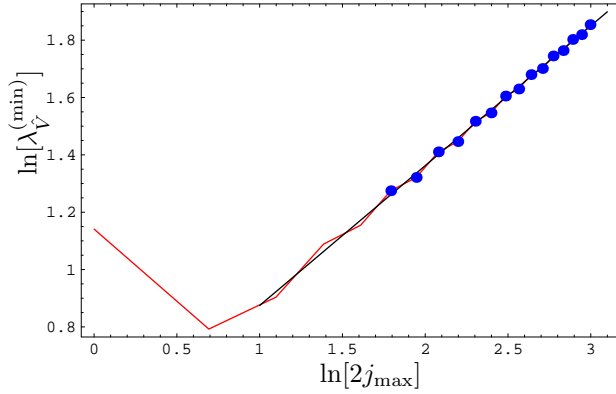


Figure 41: Fit of the smallest eigenvalue sequence at the gauge invariant cubic 6-vertex up to $j_{\max} = \frac{20}{2}$. We have used $\lambda_V^{(\min)}(j_{\max})$ for $j_{\max} = \frac{6}{2}, \dots, \frac{20}{2}$ for the fitting (blue dots). The red line indicates the minimum eigenvalue sequence, the black line the fit function.

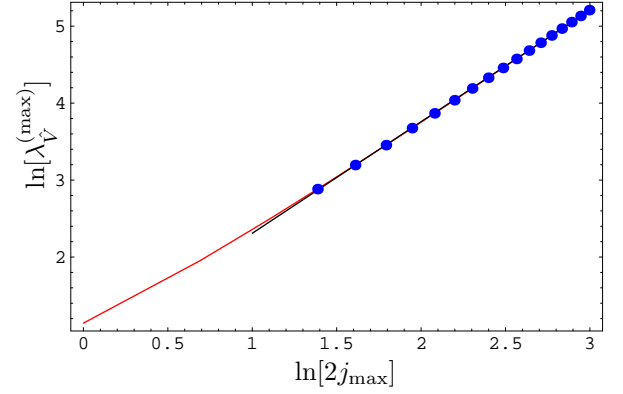


Figure 42: Fit of the largest eigenvalues at the gauge invariant cubic 6-vertex up to $j_{\max} = \frac{20}{2}$. We have used $\lambda_V^{(\max)}(j_{\max})$ for $j_{\max} = \frac{4}{2}, \dots, \frac{20}{2}$ for the fitting (blue dots). The red line indicates the maximum eigenvalue sequence, the black line the fit function.

In figures 41 and 42 we show fits of these data. The fitting functions are:

$$\lambda_V^{(\min),(fit)}(j_{\max}) = e^{0.387 \pm 0.036} (2j_{\max})^{0.4877 \pm 0.0144} \quad (6.6)$$

Here $\chi^2 := \sum_{k=1}^{15} \left(\lambda_V^{(\min),(fit)}(j_{\max}^{(k)}) - \lambda_V^{(\min)}(j_{\max}^{(k)}) \right)^2 = 0.02$ for the chosen set of 15 data points. For the largest eigenvalue sequence we obtain

$$\lambda_V^{(\max),(fit)}(j_{\max}) = e^{0.859 \pm 0.0157} (2j_{\max})^{1.44954 \pm 0.0064} \quad (6.7)$$

Here $\chi^2 := \sum_{k=1}^{17} \left(\lambda_V^{(\max),(fit)}(j_{\max}^{(k)}) - \lambda_V^{(\max)}(j_{\max}^{(k)}) \right)^2 = 4.04$ for the chosen set of 17 data points.

6.5 Gauge Invariant 7-Vertex

The 7-vertex has 3,079,875 $\vec{\sigma}$ -configurations, of which 1,912,373 are ‘non-trivial’ (not all zero, and not equivalent to another up to an overall sign). This, along with the septic number of spin configurations for a given j_{\max} , makes it extremely expensive computationally. Thus we have 7-vertex data only for much smaller spins than for the other valences (though simply in terms of number of eigenvalues our 7-vertex data vastly overwhelms that for smaller valences!).

6.5.1 Histograms

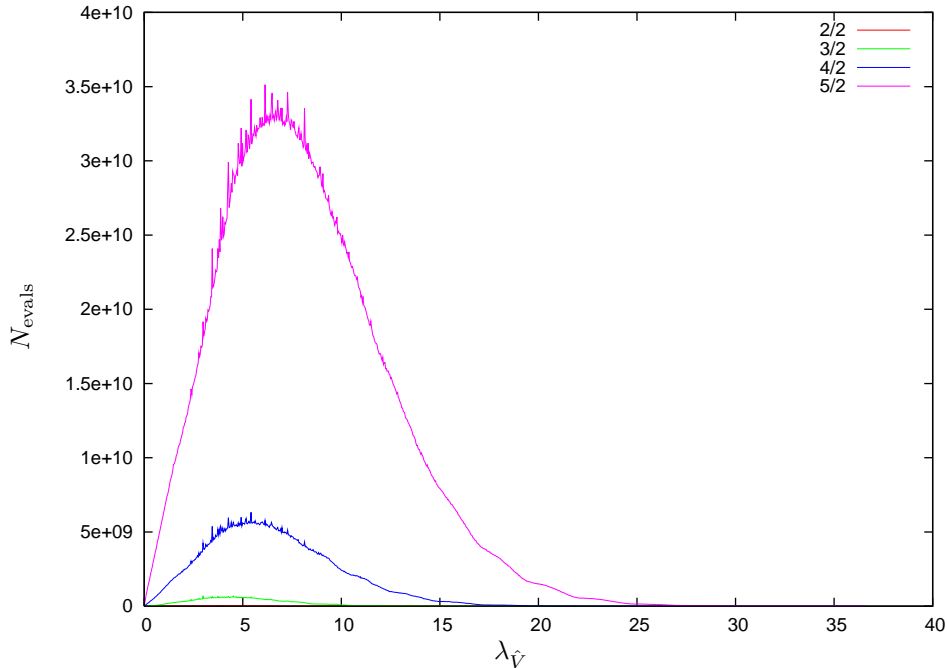


Figure 43: Overall histograms for the gauge invariant 7-vertex up to $j_{\max} = \frac{5}{2}$. There are 9,475,991,439,360 eigenvalues in all, of which 146,895,794,400 are zero. $N_{\text{bins}} = 2048$.

In figure 43 we again see no lip in the spectral density close to zero, and furthermore notice that the density appears to be linearly increasing for eigenvalues $\lesssim 3$. Both of these features are likely due to the fact that we have computed these spectra only up to the relatively small spin $j_{\max} = \frac{5}{2}$. At the 5-vertex, for small values of j_{\max} , we observe that there is no lip present (e.g. from figure 10). Additionally, at the 6-vertex, for extremely small values of j_{\max} , we also fail to observe an exponentially rising edge in the spectral density, but rather see linear growth as above. It seems likely, then, that both the exponentially increasing ‘edge’, and the lip at zero, will arise with larger j_{\max} , as it does at smaller valences.

6.5.2 Fitting of Histograms

As mentioned above, figure 43 seems to possess a spectral density which rises linearly rather than exponentially with λ_V . A fit to this rising edge is shown in figure 44, in which the logarithm of the number N_{evals} of eigenvalues as a function of the eigenvalue λ_V is given by:

$$\ln[N_{\text{evals}}(\lambda_V)]^{(fit)} = (19.72 \pm 0.084) + (0.7943 \pm 0.067)\lambda_V \quad \longrightarrow \quad N_{\text{evals}}^{(fit)}(\lambda_V) \sim 0.37 \cdot 10^9 \cdot e^{0.79 \lambda_V} \quad (6.8)$$

The quantity $\chi^2 := \sum_{k=1}^{51} (N_{\text{evals}}^{(fit)}(\lambda_V^{(k)}) - N_{\text{evals}}(\lambda_V^{(k)}))^2$ has the numerical value $\chi^2 = 1.25 \cdot 10^{16}$ on the chosen set of 51 data points. We find that, although the overall shape of the rising edge does not resemble a line in the logarithmic plot, the exponential fit is better than a linear fit, at least for the chosen set of data points.

Figure 44 seems to indicate that we have not yet entered the regime of large j_{\max} . As the exponential growth of the spectral density is expected to be a property of the spectrum at large j_{\max} , the exponential fitting is not obviously applicable for the computed range of spins.

6.5.3 Extremal Eigenvalues

As for the 5 and 6-vertices, by inspection of the eigenvalue data, we find smallest eigenvalue sequences which are decreasing, constant, or increasing as j_{\max} is increased.

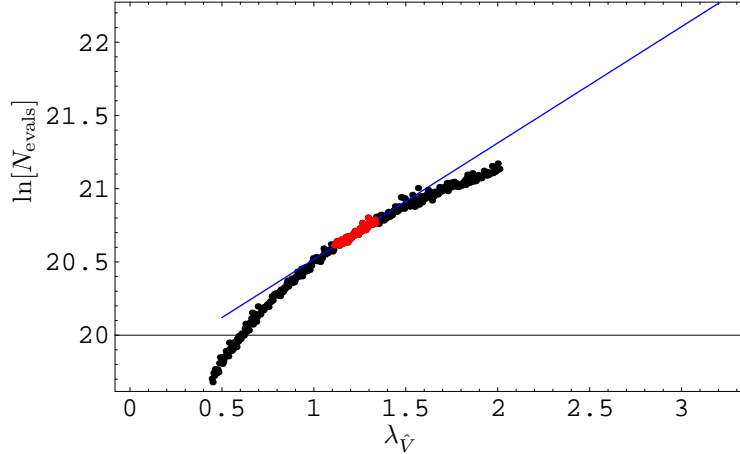


Figure 44: Logarithmic plot of the fit to the rising edge at the gauge invariant 7-vertex. The points that were used in the fitting process are colored red.

Since we can go only to a maximum spin of $j_{\max} = \frac{5}{2}$, we only have 4 data points (the case where all spins are equal to $\frac{1}{2}$ is excluded by the odd valence and the requirement that the sum of spins has to be integer in order to obtain gauge invariance), which is too few to identify an overall smallest eigenvalue sequence. However, we can take the overall smallest eigenvalue in our numerical data, which arises e.g. from $\vec{\sigma}$ -configuration $(2, 2, 2, -4, 0, 0, 0, 0, -2, -2, 2, 2, 4, -2, 4, 4, 0, 0, 0, -2)$,²⁷ and take this as the smallest eigenvalue $\vec{\sigma}$ -configuration. The smallest eigenvalues of this sequence are contributed by the following spin configurations (here $j_7 = j_{\max}$):

$2 \cdot j_1$	$2 \cdot j_2$	$2 \cdot j_3$	$2 \cdot j_4$	$2 \cdot j_5$	$2 \cdot j_6$	$2 \cdot j_7$
2	2	2	2	2	2	2
2	2	2	2	2	3	3
2	2	2	2	3	3	4
2	2	2	2	2	3	5

Table 10: The spin configurations contributing the overall smallest eigenvalue for $\vec{\sigma}_{\min} = (2, 2, 2, -4, 0, 0, 0, 0, -2, -2, 2, 2, 4, -2, 4, 4, 0, 0, 0, -2)$.

The overall smallest eigenvalue is contributed from the spin config with $j_7 = j_{\max} = \frac{5}{2}$, its numerical value is found to be $\lambda_{\vec{V}}^{(\min)}|_{j_{\max}=\frac{5}{2}} = 0.000597922$. By inspection of the data we find that this eigenvalue is in fact obtained from 120 different $\vec{\sigma}$ -configurations, each with the spin configuration in the last line of table 10. This already indicates the importance of understanding the orbits of the $\vec{\sigma}$ -configurations under permutations of the edges at a vertex [26]: We have partially fixed this symmetry by demanding ordered spins (2.39), however as 5 spins are equal in the spin configuration leading to $\lambda_{\vec{V}}^{(\min)}|_{j_{\max}=\frac{5}{2}}$, we are free to permute 5 out of 7 edges, that is we have $5! = 120$ possibilities, each giving a different $\vec{\sigma}$ -configuration.

6.6 Numerical Errors

An interesting feature of our data, which is discussed in section 6.3.1, is a ‘lip’ in the spectral density of the 5-vertex at eigenvalues near zero, as manifested in figure 9. One may be concerned whether this is a genuine feature of the theory, or if it arises from numerical noise. A look at figure 15 causes alarm, in that it shows the smallest non-zero eigenvalue decreasing monotonically to values arbitrarily close to zero. Since the numerical errors are obviously bounded away from zero by machine epsilon, for some finite j_{\max} the minimum eigenvalues must inevitably become comparable with the numerical noise.

6.6.1 Error bound provided by LAPACK

In presenting our data we regard as zero any singular value

$$s_i \leq T\delta s_i \tag{6.9}$$

where δs_i is given by eqn. (5.4) and T is a constant numerical threshold. As we reduce T , we will regard smaller and smaller eigenvalues as non-zero. For the data presented up to this point $T = 1$. From section 5.3 we recall that the

²⁷The sigmas are again ordered in the same pattern as for the smaller valences, i.e. 123 124 125 126 134 135 136 145 146 156 234 235 236 245 246 256 345 346 356 456.

eigenvalues are related to the singular values by $\lambda_{\hat{V}} = \sqrt{s_i}$, so in terms of the eigenvalues, our error bound is

$$\delta\lambda_{\hat{V}} = \frac{\delta s_i}{2\sqrt{s_i}} = \frac{\delta s_i}{2\lambda_{\hat{V}}} \quad (6.10)$$

The δs_i are proportional to the largest singular value of the matrix which gives rise to s_i . This is bounded by the square of the largest eigenvalues which occur. A more significant effect is that, because of the square root, the errors in the eigenvalues are inversely proportional to the eigenvalues themselves. Thus at large j_{\max} , as $\lambda_{\hat{V}}$ converges to zero, our errors grow without bound. Because of this the computation of volume eigenvalues for valences $N > 4$ is bounded by machine precision, rather than computation time or system memory.

The error bars in figure 15 reveal that, for the 5-vertex, the smallest non-zero eigenvalues are comparable with our error bound for $j_{\max} \gtrsim \frac{35}{2}$. Figure 45 portrays the closeness of the remainder of our 5-vertex dataset to the LAPACK

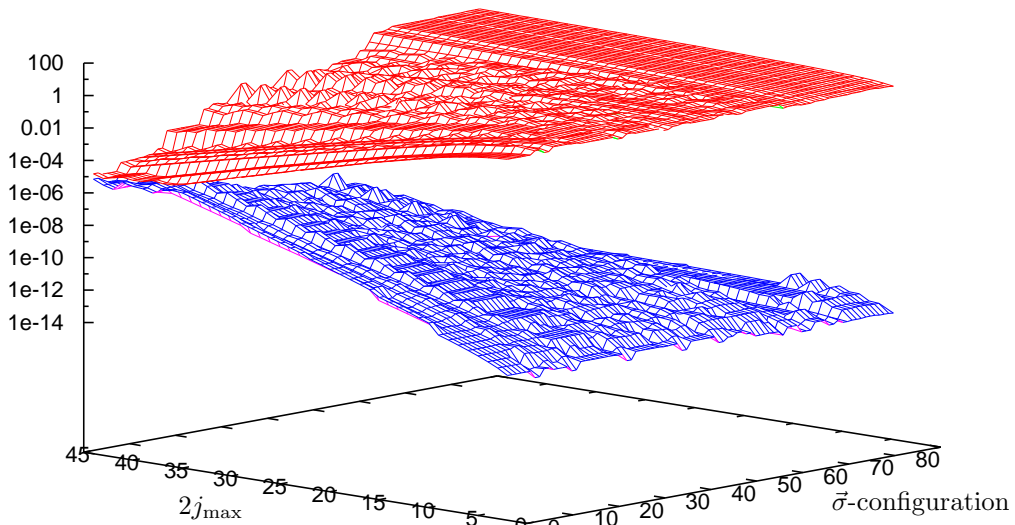


Figure 45: Smallest non-zero eigenvalues of 5-vertex (top, red), along with their LAPACK error bound (bottom, blue). The vertical axis is in logscale.

error bound. The top (red) surface is the minimum eigenvalues for each $\vec{\sigma}$ -configuration and j_{\max} . (This is equivalent to figure 15.²⁸) The bottom (blue) surface is the LAPACK error bound for these minimum eigenvalues. The vertical axis is in logscale. Note that the errors grow in inverse proportion to the eigenvalues, as expected by (6.10). They become comparable only for a tiny ‘corner’ of the dataset, with $j_{\max} \gtrsim \frac{35}{2}$, and $\vec{\sigma}$ -indices (from table 4) 1–4. (The smallest eigenvalues are always greater than the error bound by construction, c.f. (6.9) with $T = 1$.) Zooming into this corner, as shown in figure 46, illustrates the effect of the error bound. Consider the $\vec{\sigma}$ -configurations labeled 6 and 7. (These are $\vec{\sigma}$ -index 3 in table 4.) The smallest non-zero eigenvalue decreases steadily until $j_{\max} = \frac{41}{2}$, at which point it rises suddenly. For $\vec{\sigma}$ -configurations 2–4 we see similar behavior, with the smallest non-zero eigenvalue rising at $j_{\max} = \frac{41}{2}$, and $\vec{\sigma}$ -configurations 0 and 1 see a rise at both $j_{\max} = \frac{41}{2}$ and $\frac{38}{2}$. This is likely due to the smallest non-zero eigenvalue dipping below the error threshold, such that it is regarded as zero from inequality (6.9). Then the next-smallest eigenvalue is regarded as zero, resulting in an apparent jump in figure 46. Thus we can see that some small number of our non-zero eigenvalues, for $j_{\max} \gtrsim \frac{36}{2}$, are descending beneath our error bound. In section 6.6.3 we will estimate the number of eigenvalues that are thus ‘lost’.

6.6.2 Characterization of true numerical noise

How well does the error bound provided by LAPACK describe our numerical noise? To explore this question, we can vary T in (6.9), and watch what happens to our data.

²⁸The $\vec{\sigma}$ -configurations of figure 45 are labeled by a sequential index (starting from zero) over the $\vec{\sigma}$ -configurations shown in table 4, rather than the $\vec{\sigma}$ -indices of figure 15.

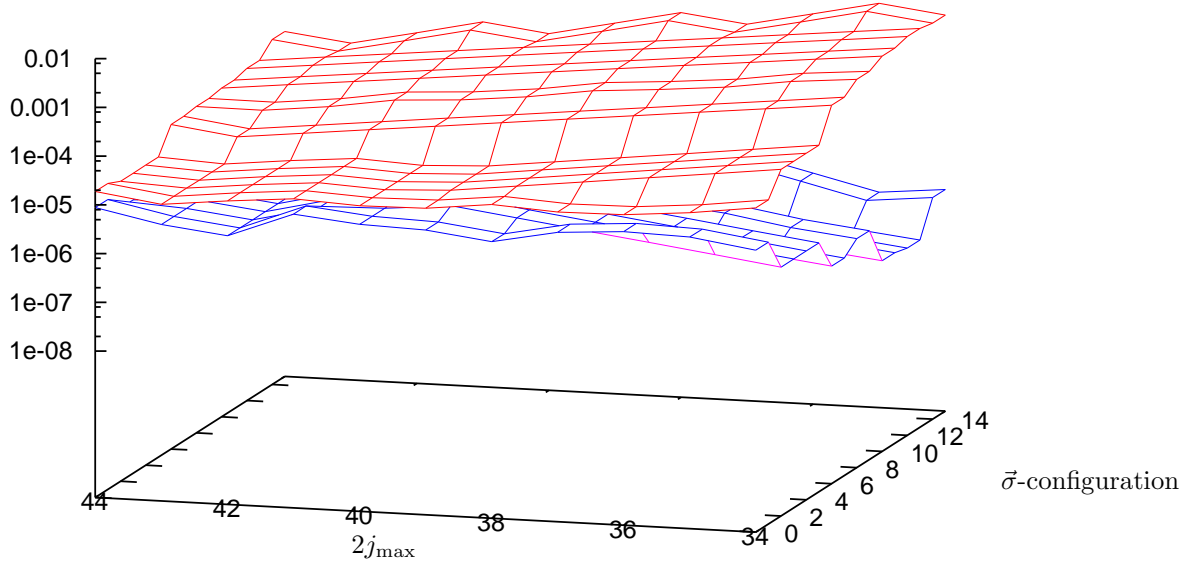


Figure 46: Smallest eigenvalues of 5-vertex (top, red), along with their LAPACK error bound (bottom, blue), for ‘large j_{\max} small $\vec{\sigma}$ -configuration corner’ of dataset. The vertical axis is in logscale.

The simplest measure of the effect of varying the error threshold is to count the number of zero eigenvalues. Figure 47 plots the overall number of zero eigenvalues as a function of T . The left figure shows that the number of zeros is essentially constant for any $T \geq 0.1$. Below that value the number of zeros drops off rapidly, indicating that a significant number of zero eigenvalues are being regarded as non-zero due to the threshold being less than the numerical noise. The plot on the right shows a relatively slow increase in the number of zeros for larger thresholds, which is expected. Here genuine non-zero eigenvalues are being regarded as zero due to the large error threshold.

Given the results of the above paragraph, we may be tempted to use $T = 0.1$, so as to catch as many genuine small but non-zero eigenvalues as possible. Figure 48 shows what happens to figure 45 when T is reduced to 0.1. Two features are of note. In our ‘large j_{\max} small $\vec{\sigma}$ -configuration corner’ we see that with $T < 1$ the error now can exceed the smallest non-zero eigenvalues, which it does. We also note a huge spike for $\vec{\sigma}$ -configuration 72 ($\vec{\sigma}$ -index 36), $j_{\max} = \frac{35}{2} - \frac{36}{2}$, for which the smallest non-zero eigenvalue and its error jump to meet (in fact cross) at around 10^{-5} . This occurs because numeric noise has exceeded the error threshold, and is now being regarded as a genuine smallest non-zero eigenvalue. Note that this essentially random event can occur at any point in our dataset. We thus see that our true numerical error can exceed one tenth of LAPACK’s bound, and thus stick with their reported bound with $T = 1$. The fact that this problem occurs just below the reported bound testifies to it being an accurate and tight estimate of the true numerical error.

At $T = 0.01$ the analog of figure 48 becomes mostly noise: The smallest non-zero eigenvalues are a constant $\sim 10^{-5}$ for most $\vec{\sigma}$ -configurations and values of j_{\max} .

6.6.3 Effect of noise on results

Reducing T allows us to probe the ‘problematic corner’ a bit closer to the numerical noise. Figure 49 portrays the effect of smaller T on the smallest non-zero eigenvalues. Clearly some valid non-zero eigenvalues are being washed out due to the noise.

The number of eigenvalues ‘between the two surfaces’ of figure 49 is the difference between the two leftmost data points on the right hand plot of figure 47, which is 413,160. The largest difference between data points on the right hand plot is 8,230,920. It is impossible to determine how many more non-zero eigenvalues there are below the bottom surface, but we expect it to be approximately of this larger order of magnitude. Now the bin width of the histogram in figure 9 is $\frac{497,223,680}{2048} = 0.242785$. Clearly this is much larger than any of the eigenvalues close to the error threshold

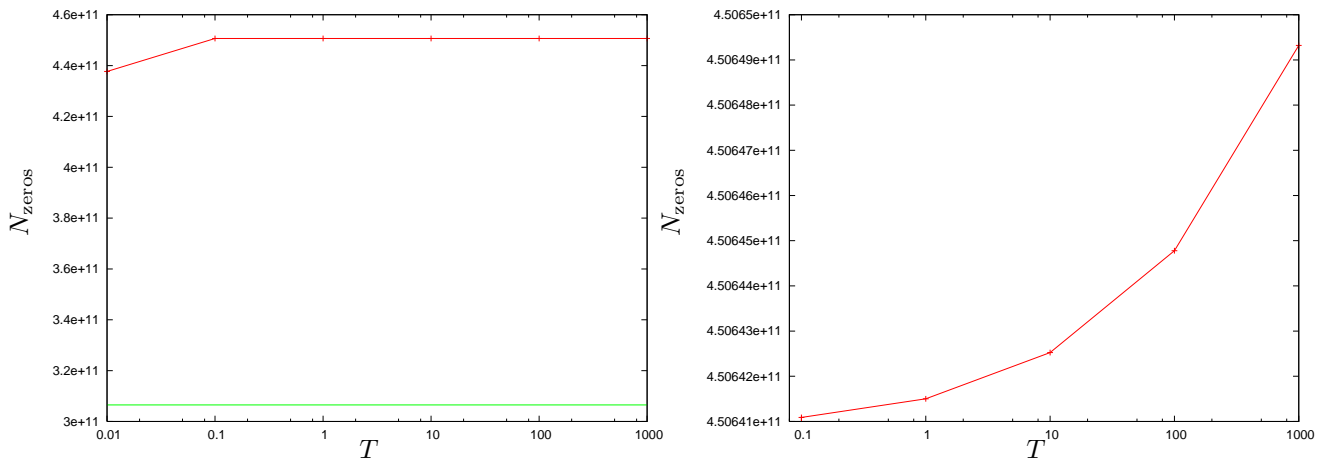


Figure 47: Number of zero eigenvalues for 5-vertex, as a function of error threshold T . The green line at the bottom of the left plot indicates the number of ‘obvious’ zeros, with $T = 0$. The plot on the right zooms in on the data points for $T > 0.08$.

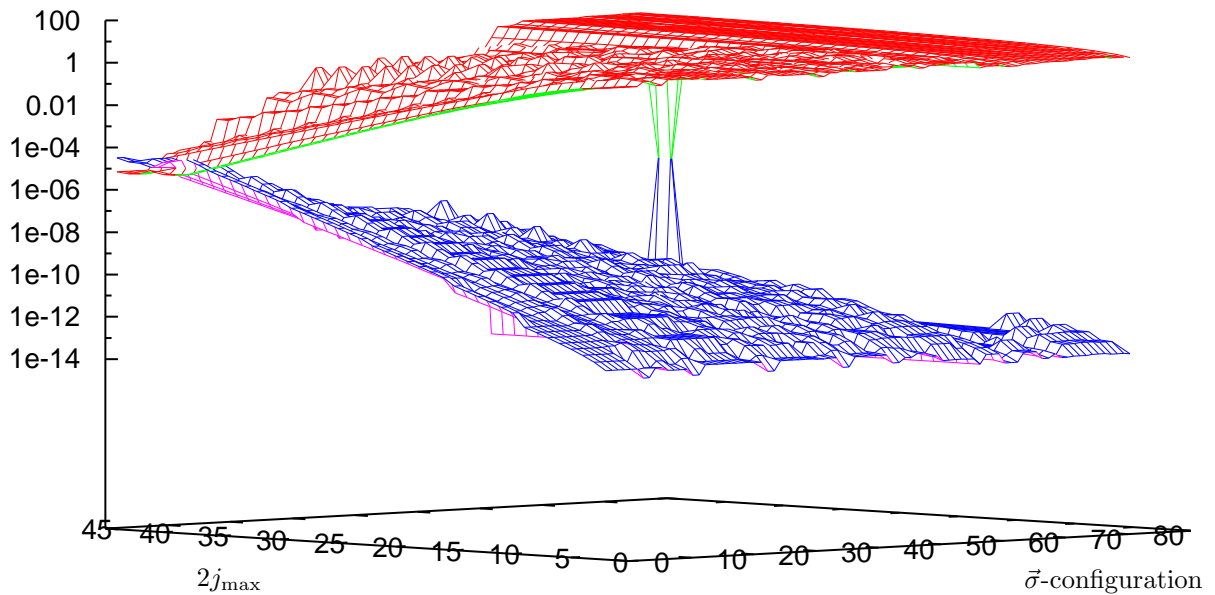


Figure 48: Smallest eigenvalues of 5-vertex (top, red), along with their LAPACK error bound (bottom, blue), for $T = 0.1$. The vertical axis is in logscale.

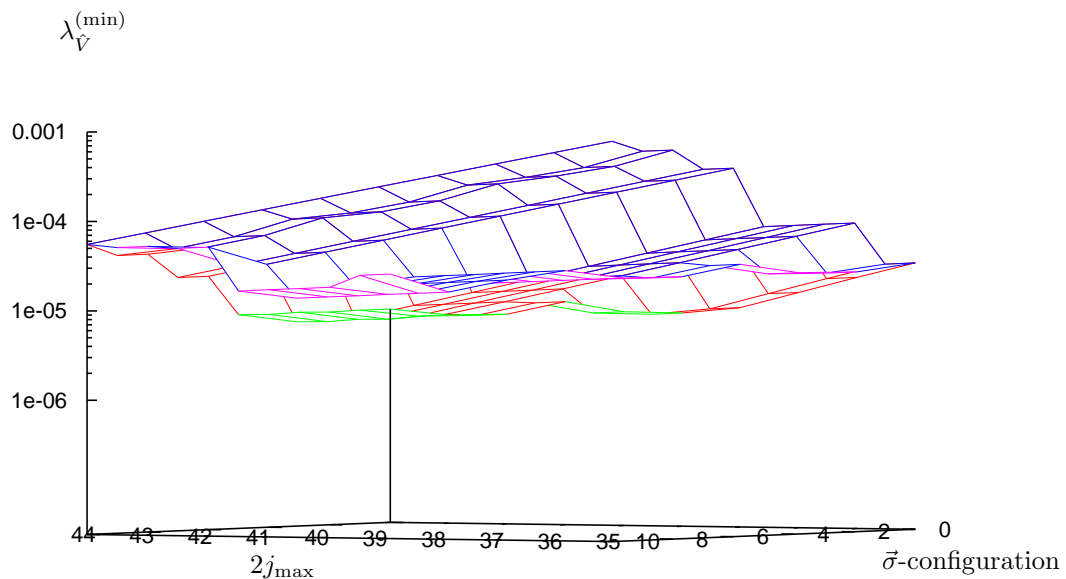


Figure 49: Smallest eigenvalues of 5-vertex, for $T = 1$ (top surface: upper side blue, bottom side magenta), and $T = 0.1$ (bottom surface: upper side red, bottom side green). The vertical axis is in logscale.

that we are considering, so the only effect of noise on the 5-vertex histogram is in the bin for smallest λ_V . The population of that bin, for $T = 1$, is 154,430,880. The true value is slightly larger than this. An addition of 8,230,920 to this number will have an indiscernible effect. In any event the lip is a genuine feature of the volume operator, and not a result of numerical error.

6.6.4 Valences $N \neq 5$

Figure 50 depicts the distance between the error bound and smallest non-zero eigenvalues for the 6-vertex. The minimal eigenvalue is closest to the error bound for the $\vec{\sigma}$ -configurations 7751 and 7752 shown, out of 8207 $\vec{\sigma}$ -configurations in total. Figure 51 shows the same numbers for $\vec{\sigma}$ -configuration 7751, with error bars. This curve also appears as one of the fifty shown in figure 31. It appears that we are just at the threshold of the numerical noise for the 6-vertex. Given the analysis of the 5-vertex errors above, we expect the errors to have negligible effect on the 6-vertex results.

(One of) the smallest eigenvalue(s) for our 7-vertex data, as described in section 6.5.3, arises from $\vec{\sigma}$ -configuration (2, 2, 2, -4, 0, 0, 0, 0, -2, -2, 2, 2, 4, -2, 4, 4, 0, 0, 0, -2), with spins (2, 2, 2, 2, 2, 3, 5). Its value is 0.000597922, with error bound $2.54519 \cdot 10^{-9}$. Clearly numerical error is not a significant issue for the 7-vertex.

Since the smallest non-zero eigenvalues for the 4-vertex rise with j_{\max} , we do not expect any effect from numerical noise. The relative error for every eigenvalue at the 4-vertex will be negligible. The same situation holds for the cubic 6-vertex of section 6.4.5.

6.6.5 Symmetric Eigenproblem

Earlier we computed eigenvalues more directly using subroutines LAPACK provides for the ‘symmetric eigenproblem’. To cast the matrices into symmetric form we computed eigenvalues for QQ^\dagger rather than Q . In this case numerical error is much more prominent, for a number of reasons.

For the symmetric eigenproblem, LAPACK employs the ‘relatively robust representation algorithm’, which involves an LDL^T factorization and a number of ‘translates’, to return the matrix eigenvalues e_i with a fixed absolute error

$$\delta e_i = \epsilon \|QQ^\dagger\|_1 \quad (6.11)$$

where $\|QQ^\dagger\|_1$ is the 1-norm (maximum column sum) of QQ^\dagger . This 1-norm is bounded from below by the largest eigenvalue. For singular value decomposition (SVD) the relative error is fixed and thus proportional to the largest eigenvalue.

We see that the relative error resulting from any algorithm is bounded below by the machine precision. Thus the error in the smallest eigenvalues can never be less than the maximum eigenvalue times machine epsilon, so that, when

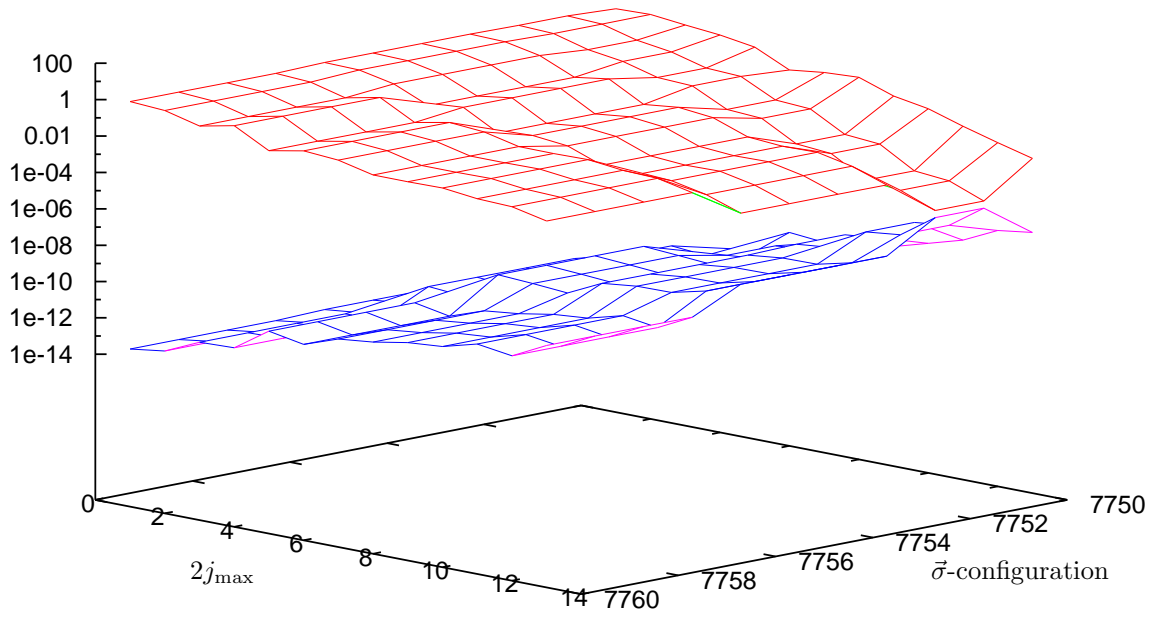


Figure 50: Some of the smallest non-zero eigenvalues of the 6-vertex (top, red), along with their LAPACK error bound (bottom, blue). The vertical axis is in logscale.

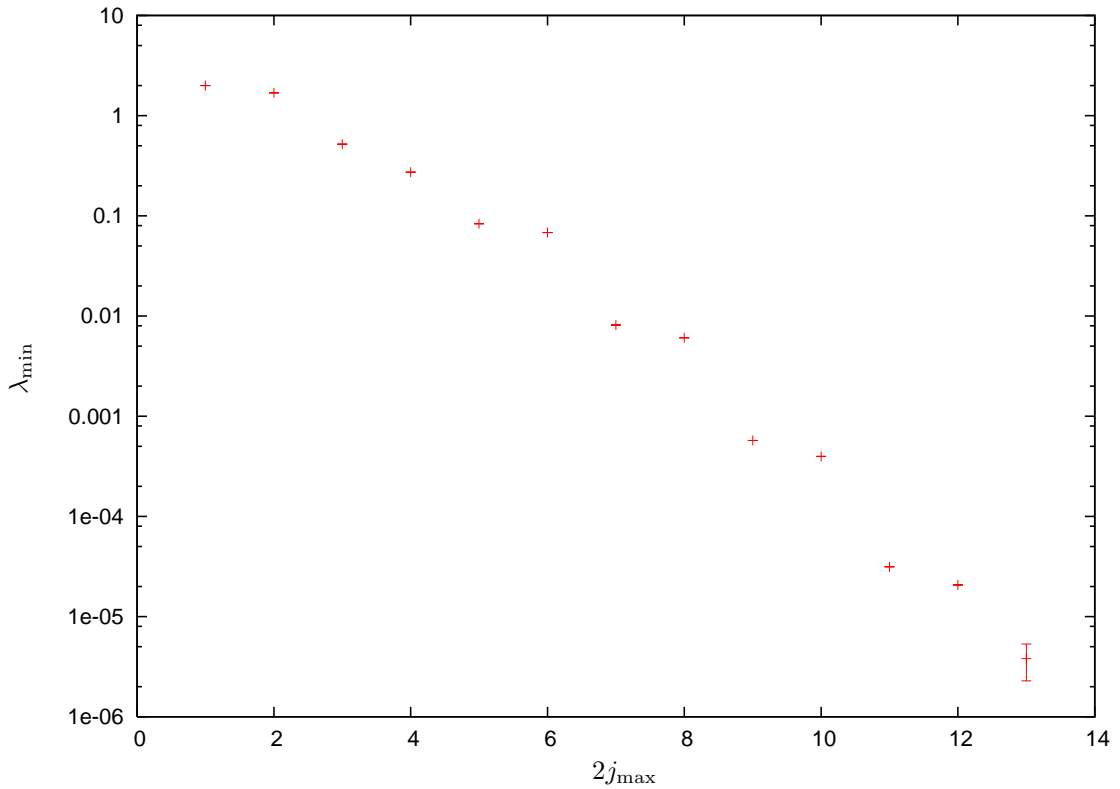


Figure 51: Minimal eigenvalues for $\vec{\sigma}$ -configuration $7751 = (0, 2, -2, 0, 0, 0, -2, 0, 2, 0)$, which yields the overall smallest non-zero eigenvalue at the 6-vertex up to $j_{\max} = \frac{13}{2}$. $T = 1$.

considering numerical error, what is important is the ratio between the largest and smallest eigenvalues which arise from a given matrix. When we square the matrix, we double this ratio, which in effect halves the relative precision of the computation.

Note that, as manifested in figures 45 and 50, the error bound in the smallest eigenvalues appears to be growing exponentially with j_{\max} . This occurs simply because we are taking the square root of the singular values to get the eigenvalues, and the minimum eigenvalues decay exponentially toward zero (as one can see from figure 17), so, according to eqn. 6.10, the error in the square root must grow exponentially. In the case of the symmetric eigenproblem, since we square Q before computing eigenvalues, we must take a 4th root to get the volume eigenvalues. In this case the analog of (6.10) has the volume eigenvalue *cubed* in the denominator. Thus the log of the errors in the volume eigenvalues will grow three times as fast as for SVD. This effect, along with the effect of squaring Q discussed in the previous paragraph, represents a considerable increase in numerical error. We are thus able to explore the spectrum to much higher values of j_{\max} with the singular value decomposition.

6.7 Histograms of Entire Data Set

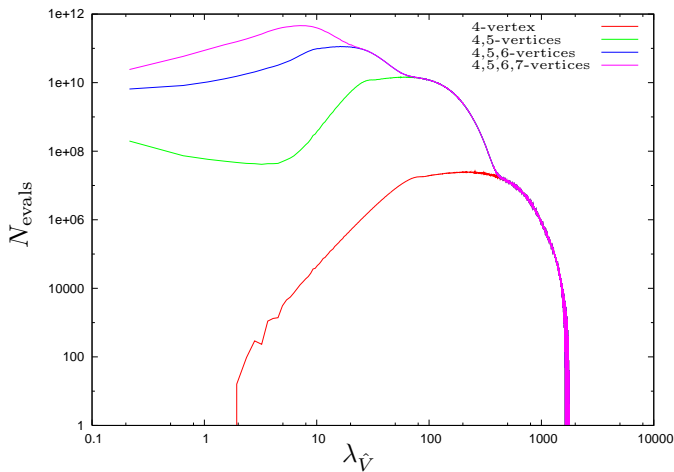


Figure 52: Histograms for entire dataset, in log-log scale. $N_{\text{bins}} = 4096$. Each successive curve adds eigenvalues for the next larger valence. Here the cutoffs for j_{\max} are: $\frac{126}{2}$ for the 4-vertex, $\frac{44}{2}$ for the 5-vertex, $\frac{13}{2}$ for the 6-vertex, and $\frac{5}{2}$ for the 7-vertex.

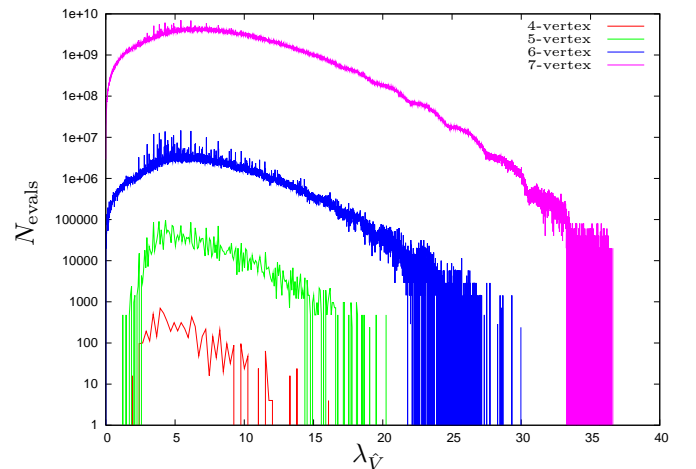


Figure 53: Histograms for entire dataset, in log-linear scale, with j_{\max} fixed at $\frac{5}{2}$. Here the histograms are not cumulative: each valence appears separately. $N_{\text{bins}} = 64, 256, 4096, 8192$, for valences 4 – 7 respectively.

Figure 52 presents four histograms of our entire data set. Each represents all eigenvalues we have computed up to a given valence. (Thus the blue curve, for example, includes all 4-, 5-, and 6-vertex eigenvalues we have computed.) There are 21,551,022,251,376 eigenvalues in all, of which 827,849,074,512 are (regarded as, c.f. discussion on errors in section 6.6 above) zero.

Figure 53 shows histograms for the entire dataset truncated to $j_{\max} = \frac{5}{2}$. We see that, as one might expect, larger valences are able to contribute larger eigenvalues, even for comparable values of spin. Note that $j_{\max} = \frac{5}{2}$ is not large enough to see the absence of a volume gap for the 5-vertex.

7 Analytical Results at the Gauge Invariant 4-Vertex

In this section we present three analytical results on the spectral properties of the volume operator at the gauge invariant 4-valent vertex. We first prove the spectral simplicity and second give a general formula for the eigenvectors of the volume operator at the 4-vertex depending on the eigenvalues, which agrees with the earlier publication [17]. Third we analyze how the smallest non-zero eigenvalue scales with the maximal spin j_{\max} at the vertex.

For the methods we are using here the particular shape of the operator, when represented as a matrix, will be crucial. In fact many theorems developed for Jacobi matrices²⁹ can be carried over to the particular case under investigation. Here [27] provides the crucial theorems and proofs.

7.1 Setup: Explicit Expression for the Volume Operator as D -dimensional Matrix \hat{Q}_D

The general case of the gauge invariant 4-vertex deals with 4 edges e_1, \dots, e_4 outgoing from the vertex v . Each edge e_K ($K = 1 \dots 4$) carries a $2j_K + 1$ dimensional representation of $SU(2)$. Due to gauge invariance the standard recoupling

²⁹That is symmetric tridiagonal matrices.

basis states (B.8) are given in this case as

$$| a_2(j_1 j_2) a_3(a_2 j_3) \stackrel{i}{=} j_4 J(a_3 j_4) = 0 M = 0 \rangle \quad (7.1)$$

where the intermediate recoupling $a_3(a_2 j_3)$ has to equal j_4 due to the Clebsch-Gordan Theorem and as a result the intermediate recoupling $a_2(j_1 j_2)$ is the only degree of freedom for fixed spins j_1, \dots, j_4 . Therefore expression (4.12) for the matrix representation of the volume operator simplifies dramatically to give

$$\hat{V}_v = \sqrt{|Z \cdot \sigma(123) \hat{q}_{123}|} = \sqrt[4]{|Z|^2 \cdot [\sigma(123)]^2 \cdot \hat{Q}^\dagger \hat{Q}} \quad (7.2)$$

where we have introduced the shorthand $\hat{Q} := \hat{q}_{123}$. Note that $\sigma(123) = \epsilon(123) - \epsilon(124) + \epsilon(134) - \epsilon(234) = 0, \pm 2, \pm 4$ gives a constant numerical prefactor depending on the relative orientations of the 4 edges only. In the following we will assume that $\sigma(123) \neq 0$ but leave its numerical value unspecified, that is we will drop it from our formulae and reinsert it at the end. We set the regularization prefactor $Z = i$, c.f. section 2.3.³⁰ Using (3.8) together with the definitions of section 3.3.1 we obtain for the matrix $\hat{Q} = \hat{Q}_D$ (D denotes the dimension) the following shape [14, 24]:

$$\hat{Q}_D = \begin{pmatrix} 0 & -q_1 & 0 & \cdots & 0 & 0 & 0 \\ q_1 & 0 & -q_2 & \cdots & 0 & 0 & 0 \\ 0 & q_2 & 0 & \cdots & 0 & 0 & 0 \\ \vdots & \vdots & \vdots & \ddots & \vdots & \vdots & \vdots \\ 0 & 0 & 0 & \cdots & 0 & -q_{D-2} & 0 \\ 0 & 0 & 0 & \cdots & q_{D-2} & 0 & -q_{D-1} \\ 0 & 0 & 0 & \cdots & 0 & q_{D-1} & 0 \end{pmatrix} \quad (7.3)$$

where the matrix elements are given by

$$q_k = \frac{i}{\sqrt{(2a_2+1)(2a_2-1)}} \left[(j_1 + j_2 + a_2 + 1)(-j_1 + j_2 + a_2)(j_1 - j_2 + a_2)(j_1 + j_2 - a_2 + 1) \times \right. \\ \left. \times (j_3 + j_4 + a_2 + 1)(-j_3 + j_4 + a_2)(j_3 - j_4 + a_2)(j_3 + j_4 - a_2 + 1) \right]^{\frac{1}{2}} \quad (7.4)$$

and the intermediate recoupling step $a_2 = a_2(j_1 j_2)$ is given as $a_2 = a_2^{(min)} + k$, that is

$$\max[|j_2 - j_1|, |j_4 - j_3|] = a_2^{(min)} \leq a_2 \leq a_2^{(max)} = \min[j_1 + j_2, j_3 + j_4] \quad (7.5)$$

and $D = \dim \hat{Q}_D = a_2^{(max)} - a_2^{(min)} + 1$.

7.1.1 Known Results

1. Spectrum: By choosing $Z = i$, (7.3) is an antisymmetric matrix with purely imaginary matrix elements. Its eigenvalues λ are thus real and come in pairs $\lambda = \pm |\lambda|$. Moreover its eigenvectors $\Psi^\lambda = (\Psi_1^\lambda, \dots, \Psi_D^\lambda)^T$ are orthogonal and there exists a unitary matrix

$$U_D = \begin{pmatrix} \Psi_1^{\lambda_1} & \Psi_1^{\lambda_2} & \cdots & \Psi_1^{\lambda_D} \\ \Psi_2^{\lambda_1} & \Psi_2^{\lambda_2} & \cdots & \Psi_2^{\lambda_D} \\ \vdots & \vdots & \cdots & \vdots \\ \Psi_D^{\lambda_1} & \Psi_D^{\lambda_2} & \cdots & \Psi_D^{\lambda_D} \end{pmatrix} \quad (7.6)$$

such that $U_D \Lambda_D = \hat{Q}_D U_D$, $\Lambda_N = U_D^{-1} \hat{Q}_D U_D = U_D^\dagger \hat{Q}_D U_D$, $\Lambda_N = \text{diag}(\lambda_1, \dots, \lambda_D)$

2. 0-eigenvalues: It has been found in [24] that 0 as a single eigenvalue is contained only in the spectrum of odd dimensional matrices \hat{Q}_D .

7.2 Simplicity of the Spectrum of the Matrix \hat{Q}_D

By inspection an eigenvector $\Psi^\lambda = (\Psi_1^\lambda, \dots, \Psi_D^\lambda)^T$ for the eigenvalue λ of (7.3) with $(\hat{Q}_D - \lambda \mathbb{1})\Psi^\lambda = 0$ will fulfill:

$$\begin{aligned} \text{(I)} \quad & -\lambda \Psi_1^\lambda - q_1 \Psi_2^\lambda = 0 \\ \text{(II)} \quad & q_{k-1} \Psi_{k-1}^\lambda - \lambda \Psi_k^\lambda - q_k \Psi_{k+1}^\lambda = 0 \quad \boxed{1 < k < D} \\ \text{(III)} \quad & q_{N-1} \Psi_{N-1}^\lambda - \lambda \Psi_N^\lambda = 0 \end{aligned} \quad (7.7)$$

³⁰ Note that due to the definition of the eigenvalue $\lambda_{\hat{V}}$ of \hat{V} as $\lambda_{\hat{V}} := \sqrt{|\lambda_Q|}$, this does not change the volume spectrum. Because Q is an antisymmetric matrix, setting its matrix elements to be real or imaginary only rotates its spectrum in the complex plane either to the complex axis or the real axis.

Now suppose $\lambda \neq 0$.³¹ Setting $\Psi_1^\lambda = 0$ leads, together with (I) and the fact that $q_k \neq 0$ for $k = 1, \dots, N-1$, to $\Psi_2^\lambda \stackrel{!}{=} 0$, which then in turn implies together with (II) that $\Psi_k^\lambda \stackrel{!}{=} 0 \forall k$. Therefore in order to get a non-vanishing eigenvector Ψ^λ , $\lambda \neq 0$ we must have $\Psi_1^\lambda \stackrel{!}{\neq} 0$.

Now suppose there exists an eigenvalue $\lambda \neq 0$ of \widehat{Q}_D that has multiplicity > 1 : Let $\Psi^\lambda, \tilde{\Psi}^\lambda$ be two eigenvectors for λ . Then we can find two constants $\alpha, \tilde{\alpha} \in \mathbb{C}$, $\alpha, \tilde{\alpha} \neq 0$, such that we can construct an eigenvector $\Phi^\lambda = \alpha\Psi^\lambda + \tilde{\alpha}\tilde{\Psi}^\lambda$ with the property $\Phi_1^\lambda = 0$. As we have seen this implies $\Phi_k^\lambda \stackrel{!}{=} 0 \forall k$, and thus $0 = \alpha\Psi^\lambda + \tilde{\alpha}\tilde{\Psi}^\lambda$, that is $\Psi^\lambda, \tilde{\Psi}^\lambda$ are linearly dependent and therefore there exists only one eigenvector Ψ^λ for each eigenvalue $\lambda \neq 0$ of \widehat{Q}_D . We have thus proved the following

Theorem 7.1 *Spectral Simplicity of \widehat{Q}_D*

(i) *The spectrum $\text{spec}(\widehat{Q}_D) \neq 0$ is simple (consists of D distinct real numbers)*

(ii) *If $\Psi^\lambda = (\Psi_1^\lambda, \dots, \Psi_D^\lambda)^T$ is an eigenvector of \widehat{Q}_D ($\widehat{Q}_D\Psi^\lambda = \lambda\Psi^\lambda$, $\lambda \neq 0$) then $\Psi_1^\lambda \neq 0, \Psi_D^\lambda \neq 0$*

7.3 Eigenvectors of the Matrix \widehat{Q}_D

Starting from (I) in (7.7) by setting $\Psi_1^\lambda = x = \text{const}$ one can explicitly construct the components Ψ_k^λ . One gets, in agreement with [17] (using the integer number $L \geq 1$ with $L \leq \frac{D}{2}$ for even D and $L \leq \frac{D-1}{2}$ for odd D):

$$\begin{aligned} \Psi_{2L}^\lambda &= \frac{-x\lambda}{\prod_{k=1}^{2L-1} q_k} \left[\lambda^{2(L-1)} + \sum_{M=1}^{L-1} \lambda^{2(L-1-M)} \sum_{k_M=2M-1}^{2L-2} \sum_{k_{M-1}=2(M-1)-1}^{k_M-2} \dots \sum_{k_{l-1}=2(M-l)-1}^{k_{l-1}-2} \dots \sum_{k_2=3}^{k_3-2} \sum_{k_1=1}^{k_2-2} q_{k_M}^2 q_{k_{M-1}}^2 \dots q_{k_l}^2 \dots q_{k_2}^2 q_{k_1}^2 \right] \\ \Psi_{2L+1}^\lambda &= \frac{x}{\prod_{k=1}^{2L} q_k} \left[\lambda^{2L} + \sum_{M=1}^L \lambda^{2(L-M)} \sum_{k_M=2M-1}^{2L-1} \sum_{k_{M-1}=2(M-1)-1}^{k_M-2} \dots \sum_{k_{l-1}=2(M-l)-1}^{k_{l-1}-2} \dots \sum_{k_2=3}^{k_3-2} \sum_{k_1=1}^{k_2-2} q_{k_M}^2 q_{k_{M-1}}^2 \dots q_{k_l}^2 \dots q_{k_2}^2 q_{k_1}^2 \right] \end{aligned} \quad (7.8)$$

where L is a positive integer $\leq \frac{N}{2}$. When $M=1$ the upper bound of the k_1 sum is that of the k_M sum. One may explicitly check that these states fulfill (II) in (7.7). In order to fulfill (III) we find the conditions

$$\boxed{D = 2L, \text{ even}} \quad 0 \stackrel{!}{=} \frac{-x}{\prod_{k=1}^{2L-1} q_k} \left[\lambda^{2L} + \sum_{M=1}^L \lambda^{2(L-M)} \sum_{k_M=2M-1}^{2L-1} \sum_{k_{M-1}=2(M-1)-1}^{k_M-2} \dots \sum_{k_2=3}^{k_3-2} \sum_{k_1=1}^{k_2-2} q_{k_M}^2 q_{k_{M-1}}^2 \dots q_{k_2}^2 q_{k_1}^2 \right] \quad (7.9)$$

$$\boxed{D = 2L + 1, \text{ odd}} \quad 0 \stackrel{!}{=} \frac{x\lambda}{\prod_{k=1}^{2L} q_k} \left[\lambda^{2L} + \sum_{M=1}^L \lambda^{2(L-M)} \sum_{k_M=2M-1}^{2L} \sum_{k_{M-1}=2(M-1)-1}^{k_M-2} \dots \sum_{k_2=3}^{k_3-2} \sum_{k_1=1}^{k_2-2} q_{k_M}^2 q_{k_{M-1}}^2 \dots q_{k_2}^2 q_{k_1}^2 \right]$$

Thus, in order for (7.9) to be satisfied, λ has to be a root of the characteristic polynomial

$$\begin{aligned} \pi_{2L}(\lambda) &= \lambda^{2L} + \sum_{M=1}^L b_M^{(k_0)} \lambda^{2(L-M)} & D = 2L \text{ even} & \quad k_0 = 2L + 1 = D + 1 \\ \pi_{2L+1}(\lambda) &= \lambda \left[\lambda^{2L} + \sum_{M=1}^L b_M^{(k_0)} \lambda^{2(L-M)} \right] & D = 2L + 1 \text{ odd} & \quad k_0 = 2L + 2 = D + 1 \end{aligned} \quad (7.10)$$

with coefficients

$$b_M^{(k_0)} = \sum_{k_M=2M-1}^{k_0-2} \sum_{k_{M-1}=2(M-1)-1}^{k_M-2} \dots \sum_{k_{l-1}=2(M-l)-1}^{k_{l-1}-2} \dots \sum_{k_2=3}^{k_3-2} \sum_{k_1=1}^{k_2-2} q_{k_M}^2 q_{k_{M-1}}^2 \dots q_{k_l}^2 \dots q_{k_2}^2 q_{k_1}^2 \quad (7.11)$$

Since the bracketed terms in the characteristic polynomials (7.10) contain only even powers of λ we may replace $\lambda^{2k} = \Lambda^k$ with $\Lambda = |\lambda|^2$ in order to arrive at a reduced purely real notation for them:

$$\begin{aligned} 0 &= \lambda^{2L} + \sum_{M=1}^L b_M^{(k_0)} \lambda^{2(L-M)} \\ &= \Lambda^L + \sum_{M=1}^L (-1)^M |b_M^{(k_0)}| \Lambda^{L-M} \end{aligned} \quad (7.12)$$

³¹The case $\lambda = 0$ is already discussed in [24].

where we have pulled out a prefactor $(-1)^M$ coming from the purely imaginary nature of the matrix elements (7.4).

7.3.1 Traces of $(\widehat{Q}_D^2)^n$

Knowing the coefficients (7.11) of the characteristic polynomial, together with Newton's equation valid for an arbitrary matrix A with $\text{tr}[A^n] = s_n$

$$s_n = -\left[n \cdot b_n^{(k_0)} + \sum_{l=1}^{n-1} b_{n-l}^{(k_0)} s_l \right] \quad n > 1 \quad (7.13)$$

we are now enabled to successively calculate the traces of all powers of $(\widehat{Q}_D^2)^n$ starting from $s_1 = -2 \sum_{k=1}^{D-1} q_k^2$. This is of special relevance because it allows us to reconstruct the spectral density function $\rho(\lambda)$ of eigenvalues λ of the hermitian operator \widehat{Q}_D in question (see e.g. [33], chapter 2).

$\rho(\lambda)$ fulfills the properties of a probability distribution

- (i) $\rho(\lambda) \geq 0 \quad \forall \lambda$ positivity
- (ii) $\int_{-\infty}^{+\infty} \rho(\lambda) = 1$ normalization
- (iii) $\rho(\lambda) = \sum_{k=1}^D \delta(\lambda - \lambda_k)$ for a discrete spectrum, as is the case for \widehat{Q}_D

Then

$$\text{tr}[(\widehat{Q}_D)^n] = \sum_{k=1}^n (\lambda_k)^n = m_n = \int_{-\infty}^{+\infty} \lambda^n \rho(\lambda) d\lambda \quad (7.14)$$

is called the n^{th} moment of the distribution $\rho(\lambda)$. The Fourier transform of $\rho(\lambda)$

$$\chi(\tau) = \int_{-\infty}^{+\infty} e^{-i\lambda\tau} \rho(\lambda) d\lambda \quad (7.15)$$

is called the characteristic function. By inversion of the Fourier transform $\rho(\lambda)$ can be reconstructed from $\chi(\tau)$:

$$\rho(\lambda) = \frac{1}{2\pi} \int_{-\infty}^{+\infty} e^{i\lambda\tau} \chi(\tau) d\tau \quad (7.16)$$

Now by expanding the exponent in (7.15) and inserting (7.14), the Fourier transform $\chi(\tau)$ of the eigenvalue distribution $\rho(\lambda)$ can be expressed in terms of the moments (7.14) as

$$\chi(\tau) = \sum_{n=0}^{\infty} \frac{(-i)^n}{n!} \tau^n \left[\int_{-\infty}^{+\infty} \lambda^n \rho(\lambda) d\lambda \right] = \sum_{n=0}^{\infty} \frac{(-i)^n}{n!} \tau^n m_n \quad (7.17)$$

Inserting this back into (7.16) one finally obtains $\rho(\lambda)$ in terms of the moments. However this formal way of obtaining $\rho(\lambda)$ will not be directly accessible in most cases, since the series (7.17) is not convergent, and one needs a closed expression for $\chi(\tau)$, as otherwise inserting the formal power series (7.17) into (7.16) will result in ill-defined divergent expressions. One then has to put in by hand an assumption on the kind of distribution one is working with (see e.g. [19]). A note on the results obtained in [18] is given in the companion paper [25]. There are also numerical procedures to reconstruct a statistical distribution from a finite number of its moments using spline interpolation [20].

7.4 Upper and Lower Bounds on the Eigenvalues of \widehat{Q}_D

7.4.1 Upper Bound

One can find upper bounds for the eigenvalues by applying the theorem of *Geršgorin* (see e.g. [31], [34]):

Theorem 7.2 *Geršgorin*

Every eigenvalue λ of an $(n \times n)$ -matrix Q lies at least in one of the discs

$$|q_{ii} - \lambda| \leq \sum_{\substack{j=1 \\ j \neq i}}^n |q_{ij}| \quad i = 1, \dots, n$$

That is every eigenvalue lies in a disc centered at the diagonal element q_{ii} with radius the sum of moduli of the off-diagonal-elements q_{ij} , $i \neq j$ of the i^{th} row or column. In the case of the gauge invariant 4-vertex this theorem simplifies, due to the banded matrix structure of (7.3) and the fact that $q_{ii} = 0$, to

$$|\lambda| \leq \sum_{j \neq i} |q_{ij}| = |q_{i \ i-1}| + |q_{i \ i+1}| \quad (7.18)$$

A general upper bound was found already in [24] by directly employing theorem 7.2.

7.4.2 Lower Bound

Finding a lower bound on the modulus of the smallest non-zero eigenvalue turns out to be a much harder task in [24]. The idea is to invert the matrix \widehat{Q}_D and find an upper bound on the eigenvalues of the inverse \widehat{Q}_D^{-1} , which then in turn would serve as a lower bound on the spectrum of \widehat{Q}_D . The problem is that in the case of odd dimensional \widehat{Q}_D we cannot directly invert the matrix but have to project out the null space first. That results in a messy matrix which has lost some of the banded structure of the original \widehat{Q}_D given in (7.3).

We will show now that this procedure is not necessary. In order to see this consider the (D, D) component of the resolvent of \widehat{Q}_D :

$$\left[\frac{1}{\widehat{Q}_D - \lambda \mathbb{1}_D} \right]_{DD} = \frac{\widetilde{[\widehat{Q}_D - \lambda \mathbb{1}_D]_{DD}}}{\det [\widehat{Q}_D - \lambda \mathbb{1}_D]} = \frac{\det [\widehat{Q}_{D-1} - \lambda \mathbb{1}_{D-1}]}{\det [\widehat{Q}_D - \lambda \mathbb{1}_D]} = \frac{\pi_{D-1}(\lambda)}{\pi_D(\lambda)} \quad (7.19)$$

where we have used the general definition of the matrix element of the inverse matrix $[\widehat{Q}^{-1}]_{jk} = (-1)^{j+k} \frac{\widetilde{Q}_{kj}}{\det \widehat{Q}}$, \widetilde{Q}_{kj} is obtained by deleting row k and column j from \widehat{Q} and taking the determinant of the remaining submatrix. Moreover $\pi_D(\lambda)$ denotes the characteristic polynomial of \widehat{Q}_D , $\pi_{D-1}(\lambda)$ is the characteristic polynomial of the $D-1$ dimensional submatrix \widehat{Q}_{D-1} one obtains by deleting row D and column D of \widehat{Q}_D . In what follows we will drop the index D from \widehat{Q}_D , U_D etc. for clarity.

From (7.6) we know that $\widehat{Q} = U\Lambda U^\dagger$, $\Lambda = \text{diag}(\lambda_1, \dots, \lambda_D)$, and $U^\dagger U = U U^\dagger = \mathbb{1}$, U being a unitary matrix. Therefore we know that

$$\widehat{Q}_{lm} = \sum_{r,s} U_{lr} \Lambda_{rs} U_{sm}^\dagger = \sum_{r,s} U_{lr} [\lambda_r \cdot \delta_{rs}] U_{sm}^\dagger = \sum_r \lambda_r U_{lr} U_{rm}^\dagger$$

and, since U diagonalizes $(\widehat{Q} - \lambda \mathbb{1})^{-1}$ as well:

$$[(\widehat{Q} - \lambda \mathbb{1})^{-1}]_{lm} = \sum_{r,s} U_{lr} [(\Lambda - \lambda \mathbb{1})^{-1}]_{rs} U_{sm}^\dagger = \sum_{r,s} U_{lr} [(\lambda_r - \lambda)^{-1} \delta_{rs}] U_{sm}^\dagger = \sum_r \frac{1}{\lambda_r - \lambda} U_{lr} U_{rm}^\dagger \quad (7.20)$$

Thus we find using (7.6):

$$[(\widehat{Q} - \lambda \mathbb{1})^{-1}]_{DD} = \frac{\pi_{D-1}(\lambda)}{\pi_D(\lambda)} = \sum_r \frac{U_{Dr} U_{rD}^\dagger}{\lambda_r - \lambda} = \sum_r \frac{\Psi_D^{\lambda_r} \overline{\Psi_D^{\lambda_r}}}{\lambda_r - \lambda} = \sum_r \frac{|\Psi_D^{\lambda_r}|^2}{\lambda_r - \lambda} \quad (7.21)$$

where the overline denotes complex conjugation.

Now from theorem 7.1 we know that we must have $\Psi_D^{\lambda_r} \neq 0 \ \forall r = 1 \dots D$. Therefore we know that

$$V(\lambda) = \frac{\pi_{D-1}(\lambda)}{\pi_D(\lambda)} = \sum_r \frac{|\Psi_D^{\lambda_r}|^2}{\lambda_r - \lambda} \quad (7.22)$$

is a real valued function and its derivative

$$\frac{d}{d\lambda} V(\lambda) = \sum_r \frac{|(\Psi^{\lambda_r})_D|^2}{(\lambda_r - \lambda)^2} > 0 \ \forall \lambda \quad (7.23)$$

That is, $V(\lambda)$ is monotonic increasing $\forall \lambda \in \mathbb{R}$, has poles at every $\lambda = \lambda_r$, $r = 1 \dots D$, and is finite $\forall \lambda \neq \lambda_r$. So we conclude that $V(\lambda)$ has the form illustrated in figure 54. The function $V(\lambda)$ has precisely one root in the interval $[\lambda_k, \lambda_{k+1}]$. This means that the roots of $\pi_{D-1}(\lambda)$, $\pi_D(\lambda)$ interlace: in between two eigenvalues λ_k, λ_{k+1} of \widehat{Q}_D there is precisely one eigenvalue of its submatrix \widehat{Q}_{D-1} . From this we conclude that the structure for the spectra of \widehat{Q}_D and its submatrices $\widehat{Q}_{D-1}, \widehat{Q}_{D-2}, \dots$ is as illustrated in figures 55 and 56. The D odd case in figure 55 shows that a lower bound for the smallest non-zero eigenvalues of \widehat{Q}_D is given by the smallest eigenvalue of the even dimensional

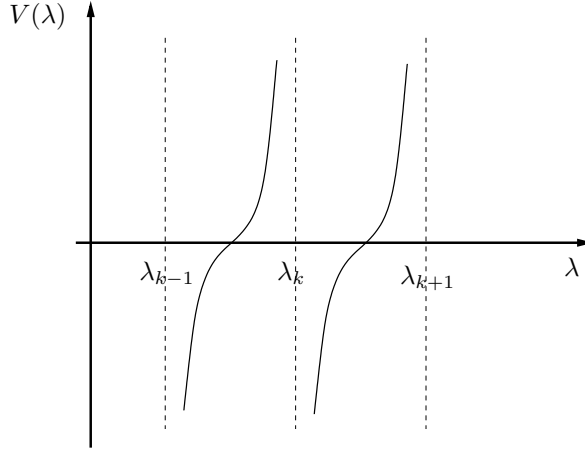


Figure 54: The function $V(\lambda)$.

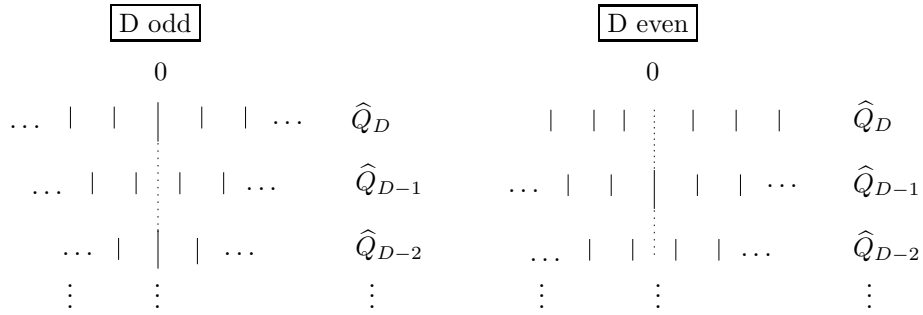


Figure 55: Interlacing of the spectra for odd dimension D .

Figure 56: Interlacing of the spectra for even dimension D .

submatrix \widehat{Q}_{D-1} . However, as mentioned above, one can show [24] that even dimensional matrices of type of \widehat{Q}_D have no zero eigenvalue in their spectrum and thus it seems feasible to give a lower bound for their eigenvalues by finding an upper bound for the eigenvalues of its inverse matrix \widehat{Q}_D^{-1} .

Set $L^{(M,N)} = \frac{1}{q_{2M-1}} \prod_{l=M}^{N-1} \frac{q_{2l}}{q_{2l+1}}$, for $M < N$ and $L^{(M,M)} = \frac{1}{q_{2M-1}}$, such that e.g. $L^{(1,1)} = \frac{1}{q_1}$, $L^{(1,2)} = \frac{q_2}{q_1 q_3}$ or $L^{(2,2)} = \frac{1}{q_3}$, $L^{(2,3)} = \frac{q_4}{q_3 q_5}$, $L^{(2,4)} = \frac{q_4 q_6}{q_3 q_5 q_7}$. Then if \widehat{Q}_D is as given in (7.3) and D is even we have for its inverse (using $n = \frac{D}{2}$):

$$\widehat{Q}_D^{-1} = \begin{pmatrix} 0 & L^{(1,1)} & 0 & L^{(1,2)} & 0 & L^{(1,3)} \dots & 0 & L^{(1,n-2)} & 0 & L^{(1,n-1)} & 0 & L^{(1,n)} \\ -L^{(1,1)} & 0 & 0 & 0 & 0 & 0 \dots & 0 & 0 & 0 & 0 & 0 & 0 \\ 0 & 0 & 0 & L^{(2,2)} & 0 & L^{(2,3)} \dots & 0 & L^{(2,n-2)} & 0 & L^{(2,n-1)} & 0 & -L^{(2,n)} \\ -L^{(1,2)} & 0 & -L^{(2,2)} & 0 & 0 & 0 \dots & 0 & 0 & 0 & 0 & 0 & 0 \\ 0 & 0 & 0 & 0 & 0 & L^{(3,3)} \dots & 0 & L^{(3,n-2)} & 0 & L^{(3,n-1)} & 0 & L^{(3,n)} \\ -L^{(1,3)} & 0 & -L^{(2,3)} & 0 & -L^{(3,3)} & 0 \dots & 0 & 0 & 0 & 0 & 0 & 0 \\ \vdots & \vdots & \vdots & \vdots & \vdots & \vdots & \vdots & \vdots & \vdots & \vdots & \vdots & \vdots \\ \vdots & \vdots & \vdots & \vdots & \vdots & \vdots & \vdots & \vdots & \vdots & \vdots & \vdots & \vdots \\ 0 & 0 & 0 & 0 & 0 & 0 \dots & 0 & L^{(n-2,n-2)} & 0 & L^{(n-2,n-1)} & 0 & L^{(n-2,n)} \\ -L^{(1,n-2)} & 0 & -L^{(2,n-2)} & 0 & -L^{(3,n-2)} & 0 \dots -L^{(n-2,n-2)} & 0 & 0 & 0 & 0 & 0 & 0 \\ 0 & 0 & 0 & 0 & 0 & 0 \dots & 0 & 0 & 0 & L^{(n-1,n-1)} & 0 & L^{(n-1,n)} \\ -L^{(1,n-1)} & 0 & -L^{(2,n-1)} & 0 & -L^{(3,n-1)} & 0 \dots -L^{(n-2,n-1)} & 0 & -L^{(n-1,n-1)} & 0 & 0 & 0 & 0 \\ 0 & 0 & 0 & 0 & 0 & 0 \dots & 0 & 0 & 0 & 0 & 0 & L^{(n,n)} \\ -L^{(1,n)} & 0 & -L^{(2,n)} & 0 & -L^{(3,n)} & 0 \dots -L^{(n-2,n)} & 0 & -L^{(n-1,n)} & 0 & -L^{(n,n)} & 0 & 0 \end{pmatrix} \quad (7.24)$$

We are now left with the task of finding an upper bound for the row/column sums of \widehat{Q}_D^{-1} in order to apply theorem

7.2. For this we have to use the explicit form of the matrix elements (7.4). Let us introduce the following shorthands:

$$\begin{aligned} R_k^{(m,n)} &= j_m + j_n - a_2^{(\min)} - k + 1 \\ U_k^{(m,n)} &= (j_m + j_n + a_2^{(\min)} + k + 1)(-j_m + j_n + a_2^{(\min)} + k)(j_m - j_n + a_2^{(\min)} + k) \end{aligned} \quad (7.25)$$

which enable us to write for $\boxed{M < N}$

$$\begin{aligned} |L^{(M,N)}|^2 &= \left| \frac{1}{q_{2M-1}} \prod_{l=M}^{N-1} \frac{q_{2l}}{q_{2l+1}} \right|^2 \\ &= [2(a_2^{(\min)} + 2M - 1) - 1] [2(a_2^{(\min)} + 2M - 1) + 1] \prod_{l=M}^{N-1} \frac{[2(a_2^{(\min)} + 2l + 1) - 1] [2(a_2^{(\min)} + 2l + 1) + 1]}{[2(a_2^{(\min)} + 2l) - 1] [2(a_2^{(\min)} + 2l) + 1]} \\ &\quad \times \frac{1}{U_{2M-1}^{(1,2)} U_{2M-1}^{(3,4)}} \prod_{l=M}^{N-1} \frac{U_{2l}^{(1,2)} U_{2l}^{(3,4)}}{U_{2l+1}^{(1,2)} U_{2l+1}^{(3,4)}} \times \frac{1}{R_{2M-1}^{(1,2)} R_{2M-1}^{(3,4)}} \prod_{l=M}^{N-1} \frac{R_{2l}^{(1,2)} R_{2l}^{(3,4)}}{R_{2l+1}^{(1,2)} R_{2l+1}^{(3,4)}} \\ &= \frac{(2a_2^{(\min)} + 4M - 3)(2a_2^{(\min)} + 4N - 1)}{U_{2M-1}^{(1,2)} U_{2M-1}^{(3,4)} R_{2N-1}^{(1,2)} R_{2N-1}^{(3,4)}} \prod_{l=M}^{N-1} \underbrace{\frac{R_{2l}^{(1,2)} R_{2l}^{(3,4)} U_{2l}^{(1,2)} U_{2l}^{(3,4)}}{R_{2l-1}^{(1,2)} R_{2l-1}^{(3,4)} U_{2l+1}^{(1,2)} U_{2l+1}^{(3,4)}}}_{=: x(2l)} \end{aligned} \quad (7.26)$$

Note that by construction (7.26) also holds for the case $\boxed{M = N}$ just by leaving out the product of the $x(2l)$, as can be seen from the fact that

$$|L^{(M,M)}|^2 = |q_{2M-1}|^{-2} = \frac{(2a_2^{(\min)} + 4M - 3)(2a_2^{(\min)} + 4M - 1)}{U_{2M-1}^{(1,2)} U_{2M-1}^{(3,4)} R_{2M-1}^{(1,2)} R_{2M-1}^{(3,4)}} \quad (7.27)$$

In the last line of (7.26) we have moreover introduced

$$x(2l) := \frac{R_{2l}^{(1,2)} R_{2l}^{(3,4)} U_{2l}^{(1,2)} U_{2l}^{(3,4)}}{R_{2l-1}^{(1,2)} R_{2l-1}^{(3,4)} U_{2l+1}^{(1,2)} U_{2l+1}^{(3,4)}} \quad (7.28)$$

Now due to positivity of all terms contained in $R_k^{(m,n)}, U_k^{(m,n)}$ we always have $\boxed{x \leq 1}$ in (7.26). Let us take a closer look at the product terms contained in (7.26) for the case that $\boxed{M < N}$.

Using $\boxed{x^{(m,n)} = j_m + j_n - a_2^{(\min)} + 1}$ we may write

$$\begin{aligned} \prod_{l=M}^{N-1} \frac{R_{2l}^{(m,n)}}{R_{2l-1}^{(m,n)}} &= \prod_{l=M}^{N-1} \frac{x^{(m,n)} - 2l}{x^{(m,n)} - 2l + 1} \\ &= \prod_{l=-M}^{-N+1} \frac{x^{(m,n)} + 2l}{x^{(m,n)} + 2l + 1} && \text{introduce: } r = l + N \\ &= \prod_{r=1}^{N-M} \frac{x^{(m,n)} - 2N + 2r}{x^{(m,n)} - 2N + 2r + 1} \\ &= \frac{\Gamma(1 + \frac{x^{(m,n)}}{2} - M)}{\Gamma(1 + \frac{x^{(m,n)}}{2} - N)} \cdot \frac{\Gamma(\frac{3}{2} + \frac{x^{(m,n)}}{2} - N)}{\Gamma(\frac{3}{2} + \frac{x^{(m,n)}}{2} - M)} \end{aligned} \quad (7.29)$$

Using $x_1^{(m,n)} = j_m + j_n + a_2^{(min)} + 1$, $x_2^{(m,n)} = -j_m + j_n + a_2^{(min)}$, $x_3^{(m,n)} = j_m - j_n + a_2^{(min)}$ we can write

$$\begin{aligned}
\prod_{l=M}^{N-1} \frac{U_{2l}^{(m,n)}}{U_{2l+1}^{(m,n)}} &= \prod_{l=M}^{N-1} \left[\prod_{\mu=1}^3 \frac{x_\mu + 2l}{x_\mu + 2l + 1} \right] && \text{introduce: } s = l - M + 1 \\
&= \prod_{\mu=1}^3 \left[\prod_{s=1}^{N-M} \frac{x_\mu + 2M + 2(s-1)}{x_\mu + 2M + 2(s-1) + 1} \right] \\
&= \prod_{\mu=1}^3 \left[\prod_{s=0}^{N-M-1} \frac{x_\mu + 2M + 2s}{x_\mu + 2M + 2s + 1} \right] \\
&= \prod_{\mu=1}^3 \left[\left(\prod_{s=1}^{N-M} \frac{x_\mu + 2M + 2s}{x_\mu + 2M + 2s + 1} \right) \cdot \frac{x_\mu + 2N + 1}{x_\mu + 2N} \cdot \frac{x_\mu + 2M}{x_\mu + 2M + 1} \right] \\
&= \prod_{\mu=1}^3 \left[\frac{\Gamma(1 + \frac{x_\mu}{2} + N)}{\Gamma(1 + \frac{x_\mu}{2} + M)} \cdot \frac{\Gamma(\frac{3}{2} + \frac{x_\mu}{2} + M)}{\Gamma(\frac{3}{2} + \frac{x_\mu}{2} + N)} \cdot \frac{x_\mu + 2N + 1}{x_\mu + 2N} \cdot \frac{x_\mu + 2M}{x_\mu + 2M + 1} \right] \\
&\leq \prod_{\mu=1}^3 \left[\frac{\Gamma(1 + \frac{x_\mu}{2} + N)}{\Gamma(1 + \frac{x_\mu}{2} + M)} \cdot \frac{\Gamma(\frac{3}{2} + \frac{x_\mu}{2} + M)}{\Gamma(\frac{3}{2} + \frac{x_\mu}{2} + N)} \right] \tag{7.30}
\end{aligned}$$

since $\frac{x_\mu + 2N + 1}{x_\mu + 2N} \frac{x_\mu + 2M}{x_\mu + 2M + 1} \leq 1$ because $M < N$ and the function $f(y) = \frac{y}{y+1}$ is monotonically increasing. Using the expansion of the Γ -function [28] one may check that

$$e^{-x} x^{x-\frac{1}{2}} \sqrt{2\pi} < \Gamma(x) < 2 \cdot e^{-x} x^{x-\frac{1}{2}} \sqrt{2\pi} \quad \forall x \in \mathbb{R} \quad x > 1 \tag{7.31}$$

moreover we have

$$\left(1 + \frac{1}{x}\right)^x < e < 2 \cdot \left(1 + \frac{1}{x}\right)^x \quad \forall x \in \mathbb{R} \quad x > 1 \tag{7.32}$$

and we can estimate

$$\frac{\Gamma(x)}{\Gamma(x + \frac{1}{2})} \leq \frac{2\sqrt{2}}{\sqrt{x}} \quad \text{and} \quad \frac{\Gamma(x + \frac{1}{2})}{\Gamma(x)} \leq 2\sqrt{x} \tag{7.33}$$

and finally obtain from (7.29)

$$\prod_{l=M}^{N-1} \frac{R_{2l}^{(m,n)}}{R_{2l-1}^{(m,n)}} = \frac{\Gamma(1 + \frac{x^{(m,n)}}{2} - M)}{\Gamma(1 + \frac{x^{(m,n)}}{2} - N)} \cdot \frac{\Gamma(\frac{3}{2} + \frac{x^{(m,n)}}{2} - N)}{\Gamma(\frac{3}{2} + \frac{x^{(m,n)}}{2} - M)} \leq 4\sqrt{2} \left[\frac{1 + \frac{x^{(m,n)}}{2} - N}{1 + \frac{x^{(m,n)}}{2} - M} \right]^{\frac{1}{2}} \tag{7.34}$$

For (7.30) we find

$$\prod_{l=M}^{N-1} \frac{U_{2l}^{(m,n)}}{U_{2l+1}^{(m,n)}} \leq \prod_{\mu=1}^3 \left[\frac{\Gamma(1 + \frac{x_\mu^{(m,n)}}{2} + N)}{\Gamma(1 + \frac{x_\mu^{(m,n)}}{2} + M)} \cdot \frac{\Gamma(\frac{3}{2} + \frac{x_\mu^{(m,n)}}{2} + M)}{\Gamma(\frac{3}{2} + \frac{x_\mu^{(m,n)}}{2} + N)} \right] \leq (4\sqrt{2})^3 \prod_{\mu=1}^3 \left[\frac{1 + \frac{x_\mu^{(m,n)}}{2} + M}{1 + \frac{x_\mu^{(m,n)}}{2} + N} \right]^{\frac{1}{2}} \tag{7.35}$$

Now recall that

$$j_1 \leq j_2 \leq j_3 \leq j_4 \tag{7.36}$$

where j_4 equals the maximal spin j_{\max} . Note the ranges of the intermediate recoupling spin $a_2 = a_2^{(min)} + k$ according to (7.5). Now without loss of generality assume $a_2^{(min)} = j_2 - j_1$.³² Then the dimension of the matrix \widehat{Q}_D is given by

$$\dim \widehat{Q}_D = a_2^{(max)} - a_2^{(min)} + 1 = 2j_1 + 1 \tag{7.37}$$

which implies $M \leq N \leq j_1 + \frac{1}{2}$. So finally by using the definitions for $x^{(m,n)}$, $x_\mu^{(m,n)}$ above with $a_2^{(min)} = j_2 - j_1$:

$$\begin{aligned}
x^{(1,2)} &= 2j_1 + 1 & x^{(3,4)} &= j_3 + j_4 - j_2 + j_1 + 1 \\
x_1^{(1,2)} &= 2j_2 + 1 & x_1^{(3,4)} &= j_3 + j_4 + j_2 - j_1 + 1 \\
x_2^{(1,2)} &= 2(j_2 - j_1) & x_2^{(3,4)} &= -j_3 + j_4 + j_2 - j_1 \\
x_3^{(1,2)} &= 0 & x_3^{(3,4)} &= j_3 - j_4 + j_2 - j_1
\end{aligned} \tag{7.38}$$

³²Note that we might equivalently choose $a_2^{(min)} = j_4 - j_3$ here, as (7.26) is symmetric with respect to interchanging $(j_1, j_2) \leftrightarrow (j_3, j_4)$.

we can estimate using (7.34)

$$\prod_{l=M}^{N-1} \frac{R_{2l}^{(1,2)} R_{2l}^{(3,4)}}{R_{2l-1}^{(1,2)} R_{2l-1}^{(3,4)}} \leq 32 \cdot \left[\frac{(3+2j_1-2N)(3+j_3+j_4-j_2+j_1-2N)}{(3+2j_1-2M)(3+j_3+j_4-j_2+j_1-2M)} \right]^{\frac{1}{2}} \quad (7.39)$$

moreover with (7.35):

$$\begin{aligned} \prod_{l=M}^{N-1} \frac{U_{2l}^{(1,2)} U_{2l}^{(3,4)}}{U_{2l+1}^{(1,2)} U_{2l+1}^{(3,4)}} &\leq (32)^3 \left[\frac{(3+2j_2+2M)}{(3+2j_2+2N)} \right]^{\frac{1}{2}} \left[\frac{(3+j_3+j_4+j_2-j_1+2M)}{(3+j_3+j_4+j_2-j_1+2N)} \right]^{\frac{1}{2}} \\ &\times \left[\frac{(1+j_2-j_1+M)}{(1+j_2-j_1+N)} \right]^{\frac{1}{2}} \left[\frac{(2-j_3+j_4+j_2-j_1+2M)}{(2-j_3+j_4+j_2-j_1+2N)} \right]^{\frac{1}{2}} \\ &\times \left[\frac{(1+M)}{(1+N)} \right]^{\frac{1}{2}} \left[\frac{(2+j_3-j_4+j_2-j_1+2M)}{(2+j_3-j_4+j_2-j_1+2N)} \right]^{\frac{1}{2}} \end{aligned} \quad (7.40)$$

Combining (7.39) and (7.40) we finally get an upper bound for the last product on the right hand side of (7.26) by taking into account that $0 < M < N$:

$$\begin{aligned} \prod_{l=M}^{N-1} x(2l) &= \prod_{l=M}^{N-1} \frac{R_{2l}^{(1,2)} R_{2l}^{(3,4)} U_{2l}^{(1,2)} U_{2l}^{(3,4)}}{R_{2l-1}^{(1,2)} R_{2l-1}^{(3,4)} U_{2l+1}^{(1,2)} U_{2l+1}^{(3,4)}} \\ &\leq (32)^4 \left[\frac{(3+2j_1-2N)}{(3+2j_1-2M)} \right]^{\frac{1}{2}} \left[\frac{(3+j_3+j_4-j_2+j_1-2N)}{(3+j_3+j_4-j_2+j_1-2M)} \right]^{\frac{1}{2}} \\ &\times \left[\frac{(3+2j_2+2M)}{(3+2j_2+2N)} \right]^{\frac{1}{2}} \left[\frac{(3+j_3+j_4+j_2-j_1+2M)}{(3+j_3+j_4+j_2-j_1+2N)} \right]^{\frac{1}{2}} \left[\frac{(1+j_2-j_1+M)}{(1+j_2-j_1+N)} \right]^{\frac{1}{2}} \\ &\times \left[\frac{(2-j_3+j_4+j_2-j_1+2M)}{(2-j_3+j_4+j_2-j_1+2N)} \right]^{\frac{1}{2}} \left[\frac{(1+M)}{(1+N)} \right]^{\frac{1}{2}} \left[\frac{(2+j_3-j_4+j_2-j_1+2M)}{(2+j_3-j_4+j_2-j_1+2N)} \right]^{\frac{1}{2}} \end{aligned} \quad (7.41)$$

By construction we have already seen that

$$\prod_{l=M}^{N-1} x(2l) \leq 1 \quad (7.42)$$

however the reason for the explicit calculation of (7.41) will become clear in a moment. Using (7.42) we give a first upper bound on $|L^{(M,N)}|^2$ in (7.26)

$$\begin{aligned} |L^{(M,N)}|^2 &\leq \frac{(2a_2^{(min)} + 4M - 3)(2a_2^{(min)} + 4N - 1)}{U_{2M-1}^{(1,2)} U_{2M-1}^{(3,4)} R_{2N-1}^{(1,2)} R_{2N-1}^{(3,4)}} \\ &= \frac{\overbrace{(2a_2^{(min)} + 4M - 3)(2a_2^{(min)} + 4N - 1)}^{T_3}}{\underbrace{(j_1 + j_2 + a_2^{(min)} + 2M)(-j_1 + j_2 + a_2^{(min)} + 2M - 1)(j_1 - j_2 + a_2^{(min)} + 2M - 1)}_{T_1}} \\ &\times \frac{1}{\underbrace{(j_3 + j_4 + a_2^{(min)} + 2M)(-j_3 + j_4 + a_2^{(min)} + 2M - 1)(j_3 - j_4 + a_2^{(min)} + 2M - 1)}_{T_2}} \\ &\times \frac{1}{\underbrace{(j_1 + j_2 - a_2^{(min)} - 2N + 2)(j_3 + j_4 - a_2^{(min)} - 2N + 2)}_{T_4}} \end{aligned} \quad (7.43)$$

In order to get an estimate for the smallest non-zero eigenvalue we will now perform a power counting in $j_4 = j_{\max}$ for all the different factors $T_1 \dots T_4$ in (7.43), that is while respecting (7.36) we have to minimize the obvious inverse power of $j_4 = j_{\max}$ in (7.43). To do so we make the following ansatz:

$$\begin{aligned} j_1 &= \alpha_1 j_{\max} + \beta_1 & M &= \alpha_M j_{\max} + \beta_M \\ j_2 &= \alpha_2 j_{\max} + \beta_2 & N &= \alpha_N j_{\max} + \beta_N \\ j_3 &= \alpha_3 j_{\max} + \beta_3 \\ j_4 &= j_{\max} \end{aligned} \quad (7.44)$$

which is justified if in the factor terms T_1, T_2, T_4 contained in (7.43) the power of j_{\max} should be lowered (raised in T_3) while simultaneously respecting (7.36) as $j_{\max} \rightarrow \infty$ ³³. Moreover by inspection we find that in (7.41) only M, N matter (and $M < N$), since all other factors in the numerator and denominator are identical and it is therefore sufficient to look at (7.41) alone.

Upon inserting (7.44) into (7.43) and again assuming $a_2^{(min)} = j_2 - j_1$ one obtains

$$\begin{aligned} |L^{(M,N)}|^2 &\leq \frac{2 \cdot 2 [(\alpha_2 - \alpha_1 + 2\alpha_M) \cdot j_4 + \beta_2 - \beta_1 + 2\beta_M - \frac{3}{2}] [(\alpha_2 - \alpha_1 + 2\alpha_N) \cdot j_4 + \beta_2 - \beta_1 + 2\beta_N - \frac{1}{2}]}{2 [c_1 \cdot j_4 + \beta_2 + \beta_M] 2 [c_2 \cdot j_4 + \beta_2 - \beta_1 + \beta_M - \frac{1}{2}] 2 [c_3 \cdot j_4 + \beta_M - \frac{1}{2}]} \\ &\quad \times \frac{1}{[c_4 \cdot j_4 + \beta_3 + \beta_2 - \beta_1 + 2\beta_M] [c_5 \cdot j_4 - \beta_3 + \beta_2 - \beta_1 + 2\beta_M - 1] [c_6 \cdot j_4 + \beta_3 + \beta_2 - \beta_1 + 2\beta_M - 1]} \\ &\quad \times \frac{1}{2 [c_7 \cdot j_4 + \beta_1 - \beta_N + 1] [c_8 \cdot j_4 + \beta_3 - \beta_2 + \beta_1 - 2\beta_N + 2]} \end{aligned} \quad (7.45)$$

where we have introduced the shorthands

$$\begin{aligned} c_1 &= \alpha_2 + \alpha_M & c_4 &= 1 + \alpha_3 + \alpha_2 - \alpha_1 + 2\alpha_M & c_7 &= \alpha_1 - \alpha_N \\ c_2 &= \alpha_2 - \alpha_1 + \alpha_M & c_5 &= 1 - \alpha_3 + \alpha_2 - \alpha_1 + 2\alpha_M & c_8 &= 1 + \alpha_3 - \alpha_2 + \alpha_1 - 2\alpha_N \\ c_3 &= \alpha_M & c_6 &= -1 + \alpha_3 + \alpha_2 - \alpha_1 + 2\alpha_M \end{aligned} \quad (7.46)$$

where $c_k \geq 0$ for all $k = 1 \dots 8$ due to positivity of the according factors in (7.45). The set of shorthands (7.46) can be seen as a system of 8 equalities for the 5 variables $\alpha_1, \alpha_2, \alpha_3, \alpha_M, \alpha_N$. Thus we can eliminate these 5 variables by using 5 equations which results in three remaining consistency equations among the constants c_1, \dots, c_8 .

$$\begin{aligned} 2c_1 &= 2 + c_6 + 2c_7 - c_8 \\ 2c_2 &= -2c_3 + c_5 + c_6 \\ c_4 &= 2 + c_6 \end{aligned} \quad \text{and } c_k \geq 0 \quad \forall k = 1 \dots 8 \quad (7.47)$$

The question is now how one can choose the maximal number of c 's equal to 0 consistently. By inspection of (7.47) we can simultaneously set at most 6 of the c 's to zero if:

$$\begin{aligned} \boxed{\text{Case 1}} \quad c_1 &= 1 \quad c_4 = 2 \\ \text{and} \\ c_2 &= c_3 = c_5 = c_6 = c_7 = c_8 = 0 \end{aligned}$$

Then the set (7.46) obeys a solution:

$$\begin{aligned} \alpha_1 &= 1 \\ \alpha_2 &= 1 \\ \alpha_3 &= 1 \\ \alpha_M &= 0 \\ \alpha_N &= 1 \end{aligned}$$

$$\begin{aligned} \boxed{\text{Case 2}} \quad c_8 &= 2 \quad c_4 = 2 \\ \text{and} \\ c_1 &= c_2 = c_3 = c_5 = c_6 = c_7 = 0 \end{aligned}$$

Then the set (7.46) obeys a solution:

$$\begin{aligned} \alpha_1 &= 0 \\ \alpha_2 &= 0 \\ \alpha_3 &= 1 \\ \alpha_M &= 0 \\ \alpha_N &= 0 \end{aligned}$$

Case 1

Here (7.45) reads as

$$\begin{aligned} |L^{(M,N)}|^2 &\leq \frac{2(\beta_2 - \beta_1 + 2\beta_M - \frac{3}{2}) 2(2j_4 + \beta_2 - \beta_1 + 2\beta_N - \frac{1}{2})}{2(j_4 + \beta_2 + \beta_M) 2(\beta_2 - \beta_1 + \beta_M - \frac{1}{2}) 2(\beta_M - \frac{1}{2})(2j_4 + \beta_3 + \beta_2 - \beta_1 + 2\beta_M)(-\beta_3 + \beta_2 - \beta_1 + 2\beta_M - 1)} \\ &\quad \times \frac{1}{(\beta_3 + \beta_2 - \beta_1 + 2\beta_M - 1) 2(\beta_1 - \beta_N + 1)(\beta_3 - \beta_2 + \beta_1 - 2\beta_N + 2)} \\ &\sim \frac{1}{j_4} \end{aligned} \quad (7.48)$$

³³Certainly the ansatz (7.44) qualifies only to estimate the largest inverse power of the maximal spin in the limit $j_{\max} \rightarrow \infty$. We could in principle assume the spins to be arbitrary polynomials of j_{\max} . However we want to look for the smallest inverse power of j_{\max} , that is we want the spins to be configured such that any higher inverse power of j_{\max} is compensated in (7.43). In the limit $j_{\max} \rightarrow \infty$ this can only be achieved if the spins scale with the same power of j_{\max} .

However (7.41) gives in this case

$$\begin{aligned}
\prod_{l=M}^{N-1} x(2l) &\leq (32)^4 \left[\frac{(3+2\beta_1-2\beta_N)}{(3+2j_4+2\beta_1-2\beta_M)} \right]^{\frac{1}{2}} \left[\frac{(3+\beta_3-\beta_2+\beta_1-2\beta_N)}{(3+2j_4+\beta_3-\beta_2+\beta_1-2\beta_M)} \right]^{\frac{1}{2}} \\
&\times \left[\frac{(3+2j_4+2\beta_2+2\beta_M)}{(3+2j_4+2\beta_2+2j_4+2\beta_N)} \right]^{\frac{1}{2}} \left[\frac{(3+j_4+\beta_3+j_4+\beta_2-\beta_1+2\beta_M)}{(3+j_4+\beta_3+j_4+\beta_2-\beta_1+2j_4+2\beta_N)} \right]^{\frac{1}{2}} \\
&\times \left[\frac{(1+\beta_2-\beta_1+\beta_M)}{(1+\beta_2-\beta_1+j_4+\beta_N)} \right]^{\frac{1}{2}} \left[\frac{(2-\beta_3+\beta_2-\beta_1+2\beta_M)}{(2-\beta_3+\beta_2-\beta_1+2j_4+2\beta_N)} \right]^{\frac{1}{2}} \\
&\times \left[\frac{(1+\beta_M)}{(1+j_4+\beta_N)} \right]^{\frac{1}{2}} \left[\frac{(2+\beta_3-\beta_4+\beta_2-\beta_1+2\beta_M)}{(2+\beta_3-\beta_4+\beta_2-\beta_1+2j_4+2\beta_N)} \right]^{\frac{1}{2}} \\
&\sim \frac{1}{(j_4)^3}
\end{aligned} \tag{7.49}$$

We therefore find that in **Case 1** $|L^{(M,N)}|$ is bounded from above by a quantity of the order $\frac{1}{(j_{\max})^2}$. Moreover according to (7.37) the dimension of the matrix \widehat{Q} is given by $\dim \widehat{Q} = 2j_1 + 1 = 2j_4 + 2\beta_1 + 1$ which is proportional to j_{\max} . Therefore upon summing up all terms in the row/column sums in order to apply theorem 7.2, we could get an additional factor of j_{\max} . However, taking this sum implies increasing M and taking $M = \beta_M \sim j_4$. This contradicts our minimization of the inverse power of j_{\max} above immediately. Despite this we still may assume $j_1 \leq j_2 \leq j_3 \leq j_4$ and if we want the dimension D of \widehat{Q}_D to scale with the maximal spin then (7.5) forces us to take $j_1 \sim j_2 \sim j_3 \sim j_4 = j_{\max}$. But then in (7.46) all constants but c_7, c_8 are non zero because for all α 's we have $0 \leq \alpha \leq 1$. Inserting this into (7.48) and (7.49) gives

$$\left| L^{(M,N)} \right|^2 \sim \frac{1}{(j_4)^4} \quad \text{and} \quad \prod_{l=M}^{N-1} x(2l) \sim \frac{1}{j_4} \quad \text{unless } \beta_M = j_4 \tag{7.50}$$

and therefore taking the row sum will not change the inverse power of j_{\max} , because $\lim_{M \rightarrow N} |L^{(M,N)}| \sim (j_{\max})^{-\frac{5}{2}}$ and thus the maximal row sum will be of an order $(j_{\max})^{-r}$ where $r > 1$.

Note that the case **M=N** contradicts the assumptions of **case 1**, since for $M = N$ it must hold that $\alpha_M = \alpha_N$. This case will be included in the following discussion.

Case 2

Using (7.44) we have

$$\begin{aligned}
j_1 &= \beta_1 & j_3 &= j_{\max} + \beta_3 & M &= \beta_M \\
j_2 &= \beta_2 & j_4 &= j_{\max} & N &= \beta_N
\end{aligned} \tag{7.51}$$

Here (7.45) reads as

$$\begin{aligned}
\left| L^{(M,N)} \right|^2 &\leq \frac{2(\beta_2 - \beta_1 + 2\beta_M - \frac{3}{2}) 2(\beta_2 - \beta_1 + 2\beta_N - \frac{1}{2})}{2(\beta_2 + \beta_M) 2(\beta_2 - \beta_1 + \beta_M - \frac{1}{2}) 2(\beta_M - \frac{1}{2})(2j_4 + \beta_3 + \beta_2 - \beta_1 + 2\beta_M)(-\beta_3 + \beta_2 - \beta_1 + 2\beta_M - 1)} \\
&\times \frac{1}{(\beta_3 + \beta_2 - \beta_1 + 2\beta_M - 1) 2(\beta_1 - \beta_N + 2)(2j_4 + \beta_3 - \beta_2 + \beta_1 - 2\beta_N + 2)} \\
&\sim \frac{1}{(j_4)^2}
\end{aligned} \tag{7.52}$$

By observation, since M, N do not scale with the largest spin, (7.41) is only sensitive to M, N and thus becomes a constant in the limit $j_4 \rightarrow \infty$. Since $j_1 \leq j_2$ we must have $\beta_1 \leq \beta_2$. Moreover $j_3 \leq j_4$ and thus $\beta_3 \stackrel{!}{=} 0$. Also recall that $1 \leq M \leq N \leq j_1 + \frac{1}{2}$ which implies, together with (7.51), that $1 \leq \beta_M \leq \beta_N \leq \beta_1 + \frac{1}{2}$. Additionally we observe that the row/column sum contains at most $N = \beta_N$ terms. Hence

$$\begin{aligned}
\left| L^{(M,N)} \right|^2 &\leq \frac{(\beta_2 - \beta_1 + 2\beta_M - \frac{3}{2}) (\beta_2 - \beta_1 + 2\beta_N - \frac{1}{2})}{4(\beta_2 + \beta_M) (\beta_2 - \beta_1 + \beta_M - \frac{1}{2}) (\beta_M - \frac{1}{2})(2j_4 + \beta_2 - \beta_1 + 2\beta_M)(\beta_2 - \beta_1 + 2\beta_M - 1)} \\
&\times \frac{1}{(\beta_2 - \beta_1 + 2\beta_M - 1) (\beta_1 - \beta_N + 2)(2j_4 - \beta_2 + \beta_1 - 2\beta_N + 2)}
\end{aligned} \tag{7.53}$$

Now by inspection of (7.53), we find that $\left| L^{(M,N)} \right|^2$ scales as $(\beta_2)^{-4}, (\beta_1)^{-4}, (\beta_M)^{-5}, (\beta_N)^{-1}$. The row sum of the inverse matrix \widehat{Q}_D^{-1} contains β_N terms. However $\beta_N \leq \beta_1 + \frac{1}{2}$ and hence β_N cannot be increased without increasing

β_1 and thus β_2 . This overcompensates the possible β_N terms of type (7.53) in a row sum. Therefore we will set $\beta_2 = \beta_1 =: \beta_{12}$ and $\beta_M = 1$. Then

$$\begin{aligned} \left|L^{(1,N)}\right|^2 &\leq \frac{\left(\frac{1}{2}\right) (2\beta_N - \frac{1}{2})}{4 (\beta_{12} + 1) \left(\frac{1}{2}\right) \left(\frac{1}{2}\right) (2j_4 + 2)(1)} \times \frac{1}{(1) (\beta_{12} - \beta_N + 2)(2j_4 - 2\beta_N + 2)} \\ &\leq \frac{\beta_N}{4(\beta_{12} + 1) (j_4 + 1)(\beta_{12} - \beta_N + 2)(j_4 - \beta_N + 1)} \\ &\leq \frac{\beta_N}{4\beta_{12} j_4(\beta_{12} - \beta_N + 2)(j_4 - \beta_N + 1)} \end{aligned} \quad (7.54)$$

If we demand (7.54) to be valid already for $j_4 = j_{\max} = \frac{1}{2}$, then we have to fix $\beta_N = 1$ due to positivity of $\left|L^{(M,N)}\right|$. In order to still obtain an upper limit for $\left|L^{(M,N)}\right|$, this implies we minimize β_{12} by setting it to $\frac{1}{2}$. Then

$$\left|L^{(1,1)}\right| \leq \frac{1}{\sqrt{3} j_4} < \frac{1}{j_4} \quad (7.55)$$

Recall that always $x(2l) < 1$, but from (7.41) it can be seen that for **Case 2** the quantity $x(2l)$ does not scale with inverse powers of j_{\max} , as j_{\max} is increased. Therefore we can obtain a row sum of an order $(j_{\max})^{-1}$.

Note that giving an upper bound on $L^{(M,N)}$ leads us to set $(M, N) = (1, 1)$, which gives the special case of (7.27). Now the finite upper bound (7.55) for the spectrum of the inverse matrix \widehat{Q}_D^{-1} provides us with a lower bound for the smallest non-zero eigenvalue of \widehat{Q}_D in leading order of the maximal spin j_{\max} . This lower bound is given, for the spins $j_1 = j_2 = \frac{1}{2}, j_3 = j_4 = j_{\max}$, as

$$\lambda_{\widehat{Q}}^{(min)} \geq \frac{1}{\left|L^{(1,1)}\right|} = j_{\max} \quad (7.56)$$

This may be compared to the numerical result $\lambda_{\widehat{Q}}^{(min)} = 2 \cdot \sqrt{j_{\max}(j_{\max} + 1)}$ obtained in [24] contributed by the spin configuration $j_1 = j_2 = \frac{1}{2}$ and $j_3 = j_4 = j_{\max}$. Our estimate above explains this combination of spins. Recall that $\lambda_{\widehat{V}}^{(min)} = \sqrt{|\lambda_{\widehat{Q}}^{(min)}|}$. Therefore we conclude that:

The smallest non-zero eigenvalue $\lambda_{\widehat{V},4\text{-vertex}}^{(min)}$ of the volume operator \widehat{V} acting on a gauge invariant four valent vertex v with spin configuration $j_1 \leq j_2 \leq j_3 \leq j_4 = j_{\max}$ is bounded from below by

$$\lambda_{\widehat{V},4\text{-vertex}}^{(min)}(j_{\max}) \geq \ell_P^3 \sqrt{|Z| \cdot |\sigma(123)|} \cdot j_{\max} \quad (7.57)$$

where Z is the regularization constant in (2.25), $\sigma(123) = 0, \pm 2, \pm 4$, and ℓ_P is the Planck length.

8 Summary

In this paper and its companion [25] we have presented a comprehensive analysis of the spectral properties of the volume operator \widehat{V} in Loop Quantum Gravity (LQG), which may serve as a starting point for a computer based analysis of the action of constraint operators in the full theory. We have shown how the volume operator \widehat{V} can be handled analytically in case of a 4-valent vertex, and numerically in the general case. In this context we have analyzed how the spatial diffeomorphism invariant properties of the graphs underlying the states of the kinematical Hilbert space, as encoded in the sign factors $\epsilon(IJK)$, become relevant in a practical computation. This aspect of the theory, although known, has not been analyzed in detail before the present work.

A further summary and outlook is given in section 6 of the companion paper [25].

9 Acknowledgments

We would like to thank Thomas Thiemann for encouraging us to start this project and for suggestions and discussion on the issue of the sign factors. His continuous, reliable support for this project and his helpful suggestions on the manuscript are gratefully acknowledged. We thank Steve White for pointing out to us the relative merit of singular value decomposition, because of its numerical stability. This resulted in a significant improvement in the quality of our numerical results. Moreover we thank Jonathan Thornburg for providing perspective into the problem of handling numerical error.

We would like to thank Luciano Rezzolla and the numerical relativity group at the Albert Einstein Institute Potsdam for support and use of computational resources at the AEI, in particular the Peyote cluster. In addition we thank the Perimeter Institute for Theoretical Physics, where parts of this project were completed, for hospitality.

JB thanks the Gottlieb-Daimler and Carl-Benz foundation, the German Academic Exchange Office as well as the Albert Einstein Institute for financial support. Furthermore JB has been supported in part by the Emmy-Noether-Programm of the Deutsche Forschungsgemeinschaft under grant FL 622/1-1. The work of DR was supported in part through the Marie Curie Research and Training Network ENRAGE (MRTN-CT-2004-005616).

We thank Simone Speziale for pointing out [17] to us.

We are grateful for valuable suggestions on improving the manuscript by anonymous referees of Classical and Quantum Gravity.

Appendices

This paper and its companion [25] make heavy use of special properties of the spin network functions, in particular the fact that the action of the flux operators on spin network basis states can be mapped to the problem of evaluating angular momentum operators on angular momentum eigenstates, the latter of which is familiar from ordinary quantum mechanics. This not only results in a great simplification, but also provides a convenient way to work in the $SU(2)$ -gauge-invariant regime by using powerful techniques from the recoupling theory of angular momenta.

We have added these appendices in order to provide the reader with details on the conventions we use, for example in the construction of recoupling schemes. Moreover the reader not familiar with these techniques is given a brief summary, in order to be able to redo the computations presented here.

The appendices are organized as follows: In appendix A we give basic properties of matrix representations of $SU(2)$, whose matrix elements are used for the definition of spin network functions. Appendix B then summarizes the theory of angular momentum from quantum mechanics, and discusses an extended notion of recoupling of an arbitrary number of angular momenta in terms of recoupling schemes, as we use them. Appendix C completes this presentation with the definition of so called $6j$ -symbols, along with an elaboration of their basic properties. This provides an explicit notion of recoupling schemes in terms of polynomials of quantum numbers. Finally A,B,C are connected in appendix D, in which the correspondence between spin network states and angular momentum states is reviewed in detail.

A Representations of $SU(2)$

Irreducible matrix representations of $SU(2)$ can be constructed in $(2j+1)$ -dimensional linear vector spaces, where $j \geq 0$ is a half integer number; $j = 0$ denotes the trivial representation. Note that we write for the defining representation of a group element $h \in SU(2)$ $[\pi_{j=\frac{1}{2}}(h)]_{mn} = h_{AB}$ and for general representation matrices $[\pi_j(h)]_{mn}$: the rows m are labelled from top to bottom by $m = j \dots -j$ and the columns n from left to right by $n = j \dots -j$.

In the following an overline denotes complex conjugation, while \cdot^T indicates the transpose.

A.1 General Conventions — Defining Representation $\boxed{j = \frac{1}{2}}$

A.1.1 Generators

As generators of $SU(2)$ we use the τ -matrices given by $\tau_k := -i\sigma_k$, with σ_k being the Pauli-matrices:

$$\begin{aligned} \sigma_1 &= \begin{pmatrix} 0 & 1 \\ 1 & 0 \end{pmatrix} & \sigma_2 &= \begin{pmatrix} 0 & -i \\ i & 0 \end{pmatrix} & \sigma_3 &= \begin{pmatrix} 1 & 0 \\ 0 & -1 \end{pmatrix} & \text{for which} & & [\sigma_i, \sigma_j] &= 2i \epsilon^{ijk} \sigma_k \\ \tau_1 &= \begin{pmatrix} 0 & -i \\ -i & 0 \end{pmatrix} & \tau_2 &= \begin{pmatrix} 0 & -1 \\ 1 & 0 \end{pmatrix} & \tau_3 &= \begin{pmatrix} -i & 0 \\ 0 & i \end{pmatrix} & \text{for which} & & [\tau_i, \tau_j] &= 2 \epsilon^{ijk} \tau_k \end{aligned} \tag{A.1}$$

Additionally we use

$$\epsilon = -\tau_2 = \begin{pmatrix} 0 & 1 \\ -1 & 0 \end{pmatrix} \quad \text{with the obvious properties} \quad \epsilon^{-1} = \epsilon^T = -\epsilon = \begin{pmatrix} 0 & -1 \\ 1 & 0 \end{pmatrix} \tag{A.2}$$

A.1.2 $SU(2)$ Representations

In the defining representation of $SU(2)$, for a group element $h \in SU(2)$, we have

$$h = \begin{pmatrix} a & b \\ -\bar{b} & \bar{a} \end{pmatrix} \quad \text{for which} \quad \det h = |a|^2 + |b|^2 = 1 \tag{A.3}$$

where $a, b \in \mathbb{C}$. Moreover

$$h^{-1} = \epsilon h^T \epsilon^{-1} = \begin{pmatrix} \bar{a} & -b \\ \bar{b} & a \end{pmatrix} \tag{A.4}$$

and we have the additional properties that

$$\bar{h} = [h^{-1}]^T = [\epsilon h^T \epsilon^T]^T = \epsilon h \epsilon^T = \epsilon h \epsilon^{-1} \quad (\text{A.5})$$

As mentioned above, we use the following convention for the matrix elements of $[\pi_{j=\frac{1}{2}}(h)]_{AB}$, with A being the row and B the column index

$$\begin{aligned} h_{11} &= h_{\frac{1}{2} \frac{1}{2}} = a & h_{12} &= h_{\frac{1}{2} -\frac{1}{2}} = b \\ h_{21} &= h_{-\frac{1}{2} \frac{1}{2}} = -\bar{b} & h_{22} &= h_{-\frac{1}{2} -\frac{1}{2}} = \bar{a} \end{aligned} \quad (\text{A.6})$$

For the τ_k 's we additionally have

$$-\overline{\tau_k}^T = \tau_k = -(\tau_k)^{-1} \quad (\text{A.7})$$

A.2 General Conventions for $(2j+1)$ -dimensional $SU(2)$ -Representation Matrices

Here we follow [32, 22, 23].

A.2.1 General Formula for $SU(2)$ Matrix Element

The $(2j+1)$ -dimensional representation matrix $[\pi_j(h)]$ of $h \in SU(2)$, given in terms of the parameters of the defining representation (A.3), can be written as

$$\boxed{[\pi_j(h)]_{mm'} = \sum_{\ell} (-1)^{\ell} \frac{\sqrt{(j+m)! (j-m)! (j+m')! (j-m')!}}{(j-m-\ell)! (j+m'-\ell)! (m-m'+\ell)! \ell!} a^{j+m'-\ell} (\bar{a})^{j-m-\ell} b^{m-m'+\ell} (\bar{b})^{\ell}} \quad (\text{A.8})$$

where ℓ takes all integer values such that none of the factorials in the denominator gets a negative argument. By construction every representation of $SU(2)$ consists of special unitary matrices $[\pi_j(g)]$ (such that $\det [\pi_j(g)] = 1$ and $[\pi_j(g)] [\pi_j(g)]^{\dagger} = [\pi_j(g)]^{\dagger} [\pi_j(g)] = [\pi_j(\mathbb{1})]$ (with $[\pi_j(g)]^{\dagger} = \overline{[\pi_j(g)]^T}$)). Using (A.8) we obtain a generalization of (A.5):

$$[\pi_j(\epsilon)] [\pi_j(h)]^T [\pi_j(\epsilon^{-1})] = [\pi_j(\epsilon^{-1})] [\pi_j(h)]^T [\pi_j(\epsilon)] = [\pi_j(h^{-1})] = [\pi_j(h)]^{\dagger} = \overline{[\pi_j(h)]^T} \quad (\text{A.9})$$

A.2.2 Generators and ϵ -Metric

Upon applying the representation matrix element formula (A.8) and the ansatz,

$$[\pi_j(\tau_k)]_{mn} = \left. \frac{d}{dt} ([\pi_j(e^{t\tau_k} \mathbb{1})]_{mn}) \right|_{t=0} \quad (\text{A.10})$$

where in the defining two dimensional representation the exponential can be explicitly evaluated, one obtains,³⁴ using $A(j, m) = [j(j+1) - m(m-1)]^{\frac{1}{2}}$ with the obvious property that $A(j, -m) = A(j, m+1)$,

$$\begin{aligned} [\pi_j(\tau_1)]_{mn} &= -i A(j, m) \delta_{m, n+1} - i A(j, m+1) \delta_{m, n-1} \\ [\pi_j(\tau_2)]_{mn} &= -A(j, m) \delta_{m, n+1} + A(j, m+1) \delta_{m, n-1} \\ [\pi_j(\tau_3)]_{mn} &= -2 i m \delta_{m, n} \end{aligned} \quad (\text{A.11})$$

Moreover one finds by plugging (A.2) into (A.8) that

$$[\pi_j(\epsilon)]_{mn} = (-1)^{j-m} \delta_{m, -n} \quad \text{and} \quad [\pi_j(\epsilon^{-1})]_{mn} = (-1)^{j+m} \delta_{m, -n} \quad (\text{A.12})$$

B Angular Momentum Theory

B.1 Basic Definitions

In this section we will summarize the results given in [29]. We have an angular momentum orthonormal basis $u(j, m; n) = |j, m; n\rangle$ of a general $(2j+1)$ dimensional representation of $SU(2)$. The index n stands for additional quantum numbers, not affected by the action of the angular momentum operators J^k fulfilling the commutation relations

$$[J^i, J^j] = i \epsilon^{ijk} J^k \quad (\text{B.1})$$

³⁴ See [22, 23] for details.

We can formulate ladder operators given as $J^+ = J^1 + iJ^2$ and $J^- = J^1 - iJ^2$ where, using the shorthand $A(j, m) = \sqrt{j(j+1) - m(m-1)}$ with the obvious property that $A(j, -m) = A(j, m+1)$, we have

$$\begin{aligned} J^- |j m; n\rangle &= A(j, m) |j m-1; n\rangle \\ J^+ |j m; n\rangle &= A(j, m+1) |j m+1; n\rangle \end{aligned} \quad (\text{B.2})$$

The $|j m; n\rangle$ simultaneously diagonalize the two operators: the squared total angular momentum³⁵ $(J)^2$ and the magnetic quantum number J^3 [29]:

$$\begin{aligned} (J)^2 |j m; n\rangle &= ((J^1)^2 + (J^2)^2 + (J^3)^2) |j m; n\rangle = \left(\frac{1}{2}(J^- J^+ + J^+ J^-) + (J^3)^2\right) |j m; n\rangle \\ &= j(j+1) |j m; n\rangle \\ J^3 |j m; n\rangle &= m |j m; n\rangle \end{aligned} \quad (\text{B.3})$$

That is, $|j m; n\rangle$ is a maximal set of simultaneous eigenvectors of $(J)^2$ and J^3 .

One then finds the following commutation relations

$$[J^3, (J)^2] = [J^+, (J)^2] = [J^-, (J)^2] = 0 \quad [J^3, J^+] = J^+ \quad [J^3, J^-] = -J^- \quad [J^+, J^-] = 2J^3 \quad (\text{B.4})$$

such that we obtain for the $(2j+1)$ -dimensional matrix representation with arbitrary weight j

$$\begin{aligned} (J^3)_{m'm} &= m \delta_{m'm} \\ (J^+)_{m'm} &= A(j, m+1) \delta_{m' m+1} \quad (J^1)_{m'm} = \frac{1}{2}(J^+ + J^-)_{m'm} = \frac{1}{2}A(j, m+1) \delta_{m' m+1} + \frac{1}{2}A(j, m) \delta_{m' m-1} \\ (J^-)_{m'm} &= A(j, m) \delta_{m' m-1} \quad (J^2)_{m'm} = -\frac{i}{2}(J^+ - J^-)_{m'm} = -\frac{i}{2}A(j, m+1) \delta_{m' m+1} + \frac{i}{2}A(j, m) \delta_{m' m-1} \end{aligned} \quad (\text{B.5})$$

B.2 Fundamental Recoupling

Now we can easily understand what happens if we couple several angular momenta. For that we first repeat the well known theorem of Clebsch & Gordan on tensorized representations of $SU(2)$:

Theorem B.1 Clebsch & Gordan

Having two irreducible representations π_{j_1}, π_{j_2} of $SU(2)$ with weights j_1 and j_2 , their tensor product space splits into a direct sum of irreducible representations $\pi_{j_{12}}$ with $|j_1 - j_2| \leq j_{12} \leq j_1 + j_2$ such that

$$\pi_{j_1} \otimes \pi_{j_2} = \pi_{j_1+j_2} \oplus \pi_{j_1+j_2-1} \oplus \dots \oplus \pi_{|j_1-j_2+1|} \oplus \pi_{|j_1-j_2|}$$

Equivalently we can write for the resulting representation space $\mathcal{H}_{(D)} = \mathcal{H}_{(D_1)} \otimes \mathcal{H}_{(D_2)}$ (where $D_1 = 2j_1 + 1$, $D_2 = 2j_2 + 1$, $D = D_1 \cdot D_2$ denote the dimensions of the Hilbert spaces):

$$\mathcal{H}_{(D)} = \mathcal{H}_{(D_1)} \otimes \mathcal{H}_{(D_2)} = \bigoplus_{j_{12}=|j_1-j_2|}^{j_1+j_2} \mathcal{H}_{(2j_{12}+1)} \quad (\text{B.6})$$

In other words, if we couple two angular momenta j_1, j_2 , we can get resulting angular momenta j_{12} varying in the range $|j_1 - j_2| \leq j_{12} \leq j_1 + j_2$. The tensor product space of two representations of $SU(2)$ decomposes into a direct sum of representation spaces, with one space for every possible value of recoupling j_{12} with the according dimension $2j_{12} + 1$.

B.3 Recoupling of n Angular Momenta — $3nj$ -Symbols

As mentioned earlier the successive coupling of three angular momenta to a resulting j can be generalized. For this purpose let us first comment on the generalization principle before we go into detailed definitions.

Theorem B.1 can be applied to an n -fold tensor product of representations $\pi_{j_1} \otimes \pi_{j_2} \otimes \dots \otimes \pi_{j_n}$ by reducing out step by step every pair of representations. This procedure has to be carried out until all tensor products are reduced out. One then ends up with a direct sum of representations, each of which has a weight corresponding to an allowed value of the total angular momentum to which the n single angular momenta j_1, j_2, \dots, j_n can couple. However, there is an arbitrariness in how one couples the n angular momenta together, that is the order in which $\pi_{j_1} \otimes \pi_{j_2} \otimes \dots \otimes \pi_{j_n}$ is reduced out (by applying B.1) matters.

³⁵Note that we denote single components of the angular momentum by J^i , $i = 1, 2, 3$, whereas the total angular momentum is denoted by (J) .

Consider a system of n angular momenta. First we fix a labelling of these momenta, such that we have j_1, j_2, \dots, j_n . Again the first choice would be a tensor basis $|\vec{j} \vec{m}\rangle$ of all single angular momentum states $|j_k m_k\rangle$, $k = 1 \dots n$ defined by:

$$|\vec{j} \vec{m}\rangle = |(j_1, j_2, \dots, j_n) (m_1, m_2, \dots, m_n)\rangle := \bigotimes_{k=1}^n |j_k m_k\rangle \quad (\text{B.7})$$

with the maximal set of $2n$ commuting operators $(J_I)^2, J_I^3$, $(I = 1, \dots, n)$.

Now we proceed in order to find a basis in which the total angular momentum $(J_{tot})^2 = (J)^2 = (J_1 + J_2 + \dots + J_n)^2$ is diagonal (quantum number j) together with the total magnetic quantum number $J_{tot}^3 = J^3 = J_1^3 + J_2^3 + \dots + J_n^3$ (quantum number M). As $(J)^2$ and J^3 are only two operators, we need $2(n-1)$ more mutually commuting operators to have again a maximal set. We choose therefore the n operators $(J_I)^2$, $I = 1, \dots, n$ of total single angular momentum (quantum numbers $(j_1, \dots, j_n) := \vec{j}$). Then we are left with the task of finding an additional $n-2$ commuting operators. For this purpose we define:

Definition B.1 *Recoupling Scheme*

A recoupling scheme $|\vec{g}(IJ) \vec{j} j m\rangle$ is an orthonormal basis which diagonalizes, besides $(J)^2$, J^3 , and $(J_I)^2$ ($I = 1, \dots, n$) the squares of the additional $n-2$ operators G_2, G_3, \dots, G_{n-1} defined as:³⁶

$$\begin{aligned} G_1 &:= J_I, \quad G_2 := G_1 + J_J, \quad G_3 := G_2 + J_1, \quad G_4 := G_3 + J_2, \quad \dots, \\ G_I &:= G_{I-1} + J_{I-2}, \quad G_{I+1} := G_I + J_{I-1}, \quad G_{I+2} := G_{I+1} + J_{I+1}, \quad G_{I+3} := G_{I+2} + J_{I+2}, \quad \dots, \\ G_J &:= G_{J-1} + J_{J-1}, \quad G_{J+1} := G_J + J_{J+1}, \quad G_{J+2} := G_{J+1} + J_{J+2}, \quad \dots, \\ G_{n-1} &:= G_{n-2} + J_{n-1} \end{aligned}$$

The vector

$$\vec{g}(IJ) := (g_2(j_I, j_J), g_3(g_2, j_1), \dots, g_{I+1}(g_I, j_{I-1}), g_{I+2}(g_{I+1}, j_{I+1}), \dots, g_J(g_{J-1}, j_{J-1}), g_{J+1}(g_J, j_{J+1}), \dots, g_{n-1}(g_{n-2}, j_{n-1}))$$

carries as quantum numbers the $n-2$ eigenvalues of the operators $(G_2)^2, \dots, (G_{n-1})^2$.

So we recouple first the angular momenta labelled by I, J where $I < J$ and secondly all the other angular momenta successively (all labels are with respect to the fixed label set), by taking into account the allowed values for each recoupling according to theorem B.1.

Let us define furthermore the so called *standard recoupling scheme* or *standard basis*:

Definition B.2 *Standard Basis*

A recoupling scheme based on the pair $(I, J) = (1, 2)$ with

$$G_K = \sum_{L=1}^K J_L$$

is called the *standard basis*.

Using definition B.1 with the commutation relations (B.4) and the fact that single angular momentum operators acting on different single angular momentum Hilbert spaces commute³⁷, one can easily check that for every recoupling scheme

- (i) the G_I 's fulfill the angular momentum algebra B.4
- (ii) $(J)^2$, $(J_I)^2$, $(G_I)^2$, $J^3 \forall I = 1 \dots n$ commute with each other

Note that it is sufficient to prove these two points in the standard basis $\vec{g}(12)$, because every other basis $\vec{g}(IJ)$ is related to it by simply relabelling the n angular momenta.

We have thus succeeded in giving an alternative description of a system of n angular momenta by all possible occurring intermediate recoupling stages G_I , instead of using the individual magnetic quantum numbers. Every recoupling scheme $|\vec{g}(IJ) \vec{j} j m\rangle$, labeled by the index pair (IJ) , gives a distinct orthonormal basis. We are then in need of a transformation connecting the different bases, i.e. we wish to express one basis, belonging to the pair (IJ) , in terms of another basis belonging to the pair (KL) . This leads to the following definition.

³⁶Note that formally $G_n := G_{n-1} + J_n = J_{total}$.

³⁷That is $[J_I^i, J_J^j] = 0$ whenever $I \neq J$.

Definition B.3 $3nj$ -Symbol

The generalized expansion coefficients of a recoupling scheme in terms of the standard recoupling scheme are called $3nj$ -symbols:

$$\left| \vec{g}(IJ) \vec{j} j m \right\rangle = \sum_{\text{all } \vec{g}'(12)} \underbrace{\left\langle \vec{g}'(12) \vec{j} j m \mid \vec{g}(IJ) \vec{j} j m \right\rangle}_{3nj\text{-symbol}} \left| \vec{g}'(12) \vec{j} j m \right\rangle$$

The summation has to be extended over all possible values of the intermediate recouplings

$\vec{g}'(12) = (g'_2(j_1, j_2), g'_3(g'_2, j_3), \dots, g'_{n-1}(g'_{n-2}, j_{n-1}))$, that is all values of each component g'_k allowed by theorem B.1.

In calculations we will suppress the quantum numbers \vec{j}, j, m , since they are identical in every expression, and write the $3nj$ -symbols as $\langle \vec{g}(IJ) \mid \vec{g}'(12) \rangle$. Note additionally the following properties of the $3nj$ -symbols:

- (i) They are unitary and real, due to the fact that they can be expressed in terms of Clebsch-Gordan-coefficients³⁸:

$$\langle \vec{g}(IJ) \mid \vec{g}'(12) \rangle = \langle \vec{g}'(12) \mid \vec{g}(IJ) \rangle$$

- (ii) They are rotationally invariant, i.e. independent of the magnetic quantum numbers m_k occurring in (B.7).

B.4 Properties of Recoupling Schemes

In this section we will briefly review the properties of recoupling schemes as defined in section B.3. In what follows we will frequently use $\tilde{m}_k := m_1 + m_2 + \dots + m_k$.

B.4.1 A General (Standard-)Recoupling Scheme

A general standard recoupling scheme is defined as follows: Fix a labelling j_1, \dots, j_N of the N spins to recouple. Then one constructs

$$\begin{aligned} \left| \vec{a}(12) J M ; \vec{n} \right\rangle = & \left| a_2(j_1 j_2) a_3(a_2 j_3) \dots a_{K-1}(a_{K-2} j_{K-1}) a_K(a_{K-1} j_K) a_{K+1}(a_K j_{K+1}) \dots a_{N-1}(a_{N-2} j_{N-1}) J(a_{N-1} j_N) M ; n_1 \dots n_N \right\rangle \\ = & \left. \begin{aligned} & \sum_{m_1 + \dots + m_N = M} \left\langle \begin{array}{l} j_1 m_1 ; j_2 m_2 \mid a_2(j_1 j_2) \tilde{m}_2 \\ a_2 \tilde{m}_2 ; j_3 m_3 \mid a_3(a_2 j_3) \tilde{m}_3 \\ \vdots \\ a_{K-2} \tilde{m}_{K-2} ; j_{K-1} m_{K-1} \mid a_{K-1}(a_{K-2} j_{K-1}) \tilde{m}_{K-1} \\ a_{K-1} \tilde{m}_{K-1} ; j_K m_K \mid a_K(a_{K-1} j_K) \tilde{m}_K \\ a_K \tilde{m}_K ; j_{K+1} m_{K+1} \mid a_{K+1}(a_K j_{K+1}) \tilde{m}_{K+1} \\ \vdots \\ a_{N-2} \tilde{m}_{N-2} ; j_{N-1} m_{N-1} \mid a_{N-1}(a_{N-2} j_{N-1}) \tilde{m}_{N-1} \\ a_{N-1} \tilde{m}_{N-1} ; j_N m_N \mid J(a_{N-1} j_N) M \end{array} \right\rangle \\ & \left. \begin{array}{l} \left| j_1 m_1 ; n_1 \right\rangle \otimes \left| j_2 m_2 ; n_2 \right\rangle \otimes \dots \otimes \left| j_{K-1} m_{K-1} ; n_{K-1} \right\rangle \otimes \left| j_K m_K ; n_K \right\rangle \otimes \left| j_{K+1} m_{K+1} ; n_{K+1} \right\rangle \otimes \\ \otimes \dots \otimes \left| j_{N-1} m_{N-1} ; n_{N-1} \right\rangle \otimes \left| j_N m_N ; n_N \right\rangle \end{array} \right\} \text{N-1 factors} \end{aligned} \right. \end{aligned} \quad (\text{B.8})$$

B.4.2 Orthogonality Relations Between Recoupling Schemes

For the scalar product of two recoupling schemes we have:

$$\left\langle a'_2 a'_3 \dots a'_{N-1} J' M' \mid a_2 a_3 \dots a_{N-1} J M \right\rangle = \delta_{MM'} \delta_{a_2 a'_2} \delta_{a_3 a'_3} \dots \delta_{a_{N-1} a'_{N-1}} \delta_{JJ'} \delta_{j'_1 j_1} \dots \delta_{j'_N j_N} \delta_{n'_1 n_1} \dots \delta_{n'_N n_N}$$

This result can be easily understood by recalling the definition of a recoupling scheme

$\left| a_2(j_1 j_2) a_3(a_2 j_3) \dots a_{N-1}(a_{N-2} j_{N-1}) J(a_{N-1} j_N) M \right\rangle$ as the simultaneous eigenstate for the operators $(G_2)^2 = (J_1 + J_2)^2$, $(G_3)^2 = (G_2 + J_3)^2$, \dots , $(G_{N-1})^2 = (G_{N-2} + J_{N-1})^2$, $J^2 = (G_{N-1} + J_N)^2 = (J_1 + \dots + J_N)^2$ with eigenvalues $a_2(a_2 + 1)$, $a_3(a_3 + 1)$, \dots , $a_{N-1}(a_{N-1} + 1)$, $J(J + 1)$.

B.4.3 Partial Orthogonality Relations Between Recoupling Schemes

The same argument can also be applied to cases where we have to calculate the scalar product of two recoupling schemes of different recoupling order. For illustration let us consider two recoupling schemes

$$\left| \vec{a} J M \right\rangle = \left| a_2(j_1 j_2) a_3(a_2 j_3) \dots a_{K-1}(a_{K-2} j_{K-1}) a_K(a_{K-1} j_K) \dots a_L(a_{L-1} j_L) a_{L+1}(a_L j_{L+1}) \dots a_{N-1}(a_{N-2} j_{N-1}) J(a_{N-1} j_N) M \right\rangle$$

$$\left| \vec{g} J M \right\rangle = \left| g_2(j_1 j_2) g_3(a_2 j_3) \dots g_{K-1}(g_{K-2} j_{K-1}) g_K(g_{K-1} j_K) \dots g_L(g_{L-1} j_L) g_{L+1}(g_L j_{L+1}) \dots g_{N-1}(g_{N-2} j_{N-1}) J(g_{N-1} j_N) M \right\rangle$$

³⁸Which are unitary and real.

Here from $2 \dots K-1$ the spins $j_1, j_2 \dots j_{K-1}$ are coupled in \vec{a} and \vec{g} in the same order. Then $j_K \dots j_L$ are coupled in the standard way for \vec{a} but in a different order for \vec{g} . After that $j_{L+1} \dots j_N$ are successively coupled to each scheme again. Now it is clear that \vec{a} and \vec{g} simultaneously diagonalize not only $(G_2)^2 = (J_1 + J_2)^2$, $(G_3)^2 = (G_2 + J_3)^2$, \dots , $(G_{K-1})^2 = (G_{K-2} + J_{K-1})^2$ but also $(G_L)^2 \dots (G_{N-1})^2$, $J^2 = (J_1 + \dots + j_N)^2$. Therefore we can write down immediately

$$\langle \vec{a} J M \mid \vec{g} J M \rangle = \langle a_K(a_{K-1} j_K) \dots a_{L-1}(a_{L-2} j_{L-1}) a_L(a_{L-1} j_L) \mid g_K(a_{K-1} j_P) \dots g_{L-1}(g_{L-2} j_Q) a_L(g_{L-1} j_R) \rangle \times \delta_{a_2 g_2} \dots \delta_{a_{K-1} g_{K-1}} \times \delta_{a_L g_L} \dots \delta_{a_{N-1} g_{N-1}} \times \delta_{JJ'} \times \delta_{MM'} \quad (\text{B.9})$$

For a more detailed derivation of (B.9) see lemmas 5.1 and 5.2 of [15].

C Properties of the $6j$ -Symbols

In this appendix we will give an overview of the $6j$ -symbols, because they are the basic structure we will use in our recoupling calculations, as every coupling of n angular momenta can be expressed in terms of them. For further details we refer the reader to [30],[29].

C.1 Definition

The $6j$ -symbol is defined in [29], p 92, as:

$$\left\{ \begin{matrix} j_1 & j_2 & j_{12} \\ j_3 & j & j_{23} \end{matrix} \right\} := [(2j_{12} + 1)(2j_{23} + 1)]^{-\frac{1}{2}} (-1)^{j_1 + j_2 + j_3 + j} \langle j_{12}(j_1, j_2), j(j_{12}, j_3) \mid j_{23}(j_2, j_3), j(j_1, j_{23}) \rangle \\ = [(2j_{12} + 1)(2j_{23} + 1)]^{-\frac{1}{2}} (-1)^{j_1 + j_2 + j_3 + j} \\ \times \sum_{m_1 m_2} \left[\langle j_1 m_1; j_2 m_2 \mid j_1 j_2 j_{12} m_1 + m_2 \rangle \langle j_{12} m_1 + m_2; j_3 m - m_1 - m_2 \mid j_{12} j_3 j m \rangle \right. \\ \left. \times \langle j_2 m_2; j_3 m - m_1 - m_2 \mid j_2 j_3 j_{23} m - m_1 \rangle \langle j_1 m_1; j_{23} m - m_1 \mid j_1 j_{23} j m \rangle \right] \quad (\text{C.1})$$

The factors in the summation are Clebsch-Gordon coefficients.

C.2 Explicit Evaluation of the $6j$ -Symbols

A general formula for the numerical value of the $6j$ -symbols has been derived by Racah [29], p.99:

$$\left\{ \begin{matrix} j_1 & j_2 & j_{12} \\ j_3 & j & j_{23} \end{matrix} \right\} = \Delta(j_1, j_2, j_{12}) \Delta(j_1, j, j_{23}) \Delta(j_3, j_2, j_{23}) \Delta(j_3, j, j_{12}) w \left\{ \begin{matrix} j_1 & j_2 & j_{12} \\ j_3 & j & j_{23} \end{matrix} \right\} \quad (\text{C.2})$$

where

$$\Delta(a, b, c) = \sqrt{\frac{(a+b-c)!(a-b+c)!(-a+b+c)!}{(a+b+c+1)!}}$$

and

$$w \left\{ \begin{matrix} j_1 & j_2 & j_{12} \\ j_3 & j & j_{23} \end{matrix} \right\} = \sum_n (-1)^n (n+1)! [(n-j_1-j_2-j_{12})! (n-j_1-j-j_{23})! (n-j_3-j_2-j_{23})! (n-j_3-j-j_{12})!]^{-1} \times \\ \times [(j_1+j_2+j_3+j-n)! (j_2+j_{12}+j+j_{23}-n)! (j_{12}+j_1+j_{23}+j_3-n)!]^{-1} \quad (\text{C.3})$$

The sum is extended over all positive integer values of n such that no factorial in the denominator has a negative argument. That is:

$$\max[j_1 + j_2 + j_{12}, j_1 + j + j_{23}, j_3 + j_2 + j_{23}, j_3 + j + j_{12}] \leq n \leq \min[j_1 + j_2 + j_3 + j, j_2 + j_{12} + j + j_{23}, j_{12} + j_1 + j_{23} + j_3]$$

Remark From (C.2) we are provided with some additional requirements the arguments of the $6j$ -symbols must fulfill: Certain sums or differences of them must be integers to be proper (\equiv integer) arguments for the factorials:

From $\Delta(a, b, c)$ one gets:

- a, b, c must fulfill the triangle inequalities: $(a + b - c) \geq 0$, $(a - b + c) \geq 0$, $(-a + b + c) \geq 0$,
- $(\pm a \pm b \pm c)$ must be an integer

From the w -coefficient one gets:

- $j_1 + j_2 + j_3 + j$, $j_2 + j_{12} + j + j_{23}$, $j_{12} + j_1 + j_{23} + j_3$ are integers.

The following (trivial but important) relations are frequently used in calculations involving $6j$ -symbols:

$$\begin{aligned} (-1)^z &= (-1)^{-z} \quad \forall z \in \mathbb{Z} \\ (-1)^{2z} &= 1 \quad \forall z \in \mathbb{Z} \\ (-1)^{3k} &= (-1)^{-k} \quad \forall k = \frac{z}{2} \quad \text{with } z \in \mathbb{Z} \end{aligned} \quad (\text{C.4})$$

C.3 Symmetry Properties

The $6j$ -symbols are invariant under

- any permutation of the columns:

$$\left\{ \begin{matrix} j_1 & j_2 & j_3 \\ j_4 & j_5 & j_6 \end{matrix} \right\} = \left\{ \begin{matrix} j_2 & j_3 & j_1 \\ j_5 & j_6 & j_4 \end{matrix} \right\} = \left\{ \begin{matrix} j_3 & j_1 & j_2 \\ j_6 & j_4 & j_5 \end{matrix} \right\} = \left\{ \begin{matrix} j_2 & j_1 & j_3 \\ j_5 & j_4 & j_6 \end{matrix} \right\} = \left\{ \begin{matrix} j_1 & j_3 & j_2 \\ j_4 & j_6 & j_5 \end{matrix} \right\} = \left\{ \begin{matrix} j_3 & j_2 & j_1 \\ j_6 & j_5 & j_4 \end{matrix} \right\} \quad (\text{C.5})$$

- simultaneous interchange of the upper and lower arguments of two columns, e.g.

$$\left\{ \begin{matrix} j_1 & j_2 & j_3 \\ j_4 & j_5 & j_6 \end{matrix} \right\} = \left\{ \begin{matrix} j_1 & j_5 & j_6 \\ j_4 & j_2 & j_3 \end{matrix} \right\} \quad (\text{C.6})$$

C.4 Orthogonality and Sum Rules

Orthogonality Relations

$$\sum_{j_{23}} (2j_{12} + 1)(2j'_{12} + 1) \left\{ \begin{matrix} j_1 & j_2 & j_{12} \\ j_3 & j & j_{23} \end{matrix} \right\} \left\{ \begin{matrix} j_1 & j_2 & j'_{12} \\ j_3 & j & j_{23} \end{matrix} \right\} = \delta_{j_{12}j'_{12}} \quad (\text{C.7})$$

Composition Relation

$$\sum_{j_{23}} (-1)^{j_{23}+j_{31}+j_{12}} (2j_{23} + 1) \left\{ \begin{matrix} j_1 & j_2 & j_{12} \\ j_3 & j & j_{23} \end{matrix} \right\} \left\{ \begin{matrix} j_2 & j_3 & j_{23} \\ j_1 & j & j_{31} \end{matrix} \right\} = \left\{ \begin{matrix} j_3 & j_1 & j_{31} \\ j_2 & j & j_{12} \end{matrix} \right\} \quad (\text{C.8})$$

Sum Rule of Elliot and Biedenharn

$$\begin{aligned} \left\{ \begin{matrix} j_1 & j_2 & j_{12} \\ j_3 & j_{123} & j_{23} \end{matrix} \right\} \left\{ \begin{matrix} j_{23} & j_1 & j_{123} \\ j_4 & j & j_{14} \end{matrix} \right\} &= (-1)^{j_1+j_2+j_3+j_4+j_{12}+j_{23}+j_{14}+j_{123}+j} \\ &\times \sum_{j_{124}} (-1)^{j_{124}} (2j_{124} + 1) \left\{ \begin{matrix} j_3 & j_2 & j_{23} \\ j_{14} & j & j_{124} \end{matrix} \right\} \left\{ \begin{matrix} j_2 & j_1 & j_{12} \\ j_4 & j_{124} & j_{14} \end{matrix} \right\} \left\{ \begin{matrix} j_3 & j_{12} & j_{123} \\ j_4 & j & j_{124} \end{matrix} \right\} \end{aligned} \quad (\text{C.9})$$

D Spin Networks and Representation Theory

Concrete calculations performed in Loop Quantum Gravity heavily rest on the fact that the representation theory of $SU(2)$ is closely related to the theory of angular momenta familiar from quantum mechanics. Employing this correspondence we are able to use the powerful techniques provided by recoupling theory of angular momenta in Loop Quantum Gravity. However, as we will describe in this section, there are certain subtleties which have to be worked out carefully in order to fully establish the indicated correspondence.

D.1 Spin Network Functions

D.1.1 Defining a Basis of Angular Momentum Eigenstates

Due to the *Peter & Weyl* theorem we have [1] :

$$\int_{SU(2)} d\mu_H(h) \overline{[\pi_{j'}(h)]_{m'n'}} [\pi_j(h)]_{mn} = \frac{1}{2j+1} \delta_{j'j} \delta_{m'm} \delta_{n'n} \quad (\text{D.1})$$

which states that the representation matrix element functions $[\pi_j(h)]_{mn}$ are orthogonal with respect to the Haar measure $d\mu_H(h)$ on $SU(2)$. Theorem (D.1) enables us to introduce an orthonormal basis³⁹ on the total Hilbert space

$$\mathcal{H} = \bigoplus_j \mathcal{H}^{(j)} \quad (\text{D.2})$$

by

$$\langle h | jmn \rangle := \sqrt{2j+1} [\pi_j(h)]_{mn} \quad \text{and} \quad \langle jmn | h \rangle := \sqrt{2j+1} \overline{[\pi_j(h)]_{mn}} = \sqrt{2j+1} [\pi_j(h)]_{nm}^{-1} \quad (\text{D.3})$$

where by construction

$$\begin{aligned} \langle jmn | j'm'n' \rangle &:= \int_{SU(2)} d\mu_H(h) \langle jmn | h \rangle \langle h | j'm'n' \rangle = \sqrt{(2j'+1)(2j+1)} \int_{SU(2)} d\mu_H(h) \overline{[\pi_j(h)]_{mn}} [\pi_{j'}(h)]_{m'n'} \\ &= \delta_{j'j} \delta_{m'm} \delta_{n'n} \end{aligned} \quad (\text{D.4})$$

Therefore the meaning of the representation matrices is twofold: On the one hand the rescaled representation matrix element functions $\sqrt{2j+1} [\pi_j(\cdot)]_{mn} =: | j m n \rangle$ provide an orthonormal basis, whereas the representation matrix $[\pi_j(h)]_{mn}$ of a specific group element $h \in SU(2)$ should act as a unitary transformation matrix on the basis states as

$$[\pi_j(h)] | j m n \rangle = \sum_{m'} [\pi_j(h)]_{m'm} | j m' n \rangle \quad (\text{D.5})$$

D.2 Right Invariant Vector Fields

D.2.1 Action on Group Valued Functions

The action of right invariant vector fields $(X_k f)(g) = \left. \frac{d}{dt} f(\mathbb{e}^{t\tau_k} g) \right|_{t=0}$ on group valued functions $f(g)$, $g \in SU(2)$ is evaluated as:

$$\begin{aligned} (X_k f)(g) &= \left. \frac{d}{dt} f(\mathbb{e}^{t\tau_k} g) \right|_{t=0} = \sum_{A B} \frac{\partial f(\mathbb{e}^{t\tau_k} g)}{\partial (\mathbb{e}^{t\tau_k} g)_{AB}} \left. \frac{d}{dt} (\mathbb{e}^{t\tau_k} g)_{AB} \right|_{t=0} = \sum_{A B C} \frac{\partial f(\mathbb{e}^{t\tau_k} g)}{\partial (\mathbb{e}^{t\tau_k} g)_{AB}} \left. \frac{d}{dt} (\mathbb{e}^{t\tau_k})_{AC} (g)_{CB} \right|_{t=0} \\ &= \text{tr} \left[\tau_k g \frac{\partial}{\partial g} \right] f(g) \end{aligned} \quad (\text{D.6})$$

where we have used the defining ($j = \frac{1}{2}$) representation of $SU(2)$ in order to define the derivation of the group element. In the last line we then express the sum over the defining representation indices as a trace. Note, however, that using the defining representation here is a matter of choice, we are free to choose any other representation and accordingly the trace in (D.6) is then defined with respect to the chosen representation. From (D.6) the commutation relations of the X_k are found to be

$$\left([X_i, X_j] f \right)(g) = -2\epsilon^{ijk} (X_k f)(g) \quad (\text{D.7})$$

The action of the right invariant vector fields on representation matrix element functions can be evaluated as:

$$\begin{aligned} (X_k [\pi_j(\cdot)]_{mn})(g) &= \left. \frac{d}{dt} [\pi_j(\mathbb{e}^{t\tau_k} g)]_{mn} \right|_{t=0} = \sum_r \left. \frac{d}{dt} [\pi_j(\mathbb{e}^{t\tau_k} \mathbb{1})]_{mr} \right|_{t=0} [\pi_j(g)]_{rn} = \sum_r [\pi_j(\tau_k)]_{mr} [\pi_j(g)]_{rn} \\ &\equiv \sum_r [\tau_k]_m^{(j)}{}_r [\pi_j(g)]_{rn} \end{aligned} \quad (\text{D.8})$$

where we use the representation property⁴⁰ and the definition of the τ_k 's as a basis for the tangent space of the group at the identity element $\mathbb{1}_{SU(2)}$. Note that we have changed the notation in the last line to indicate that the resulting $(2j+1)$ dimensional matrix $[\tau_k]_r^{(j)}{}_m$ is an element of the Lie algebra $su(2)$ rather than a group element. Moreover as mentioned above we choose here the representation of weight j in order to evaluate the trace.

However (D.8) yields a possible obstacle: while we would like to write the action of any transformation on the basis states (D.3) to be according to (D.5), the action of the right invariant vector fields (D.8) is defined as a matrix multiplication, that is it transforms the basis states (D.3) as vectors rather than as basis states. Therefore we have to take a closer look at the group multiplication properties.

³⁹We will use Dirac's bracket notation here.

⁴⁰ $[\pi_j(g_1 g_2)] = [\pi_j(g_1)] [\pi_j(g_2)]$

D.2.2 Group Multiplication — Introducing a New Basis

For the representation of a general group multiplication we find

$$\begin{aligned}
[\pi_j(gh)]_{mn} &= \sum_{m''} [\pi_j(g)]_{mm''} [\pi_j(h)]_{m''n} = \frac{1}{\sqrt{2j+1}} \sum_{m''} [\pi_j(g)]_{m''m}^T \langle h | j m'' n \rangle \\
&= \frac{1}{\sqrt{2j+1}} \sum_{m''} [\pi_j(\epsilon^{-1} g^{-1} \epsilon)]_{m''m} \langle h | j m'' n \rangle \\
&= \frac{1}{\sqrt{2j+1}} \sum_{r s m''} [\pi_j(\epsilon)]_{sm} [\pi_j(g^{-1})]_{rs} [\pi_j(\epsilon^{-1})]_{m''r} \langle h | j m'' n \rangle
\end{aligned} \tag{D.9}$$

By observation, (D.9) suggests a solution to the problem above: If we slightly modify our preliminary basis (D.3) by absorbing the according ϵ components, we can introduce a new basis $| j m ; n \rangle$ as

$$\begin{aligned}
| j m ; n \rangle &:= \sum_r [\pi_j(\epsilon^{-1})]_{rm} | j r n \rangle = (-1)^{j-m} | j -m n \rangle = (-1)^{j-m} \sqrt{2j+1} [\pi_j(\cdot)]_{-m n} \\
\langle j m ; n | &:= \sum_r [\pi_j(\epsilon)]_{mr} \langle j r n | = (-1)^{j-m} \langle j -m n | = (-1)^{j-m} \sqrt{2j+1} \overline{[\pi_j(\cdot)]_{-m n}}
\end{aligned} \tag{D.10}$$

which is orthonormal as well by the unitarity of $[\pi_j(\epsilon)]_{mn}$ ⁴¹. Note that there is an ambiguity in the definition (D.10) coming from the fact that due to (A.9) $[\pi(\epsilon^{-1} g^{-1} \epsilon)] = [\pi(\epsilon g^{-1} \epsilon^{-1})]$, and therefore we can exchange $\epsilon^{-1} \leftrightarrow \epsilon$ consistently in (D.10).

Now continuing from (D.9), and using (D.10), group multiplication can be rewritten as

$$\begin{aligned}
[\pi_j(gh)]_{mn} &= \frac{1}{\sqrt{2j+1}} \sum_{r s} [\pi_j(\epsilon^{-1})]_{ms} [\pi_j(g^{-1})]_{rs} \langle h | j r ; n \rangle = \frac{1}{\sqrt{2j+1}} \sum_{r s} (-1)^{j+m} \delta_{m -s} [\pi_j(g^{-1})]_{rs} \langle h | j r ; n \rangle \\
&= \frac{1}{\sqrt{2j+1}} \sum_r (-1)^{j+m} [\pi_j(g^{-1})]_{r -m} \langle h | j r ; n \rangle
\end{aligned} \tag{D.11}$$

We have now formally achieved a form analogous to the transformation property (D.5) on the redefined basis (D.10).

D.2.3 Rewriting the Action of the Right Invariant Vector Fields

Let us evaluate the action of the modified right invariant vector fields X_k on the representation matrix element functions $[\pi_j(\cdot)]_{mn}$. By using (A.7) as $-\overline{\tau_k^T} = \tau_k = -\tau_k^{-1}$ we can evaluate the action of the X_k on the states $| j m ; n \rangle$ as follows

$$\begin{aligned}
X_k \langle h | j m ; n \rangle &= \sqrt{2j+1} (-1)^{j-m} \left(X_k [\pi_j(\cdot)]_{-m n} \right) (h) = \sqrt{2j+1} (-1)^{j-m} \frac{d}{dt} \left([\pi_j(e^{t\tau_k} h)]_{-m n} \right) \Big|_{t=0} \\
&\stackrel{(D.11)}{=} \sum_r (-1)^{2(j-m)} \frac{d}{dt} \left([\pi_j(e^{t\tau_k} \mathbb{1})]_{r m}^{-1} \right) \Big|_{t=0} \langle h | j r ; n \rangle \\
&= - \sum_r [\tau_k]_{r m}^{(j)} \langle h | j r ; n \rangle
\end{aligned} \tag{D.12}$$

where the action of the right invariant vector fields may now be interpreted as a basis transformation. The prefactor $(-1)^{2(j-m)} = 1$ because $j - m$ is an integer number. Here we again have changed the notation in the last line to indicate that the resulting $(2j+1)$ -dimensional matrix $[\tau_k]_{r m}^{(j)}$ is an element of the Lie algebra $su(2)$ rather than a group element. However, we will abuse the notation a tad by writing $[\tau_k]_{r m}^{(j)}$ as $[\pi_j(\tau_k)]_{rm}$.

D.3 Correspondence to Angular Momentum Theory

Now we introduce the modified vector fields⁴² $Y^k := -\frac{i}{2} X_k$, and their commutation relations as evaluated on group valued functions, which easily follows from (D.7):

$$[Y^i, Y^j] \langle h | j m ; n \rangle = i \epsilon^{ijk} Y^k \langle h | j m ; n \rangle \tag{D.13}$$

These are the commutation relations of angular momentum operators. Moreover using (D.12) the Y_k act on the basis states (D.10) as

$$Y^k = \frac{i}{2} \sum_r [\pi_j(\tau_k)]_{r m} \langle h | j r ; n \rangle \tag{D.14}$$

⁴¹ Also this can easily be seen from (D.4) and the fact that $(-1)^{2(j-m)} = 1$.

⁴² Note that we can raise and lower $su(2)$ -indices with the Cartan metric on $su(2)$. Since this is simply $\delta_{ij} = \delta^{ij}$, there is no difference between upper and lower indices. We thus place $su(2)$ -indices as is convenient throughout the paper.

Thus we can identify the action of Y^k on the new basis states $|j\ m\ ;\ n\rangle$ with the usual action of the angular momentum operators $Y^k = J^k$ on basis states of an abstract spin system $|j\ m\rangle_{(n)}$ ⁴³:

$$Y^k |j\ m\ ;\ n\rangle \Leftrightarrow J^k |j\ m\rangle_{(n)} \quad (\text{D.15})$$

and obtain the usual angular momentum and ladder operator algebra and the algebra of ladder operators as can be found in [29]. Upon defining the action of the Y 's in this way there is a correspondence $Y^\pm \leftrightarrow J^\pm$ and therefore one realizes the following commutation relations (which are compared to the commutation relations of the usual angular momentum operators acting on spin states $|j\ m\rangle$).

$$\begin{aligned} [(Y)^2, Y^k] &= 0 & [(J)^2, J^k] &= 0 & [Y^3, Y^+] &= Y^+ & [J^3, J^+] &= J^+ \\ [Y^i, Y^j] &= i\epsilon^{ijk} Y^k & [J^i, J^j] &= i\epsilon^{ijk} J^k & [Y^3, Y^-] &= -Y^- & [J^3, J^-] &= -J^- \\ & & & & [Y^+, Y^-] &= 2Y^3 & [J^+, J^-] &= 2J^3 \end{aligned} \quad (\text{D.16})$$

D.3.1 Rewriting Right Invariant Vector Field Expressions

We can now give the general prescription for translating the action of the modified right invariant vector fields Y_k on holonomies into the action of usual angular momentum operators on abstract spin systems.

$$\boxed{Y^k \sqrt{2j+1} [\pi_j(\cdot)]_{mn} = Y^k (-1)^{j+m} |j\ -m\ ;\ n\rangle \Leftrightarrow (-1)^{j+m} J^k |j\ -m\rangle_{(n)}} \quad (\text{D.17})$$

D.3.2 Recoupling Schemes

Due to (D.17) we can therefore apply recoupling theory to the states $|j\ m\ ;\ n\rangle$ as follows:

$$\begin{aligned} |\vec{a}\ J\ M\ ;\ \vec{n}\ \vec{j}\rangle := & \sum_{m_1+m_2+\dots+m_N=M} \langle j_1\ m_1\ ;\ j_2\ m_2\ | a_2\ \tilde{m}_2\rangle \times \dots \times \langle a_{N-1}\ \tilde{m}_{N-1}\ ;\ j_N\ m_N\ | J\ M\rangle \\ & \times |j_1\ m_1\ ;\ n_1\rangle \otimes |j_2\ m_2\ ;\ n_2\rangle \otimes \dots \otimes |j_N\ m_N\ ;\ n_N\rangle \end{aligned} \quad (\text{D.18})$$

D.4 Historical Remark

For the sake of completeness we would like to add a remark on the development of correspondence (D.17) here. The necessity of (D.5) leading to

$$Y^k \langle h\ |j\ m\ ;\ n\rangle = \frac{i}{2} \sum_r [\pi_j(\tau_k)]_{r\ m} \langle h\ |j\ r\ ;\ n\rangle \quad (\text{D.19})$$

was realized for the first time in [22, 23], where the authors evaluated the detailed matrix elements for the Y_k . In calculations in the spin network formalism before [22, 23] one always used the preliminary basis (D.3) and directly evaluated the action of the Y_k resulting from the group multiplication (D.8) as

$$Y^k \langle h\ |j\ m\ n\rangle = -\frac{i}{2} \sum_r [\pi_j(\tau_k)]_{m\ r} \langle h\ |j\ r\ ;\ n\rangle \quad (\text{D.20})$$

This was justified because the commutation relations of the Y^k resulting from (D.20)

$$[Y^i, Y^j] \langle h\ |j\ m\ n\rangle = i\epsilon^{ijk} Y^k \langle h\ |j\ m\ n\rangle \quad (\text{D.21})$$

are identical to those of (D.13). As a result one directly identified

$$Y^k |j\ m\ n\rangle \Leftrightarrow J^k |j\ m\rangle_{(n)} \quad (\text{D.22})$$

However, comparing the operators obtained from (D.20) on a representation of weight j we find:

$$\begin{aligned} [Y_{(j)}^1]_{mn} &= -\frac{i}{2} [\pi_j(\tau_1)]_{mn} = -\frac{1}{2} A(j, n+1) \delta_{m\ n+1} - \frac{1}{2} A(j, n) \delta_{m\ n-1} \\ [Y_{(j)}^2]_{mn} &= -\frac{i}{2} [\pi_j(\tau_2)]_{mn} = \frac{i}{2} A(j, n+1) \delta_{m\ n+1} - \frac{i}{2} A(j, n) \delta_{m\ n-1} \\ [Y_{(j)}^3]_{mn} &= -\frac{i}{2} [\pi_j(\tau_3)]_{mn} = -m \delta_{m\ n} \end{aligned} \quad (\text{D.23})$$

⁴³Here n denotes an additional quantum number which is irrelevant for the action of J^k .

One can already see an overall minus sign compared to (B.5). From this one can formulate ladder operators

$$\begin{aligned} Y_{(j)}^+ &:= [Y_{(j)}^1 - iY_{(j)}^2] = -A(j, m+1) \delta_{m, n-1} \\ Y_{(j)}^- &:= [Y_{(j)}^1 + iY_{(j)}^2] = -A(j, m) \delta_{m, n+1} \end{aligned} \quad (\text{D.24})$$

but notices the difference in their definition as compared to (B.2), due to the assumed matrix multiplication instead of the contragredient action. One finds

$$\begin{aligned} \sum_r [Y_{(j)}^+]_{mr} |j\ r\ n\rangle &= -A(j, m+1) |j\ m+1\ n\rangle & \sum_r [Y_{(j)}^-]_{mr} |j\ r\ n\rangle &= -A(j, m) |j\ m-1\ n\rangle \\ \sum_r [Y_{(j)}^3]_{mr} |j\ r\ n\rangle &= -m |j\ m\ n\rangle & \sum_r [(Y_{(j)})^2]_{mr} |j\ r\ n\rangle &= j(j+1) |j\ m\ n\rangle \end{aligned} \quad (\text{D.25})$$

where $(Y)^2 = (Y^1)^2 + (Y^2)^2 + (Y^3)^2 = \frac{1}{2}Y^-Y^+ + \frac{1}{2}Y^+Y^- + (Y^3)^2$. Upon defining the action of the Y 's in this way there is a correspondence $Y^\pm \leftrightarrow J^\mp$ and therefore one realizes the following commutation relations (as compared to the commutation relations of the usual angular momentum operators acting on spin states $|j\ m\rangle$).

$$\begin{aligned} [(Y)^2, Y^k] &= 0 & [(J)^2, J^k] &= 0 & [Y^3, Y^+] &= -Y^+ & [J^3, J^+] &= J^+ \\ [Y^i, Y^j] &= i\epsilon^{ijk} Y^k & [J^i, J^j] &= i\epsilon^{ijk} J^k & [Y^3, Y^-] &= Y^- & [J^3, J^-] &= -J^- \\ [Y^+, Y^-] &= -2Y^3 & [J^+, J^-] &= 2J^3 \end{aligned} \quad (\text{D.26})$$

Although the Y 's obey the usual angular momentum commutation relations on the left hand side of (D.26), there is a difference in the signs of the ladder operator commutator algebra, providing possible phase convention obstacles when applying techniques of recoupling theory of angular momentum.

D.4.1 Recoupling Schemes

In (D.17) we have found a matching between the basis states $|j\ m; n\rangle$ as defined in (D.10) to the states $|j\ m\rangle_{(n)}$ of an ordinary angular momentum system. Using (D.10), where

$$|j\ m; n\rangle = (-1)^{j-m} |j\ -m\ n\rangle \quad \text{and} \quad \langle j\ m; n| = (-1)^{j-m} \langle j\ -m\ n| \quad (\text{D.27})$$

we can relate the states $|j\ -m\ n\rangle$ to the abstract spin states $|j\ m\rangle_{(n)}$ and can relate the recoupling scheme (D.18)

$$\begin{aligned} |\vec{a}\ J\ M; \vec{n}\ \vec{j}\rangle &:= \sum_{m_1+m_2+\dots+m_N=M} \langle j_1\ m_1; j_2\ m_2 | a_2\ \tilde{m}_2\rangle \times \dots \times \langle a_{N-1}\ \tilde{m}_{N-1}; j_N\ m_N | J\ M\rangle \\ &\quad \times |j_1\ m_1; n_1\rangle \otimes |j_2\ m_2; n_2\rangle \otimes \dots \otimes |j_N\ m_N; n_N\rangle \\ &:= \sum_{m_1+m_2+\dots+m_N=M} \langle j_1\ m_1; j_2\ m_2 | a_2\ \tilde{m}_2\rangle \times \dots \times \langle a_{N-1}\ \tilde{m}_{N-1}; j_N\ m_N | J\ M\rangle \\ &\quad \times (-1)^{j_1+\dots+j_N} (-1)^{-m_1-\dots-m_N} \times |j_1\ -m_1\ n_1\rangle \otimes |j_2\ -m_2\ n_2\rangle \otimes \dots \otimes |j_N\ -m_N\ n_N\rangle \\ &\quad \boxed{\text{Introduce } \mu_k = -m_k, \tilde{\mu}_k = -\tilde{m}_k, \mu = -M} \\ &= \sum_{\mu_1+\mu_2+\dots+\mu_N=\mu} \langle j_1\ -\mu_1; j_2\ -\mu_2 | a_2\ -\tilde{\mu}_2\rangle \times \dots \times \langle a_{N-1}\ -\tilde{\mu}_{N-1}; j_N\ -\mu_N | J\ -\mu\rangle \\ &\quad \times (-1)^{j_1+\dots+j_N} (-1)^\mu \times |j_1\ \mu_1\ n_1\rangle \otimes |j_2\ \mu_2\ n_2\rangle \otimes \dots \otimes |j_N\ \mu_N\ n_N\rangle \end{aligned} \quad (\text{D.28})$$

Using a symmetry property (See e.g. [29], p.42) of the Clebsch-Gordan coefficients with respect to permutation of their arguments⁴⁴

$$\langle j_1\ -m_1; j_2\ -m_2 | a_2\ -\tilde{m}_2\rangle = (-1)^{-j_1-j_2+a_2} \langle j_1\ m_1; j_2\ m_2 | a_2\ \tilde{m}_2\rangle \quad (\text{D.29})$$

we can continue

$$\begin{aligned} |\vec{a}\ J\ M; \vec{n}\ \vec{j}\rangle &= \sum_{\mu_1+\mu_2+\dots+\mu_N=\mu} \langle j_1\ \mu_1; j_2\ \mu_2 | a_2\ \tilde{\mu}_2\rangle \times \dots \times \langle a_{N-1}\ \tilde{\mu}_{N-1}; j_N\ \mu_N | J\ \mu\rangle \\ &\quad \times (-1)^J (-1)^\mu \times |j_1\ \mu_1\ n_1\rangle \otimes |j_2\ \mu_2\ n_2\rangle \otimes \dots \otimes |j_N\ \mu_N\ n_N\rangle \end{aligned} \quad (\text{D.30})$$

⁴⁴The sum $j_1 + j_2 - a_2$ is an integer number.

in complete analogy to (D.27). A similar calculation gives for the bra state

$$\begin{aligned} \langle \vec{a} J M ; \vec{n} \vec{j} | = & \sum_{\mu_1 + \mu_2 + \dots + \mu_N = \mu} \langle j_1 \mu_1 ; j_2 \mu_2 | a_2 \tilde{\mu}_2 \rangle \times \dots \times \langle a_{N-1} \tilde{\mu}_{N-1} ; j_N \mu_N | J \mu \rangle \\ & \times (-1)^J (-1)^\mu \times \langle j_1 \mu_1 n_1 | \otimes \langle j_2 \mu_2 n_2 | \otimes \dots \otimes \langle j_N \mu_N n_N | \end{aligned} \quad (\text{D.31})$$

We can thus conclude that for gauge invariant states $J = 0$, $M = \mu = 0$ the recoupling schemes built from the preliminary basis $| j m n \rangle$ and the final basis $| j m ; n \rangle$ are identical and thus as long as one works with gauge invariant states the “historical” approach coincides with the construction implemented in the previous section. Moreover, since $J + \mu = J - M$ is an integer number, the expectation values of operators diagonal⁴⁵ with respect to J, M will also be identical using the conventions (D.3), (D.20) with respect to our conventions (D.10), (D.14). This is in particular the case for the volume operator.

References

- [1] T. Thiemann, “Introduction to Modern Canonical Quantum General Relativity”, Cambridge University Press, Cambridge 2006; [arXiv: gr-qc/0110034].
- [2] C. Rovelli, “Quantum Gravity”, Cambridge University Press, Cambridge, 2004.
- [3] A. Ashtekar and J. Lewandowski, “Background independent quantum gravity: A status report,” *Class. Quant. Grav.* **21** (2004) R53; [arXiv:gr-qc/0404018].
- [4] R. Arnowitt, S. Deser, C.W.Misner, in: *Gravitation: An Introduction to current Research*, L. Witten (ed.), Wiley, New York, 1962.
- [5] P.A.M. Dirac, “Lectures on Quantum Mechanics”, Academic Press INC. New York/London, Second printing 1967.
- [6] T. Thiemann, “Quantum Spin Dynamics (QSD)”, *Class.Quant.Grav.* **15** (1998) 839-873; [arXiv: gr-qc/9606089].
- [7] T. Thiemann, “QSD V. Quantum Gravity as the Natural Regulator of the Hamiltonian Constraint of Matter Quantum Field Theories”, *Class. Quantum Grav.* **15** (1998) 1281-1314; [arXiv:gr-qc/9705019].
- [8] T. Thiemann, “Quantum spin dynamics. VIII: The master constraint”, *Class. Quant. Grav.* **23**, 2249 (2006); [arXiv:gr-qc/0510011].
- [9] H. Sahlmann and T. Thiemann, “Towards the QFT on curved spacetime limit of QGR. II: A concrete implementation”, *Class. Quant. Grav.* **23** (2006) 909; [arXiv:gr-qc/0207031].
- [10] K. Giesel and T. Thiemann, “Algebraic quantum gravity (AQG). I: Conceptual setup”; [arXiv:gr-qc/0607099].
“Algebraic quantum gravity (AQG). II: Semiclassical analysis”; [arXiv:gr-qc/0607100].
“Algebraic quantum gravity (AQG). III: Semiclassical perturbation theory”; [arXiv:gr-qc/0607101].
- [11] J. Brunnemann and T. Thiemann, “On (cosmological) singularity avoidance in loop quantum gravity”, *Class. Quant. Grav.* **23** (2006) 1395; [arXiv:gr-qc/0505032].
- [12] J. Brunnemann and T. Thiemann, “Unboundedness of triad – like operators in loop quantum gravity”, *Class. Quant. Grav.* **23** (2006) 1429; [arXiv:gr-qc/0505033].
- [13] C. Rovelli and L. Smolin, “Discreteness of area and volume in quantum gravity”, *Nucl. Phys. B* **442** (1995) 593 [Erratum-ibid. B **456** (1995) 753]; [arXiv:gr-qc/9411005].
- [14] R. De Pietri, “Spin Networks and Recoupling in Loop Quantum Gravity”, *Nucl. Phys. Proc. Suppl.* **57**, 251 (1997); [arXiv:gr-qc/9701041].
- [15] T. Thiemann, “Closed formula for the matrix elements of the volume operator in canonical quantum gravity”, *J. Math. Phys.* **39**, 3347 (1998); [arXiv: gr-qc/9606091].
- [16] A. Ashtekar and J. Lewandowski, “Quantum theory of geometry. II: Volume operators”, *Adv. Theor. Math. Phys.* **1**, 388 (1998); [arXiv:gr-qc/9711031].
- [17] G. Carbone, M. Carfora, A. Marzouli, “Quantum states of elementary three-geometry”, *Class. Quant. Grav.* **19** (2002) 3761; [arXiv:gr-qc/0112043].

⁴⁵By diagonal we mean that these operators require identical J, M upon evaluation in a recoupling scheme basis.

- [18] K. A. Meissner, “Eigenvalues of the volume operator in loop quantum gravity”, *Class. Quant. Grav.* **23** (2006) 617; [arXiv:gr-qc/0509049].
- [19] F.J. Dyson, “The Dynamics of a Disordered Linear Chain”, *Phys. Rev.* **92**, 1331 (1953).
- [20] V. John, I. Angelov, A. A. Öncül, K. Sundmacher, D. Thevenin, “Towards the Optimal Reconstruction of a Distribution From its Moments”, Proceedings of the AIChE Annual Meeting, 2005, available at <http://www.math.uni-sb.de/ag/john/AIChE.pdf>.
- [21] O. Dreyer, private communication.
- [22] K. Giesel and T. Thiemann, “Consistency check on volume and triad operator quantisation in loop quantum gravity. I”, *Class. Quant. Grav.* **23** (2006) 5667; [arXiv:gr-qc/0507036].
- [23] K. Giesel and T. Thiemann, “Consistency check on volume and triad operator quantisation in loop quantum gravity. II”, *Class. Quant. Grav.* **23** (2006) 5693; [arXiv:gr-qc/0507037].
- [24] J. Brunnemann and T. Thiemann, “Simplification of the spectral analysis of the volume operator in loop quantum gravity”, *Class. Quant. Grav.* **23** (2006) 1289; [arXiv:gr-qc/0405060].
- [25] J. Brunnemann and D. Rideout, “Properties of the Volume Operator in Loop Quantum Gravity I: Results”; [arXiv:0706.0469v1] [gr-qc].
- [26] J. Brunnemann and D. Rideout, “Embeddable Vertex Geometries in Three Dimensional Riemannian Space”, work in progress.
- [27] P. Deift, “Orthogonal Polynomials and Random Matrices: A Riemann-Hilbert Approach”, Courant Lecture Notes 3, Courant Institute of Mathematical Sciences, New York University, 1999.
- [28] M. Abramowitz, I. Stegun, “Handbook of Mathematical Functions”, Dover Publications, Inc., New York, 1970, Online version available at <http://www.math.sfu.ca/~cbm/aands>.
- [29] A. R. Edmonds, “Angular Momentum in Quantum Mechanics”, Princeton University Press, Fourth printing 1996.
- [30] D. A. Varshalovich, A. N. Moskalev, V. K. Khersonskii, “Quantum Theory of Angular Momentum”, World Scientific, 1988.
- [31] M. Marcus H. Minc, “A Survey of Matrix Theory and Matrix Inequalities”, Dover Publications, Inc. New York, 1992.
- [32] R.U. Sexl H.K. Urbantke, “Relativität, Gruppen, Teilchen”, Springer Verlag Wien/New York 1982, second extended edition.
- [33] F. Schwabl, “Quantum Mechanics”, translated by R. Kates, Secon Revised Edition, Springer-Verlag, Berlin/Heidelberg/New York, 1995.
- [34] F. R. Gantmacher “Matrizentheorie”, VEB Deutscher Verlag der Wissenschaften, Berlin 1986.
- [35] LAPACK Linear Algebra Package, <http://www.netlib.org/lapack>.
- [36] T. Goodale, G. Allen, G. Lanfermann, J. Massó, T. Radke, E. Seidel, and J. Shalf, “The Cactus Framework and Toolkit: Design and Applications” in *Vector and Parallel Processing — VECPAR 2002, 5th International Conference*, Springer, pp. 197–227.
- [37] <http://www.netlib.org>.